

AD-A055 177

OPTICAL SCIENCES CO PLACENTIA CA
ADAPTIVE COMPENSATION TECHNIQUES.(U)

F/G 17/8

MAY 78 D L FRIED, E J SCHONHEINZ, R B ASHER

F30602-77-C-0099

UNCLASSIFIED

DR-105

RADC-TR-78-101

NL

1 OF 5
AD
A055177



FOR FURTHER TRAN *W.L.L.*

② ✓



AD A 055177

RADC-TR-78-101
Final Technical Report
May 1978

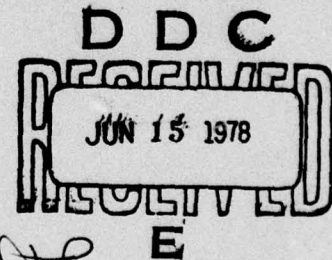
ADAPTIVE COMPENSATION TECHNIQUES

Dr. David L. Fried
Emil J. Schonheinz
Professor Robert B. Asher

The Optical Sciences Company

THIS DOCUMENT IS BEST QUALITY PRACTICABLE.
THE COPY FURNISHED TO DDC CONTAINED A
SIGNIFICANT NUMBER OF PAGES WHICH DO NOT
REPRODUCE LEGIBLY.

Approved for public release; distribution unlimited.



AD NO.
DDC FILE COPY

ROME AIR DEVELOPMENT CENTER
Air Force Systems Command
Griffiss Air Force Base, New York 13441

78 06 14 010

This report contains a large percentage of machine-produced copy which is not of the highest printing quality but because of economical consideration, it was determined in the best interest of the government that they be used in this publication.

This report has been reviewed by the RADC Information Office (OI) and is releasable to the National Technical Information Service (NTIS). At NTIS it will be releasable to the general public, including foreign nations.

RADC-TR-78-101 has been reviewed and is approved for publication.

APPROVED:

Robert F. Ogrodnik

ROBERT F. OGRODNIK
Project Engineer

APPROVED:

Joseph L. Ryerson

JOSEPH L. RYERSON
Technical Director
Surveillance Division

FOR THE COMMANDER:

John P. Huss

JOHN P. HUSS
Acting Chief, Plans Office

If your address has changed or if you wish to be removed from the RADC mailing list, or if the addressee is no longer employed by your organization, please notify RADC (OCTM) Griffiss AFB NY 13441. This will assist us in maintaining a current mailing list.

Do not return this copy. Retain or destroy.

DISCLAIMER NOTICE

**THIS DOCUMENT IS BEST QUALITY
PRACTICABLE. THE COPY FURNISHED
TO DDC CONTAINED A SIGNIFICANT
NUMBER OF PAGES WHICH DO NOT
REPRODUCE LEGIBLY.**

UNCLASSIFIED

SECURITY CLASSIFICATION OF THIS PAGE (When Data Entered)

REPORT DOCUMENTATION PAGE		READ INSTRUCTIONS BEFORE COMPLETING FORM	
1. REPORT NUMBER RADC-TR-78-141	2. GOVT ACCESSION NO.	3. RECIPIENT'S CATALOG NUMBER	
4. TITLE (and Subtitle) ADAPTIVE COMPENSATION TECHNIQUES		5. TYPE OF REPORT & PERIOD COVERED Final Technical Report, Jun 77 - Feb 78	
6. AUTHOR(s) David L. Fried, and Emil J. Schonheinz with contribution of Prof. Robert B. Asher		7. PERFORMING ORG. REPORT NUMBER DR-105	
8. PERFORMING ORGANIZATION NAME AND ADDRESS The Optical Sciences Company P O Box 446 Placentia CA 92670		9. CONTRACT OR GRANT NUMBER(s) F30602-77-C-0099	
10. CONTROLLING OFFICE NAME AND ADDRESS Rome Air Development Center (OCTM) Griffiss AFB NY 13441		11. PROGRAM ELEMENT, PROJECT, TASK AREA & WORK UNIT NUMBERS 62702F 65270217	
12. MONITORING AGENCY NAME & ADDRESS (if different from Controlling Office) Same		13. REPORT DATE May 78	
14. DISTRIBUTION STATEMENT (of this Report) Approved for public release; distribution unlimited.		15. NUMBER OF PAGES 385	
16. DISTRIBUTION STATEMENT (of the abstract entered in Block 20, if different from Report) Same		17. SECURITY CLASS. (of this report) UNCLASSIFIED	
18. SUPPLEMENTARY NOTES RADC Project Engineer: Robert F. Ogradnik (OCTM)		19. DECLASSIFICATION/DOWNGRADING SCHEDULE N/A	
20. KEY WORDS (Continue on reverse side if necessary and identify by block number) Long Range Tracking Adaptive Optics Target Scattering Optimal Estimation			
21. ABSTRACT (Continue on reverse side if necessary and identify by block number) This report is the final technical report on work performed on Contract F30602-77-C-0099, and covers all work done under this contract. This report presents analysis, a set of computer simulation programs, and a set of simulation results that demonstrate that an adaptive compensation pointing and tracking servo loop can be closed in a long range space engagement that permits high servo bandwidth tracking performance with point-ahead and boresight error compensation that adapts to insure that the laser spot			

DD FORM 1 JAN 73 1473 EDITION OF 1 NOV 65 IS OBSOLETE

UNCLASSIFIED

SECURITY CLASSIFICATION OF THIS PAGE (When Data Entered)

78 06 14 010
397 358

UNCLASSIFIED

SECURITY CLASSIFICATION OF THIS PAGE(When Data Entered)

is held on the desired aimpoint. A laser spot position technique based on exploitation of speckle statistics is developed that allows the true laser spot position to be sensed and compensated for whether or not a glint point (even a strong glint point) is present. Simulation results demonstrate the performance at the concept and lead to the conclusion that the technique should be applicable with extension, to higher order adaptive optics control problems - thus providing high servo bandwidth performance together with compensation for any bias errors.

ACCESSION for	
NTIS	White Section <input checked="" type="checkbox"/>
DDC	Buff Section <input type="checkbox"/>
UNANNOUNCED	<input type="checkbox"/>
JUSTIFICATION.....	
BY.....	
DISTRIBUTION/AVAILABILITY CODES	
Dist.	AVAIL. and/or SPECIAL
A	23 24

UNCLASSIFIED

SECURITY CLASSIFICATION OF THIS PAGE(When Data Entered)

TABLE OF CONTENTS

<u>Chapter</u>	<u>Section</u>	<u>Title</u>	<u>Page</u>
		Overview and Summary	1
1		Adaptive Compensation Baseline Optical System Concept	8
	1.1	Baseline System Concept	9
2		Modeling the Basic Engagement Scenario for ACT	16
	2.1	Introduction	17
	2.2	Basic Engagement Geometry	18
	2.3	Gimbal Angle and Target Track Error Signal	21
	2.4	Gimbal Servo Computation	24
	2.5	Laser Miss Distance	27
	2.6	Computer Simulation	29
		Appendix to Chapter 2	45
3		Outer Loop Control of Laser Pointing Boresight Error	60
	3.1	Introduction	61
	3.2	Inner Loop/Outer Loop Servo Considerations	63
	3.3	Ideal Sensor Bias Control Servo Simulation	68
		Appendix to Chapter 3	96
4		Diffuse Backscatter Focal Plane Statistics for a Laser Transmitter/Receiver	103
	4.1	Introduction	104
	4.2	Encounter Geometry	106
	4.3	Surface Roughness Statistics	109
	4.4	Propagation Formulation	112
	4.5	Point-Intensity Statistics	116
	4.6	Evaluation With a Gaussian-Taper Aperture	126

Table of Contents (Continued)

<u>Chapter</u>	<u>Section</u>	<u>Title</u>	<u>Page</u>
5		Laser Transmitter/Receiver Sensor Definition and Signal Simulation	134
	5.1	Introduction	135
	5.2	Focal Plane Array Definition	137
	5.3	Glint Return	140
	5.4	Array Output Simulation	144
6		Simulation of Random Laser Backscatter	155
	6.1	Introduction	156
	6.2	System and Engagement Parameters	158
	6.3	Synopsis of the Required Backscatter Statistics	165
	6.4	Generation of the \tilde{A} -Quantities	168
	6.5	Sample Results	172
		Appendix to Chapter 6	229
7		Outer Loop Laser Boresight Error Control By Sensing the Backscatter Signal	243
	7.1	Introduction	244
	7.2	Separation of Diffuse and Glint Returns	247
	7.3	Laser Spot Position Estimation	253
	7.4	Boresight Error Control Simulation	256
		Appendix I to Chapter 7	338
		Appendix II to Chapter 7	346
		Addendum on Adaptive Estimation for ACT Signal Processing	355
	A.1	Introduction	357
	A.2	Problem Statement	359
	A.3	Measurement Models	360
	A.4	State Space Realization	363
	A.5	Adaptive Estimator	370
	A.6	Conclusions	378
		References for Addendum Section	379

LIST OF FIGURES

<u>Figure No.</u>	<u>Title</u>	<u>Page</u>
1.1	Block Diagram of the Major Components of the Adaptive Compensation Laser Pointing and Tracking System.	14
1.2	Block Diagram of the Internal Arrangement of the Track and Boresight Sensor.	15
2.1	Basic Engagement Geometry.	31
2.2	Servo Block Diagram.	32
3.1	Local Inner Servo Imbedded in a R/T Delayed Outer Servo Loop.	71
3.2	Laser/Target Miss Distance Without Bias Update for a Time-Varying Bias Error.	72
3.3	Laser/Target Miss Distance With Bias Update for Various Stability Factors.	73
3.4	Laser/Target Miss Distance With Bias Update for Various Update Times.	74
4.1	Engagement Geometry.	133
7.1a	Estimated Laser Spot Position Along $\hat{\xi}$ - Axis.	258
7.1b	Estimated Laser Spot Position Along $\hat{\eta}$ - Axis.	259
7.2	Relative Glint Strength.	260
7.3a	Closed Loop Boresight Error Control	261
7.3b	Closed Loop Boresight Error Control	261
7.3c	Closed Loop Boresight Error Control	261
7.3d	Closed Loop Boresight Error Control	261

LIST OF TABLES

<u>Table</u>	<u>Title</u>	<u>Page</u>
2.1	High Crossing Velocity Engagement	33
2.2	Low Crossing Velocity Engagement	36
2.3	Low Crossing Velocity Engagement With Laser Boresight Error	39
2.4	Low Crossing Velocity Engagement With Laser Boresight Error and Boresight Error Estimates	42
3.1a	Outer Loop Bias Control of a Time-Dependent Boresight Error, With a Servo Stability Factor of $\alpha = 8$, and a $\tau_0 = 20$ msec Update Time.	75
3.1b	Outer Loop Bias Control of a Time-Dependent Boresight Error, With a Servo Stability Factor of $\alpha = 6$, and a $\tau_0 = 20$ msec Update Time.	77
3.1c	Outer Loop Bias Control of a Time-Dependent Boresight Error, With a Servo Stability Factor of $\alpha = 4$, and a $\tau_0 = 20$ msec Update Time.	79
3.1d	Outer Loop Bias Control of a Time-Dependent Boresight Error, With a Servo Stability Factor of $\alpha = 3$, and a $\tau_0 = 20$ msec Update Time.	81
3.2a	Outer Loop Bias Control of a Fixed Boresight Error, With a Servo Stability Factor of $\alpha = 8$, and a $\tau_0 = 20$ msec Update Time.	83
3.2b	Outer Loop Bias Control of a Fixed Boresight Error, With a Servo Stability Factor of $\alpha = 6$, and a $\tau_0 = 20$ msec Update Time.	85
3.2c	Outer Loop Bias Control of a Fixed Boresight Error, With a Servo Stability Factor of $\alpha = 4$, and a $\tau_0 = 20$ msec Update Time.	87
3.2d	Outer Loop Bias Control of a Fixed Boresight Error, With a Servo Stability Factor of $\alpha = 3$, and a $\tau_0 = 20$ msec Update Time.	89

List of Tables (Continued)

<u>Table</u>	<u>Title</u>	<u>Page</u>
3.3a	Outer Loop Bias Control of a Time-Dependent Boresight Error, With a Servo Stability Factor of $\alpha = 6$, and a $\tau_0 = 20$ msec Update Time	91
3.3b	Outer Loop Bias Control of a Time-Dependent Boresight Error, With a Servo Stability Factor of $\alpha = 6$, and a $\tau_0 = 40$ msec Update Time	92
3.3c	Outer Loop Bias Control of a Time -Dependent Boresight Error, With a Servo Stability Factor of $\alpha = 6$, and a $\tau_0 = 80$ msec Update Time.	94
6.1	Target Tracking Kinematics	175
6.2	Laser Backscatter Detector Array Outputs for $V_{\perp} = 50$ m/sec and $I_{e,0} = 0.0$	178
6.3	Laser Backscatter Detector Array Outputs for $V_{\perp} = 50$ m/sec and $I_{e,0} = 100$.	188
6.4	Laser Backscatter Detector Array Outputs for $V_{\perp} = 50$ m/sec and $I_{e,0} = 10,000$.	199
6.5	Laser Backscatter Detector Array Outputs for $V_{\perp} = 100$ m/sec and $I_{e,0} = 0.0$	209
6.6	Laser Backscatter Detector Array Outputs for $V_{\perp} = 200$ m/sec and $I_{e,0} = 0.0$	219
7.1	Laser Spot Position Estimation	262
7.2	Closed Loop Boresight Error Control	287

EVALUATION

The objective of this program was to devise control techniques based on optimal estimation principles which promote closed loop adaptive optical control independent of transit time delay limitations in long range optical applications of precision pointing, tracking and high resolution surveillance.

Analytical development was completed for estimation modeling of the target backscatter, both specular (glint returns) and random scatter (diffuse returns), as well as for receiver tracking error detection, and estimations of signal strength, target motion rates and update line-of-sight pointing correction. This development allowed tracking error control in the presence of track error return delays due to long transit time applications. That is, the estimation modeling potentially eliminated servo bandwidth limitations for tracking error correction due to transmit delays. The ability to implement the estimation modeling in computer simulation studies was restrictive, however, due to the complex structure of the estimation models and computational load requirements in its related computing algorithms. Further work is needed (beyond the scope of this program) to either simplify the estimator structure to enable simulation feasibility, or to reformat its structure into a computationally feasible architecture (such as FFT version of transformation processes). Analytical tests of the estimation algorithms verified its performance in removing bandwidth restrictions due to transit time factors. Another aspect of the estimation algorithm was also verified. This was the use of backscattered signal statistics discrimination to isolate three factors in the target plane as observed in the receiver domain. These are the isolation and spatial location of target specular regions (glint) from spatially extended random (diffuse scattering) textured regions; and, the identification of actual beam centroid location on target (in the specular or diffuse target regions) discriminated against general target surface texture. This was performed by using spatial correlation techniques in a 20 by 20 detector element mosaic receiver, and statistical processing of signal returns. These functions were successfully

computer simulated and represented the bulk of the algorithm analysis conducted in this program. Included in this study was the correlation of target loop (external transit time delayed path) and local loop correction methods to achieve wide bandwidth system control performance (energy maximization at selected target aimpoint) while minimizing transit time bandwidth limitations.

The development of techniques which minimize or eliminate closed loop bandwidth restrictions due to transit time delays is contributory to the successful application of surveillance and directed weapons for long range applications. The target-local loop correlation schemes successfully demonstrated the minimization of transit bandwidth limitations, while the estimation algorithm techniques potentially provided methods which were capable of totally eliminating such restrictions. Continued work is desirable for this latter case for algorithm implementation in a computationally efficient manner. The removal of transit time delay restrictions on the operation of real time target detection and location is directly contributory to the success of surveillance and defense missions in long range applications whether they are strategic or tactical in nature. This directly supports the RADC Technology Plan under TPO Thrust III-STs.

This effort successfully verified that techniques can be devised to either minimize or eliminate transit limit performance limitation experienced in long range surveillance and energy directed defense systems. Continued work is planned to assess methods which will enable optimal estimation approaches computationally efficient and feasible to implement.

Robert F. Ogrodnik

ROBERT F. OGRODNIK
Project Engineer

OVERVIEW AND SUMMARY

The fundamental objective of this program has been to develop a basis for closed loop laser beam control in a space engagement that would insure that the laser spot was properly focused on the desired target aimpoint. The driving consideration has been that with the long ranges and concomitant large round-trip speed-of-light transit times involved, it is not clear how a high performance true closed loop control could be achieved. There is an apparent servo bandwidth limit associated with this round-trip transit time delay, and this necessarily restricts the achievable servo performance. This would, for example, appear to preclude the use of a conventional transmitter multidither adaptive optics system for the target tracking, focus adjustment, and wavefront distortion control functions in a long range space engagement.

In this work we have been seeking a way around this apparent restriction. To keep our task at a reasonably manageable level, we have restricted our attention to the target tracking function. Our understanding has been that, if we could find a way to control the laser spot position on the target, i. e. insure that the laser spot was striking the aimpoint, (and not just pointed in the direction we thought was proper), and yet realize high servo bandwidth type performance despite the long range to the target, then this method could probably be generalized to apply to the focus and adaptive optics control functions. However, we have left consideration of this generalization procedure as a matter to be treated in later work.

Our initial hope was that some form of adaptive estimation, i. e. an extension of the Kalman-Bucy filter technique, might allow this objective to be realized. Accordingly, we had an analysis performed to develop such a technique. The results of this work are reported in

an Addendum to this report. In studying these results we reached the conclusion that while this technique might be theoretically relevant, it was so complex that its practical implementation did not appear reasonable. This was a particularly significant point for us since a major part of the program effort was to be concerned with computer simulation of a space engagement. (We could not simply ignore the difficulty in the practical implementation of the adaptive estimation processor — we would have to program it.) In addition, we were somewhat concerned that the adaptive estimator might have been overly sensitive to model details, but we never got to test this as we did not attempt to pursue the adaptive estimation technique to the point of computer simulation.

In place of this adaptive estimation procedure, we have built the work reported here around a much more straightforward adaptive compensation concept. We assume that the basic laser beam control is provided by an entirely local high bandwidth, high performance servo. Because it is entirely local, the bandwidth can be high, but also because it is entirely local, it can only point the laser beam where it "thinks" the beam should be directed. It does not know where the beam actually strikes the target as this would involve a round-trip transit time delay and would not be compatible with the desired high servo bandwidth. Adaptive compensation to correct for this is introduced by another sensor and an outer "servo" loop which "sees" where the laser beam is striking the target and compensates for any offset by biasing the local high bandwidth servo loop. The adaptive compensation corresponds to an outer loop which, because of the round-trip transit time delay, necessarily has a low servo bandwidth. The underlying assumption is that, while

tracking may require a high bandwidth, (particularly because of gimbal vibration), the things like boresight error and point ahead requirement only change slowly and so do not require a high servo bandwidth for their compensation. This basic concept is described in Chapter 1, together with a generalized description of a baseline optical system that could utilize this approach.

Chapter 2 sets up the basic computer simulation for a laser space engagement. In particular, it models a two-axis laser transmitter/target sensor gimbal system, and properly simulates the speed-of-light round-trip transit time delay effects, as well as allowing the introduction of boresight error effects. The simulation results shown in Chapter 2 manifest the expected point-ahead effect.

Chapter 3 extends this computer simulation model to include the adaptive compensation outer loop. It is assumed that a sensor is available that can see where the laser is, (was — one transit time ago), striking the target. The error signal thus provided is used to bias the high servo bandwidth target tracking loop. It is demonstrated by computer simulation results that the residual laser miss distance will be negligibly small for a target at 1.0 Mm range and a laser boresight error drift rate of as much as 10 μ rad/sec. The adaptive compensation outer loop is configured as a nonstandard version of a type-1 sampled data servo loop with a servo bandwidth that automatically adjusts for the sample data rate. The simulations were run with a data rate significantly slower than that implied by the round-trip transit time delay.

The assumption that the position where the laser spot strikes the target can be inferred from the backscatter signal poses a potential problem when a glint point is present on the target. In such a case the glint point return can be so much greater than the diffuse scattering return,

which is the actual indicator of the laser spot position on the target, that simple backscatter signal intensity centroiding will give the wrong result for the laser spot position on the target. The reported position will very nearly correspond to that of the glint point rather than the position of the laser spot. To avoid this problem, we have decided to make use of the fact that the glint return is essentially constant while the diffuse return from the target is a randomly fluctuating quantity.

The rate of fluctuation is set by the target vibration spectrum and by the rate of rotation of the laser beam/line-of-sight with respect to the target surface normal. At a minimum this rate of rotation is set by the changing target and laser system positions, assuming that the target is not on an exact collision course with the laser system. In our simulations we have assumed that this angular rotation was quite low, corresponding to a crossing velocity of 50 m/sec at about 1.0 Mm range. This represented a worse case for the simulated performance of the adaptive compensation.

The problem of how to separate the fluctuating from the non-fluctuating portions of the return is taken up in Chapter 7. First, however, we needed to develop a basis for simulation of the random backscatter signal. In Chapter 4 we developed the basic statistical theory for the backscatter signal fluctuations as they would be seen in a shared aperture imaging focal plane. In Chapter 5 the details implicit in this theory are amplified and used to formulate a basis for simulation of the time varying backscatter signal on each element of a 20×20 element imaging detector array. The critical feature of Chapters 4 and 5 is that the randomly fluctuating signals vary with the appropriate spatial and temporal covariance.

Chapter 6 presents a computer program that implements the theory and simulation algorithms of the preceding two chapters. It produces a time varying 20×20 array of detector output corresponding to the laser backscatter image in a realistically modeled space engagement. Sample output results are presented for different levels of glint strength compared to diffuse return strength, and for different engagement kinematics corresponding to different correlation times.

Chapter 7 brings all of the work together in a realistic adaptive control system simulation based on observing the laser backscatter in the presence of a strong glint return. The chapter starts by taking note of the fact that there is a heterodyning effect when glint and diffuse returns are added, so that the signal intensity variance is greater than it would be, if only the diffuse return were present. A formula is developed for extracting the intensity to be associated with the diffuse return from the total signal's mean and variance. Using this formula a set of simulation runs are performed with the adaptive compensation loop open to demonstrate that the laser spot position calculated from the centroid of the estimated diffuse return is a good estimate of the actual laser spot position on the target. It is found that even in the presence of a glint return of up to one thousand times the diffuse return there is no apparent bias toward the glint point's position in the estimated position of the laser spot. It is found that reasonable laser spot position estimates can be formed in as little as a few times the fluctuation correlation period. Finally, using the adaptive compensation loop demonstrated initially in Chapter 3 but this time estimating the laser spot position from the randomly fluctuating backscatter signal, a series of computer simulation runs are performed to demonstrate adaptive compensation in the presence of a strong glint return, in a laser space engagement. The simulation

results demonstrate the ability of the adaptive compensation procedure to correct for point-ahead and laser bias errors to a function of a laser spot diameter. Based on these very encouraging results, we feel justified in concluding that the same technique, with certain modifications, can be applied to transmitter focus and adaptive optics control. This will allow high servo bandwidth performance of the control system, but will insure that bias errors will be sensed and corrected, so that a near perfect focusing of the laser spot on the desired aimpoint will be achieved.

Chapter 1

Adaptive Compensation

Baseline Optical System Concept

1. Baseline System Concept

To provide a framework for the adaptive compensation study we have defined a laser transmitter/target tracking system for space operation which seems to offer the potential for tracking targets at long range with high servo bandwidth.

Pointing and tracking, per se, can be implemented with a high servo bandwidth without any special control system features. However, the nulling of alignment errors in the system can only be truly insured by closing a sensing loop around the target. Because of the long range involved, the alignment control aspects of the servo may be rather slow. To prevent this from depriving the system of high bandwidth pointing and tracking servo performance, we plan to make use of the very plausible feature of the plant model, that alignment errors change only rather slowly so that they can be adequately controlled by a low servo bandwidth control loop, closed by sensing over a round-trip path to the target and back. This can then be an outer loop around the rest of the pointing and tracking controls which themselves constitute a conventional high bandwidth system. To insure that the slow outer loop is not excessively slow, so that the alignment errors will be nulled rapidly, we plan to use adaptive compensation in the alignment control outer loop.

Though our concern here is with the pointing and tracking task only, we have kept in mind an ultimate interest in the problem of controlling adaptive optics and, accordingly, have defined a shared aperture system which should prove directly applicable to control of an adaptive optics system. In this case it should also be possible to close a local high servo bandwidth pointing, tracking, and adaptive optics control loop by viewing the target through the shared aperture, but leaving the alignment of the pointing and tracking, and of the adaptive optics control to a slower round-trip control loop, whose speed we will maximize by use of an adaptive compensation control.

In Fig. 's 1 and 2 we define the basic features of the sample laser pointing and tracking system. For convenience we have postulated a pulsed high energy laser so that some form of T/R switch can be used to allow the same telescope aperture to function both as a transmitter of the laser radiation and as a receiver for the backscattered laser radiation.* The operation of the system is best understood by considering the two sensor packages, namely the Laser Alignment Sensor (the LAS) and the Track and Boresight Sensor (the T+BS). The LAS and T+BS, together with the Laser Beam Splitter (the LBS) which may be considered to be a part of the LAS, are physically proximate and so may be considered to drift with respect to each other only rather slowly. Because they are close enough to be integrated into one compact housing, there should be no vibration-induced variation in the relative alignment of the LAS and the T+BS. Only the very low frequencies associated with

* There are other techniques that will allow the telescope aperture to function in a dual role, as transmitter and receiver for the laser radiation, even if the laser operates continuously rather than in a pulsed mode. For example, the laser can be designed to transmit right circular polarized radiation. In the backscatter process, (without any depolarization) this will be converted to left circular polarized radiation. If, in place of the T/R switch of Fig. 1, the system contained a circular polarization analyzer, the right circular polarized laser radiation would all be transmitted, while the left circular polarized backscatter signal would all be sent to the sensor package, just as is the case for the pulsed laser with the T/R switch. As another alternative when the laser operation is continuous instead of pulsed, the T/R switch can be replaced by a beam splitter and the laser detection portion of the sensor could be a heterodyne system. In this case, the doppler shift of the backscattered laser radiation would allow the sensor to easily separate it from the direct leakage of the laser radiation. In this case, of course, because of the use of a beam splitter, the net utilization of optical radiation would be less than with the T/R switch.

structural creep, and with changing thermal gradients should be expected in the variations of the alignment of the LAS relative to the T+BS.

The LAS will receive a sample of the outgoing laser beam and will be able to monitor its orientation. The null position of the LAS is somewhat arbitrary so that, in a d. c. sense, the signal from the LAS has questionable meaning. However, any fluctuations in the laser beam direction corresponding to variations in the laser output will be accurately reflected in the LAS output signal.

The T+BS consists of two focal planes sharing a common input via a dichroic beam splitter, as indicated in Fig. 2. The imaging sensor will observe the target image as seen through the shared aperture of the transmitter/receiver telescope (and the hollow-axis gimbal train). Any deviation of the target position relative to the pointing of the telescope will be immediately sensed as apparent motion of the target image. We will not be particularly concerned here with the details of the image sensor, other than to note the following features. 1) It provides high data rate information on the location of the planned aim-point on the target (relative to the telescopic orientation). 2) It operates in a wavelength band distinct from that of the high energy laser, so that the dichroic beam splitter provides adequate separation of the target image photons from the backscattered laser photons.

The combination (actually the difference) of the target image tracker data and the laser alignment sensor provides sufficient information to hold the laser spot fixed with respect to the desired aim-point on the target. If the telescope pointing changes in a way not corresponding to the target motion, or if one of the relay mirrors in the hollow-axis gimbal train moves unintentionally, the image will move relative to the image tracker as much as the transmitted laser beam moves relative to the aim-point. The observed change in the target image position will provide the necessary information to correct the telescope pointing. If,

due to some instability in the laser itself, the direction of the outgoing laser beam shifts, the LAS will sense this and provide the necessary information to cause a compensating change in the telescope pointing.

In either case, by closing a servo loop to hold the difference between the image tracker signal and the LAS signal constant, the position of the laser spot relative to the aim-point on the target will be held constant. But this, by itself, does not get the laser spot on the desired aim-point—it just holds the miss distance fixed in time. To null out this remaining error, which is due to the slowly changing relationship between the LAS and the image tracker portion of the T+BS, it is necessary to close a sensor/servo loop involving a propagation path to the target and back. This function is performed by the laser position sensor portion of the T+BS.

The laser position sensor is simply a quadrant detector (and narrow band filter) aligned with the imaging sensor and viewing the backscattered laser signal from the target.* This sensor simply reports the laser spot position relative to the quadrant detector null and thus, since the laser position sensor is aligned to the imaging tracker, relative to the center of the image tracker focal plane. Thus, it is possible to determine the laser spot position relative to the desired aim-point. Because of the slowly changing nature of the alignment errors, the determination of the laser spot position relative to the center of the image tracker's focal plane only has to be done with a moderate (or low) data rate. The key problem in the operation of the quadrant detector laser position

* Because the laser position sensor and the image tracker share common input optics it is possible to combine them in a way that insures that there will be no alignment error. This cannot be achieved with respect to the LAS because of the fact that the input optics cannot be common between the LAS and the T+BS.

sensor, and the thing that drives us to utilize adaptive compensation, is the effect of glint. The presence of a strong glint point on the target, anywhere near the first few side-lobes of the laser spot, will cause the apparent centroid of the laser spot to be significantly closer to the glint point than the laser spot actually is. To circumvent this difficulty, we plan to make use of the difference between the speckle statistics of the diffuse backscatter from the main lobe of the laser spot and the essentially nonvarying backscatter from the glint point, to separate the two returns and determine the true laser spot position.

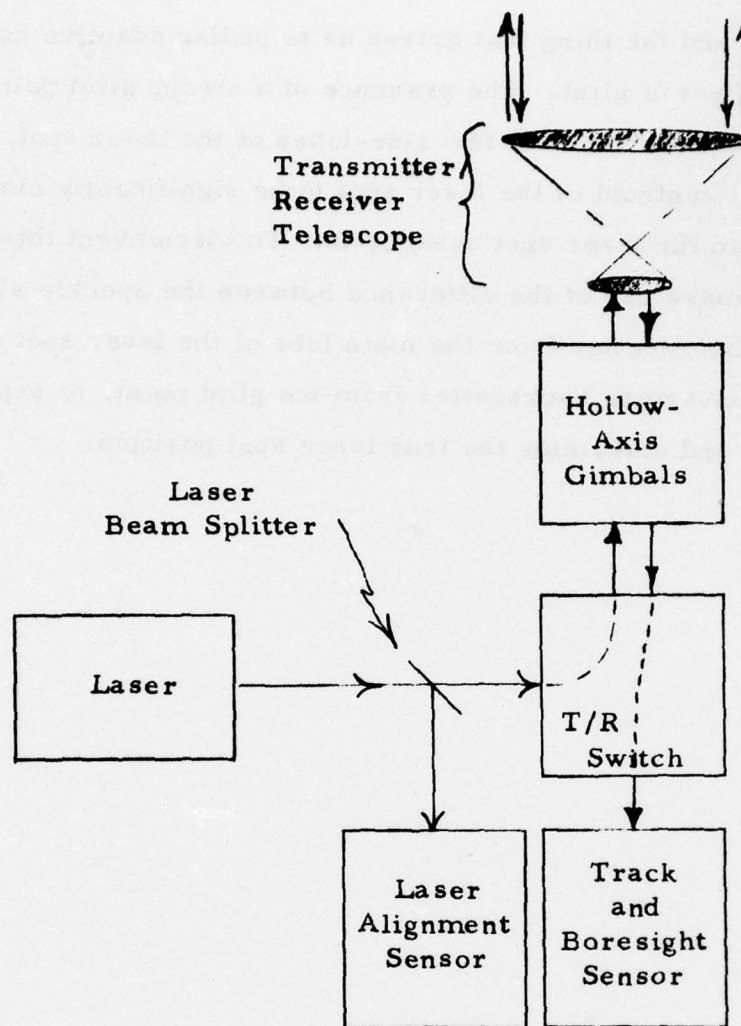


Figure 1.1 Block Diagram Of The Major Components Of The Adaptive Compensation Laser Pointing And Tracking System. Details of the Track and Boresight Sensor are shown in Fig. 2.

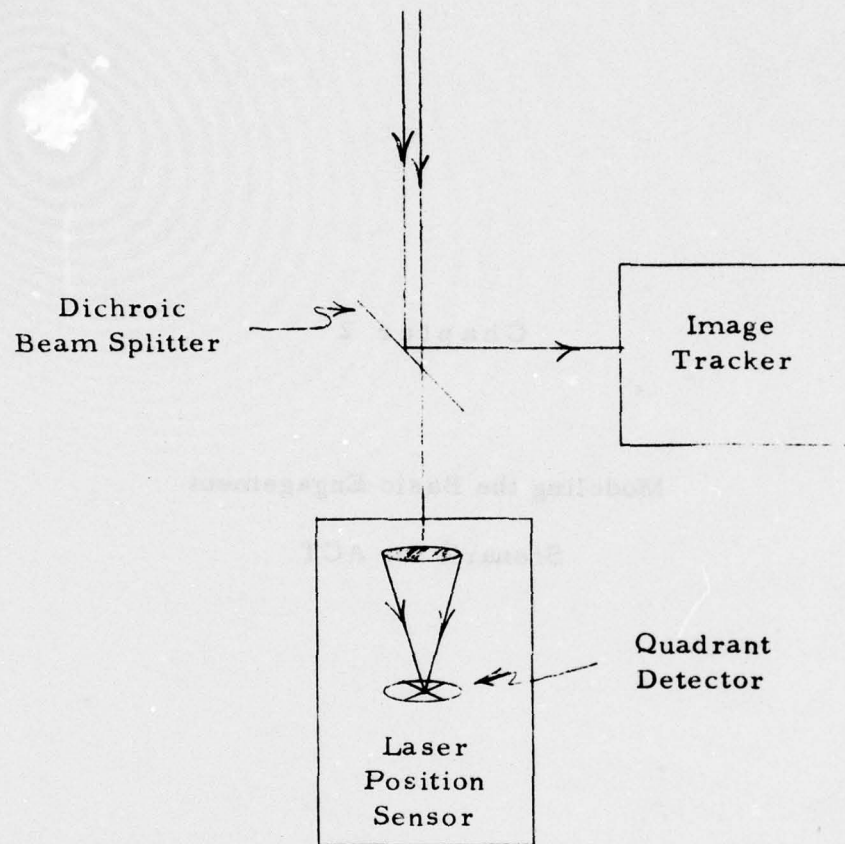


Figure 1.2 Block Diagram Of The Internal Arrangement Of The Track And Boresight Sensor.

Chapter 2

Modeling the Basic Engagement Scenario for ACT

2.1 Introduction

This chapter is concerned with the problem of simulating a space engagement between a laser weapon armed satellite (referred to hereafter as the satellite) and some target space object. The simulation will assume non-accelerating flight paths. The laser weapon gimbal system carries a (shared aperture) target imaging system which can see the target and issue tracking commands to the gimbal pointing servo. The simulation which is described here incorporates a high bandwidth servo pointing capability. A major feature of the simulation is the provision of time delays involving speed-of-light time of flight.

We are concerned here with the most straightforward aspects of the engagement — very simple flight kinematics and a high bandwidth pointing/tracking servo are assumed. Our interest is in determining the laser miss distance to be associated with laser bias and with round-trip (speed-of-light) transit time delay effects. The necessary details for simulation of these effects are provided in the engagement simulation discussed here. It has been a major objective in the development of this simulation to build a foundation upon which a much more extensive engagement simulation considering the statistics of the laser backscatter signal could be modeled. This, however, is only a background consideration in what we report here. Backscatter signal modeling and its utilization in an adaptive compensation system will be treated in later chapters.

2.2 Basic Engagement Geometry

We shall utilize a rectangular stationary coordinate frame of reference, with coordinates (x, y, z) to define the flight paths of the satellite and the target. We shall let $\vec{r}_s(t)$ denote the time dependent position vector for the satellite, and let $\vec{r}_t(t)$ denote the target position vectors. Based on our assumption that neither the satellite nor the target is accelerating, we utilize the constant vectors \vec{v}_s and \vec{v}_t to denote the satellite's velocity vector and the target's velocity vector, respectively. If we let $\vec{r}_{s,0}$ and $\vec{r}_{t,0}$ denote the positions of the satellite and of the target, respectively, at some time $t = 0$, then we can write

$$\vec{r}_s(t) = \vec{r}_{s,0} + \vec{v}_s t \quad , \quad (1)$$

$$\vec{r}_t(t) = \vec{r}_{t,0} + \vec{v}_t t \quad . \quad (2)$$

It will be useful in our work to be able to calculate the expected distance of closest approach between the satellite and the target, and the time dependent angular rate at which the target crosses the field-of-view of the satellite. To carry out these calculations, and as a general matter of policy to insure that all appropriate relativistic-type considerations are automatically taken into account in our analysis, we shall switch our attention to an inertial frame of reference fixed in the satellite. In this frame of reference, the satellite's coordinates are always $(0, 0, 0)$ and its velocity is similarly $(0, 0, 0)$, while the target's velocity is

$$\vec{v}_0 = \vec{v}_t - \vec{v}_s \quad , \quad (3)$$

i. e., the difference velocity, and the target's position vector is

$$\vec{r}_0(t) = (\vec{r}_{t,0} - \vec{r}_{s,0}) + \vec{v}_0 t \quad , \quad (4)$$

which is the difference of the position vectors. Hereafter, when we speak of position or velocity, we shall be referring to that of the target with respect to the coordinate system fixed in the satellite.

In developing our results for the distance of closest approach and for the target's apparent angular velocity, it will be convenient to have available unit vectors corresponding to \vec{v}_0 and $\vec{r}_0(t)$. We shall denote these as

$$\hat{v}_0 = \vec{v}_0 / v_0, \quad (5)$$

$$\hat{r}_0(t) = \vec{r}_0(t) / r_0(t), \quad (6)$$

where

$$v_0 = |\vec{v}_0|, \quad (7)$$

$$r_0(t) = |\vec{r}_0(t)|, \quad (8)$$

denote the respective magnitudes.

To calculate the distance of closest approach, it will facilitate our analysis to consider the plane containing the origin and the target velocity vector drawn through the target position. This is illustrated in Fig. 1.

The distance of closest approach, which we denote by the vector \vec{d} , with magnitude

$$d = |\vec{d}|, \quad (9)$$

is defined by the well-known fact that the minimum distance between a point and a line is defined by the perpendicular to the line that passes through the point. If β denotes the angle between the position vector and the velocity vector, as indicated in Fig. 1, then its cosine equals the dot product of the corresponding unit vectors, namely,

$$\cos \beta = \hat{r}_0(t) \cdot \hat{v}_0. \quad (10)$$

The distance of closest approach, as can be seen from Fig. 1, is

$$\begin{aligned} d &= r_0(t) \sin(\beta) \\ &= r_0(t) [1 - \cos^2(\beta)]^{1/2} \end{aligned} \quad (11)$$

Though the right-hand-side of this expression is apparently a function of time, a detailed evaluation of this expression will show that, in fact, it is time-independent, as we would expect from consideration of the nature of d .

The apparent angular velocity of the target, α , can be calculated by considering the component of the target velocity that is perpendicular to the position vector. [We note that the position vector $\vec{r}_0(t)$ is also the line-of-sight vector — hence this relationship.] From consideration of Fig. 1, we can see that the angle between the target velocity vector \vec{v}_0 and a line (in the plane and) perpendicular to the line-of-sight is $\beta - \frac{1}{2}\pi$. From this, it follows that the magnitude of the target velocity vector component perpendicular to the line-of-sight is

$$\begin{aligned} v_{\perp} &= v_0 \cos(\beta - \tfrac{1}{2}\pi) \\ &= v_0 \sin(\beta) \\ &= v_0 [1 - \cos^2(\beta)]^{1/2} \end{aligned} \quad (12)$$

Thus we can write for the angular rate

$$\begin{aligned} \alpha &= v_{\perp} / r_0(t) \\ &= \frac{v_0}{r_0(t)} [1 - \cos^2(\beta)]^{1/2} \end{aligned} \quad (13)$$

With the basic engagement geometry thus defined, we are now ready to turn our attention to the gimbal orientation and tracking error sensing formulation. We take this up in the next section.

2.3 Gimbal Angle and Target Track Error Signal

We assume that the pointing and tracking process is performed by a two-axis "elevation inside of azimuth" type of gimbal system. We shall use θ to denote the "inverse" of the elevation (i.e., the polar angle or ninety-degrees minus the actual elevation angle), and will use ϕ to denote the azimuth angle. We will let the ϕ -coordinate be referenced and oriented so that the x-axis corresponds to $\phi = 0$, and the y-axis to $\phi = \frac{1}{2}\pi$. The target imaging sensor mounted in the gimbals has a focal plane defined by a pair of unit vectors, $\hat{\xi}$ and $\hat{\eta}$, which we take to define a two-dimensional rectangular coordinate system so oriented that when $\theta = \frac{1}{2}\pi$, i.e., the line-of-sight is in the x,y-plane, the ξ -axis is also in the x,y-plane. These two axes, i.e., $\hat{\xi}$ and $\hat{\eta}$, are assumed to be perpendicular to the gimbal/sensor line-of-sight vector.

The gimbal line-of-sight unit vector, which we denote by $\hat{u}_g(t)$ has the three components

$$[\hat{u}_g(t)]_x = \cos(\phi) \sin(\theta) \quad , \quad (14)$$

$$[\hat{u}_g(t)]_y = \sin(\phi) \sin(\theta) \quad , \quad (15)$$

$$[\hat{u}_g(t)]_z = \cos(\theta) \quad . \quad (16)$$

We shall let \hat{z} denote a unit vector in the z-axis direction, i.e., $\hat{z} = (0, 0, 1)$. Then by virtue of the fact that the ξ -axis in the sensor focal plane is perpendicular to the gimbal/sensor unit vector, and because the elevation inside azimuth configuration keeps it always perpendicular to the z-axis (so long as it is perpendicular to the z-axis where $\theta = \frac{1}{2}\pi$), then we can write

$$\hat{\xi} = \frac{\hat{z} \times \hat{u}_g(t)}{|\hat{z} \times \hat{u}_g(t)|} \quad . \quad (17)$$

The normalization introduced by the $|\hat{z} \times \hat{u}_g|$ factor in the denominator is required since \hat{z} and \hat{u}_g are in general not perpendicular. [We note that the vector cross-product in Eq. (17) yields zero when \hat{z} and \hat{u}_g are parallel, so that in this case $\hat{\xi}$ is undefined. However, since this corresponds to a gimbal lock condition, which we should never normally encounter, we need not concern ourselves with an alternate definition for $\hat{\xi}$ in this case.] The unit vector $\hat{\eta}$ is defined by the fact that it is perpendicular to both the gimbal/sensor line-of-sight unit vector, $\hat{u}_g(t)$ and the $\hat{\xi}$ -axis. Thus we can write

$$\hat{\eta} = \hat{u}_g(t) \times \hat{\xi} \quad . \quad (18)$$

In this case, there is no need for a normalization factor since $\hat{u}_g(t)$ and $\hat{\xi}$ are, by definition, perpendicular so that their cross product is necessarily a unit vector.

The target track error as seen by the gimbal-mounted sensor is the difference between the gimbal/sensor unit vector, $\hat{u}_g(t)$, and the unit vector to the target position, $\hat{r}_p(t)$. Thus we can write for the track error vector

$$\vec{e}(t) = \hat{r}_p(t') - \hat{u}_g(t) \quad . \quad (19)$$

Here t' differs from t by the time it takes light to travel from the target to a satellite. This is $r_p(t)/c$, where $c = 3 \times 10^8$ m/sec is the speed of light. Thus

$$t' = t - r_p(t)/c \quad . \quad (20)$$

$\vec{e}(t)$, of course, is not a unit vector. (With reasonable target tracking performance, it is much smaller than a unit vector.) What is reported by the sensor track error demodulator is the two components of $\vec{e}(t)$ along the $\hat{\xi}$ - and $\hat{\eta}$ -axes. These we may write as

$$\epsilon_g = \hat{\xi} \cdot \vec{e}(t) \quad (21)$$

for the azimuth-related error, * and

$$\epsilon_{EL} = - \hat{\eta} \cdot \vec{e}(t) \quad (22)$$

for the elevation error. The minus sign is included here because the sense of θ is reversed from that of $\hat{\eta}$.

* There is an elevation angle related "correction" to ϵ_g , which we treat in discussing the gimbal servo loop, and which makes ϵ_g only related rather than being exactly the azimuth error.

2.4 Gimbal Servo Computation

We contemplate servo control of each gimbal axis based on a second order servo loop with a closed loop bandwidth, f_{BW} , equal to 100 Hz. The servo is critically tuned in the sense that the break in the lead network is set to this same frequency. This means that the servo phase margin is 45° at the $f_{BW} = 100$ Hz, 0 dB open loop gain point. In our simulation, this ignores practical niceties of the servo/gimbal hardware — our reason for doing this being that this portion of the point and tracking problem, i.e., the gimbal response, is only a matter of incidental interest.*

The basic servo block diagram is as shown in Fig. 2. The key to the proper simulation of the servo is in the appropriate selection of the gain, G , and the implementation of the lead network, $1 + \tau s$. It can be shown that to achieve the desired servo bandwidth, the gain constant, G , should have the value

$$\begin{aligned} G &= \frac{(2\pi)^2}{\sqrt{2}} f_{BW}^2 \\ &= 27.915 \times 10^4 \end{aligned} \quad (23)$$

The corresponding lead network characteristics are achieved in our computer simulation using a feed forward configuration with the lead filter constant, C_{LEAD} , set equal to

$$\begin{aligned} C_{LEAD} &= \exp(-2\pi f_{BW} \delta t) \\ &= 0.49751 \end{aligned} \quad (24)$$

* As will be developed in subsequent work, our real interest is in developing a way of analyzing the laser backscattered signal through adaptive techniques to control the laser point bias aspect of the pointing and tracking problem, and thus set the stage for even more advanced aspects of the pointing and tracking control problem — such as how to estimate from the backscattered signal the extent of defocus and astigmatism in the beam, in the presence of a glint-contaminated return.

where $\delta t = 0.001$ sec is the basic time increment in our simulation. The lead network output on the n^{th} time-step is

$$O(n) = [I(n) - C_{LEAD} I(n-1)] / (1 - C_{LEAD}) \quad , \quad (25)$$

where $O(n)$ denotes the output of the n^{th} cycle, while $I(n)$ denotes the input.

To accommodate our planned ability to estimate the laser pointing boresight error and to adjust for this, the actual error signals input into the servo loop include addition of two bias estimates, $\epsilon_{B,\xi}$ and $\epsilon_{B,\eta}$, to the calculated values of ϵ_{ξ} and ϵ_{EL} . It is these bias "corrected" values rather than the expressions given in Eq.'s (21) and (22) that are actually used. Thus we would write

$$\epsilon_{\xi} = \hat{\xi} \cdot \vec{e}(t) + \epsilon_{B,\xi} \quad , \quad (21')$$

$$\epsilon_{EL} = -\hat{\eta} \cdot \vec{e}(t) + \epsilon_{B,\eta} \quad . \quad (22')$$

The implementation of the integrators is simply a matter of multiplying the input by the time increment, δt , and adding it to the previous integrator output. Thus for the integrator we write

$$O(n) = O(n-1) + \delta t I(n) \quad . \quad (26)$$

The error inputs to the servo are just ϵ_{EL} , as defined by Eq. (22') for the elevation error, and

$$\epsilon_{AZ} = \epsilon_{\xi} / \sin(\theta) \quad , \quad (27)$$

for the azimuth error. The factor of $1/\sin(\theta)$ is required because as the gimbal pointing approaches the polar position, i.e., θ goes to zero,

it takes a larger and larger azimuthal rotation to induce a change in the ξ -component of the target position error. The scale factor for this increase in required rotation is exactly $1/\sin(\theta)$.

The only other special considerations in our simulation of the servo loops is the initiation of servo loop operation. This is, of course, a somewhat arbitrary matter — i.e., what shall we assume as our initial conditions? We have chosen to set the values of the second integrator (i.e., the position integrators) in each loop, and thus the gimbal position, to initial values that correspond to an initial zero pointing error. However, we have set all other memory elements, namely, the first integrator (or velocity integrator) and the feed forward memory in the lead network, to zero values. We believe that this arbitrary set of initial conditions is reasonable and in no way biases our results.

With this definition of the details of the servo operation, we are now ready to consider the question of the laser miss distance, or where the laser is incident on the target. We present the pertinent formulas for this in the next section.

2.5 Laser Miss Distance

To accommodate a laser boresight error in our simulation, we assume that there are two boresight error bias components, $\Delta_{\theta, \theta}$ and $\Delta_{\theta, \phi}$, respectively, and accordingly associate a unit vector $\hat{l}(t)$ with the laser pointing direction, where the three components of this unit vector are

$$[\hat{l}(t)]_x = \cos(\phi + \Delta_{\theta, \phi}) \sin(\theta + \Delta_{\theta, \theta}) \quad , \quad (28)$$

$$[\hat{l}(t)]_y = \sin(\phi + \Delta_{\theta, \phi}) \sin(\theta + \Delta_{\theta, \theta}) \quad , \quad (29)$$

$$[\hat{l}(t)]_z = \cos(\theta + \Delta_{\theta, \theta}) \quad . \quad (30)$$

To obtain an expression for the vector that measures the displacement of the laser at the point where it is closest to the target, we project the radius vector from the satellite to the target, $\vec{r}_p(t)$, onto the laser direction, as defined by $\hat{l}(y)$, using the factor $\hat{r}_p(t) \cdot \hat{l}(t)$, and subtract that vector from the radius vector to the target, $\vec{r}_p(t)$. Thus the result is of the form $\vec{r}_p(t) - [\hat{r}_p(t) \cdot \hat{l}(t)] \hat{l}(t)$. However, as just written the formulation makes no allowance for the speed of light transit time delay. The laser miss distance as seen by the satellite at time t is based on the target position at time t' , and the laser beam direction at time t'' , where as before

$$t' = t - r_p(t)/c \quad , \quad (20)$$

and

$$t'' = t - 2 r_p(t)/c \quad . \quad (31)$$

Thus we would write for the laser miss distance vector

$$\vec{\Delta}_l(t) = \vec{r}_p(t') - [\hat{r}_p(t') \cdot \hat{l}(t'')] \hat{l}(t'') \quad . \quad (32)$$

With this expression in hand, we are now ready to take up the details of the computer simulation and presentation of simulation results. We take this up in the next section.

2.6 Computer Simulation

The computer simulation program is listed in the appendix, with sample results listed in Tables 1, 2, 3, and 4. The computer simulation is based on a $\delta t = 0.001$ sec time increment, as indicated in Section 4. To accommodate the need for time delayed information, as in Eq.'s (19) and (32), a set of push-down memory stacks were implemented in the program to store values of $\vec{r}_p(t)$ and $\hat{l}(t)$ as they are generated. The push-down stack is indexed, i.e., new values are put in at the top and the oldest value pushed out at the bottom, each time cycle, δt . When delayed data is required, old values are taken from the stack at the appropriate depth, and linear interpolation is used to get the value exactly appropriate to the transit time delay. The stack depth has arbitrarily been set at 10, limiting the maximum time delay to 0.01 sec, and the maximum tractable target range to 1.5 Mm. The implementation of the push-down stack and of the retrieval of delayed data is through a pair of subroutines.

Because most of the formulation in the preceding sections was most conveniently left written in vector notation, it was decided to implement the simulation program with vector operations. Accordingly a set of vector operation subroutines was prepared and called as necessary in the main program. These subroutines, together with the time delay subroutines, are included in the appendix.

To check out the validity of the engagement simulation and thus set the stage for our further more detailed work, we have run a set of four engagements covering a three second period with printouts every 50 msec. In each case, the target range is about 1.0 Mm. The results listed in Table 1 concern a high angular rate tracking problem with zero laser boresight error and zero estimated boresight error. As can be seen, the tracking is stable, but with a laser miss distance of about 33.0 m.

It is easy to see that this miss distance almost exactly corresponds to the range, $r_0 \approx 1.0 \times 10^8$ m, times the standard $2(v/c) = 2(4.95 \times 10^8 / 3.0 \times 10^8) = 3.30 \times 10^{-6}$ rad point ahead angle.

In Table 2, we list results for another engagement with no laser boresight error and no estimated boresight error, but with a much smaller crossing velocity. The point ahead angle in this case is $2(v/c) = 2(5.39 \times 10^8 / 3.0 \times 10^8) = 3.59 \times 10^{-6}$ rad, and the listed miss distance of about 2.71 m is in reasonable agreement with this. (The slight discrepancy can be attributed to an additional time delay of the order of one-half of a time increment, i.e. $\frac{1}{2} \delta t = 0.0005$ sec).

In Table 3, we list results corresponding to the same case as for Table 2, except that laser boresight error angles of $(6.0 \mu\text{rad}, 8.0 \mu\text{rad})$ are also included. The reported laser miss distance of about 8.6 m is in good agreement with this, considering that the $6.0 \mu\text{rad}$ produces a 6.0 m displacement oppositely oriented to the 2.71 m point ahead induced miss distance. Quantitatively, we see this by noting that $[(6.0 - 2.71)^2 + (8.0)^2]^{1/2} = 8.65$ m.

Table 4 lists results for the same case as Table 3, but with the inclusion of non-zero estimated boresight errors of $(6.0 \mu\text{rad}, 8.0 \mu\text{rad})$. This estimate reduces the laser miss distance to very nearly the values in Table 2. The inability to exactly reduce it to that value is indicative of the fact that slightly different nonlinearities are involved in generation of the boresight error effects and of the effects of the estimated boresight error compensation.

Based on a consideration of the results in these four tables, we conclude that the basic engagement scenario simulation is working effectively. Accordingly, we consider that we are nearly ready to proceed to the next phase of the engagement simulation — namely, the generation of the random laser backscatter signals, with appropriate statistics. This will be treated in a subsequent chapter. In the next chapter, however, consider how boresight error information would be used, if available.

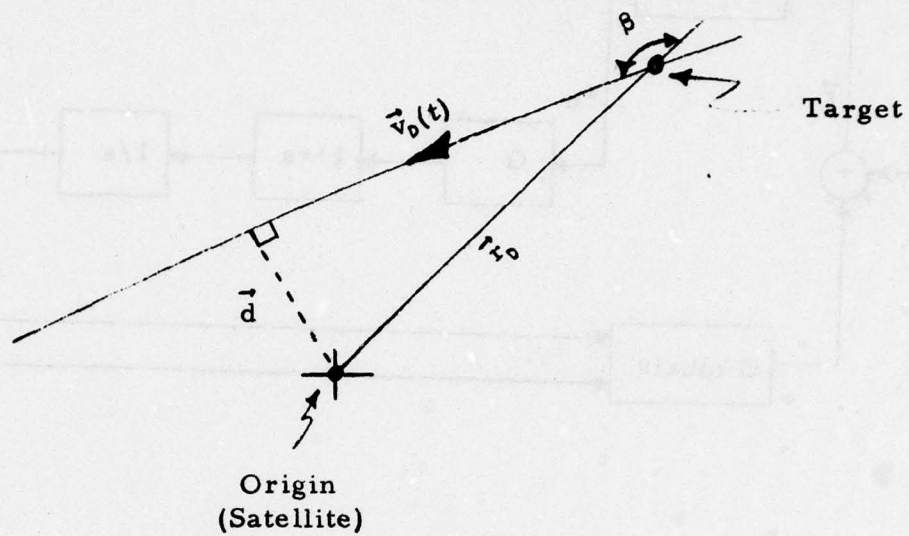


Figure 2.1 Basic Engagement Geometry.

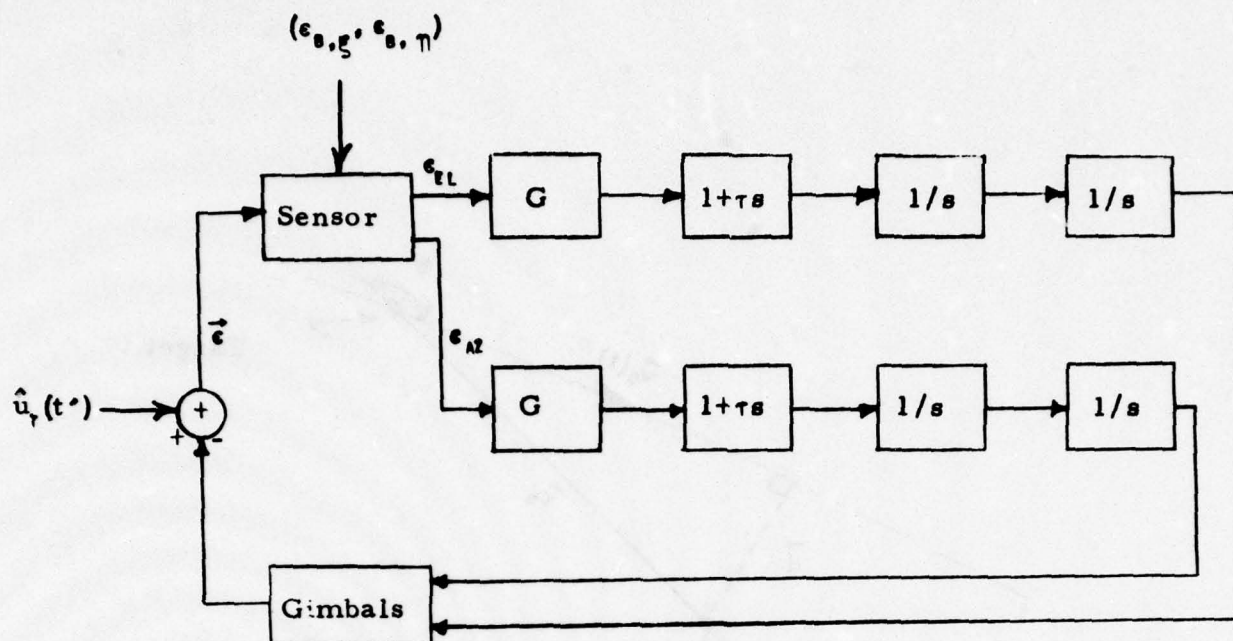


Figure 2.2 Servo Block Diagram.

Table 2.1

High Crossing Velocity Engagement

$$\vec{r}_0(0) = (6.0 \times 10^5, 6.0 \times 10^5, 5.29 \times 10^5) \text{ m}$$

$$\vec{v}_0 = (-3.5 \times 10^3, 3.5 \times 10^3, 0.0) \text{ m/sec}$$

$$\Delta_{\theta, \phi} = 0.0 \qquad \Delta_{\theta, \theta} = 0.0$$

$$\epsilon_{\theta, \xi} = 0.0 \qquad \epsilon_{\theta, \eta} = 0.0$$

TIME (SEC.)	RANGE (METERS)	MISS DISTANCE (METERS)	THETA (RAD.)	PHI (RAD.)
0.050	1.0002E+06	3.2923E+01	1.012911	0.785682
0.100	1.0003E+06	3.2941E+01	1.012660	0.785974
0.150	1.0005E+06	3.2926E+01	1.012409	0.786266
0.200	1.0006E+06	3.2921E+01	1.012159	0.786558
0.250	1.0008E+06	3.2927E+01	1.011908	0.786850
0.300	1.0010E+06	3.2942E+01	1.011658	0.787142
0.350	1.0011E+06	3.2941E+01	1.011408	0.787434
0.400	1.0013E+06	3.2945E+01	1.011157	0.787726
0.450	1.0014E+06	3.2944E+01	1.010907	0.788018
0.500	1.0016E+06	3.2925E+01	1.010657	0.788310
0.550	1.0017E+06	3.2947E+01	1.010408	0.788602
0.600	1.0019E+06	3.2955E+01	1.010158	0.788894
0.650	1.0021E+06	3.2943E+01	1.009908	0.789186
0.700	1.0022E+06	3.2955E+01	1.009659	0.789478
0.750	1.0024E+06	3.2962E+01	1.009409	0.789770
0.800	1.0025E+06	3.2964E+01	1.009160	0.790062
0.850	1.0027E+06	3.2946E+01	1.008911	0.790354
0.900	1.0029E+06	3.2955E+01	1.008662	0.790646
0.950	1.0030E+06	3.2965E+01	1.008413	0.790938
1.000	1.0032E+06	3.2966E+01	1.008164	0.791230
1.050	1.0033E+06	3.2967E+01	1.007916	0.791522
1.100	1.0035E+06	3.2967E+01	1.007667	0.791814
1.150	1.0036E+06	3.2977E+01	1.007419	0.792106
1.200	1.0038E+06	3.2973E+01	1.007171	0.792398
1.250	1.0040E+06	3.2995E+01	1.006923	0.792690
1.300	1.0041E+06	3.2991E+01	1.006674	0.792982
1.350	1.0043E+06	3.2974E+01	1.006426	0.793274
1.400	1.0044E+06	3.2983E+01	1.006178	0.793566
1.450	1.0046E+06	3.2987E+01	1.005931	0.793858
1.500	1.0048E+06	3.2990E+01	1.005683	0.794150
1.550	1.0049E+06	3.2990E+01	1.005436	0.794442
1.600	1.0051E+06	3.2990E+01	1.005188	0.794734
1.650	1.0053E+06	3.2991E+01	1.004941	0.795026
1.700	1.0054E+06	3.2991E+01	1.004694	0.795318
1.750	1.0056E+06	3.2999E+01	1.004447	0.795610
1.800	1.0057E+06	3.2991E+01	1.004200	0.795902
1.850	1.0059E+06	3.2997E+01	1.003953	0.796194
1.900	1.0060E+06	3.2999E+01	1.003707	0.796486
1.950	1.0062E+06	3.2991E+01	1.003460	0.796778
2.000	1.0064E+06	3.2986E+01	1.003214	0.797070
2.050	1.0066E+06	3.2997E+01	1.002967	0.797362
2.100	1.0067E+06	3.2995E+01	1.002721	0.797654
2.150	1.0069E+06	3.2995E+01	1.002475	0.797946
2.200	1.0070E+06	3.2997E+01	1.002229	0.798238
2.250	1.0072E+06	3.2995E+01	1.001983	0.798530
2.300	1.0073E+06	3.2995E+01	1.001737	0.798822
2.350	1.0075E+06	3.2995E+01	1.001491	0.799114
2.400	1.0077E+06	3.2995E+01	1.001247	0.799406
2.450	1.0078E+06	3.2994E+01	1.001001	0.799698

2.500	1.00903E+00	3.30788E+01	1.000756	0.799989
2.550	1.00917E+00	3.30775E+01	1.000711	0.800029
2.600	1.00931E+00	3.30744E+01	1.000666	0.800057
2.650	1.00953E+00	3.30744E+01	1.000621	0.800166
2.700	1.00966E+00	3.30711E+01	0.999776	0.801137
2.750	1.00988E+00	3.30545E+01	0.999532	0.801449
2.800	1.00908E+00	3.30439E+01	0.999237	0.801741
2.850	1.00918E+00	3.30505E+01	0.999043	0.802033
2.900	1.00930E+00	3.30480E+01	0.998798	0.802324
2.950	1.00953E+00	3.30655E+01	0.998554	0.802615
3.000	1.00966E+00	3.30665E+01	0.998310	0.802906
3.050	1.00998E+00	3.30545E+01	0.998066	0.803200

Table 2.2

Low Crossing Velocity Engagement

$$\vec{r}_D(0) = (6.0 \times 10^5, 6.0 \times 10^5, 5.29 \times 10^5) \text{ m}$$

$$\vec{v}_D = (-200.0, 500.0, 490.0) \text{ m/sec}$$

$$\Delta_{B,\phi} = 0.0$$

$$\Delta_{B,\theta} = 0.0$$

$$\epsilon_{B,\xi} = 0.0$$

$$\epsilon_{B,\eta} = 0.0$$

TIME (SEC.)	RANGE (METERS)	MISS DISTANCE (METERS)	THETA (RAD.)	PHI (RAD.)
0.050	1.0000E+06	2.7170E+00	1.013141	0.785427
0.100	1.0001E+06	2.7070E+00	1.013126	0.785456
0.150	1.0001E+06	2.7105E+00	1.013111	0.785485
0.200	1.0001E+06	2.7139E+00	1.013096	0.785515
0.250	1.0001E+06	2.7105E+00	1.013081	0.785544
0.300	1.0002E+06	2.7105E+00	1.013066	0.785573
0.350	1.0002E+06	2.7132E+00	1.013051	0.785602
0.400	1.0002E+06	2.7070E+00	1.013036	0.785632
0.450	1.0002E+06	2.7172E+00	1.013021	0.785661
0.500	1.0002E+06	2.7236E+00	1.013006	0.785690
0.550	1.0003E+06	2.7201E+00	1.012991	0.785720
0.600	1.0003E+06	2.7172E+00	1.012976	0.785749
0.650	1.0003E+06	2.7041E+00	1.012961	0.785778
0.700	1.0003E+06	2.7132E+00	1.012946	0.785807
0.750	1.0004E+06	2.7132E+00	1.012931	0.785837
0.800	1.0004E+06	2.7199E+00	1.012916	0.785866
0.850	1.0004E+06	2.7234E+00	1.012901	0.785895
0.900	1.0004E+06	2.7105E+00	1.012886	0.785925
0.950	1.0004E+06	2.7098E+00	1.012871	0.785954
1.000	1.0005E+06	2.7003E+00	1.012856	0.785983
1.050	1.0005E+06	2.7068E+00	1.012841	0.786012
1.100	1.0005E+06	2.7139E+00	1.012826	0.786042
1.150	1.0005E+06	2.7209E+00	1.012811	0.786071
1.200	1.0005E+06	2.7236E+00	1.012796	0.786100
1.250	1.0006E+06	2.7134E+00	1.012781	0.786130
1.300	1.0006E+06	2.7201E+00	1.012766	0.786159
1.350	1.0006E+06	2.7134E+00	1.012751	0.786188
1.400	1.0006E+06	2.7201E+00	1.012736	0.786217
1.450	1.0007E+06	2.7266E+00	1.012721	0.786247
1.500	1.0007E+06	2.7132E+00	1.012706	0.786276
1.550	1.0007E+06	2.7201E+00	1.012691	0.786305
1.600	1.0007E+06	2.7103E+00	1.012676	0.786335
1.650	1.0007E+06	2.7065E+00	1.012661	0.786364
1.700	1.0008E+06	2.7266E+00	1.012646	0.786393
1.750	1.0008E+06	2.7107E+00	1.012632	0.786422
1.800	1.0008E+06	2.7098E+00	1.012617	0.786452
1.850	1.0008E+06	2.7139E+00	1.012602	0.786481
1.900	1.0009E+06	2.7201E+00	1.012587	0.786510
1.950	1.0009E+06	2.7077E+00	1.012572	0.786539
2.000	1.0009E+06	2.7043E+00	1.012557	0.786569
2.050	1.0009E+06	2.7167E+00	1.012542	0.786598
2.100	1.0009E+06	2.7199E+00	1.012527	0.786627
2.150	1.0010E+06	2.7201E+00	1.012512	0.786656
2.200	1.0010E+06	2.7134E+00	1.012497	0.786686
2.250	1.0010E+06	2.7070E+00	1.012482	0.786715
2.300	1.0010E+06	2.7070E+00	1.012467	0.786744
2.350	1.0010E+06	2.7167E+00	1.012452	0.786774
2.400	1.0011E+06	2.7171E+00	1.012437	0.786803
2.450	1.0011E+06	2.7266E+00	1.012422	0.786832

2.500	1.0011E+06	2.7105E+00	1.012407	0.786861
2.550	1.0011E+06	2.7105E+00	1.012392	0.786891
2.600	1.0012E+06	2.7107E+00	1.012377	0.786920
2.650	1.0012E+06	2.7132E+00	1.012362	0.786949
2.700	1.0012E+06	2.7037E+00	1.012347	0.786978
2.750	1.0012E+06	2.7172E+00	1.012333	0.787008
2.800	1.0012E+06	2.7075E+00	1.012319	0.787037
2.850	1.0013E+06	2.7070E+00	1.012303	0.787066
2.900	1.0013E+06	2.7099E+00	1.012289	0.787096
2.950	1.0013E+06	2.7110E+00	1.012273	0.787125
3.000	1.0013E+06	2.7099E+00	1.012258	0.787154
3.050	1.0014E+06	2.7099E+00	1.012243	0.787183

Table 2.3

Low Crossing Velocity Engagement

With Laser Boresight Error

$$\vec{r}_0(0) = (6.0 \times 10^5, 6.0 \times 10^5, 5.29 \times 10^5) \text{ m}$$

$$\vec{v}_0 = (-200.0, 500.0, 490.0) \text{ m/sec}$$

$$\Delta_{B,\phi} = 8.0 \mu\text{rad} \quad \Delta_{B,\theta} = 6.0 \mu\text{rad}$$

$$\epsilon_{B,\xi} = 0.0 \quad \epsilon_{B,\eta} = 0.0$$

TIME (SEC.)	RANGE (METERS)	MISS DISTANCE (METERS)	THETA (RAD.)	PHI (RAD.)
0.050	1.0000E+06	8.6205E+00	1.013141	0.785427
0.100	1.0001E+06	8.6319E+00	1.013126	0.785456
0.150	1.0001E+06	8.6311E+00	1.013111	0.785485
0.200	1.0001E+06	8.6372E+00	1.013096	0.785515
0.250	1.0001E+06	8.6429E+00	1.013081	0.785544
0.300	1.0002E+06	8.6369E+00	1.013066	0.785573
0.350	1.0002E+06	8.6433E+00	1.013051	0.785602
0.400	1.0002E+06	8.6312E+00	1.013036	0.785632
0.450	1.0002E+06	8.6376E+00	1.013021	0.785661
0.500	1.0002E+06	8.6425E+00	1.013006	0.785690
0.550	1.0002E+06	8.6486E+00	1.012991	0.785720
0.600	1.0002E+06	8.6429E+00	1.012976	0.785749
0.650	1.0002E+06	8.6262E+00	1.012961	0.785778
0.700	1.0002E+06	8.6319E+00	1.012946	0.785807
0.750	1.0004E+06	8.6311E+00	1.012931	0.785837
0.800	1.0004E+06	8.6311E+00	1.012916	0.785866
0.850	1.0004E+06	8.6365E+00	1.012901	0.785895
0.900	1.0004E+06	8.6322E+00	1.012886	0.785925
0.950	1.0004E+06	8.6319E+00	1.012871	0.785954
1.000	1.0005E+06	8.6319E+00	1.012856	0.785983
1.050	1.0005E+06	8.6262E+00	1.012841	0.786012
1.100	1.0005E+06	8.6429E+00	1.012826	0.786042
1.150	1.0005E+06	8.6525E+00	1.012811	0.786071
1.200	1.0005E+06	8.6376E+00	1.012796	0.786100
1.250	1.0006E+06	8.6436E+00	1.012781	0.786120
1.300	1.0006E+06	8.6529E+00	1.012766	0.786159
1.350	1.0006E+06	8.6422E+00	1.012751	0.786188
1.400	1.0006E+06	8.6482E+00	1.012736	0.786217
1.450	1.0007E+06	8.6479E+00	1.012721	0.786247
1.500	1.0007E+06	8.6322E+00	1.012706	0.786276
1.550	1.0007E+06	8.6482E+00	1.012691	0.786305
1.600	1.0007E+06	8.6322E+00	1.012676	0.786335
1.650	1.0007E+06	8.6319E+00	1.012661	0.786364
1.700	1.0008E+06	8.6482E+00	1.012646	0.786393
1.750	1.0008E+06	8.6418E+00	1.012632	0.786422
1.800	1.0008E+06	8.6429E+00	1.012617	0.786452
1.850	1.0008E+06	8.6433E+00	1.012602	0.786481
1.900	1.0009E+06	8.6522E+00	1.012587	0.786510
1.950	1.0009E+06	8.6418E+00	1.012572	0.786539
2.000	1.0009E+06	8.6376E+00	1.012557	0.786569
2.050	1.0009E+06	8.6322E+00	1.012542	0.786598
2.100	1.0009E+06	8.6429E+00	1.012527	0.786627
2.150	1.0010E+06	8.6429E+00	1.012512	0.786656
2.200	1.0010E+06	8.6429E+00	1.012497	0.786686
2.250	1.0010E+06	8.6255E+00	1.012482	0.786715
2.300	1.0010E+06	8.6266E+00	1.012467	0.786744
2.350	1.0010E+06	8.6422E+00	1.012452	0.786774
2.400	1.0011E+06	8.6489E+00	1.012437	0.786803
2.450	1.0011E+06	8.6539E+00	1.012422	0.786832

2.500	1.0011E+06	8.6429E+00	1.012407	0.786361
2.550	1.0011E+06	8.6436E+00	1.012392	0.786391
2.600	1.0012E+06	8.6442E+00	1.012377	0.786420
2.650	1.0012E+06	8.6472E+00	1.012362	0.786449
2.700	1.0012E+06	8.6425E+00	1.012347	0.786478
2.750	1.0012E+06	8.6486E+00	1.012333	0.786508
2.800	1.0012E+06	8.6372E+00	1.012318	0.786537
2.850	1.0013E+06	8.6319E+00	1.012303	0.786566
2.900	1.0013E+06	8.6319E+00	1.012288	0.786595
2.950	1.0013E+06	8.6425E+00	1.012273	0.786625
3.000	1.0013E+06	8.6372E+00	1.012258	0.786654
3.050	1.0014E+06	8.6543E+00	1.012243	0.786683

Table 2.4

Low Crossing Velocity Engagement

With Laser Boresight Error

And Boresight Error Estimates

$$\vec{r}_0(0) = (6.0 \times 10^5, 6.0 \times 10^5, 5.29 \times 10^5) \text{ m}$$

$$\vec{v}_0 = (-200.0, 500.0, 490.0) \text{ m/sec}$$

$$\Delta_{B,\phi} = 8.0 \text{ } \mu\text{rad}$$

$$\Delta_{B,\theta} = 6.0 \text{ } \mu\text{rad}$$

$$\epsilon_{B,\xi} = 8.0 \text{ } \mu\text{rad}$$

$$\epsilon_{B,\eta} = -6.0 \text{ } \mu\text{rad}$$

TIME (SEC.)	RANGE (METERS)	MISS DISTANCE (METERS)	THETA (RAD.)	PHI (RAD.)
0.050	1.0000E+06	3.8133E+00	1.013135	0.785417
0.100	1.0001E+06	3.7976E+00	1.013120	0.785447
0.150	1.0001E+06	3.7981E+00	1.013105	0.785476
0.200	1.0001E+06	3.7965E+00	1.013090	0.785505
0.250	1.0001E+06	3.8092E+00	1.013075	0.785534
0.300	1.0002E+06	3.7967E+00	1.013060	0.785564
0.350	1.0002E+06	3.7961E+00	1.013045	0.785593
0.400	1.0002E+06	3.8109E+00	1.013030	0.785622
0.450	1.0002E+06	3.8022E+00	1.013015	0.785652
0.500	1.0002E+06	3.8064E+00	1.013000	0.785681
0.550	1.0003E+06	3.7858E+00	1.012985	0.785710
0.600	1.0003E+06	3.8117E+00	1.012970	0.785739
0.650	1.0003E+06	3.8088E+00	1.012955	0.785769
0.700	1.0003E+06	3.8068E+00	1.012940	0.785798
0.750	1.0004E+06	3.8019E+00	1.012925	0.785827
0.800	1.0004E+06	3.8072E+00	1.012910	0.785857
0.850	1.0004E+06	3.8109E+00	1.012895	0.785886
0.900	1.0004E+06	3.8035E+00	1.012880	0.785915
0.950	1.0004E+06	3.8084E+00	1.012865	0.785944
1.000	1.0005E+06	3.8047E+00	1.012850	0.785974
1.050	1.0005E+06	3.8105E+00	1.012835	0.786003
1.100	1.0005E+06	3.8031E+00	1.012820	0.786032
1.150	1.0005E+06	3.8006E+00	1.012805	0.786062
1.200	1.0005E+06	3.8043E+00	1.012790	0.786091
1.250	1.0006E+06	3.7944E+00	1.012775	0.786120
1.300	1.0006E+06	3.8026E+00	1.012760	0.786149
1.350	1.0006E+06	3.8022E+00	1.012745	0.786179
1.400	1.0006E+06	3.8068E+00	1.012730	0.786208
1.450	1.0007E+06	3.8006E+00	1.012715	0.786237
1.500	1.0007E+06	3.7985E+00	1.012700	0.786267
1.550	1.0007E+06	3.8064E+00	1.012685	0.786296
1.600	1.0007E+06	3.7985E+00	1.012670	0.786325
1.650	1.0007E+06	3.8047E+00	1.012655	0.786354
1.700	1.0008E+06	3.8047E+00	1.012640	0.786384
1.750	1.0008E+06	3.7985E+00	1.012626	0.786413
1.800	1.0008E+06	3.8022E+00	1.012611	0.786442
1.850	1.0008E+06	3.8158E+00	1.012596	0.786471
1.900	1.0009E+06	3.8068E+00	1.012581	0.786501
1.950	1.0009E+06	3.8043E+00	1.012566	0.786530
2.000	1.0009E+06	3.8060E+00	1.012551	0.786559
2.050	1.0009E+06	3.8006E+00	1.012536	0.786589
2.100	1.0009E+06	3.8092E+00	1.012521	0.786618
2.150	1.0010E+06	3.7916E+00	1.012506	0.786647
2.200	1.0010E+06	3.8133E+00	1.012491	0.786676
2.250	1.0010E+06	3.8047E+00	1.012476	0.786706
2.300	1.0010E+06	3.8047E+00	1.012461	0.786735
2.350	1.0010E+06	3.8006E+00	1.012446	0.786764
2.400	1.0011E+06	3.8092E+00	1.012431	0.786793
2.450	1.0011E+06	3.8133E+00	1.012416	0.786823

2.500	1.0011E+06	3.7474E+00	1.012401	0.786852
2.550	1.0011E+06	3.9092E+00	1.012466	0.786881
2.600	1.0012E+06	3.9123E+00	1.012471	0.786910
2.650	1.0012E+06	3.9048E+00	1.012356	0.786940
2.700	1.0012E+06	3.9018E+00	1.012341	0.786969
2.750	1.0012E+06	3.9022E+00	1.012427	0.786998
2.800	1.0012E+06	3.9043E+00	1.012312	0.787027
2.850	1.0012E+06	3.9103E+00	1.012297	0.787057
2.900	1.0012E+06	3.9174E+00	1.012282	0.787086
2.950	1.0013E+06	3.9060E+00	1.012267	0.787115
3.000	1.0013E+06	3.8984E+00	1.012252	0.787144
3.050	1.0014E+06	3.9150E+00	1.012237	0.787174

Appendix to Chapter 2

Computer Main Program

and

Subroutine Listings

Main Program

```

DIMENSION RSZ(3), VS(3), RTZ(3), VT(3),%
DR(3), DV(3), LDV(3), D(3), DVSF(3), UT(3), UG(3), ERR(3),%
Z(3), XI(3), ETA(3), DB(3), UL(3), RTS(3), DLM(3), UDF(3),%
RTCLC(3), RSCLC(3), ULOLD(3), ER(2), GC(3)
NAMelist /INPUT/ RSZ, VS, RTZ, VT, DB, GC, ER

```

```

NPRINT = 50
PI = 3.141592654
Z(1) = 0.
Z(2) = 0.
Z(3) = 1.
T = 0.
DT = 1.E-3
N = 0.

```

```

C*****
C*
C* SPECIFY ENGAGEMENT PARAMETERS.
C*
C*****

```

```

RSZ(1) = 0.
RSZ(2) = 0.
RSZ(3) = 0.
VS(1) = 4.9E3
VS(2) = 7.1E2
VS(3) = 7.1E2
RTZ(1) = 6.E5
RTZ(2) = 6.E5
RTZ(3) = 5.291E5
VT(1) = 4.7E3
VT(2) = 1.21E3
VT(3) = 1.2E3
DB(1)=6.E-6
DB(2)=3.E-6
ER(1)=-6.E-6
ER(2)=-8.E-6
GC(1)=1.
GC(2)=1.
GC(3)=0.

```

```

C*****
C*
C* CONVERT TO DIFFERENCE COORDINATES.
C*
C*****

```



```

C*****
C*
C*      CALCULATE DISTANCE AT CLOSEST APPROACH.
C*
C*****

```

```
C*****
C*
C*      INITIALIZE SERVO/GIMBAL AND SET SERVO PARAMETERS.
C*
C*****
```

- 47 -

```

C*****
C*
C*      INCREMENT CLOCK.
C*
C*****

```

```

100 N = N + 1
    T = T + DT

```

```

C*****
C*
C*      INCREMENT TARGET POSITION AND STORE.
C*      OBTAIN DELAYED TARGET POSITION.
C*
C*****

```

```

CALL WSLM (1., DT, DR, DV, DR)
CALL STACIN (1, DR)
CALL LVECT(DP, LDR, DRM, IF)
TTF = DRM/(3.53*DT)
IF (N.LT.TTF) GO TO 100
CALL STACCT (1, TTF, RTOLD)

```

```

C*****
C*
C*      COMPUTE TARGET TRACKING ERROR AS SEEN BY
C*      SENSOR ON THE GIMBALS (USING THE DELAYED
C*      TARGET POSITION).
C*
C*****

```

```

CALL LVECT (RTOLD, UT, R, IF)
CALL SUM (UT,UG, EFF, -1)
CALL CROSS (7, UG, XI)
CALL LVECT (XI, XI, XIM, IF)
CALL CROSS (UC, XI, ETA)
CALL DOT (ERR, ETA, ERREL)
ERRRL=ERRRL+ERR(1)
CALL DOT (ERR, XI, ERRAZ)
ERRAZ=ERRAZ+ERR(2)

```

```

C*****
C*
C*      IMPLEMENT GIMBAL SERVO POINTING UPDATE.
C*
C*****

```

```

ERRAZ = ERRAZ/SIN (THETA)
DITH = (ERRRL - CLPAD * OTHER)/(1. - CLPAD)
DIPR = (ERRAZ - CLPAD * OTHER)/(1. - CLPAD)

```

```

OTHER = ESREL
OFHER = ESRAZ
Q2TH = Q1TH * GAIN
Q2PH = Q1PH * GAIN
THINT1 = THINT1 + DT*Q2TH
PHINT1 = PHINT1 + DT * Q2PH
THINT2 = THINT2 + DT * THINT1
PHINT2 = PHINT2 + DT * PHINT1
THETA = THINT2
PHI = PHINT2
CALL SPHREC (THETA, PHI, 1., US)

```

```

C*****
C*
C*   INTRODUCE LASER SIGHT ERROR.
C*
C*****

```

```

T1= THETA+DE(1)
P1=PHI+DB(2)
CALL SPHREC(T1,P1,1.,UL)

```

```

C*****
C*
C*   CALCULATE LASER TARGET MISS DISTANCE.
C*
C*****

```

```

CALL STACIN (2,UL)
TTF2=2*TTF
CALL STACCT (2, TTF2, ULOLD)
CALL DOT (DT, ULOLD, DTL)
SF = -DTL*R
CALL WSUM (1., SF, STOLD, ULOLD, DLM)
CALL LVECT (DLM, DLM, DLM, IE)
IF ((N/NPRINT)*NPRINT.NE.N) GO TO 100
PRINT 200, T, R, DLM, THETA, PHI
200 FORMAT ( F10.3,5X,1P F10.4,5X,F10.4,5X, 5P F10.6,5X, F10.6)
IF (N.LE.3000) GO TO 100

END

```


SPHREC.FORTRAN

```

C*****
C*
C*   THIS SUBROUTINE DEFINES THE RELATIONSHIP BETWEEN
C*   THE SPHERICAL COORDINATES OF A VECTOR AND ITS
C*   RECTANGULAR COORDINATES.
C*
C*****

```

```

SUBROUTINE SPHREC (THETA, PHI, R, V)
DIMENSION V(3)
V(1) = SIN(THETA)*COS(PHI)*R
V(2) = SIN(THETA)*SIN(PHI)*R
V(3) = COS(THETA)*R

```

```

RETURN
END

```

DCT.FORTRAN

```
C*****
C*
C*   THIS SUBROUTINE TAKES THE DOT PRODUCT OF
C*   TWO VECTORS.
C*****
```

```
      SUBROUTINE DCT (V1, V2, A)
      DIMENSION V1(3), V2(3)
      A = V1(1)*V2(1) + V1(2)*V2(2) + V1(3)*V2(3)
      RETURN
      END
```

CROSS.FORTRAN

```
C*****  
C*  
C*      THIS SUBROUTINE TAKES THE CROSS PRODUCT OF  
C*      TWO VECTORS.  
C*  
C*****
```

```
SUBROUTINE CROSS (V1, V2, V3)  
  DIMENSION V1(3), V2(3), V3(3)  
  V3(1) = V1(2)*V2(3) - V1(3)*V2(2)  
  V3(2) = V1(3)*V2(1) - V1(1)*V2(3)  
  V3(3) = V1(1)*V2(2) - V1(2)*V2(1)
```

```
  RETURN  
  END
```


EQUIV.FORTRAN

```
C*****  
C*  
C*   THIS SUBROUTINE DEFINES EQUIVALENCE BETWEEN  
C*   TWO VECTORS.  
C*  
C*****
```

```
      SUBROUTINE EQUIV (V1, V2)  
      DIMENSION V1(3), V2(3)  
      V2(1) = V1(1)  
      V2(2) = V1(2)  
      V2(3) = V1(3)
```

```
      RETURN  
      END
```

WSUP.FORTRAN

```
C*****  
C*  
C*      THIS SUBROUTINE CALCULATES THE WEIGHTED SUM  
C*      OF TWO VECTORS.  
C*  
C*****
```

```
SUBROUTINE WSUP (A1, A2, V1, V2, V3)  
  DIMENSION V1(3), V2(3), V3(3)  
  V3(1) = A1*V1(1) + A2*V2(1)  
  V3(2) = A1*V1(2) + A2*V2(2)  
  V3(3) = A1*V1(3) + A2*V2(3)
```

```
  RETURN  
  END
```

SLM.FORTRAN

```
C*****
C*
C*   THIS SUBROUTINE TAKES THE SUM OR DIFFERENCE OF
C*   TWO VECTORS.
C*
C*****
```

```
      SUBROUTINE SUM(V1, V2, V3, I)
      DIMENSION V1(3), V2(3), V3(3)
      IF (I.EQ.1) GO TO 10
      V3(1) = V1(1) - V2(1)
      V3(2) = V1(2) - V2(2)
      V3(3) = V1(3) - V2(3)
      RETURN
```

```
10    V3(1) = V1(1) + V2(1)
      V3(2) = V1(2) + V2(2)
      V3(3) = V1(3) + V2(3)
      RETURN
      END
```


SCMULT.FORTRAN

```
C*****  
C*  
C*   THIS SUBROUTINE MULTIPLIES A VECTOR BY A SCALAR.  
C*  
C*****
```

```
      SUBROUTINE SCMLLT (A, V1, V2)  
      DIMENSION V1(3), V2(3)  
      V2(1) = A*V1(1)  
      V2(2) = A*V1(2)  
      V2(3) = A*V1(3)
```

```
      RETURN  
      END
```

UVECT.FORTRAN

```

C*****
C*
C*   THIS SUBROUTINE CALCULATES A UNIT VECTOR FROM ITS
C*   ARGUMENT AND RETAINS THE MAGNITUDE.
C*
C*****

```

```

SUBROUTINE UVECT (V1, V2, P, I)
DIMENSION V1(3), V2(3)
CALL DCT (V1, V1, P)
IF (P.LE.0) GO TO 10
F = C.
F = SQRT (F)
V2(1) = V1(1)/F
V2(2) = V1(2)/F
V2(3) = V1(3)/F

```

```

10  RETURN
    I = 1
    V2(1) = 0.
    V2(2) = 0.
    V2(3) = 0.

```

```

RETURN
END

```

STACOT.FORTRAN

```
C*****  
C*  
C*   THIS SUBROUTINE PROVIDES A PAST VALUE.  
C*  
C*****
```

```
      SUBROUTINE STACOT (I, XJ, V)  
      DIMENSION V(3)  
      COMMON VS(4, 10, 4)
```

```
      J = INT(XJ)  
      J1 = J+1  
      DXJ = XJ - J  
      CXJ = 1 - DXJ  
      V(1) = VS(I, J, 1)*CXJ + VS(I, J1, 1)*DXJ  
      V(2) = VS(I, J, 2)*CXJ + VS(I, J1, 2)*DXJ  
      V(3) = VS(I, J, 3)*CXJ + VS(I, J1, 3)*DXJ
```

```
      RETURN  
      END
```


STACIN.FORTRAN

```

C*****
C*
C*   THIS SUBROUTINE STORES PAST VALUES.
C*
C*****

```

```

      SUBROUTINE STACIN (I, V)
      DIMENSION V(3)
      COMMON VS(4, 10, 4)
      DO 10 J = 1, 9
        VS(I, 11-J, 1) = VS(I, 10-J, 1)
        VS(I, 11-J, 2) = VS(I, 10-J, 2)
10    VS(I, 11-J, 3) = VS(I, 10-J, 3)

      VS(I, 1, 1) = V(1)
      VS(I, 1, 2) = V(2)
      VS(I, 1, 3) = V(3)
      RETURN
      END

```

Chapter 3

Outer Loop Control of Laser Pointing Boresight Error

3.1 Introduction

In Chapter 2, we considered the problem of modeling a laser weapon space engagement. We showed how a high servo bandwidth pointing system could be implemented to maintain a tight track on the target by means of a shared aperture sensor. (The concept of a shared aperture, though not explicitly spelled out there, was implicit in the assumption that the transmitted laser beam direction was directly tied to the sensor field-of-view centerline (i. e., if one changed, the other changed by the same amount). The target tracking was tight in the sense that the image of the aimpoint on the target could be kept very well centered in the sensor's field-of-view. However, this provided no assurance that the laser beam actually was incident on the desired aimpoint. In fact, as was shown previously, because of laser pointing bias and because of the failure to correctly accommodate the point-ahead effect, the laser beam generally missed the aimpoint.

It should be possible to control this error by observing the laser miss distance and closing a laser pointing servo loop with this information. Unfortunately, because of the large delay time involved in the round-trip, speed of light, transit from the laser to the target and back, such a servo must have a rather low servo bandwidth if it is to be stable. If we were to use this kind of a servo to track the target, because of the low bandwidth its basic performance would be poor. The system would be sluggish, the servo settling time would be long, and against rapidly moving targets, the servo lag would be unacceptably long.

There is, however, a way around this problem — a way to have our cake and eat it too! We can have high bandwidth laser pointing control, and yet use the observed laser miss distance to control the pointing — nulling

the miss distance and yet retaining stable, high servo bandwidth performance. The key to this concept is to start with the ordinary shared aperture image tracking high bandwidth servo, and embed this servo loop within a much lower bandwidth servo loop designed to only control the bias error. The underlying assumption in this concept is that the laser pointing bias error only varies very slowly, and so can be adequately controlled by this outer loop low bandwidth servo.

The outer loop servo interacts with the inner loop in the sense that its output serves as a bias in the demodulation of the high data rate target image sensor, thus biasing the pointing. It accepts as input the laser miss distance, which is determined by the gimbal pointing one round-trip transit time ago. (In this report, we ignore the question of how this outer loop senses the laser miss distance. This is to be taken up in a subsequent report.) Because of the round-trip transit time delay, this outer loop must have a low servo bandwidth if it is to be stable; but this does not prevent the inner loop from tracking the target image with a high servo bandwidth — this is tracking with a slowly adjusted bias correction imposed on the track.

In the next section, we discuss this inner loop/outer loop tracking arrangement in more detail, and consider some of the special features we shall incorporate in the outer, bias control, servo loop. In the section after that, we shall present a set of sample results, evaluating some of the design parameters and showing what kind of performance we may expect against a fixed boresight error and against a linearly varying boresight error.

3.2 Inner Loop/Outer Loop Servo Considerations

The basic inner loop high servo bandwidth target tracking/outer loop low servo bandwidth bias error control concept that we shall be working with is depicted in Fig. 1. The inner loop consists of 1) the high bandwidth local servo network, 2) the gimbal and shared aperture optics, 3) the target sensor, and 4) the summing node. This portion of the system operates in just the manner that we described in Chapter 2, and we need not discuss its details further here, except to remark that it is a type two servo with a 100 Hz servo bandwidth. The outer loop takes as one of its components the entire inner loop, taking as its output from that "unit" the gimbal and shared aperture optics pointing and taking as its input point to that "unit" the summing node. The gimbal and shared aperture optics provide pointing for the laser beam and also for the target backscatter sensor, allowing the backscatter sensor not only to view the laser backscatter, but also the target (in the target tracking sense), so that the backscatter sensor can measure the distance by which the laser beam missed the target aimpoint.[†] The outer loop can be considered to consist of 1) the inner servo loop unit, 2) the laser, 3) the target, 4) the target backscatter sensor, and 5) the low bandwidth servo network.

Assuming that the target backscatter sensor can actually tell what the laser/target miss distance was, then it can form a bias control signal to compensate for this miss distance. This control signal, if used to bias the inner loop track error demodulation, as indicated in Fig. 1, will cause inner loop pointing of the gimbal and shared aperture optics to "point away from" the apparent target position by just enough to compensate for the

[†] It should be recognized that the laser beam miss distance, as determined by the target backscatter sensor, is not really dependent on the shared aperture pointing. Thus in the sense of servo theory control, there is no link from the shared aperture optics to the target backscatter sensor.

laser bias and round-trip transit time delay point-ahead effects — so that the laser beam will be exactly incident on the target aimpoint. Because the target backscatter sensor is sensing the effect of laser pointing as performed one round-trip transit time ago and controlling the present laser pointing, there is a potential servo stability problem. To insure that this bias control servo is stable, the servo bandwidth must be low enough that the phase shift and the bandwidth limit (0 dB open loop gain) frequency is much less than $\pi/2$ for a time delay equal to the round-trip transit time. Thus, with a round-trip transit time of

$$\tau_{R/T} = 2 R/c \quad , \quad (1)$$

where R is the target range, and $c = 3 \times 10^8$ m/sec is the speed of light, the outer loop bias control servo bandwidth f_{bc} must be such that

$$2 \pi f_{bc} \tau_{R/T} < \frac{1}{2} \pi \quad , \quad (2)$$

or

$$f_{bc} < (4 \tau_{R/T})^{-1} \quad . \quad (3)$$

In practice, there is a further constraint associated with the time for the target backscatter sensor to process the signals it receives and determine the apparent laser target miss distance. All of this time should be incorporated into a time delay, τ_d , which actually constrains the servo bandwidth so that

$$f_{bc} < (4 \tau_d)^{-1} \quad . \quad (4)$$

We shall, somewhat arbitrarily, restrict our attention to a type-one servo for the boresight error control outer servo loop. Thus the low

bandwidth servo network of Fig. 1 may be considered to consist of a gain factor G followed by an integrator. Operating open loop, if the target backscatter sensor output is $\epsilon(t)$, then the network output would be

$$G \int_0^t dt' \epsilon(t') \quad .$$

Operating in a sample data sense with a sample time, δt , the corresponding output at time $t = N \delta t$ would be

$$G \sum_{n=1}^N \delta t \epsilon(n \delta t) \quad .$$

In the context in which we shall later wish to apply our results, it is convenient to consider a network input update at a time interval τ_0 , in which case the output at time $t = N \tau_0$ would be

$$C \sum_{n=1}^N \epsilon(n \tau_0) \quad ,$$

where

$$C = G \tau_0 \quad . \quad (5)$$

For a type-one servo, the gain is related to the bandwidth by the expression

$$G = 2\pi f_{bc} \quad . \quad (6)$$

If we replace Eq. (4) by the equality,

$$f_{bc} = (\alpha \tau_0)^{-1} \quad , \quad (7)$$

where α is a quantity which determines the time delay/servo stability margin, then we can rewrite Eq. (5) as

$$C = 2\pi/\alpha$$

This then allows us to consider the incremental update version of the outer loop servo network as having an output equal to

$$(2\pi/\alpha) \sum_{n=1}^N e(N\tau_0)$$

In this form, α specifies the desired servo stability parameter with the update time interval, τ_0 , in effect, defining the servo bandwidth. It is never necessary to explicitly calculate the servo bandwidth or the gain (i.e., the gain in the conventional sense). With this definition of the outer loop servo network, we are directly able to carry out numerical simulation.

It is interesting to note that, with this definition of the servo network, it is possible to operate with a variable time delay. During the laser firing engagement, the time delay for bias control servo update can be continuously changing. Nonetheless, a servo implemented in accordance with this servo network approach will maintain a constant stability level (as specified by α), continuously adjusting the effective servo gain and bandwidth to match the update time interval. The ability to accept a changing update time without a major servo modification is potentially significant in the work we shall be doing later, where we consider the practical aspects of the target/backscatter sensor's realization.

With this definition for the bias control servo network, we are prepared to simulate the system of Fig. 1. In the next section, we describe

this simulation and present results, based on the assumption that the target backscatter sensor can function "perfectly" to determine the laser/target miss distance at the desired data rate.

3.3 Ideal Sensor Bias Control Servo Simulation

In Chapter 2 , we developed the details of a laser weapon space-to-space engagement computer simulation. We shall use that same computer simulation model here, except that we shall add to it a sensor capability to determine the laser/target miss distance, taking proper account of the round-trip transit time delays, and a servo network, simulated in accordance with the discussion in the previous section to control the bias error nulling outer servo loop. The output of the network is input to the target sensor track error demodulator at the point previously provided for input of a boresight error estimate.

In the appendix, we list the resultant computer program, with a set of outer DO-loops that allows us to cycle through an engagement with various values of α , and with different inherent boresight errors. Using this program, we have generated results for $\alpha = 3, 4, 6, 8$, and for the case of a fixed boresight error of $50 \mu\text{rad}$ in each axis, and for a boresight error that starts at zero, but grows at a rate of $10 \mu\text{rad}$ in each axis. The engagement corresponds to a starting range of 1.0 Mm . The closing velocity is 440 m/sec , while the crossing velocity (i.e., the relative velocity perpendicular to the line-of-sight) is 580 m/sec . We have run engagements with boresight error update times of 20 msec , 40 msec , and 80 msec , always using 1.0 msec as our basic simulation clock time. Selected portions of these results are listed in Tables 1 , 2 , and 3 , and graphed in Fig.'s 2 , 3 , and 4 .

In Fig. 2, we show the laser miss distance that we would expect for this engagement if there is no bias update. As can be seen, after the first $.02 \text{ sec}$, the initial transients have, for the most part, settled out and we appear to be pointing with about a 2.6 m bias error. (This can be attributed, in part, to the point-ahead requirement which is not being fulfilled, and, in part, to a small amount of pseudo servo lag inherent in our

finite time increment simulation.) After this, the miss distance can be seen to be growing with time, just as we would expect. In Fig.'s 3a , 3b , and 3c , we show the results of closing the boresight error control loop with a miss distance update every 0.020 sec (i.e., $\tau_b = 2 \times 10^{-2}$ sec). Results are shown for the stability factor, α , set equal to 8 , 6 , and 4 . The corresponding tables of results are listed in Tables 1a , 1b , 1c , and 1d , where Table 1d corresponds to $\alpha = 3$, for which we have not shown any corresponding figure, since the servo performance is apparently unstable. It is obvious that the optimum compromise between servo stability and boresight error drift tracking is achieved with $\alpha = 6$. In Tables 2a , 2b , 2c , and 2d , we show corresponding results for a fixed boresight error of 50 μ rad in each axis. Here again we see that with $\alpha = 3$, the bias control servo loop is unstable, and that with $\alpha = 4$, the damping of errors is unacceptably slow. The results with $\alpha = 6$ indicate that this value of α represents a good choice of the stability factor. Accordingly, our other results will be for this value of the stability parameter.

In Fig.'s 4a , 4b , and 4c , we show the dependence of the residual laser miss distance on the boresight error update time, τ_b . (Fig. 4a is identical to Fig. 3b .) Results are shown for $\alpha = 6$ and $\tau_b = 0.020$, 0.040 , and 0.080 sec , respectively. The corresponding results are listed in Tables 3a , 3b , and 3c . As can be seen from these results, the longer the update period, the poorer the performance — but there is no sharp breakpoint. It is obviously desirable to work with as short an update time as we can realize. (Obviously, however, we must not try to make the update time shorter than the round-trip transit time or the loop will necessarily be unstable.)

In reviewing these results, it is important to realize that we have deliberately picked a very large boresight error and boresight error drift rate — so that the residual errors would be clearly discernible. Obviously,

a $10 \mu\text{rad/sec}$ boresight error drift rate is much larger than we would reasonably expect in a fielded laser weapon system. If we could keep the boresight error drift rate to one-tenth that value, the residual error would be correspondingly smaller. With this thought in mind, we can see that even the $\tau_0 = 0.080 \text{ sec}$ update period, as shown in Fig. 4c but scaled by a factor of one-tenth, would yield very good performance. The worst case laser miss distance would be only about 10 cm , as compared to an uncontrolled laser drift rate across the target of 1.0 m/sec . It is fairly obvious from these results that the concept of an outer loop bias control, operating in the type-one servo mode with a stability factor of $\alpha = 6$, provides a basic capability to constrain boresight error effects. Our basic problem at this point is to define a basis for operation of our target/backscatter sensor so as to provide a measurement of the laser miss distance. We will take this up in the following chapters.

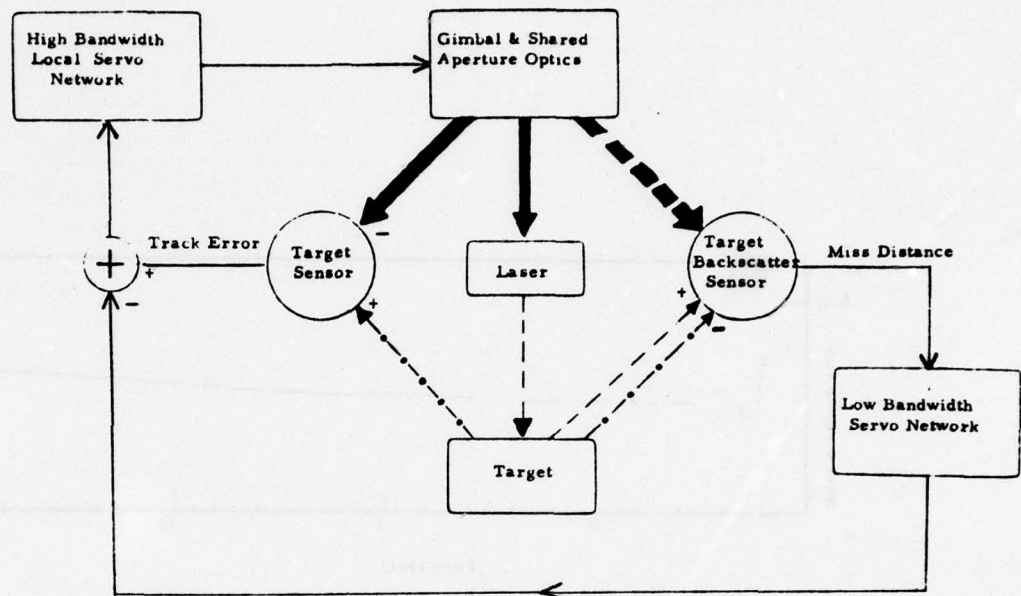


Figure 3.1 Local Inner Servo Imbedded in a R/T Delayed Outer Servo Loop.

The outer servo loop, based on observing the laser backscatter signal, compensates for the bias errors in the local loop. The low bandwidth of the outer loop is directly related to the round-trip transit time delay from the laser to the target and then back to the backscatter sensor. The heavy lines indicate the gimbal/shared aperture optics effect on the target sensor, the laser transmitter, and the target backscatter sensor — which because of the shared aperture arrangement are all identical. The broken heavy line indicates that while the gimbal/shared aperture optics control the orientation of the target backscatter sensor, it does not influence the miss distance value measured by the target backscatter sensor. The thin broken lines indicate a light propagation between the target and the shared aperture. Each of these dotted lines implies a one-way speed-of-light transit time delay. The dash-dot lines (-.-.-) carry target position information, while the dash-dash (---) lines indicate laser light propagation.

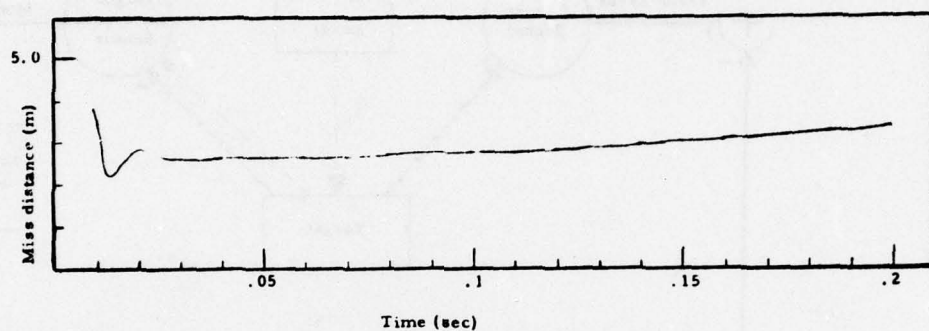


Figure 3.2 Laser/Target Miss Distance Without Bias Update for a Time-Varying Bias Error.

The target range is 1.0 Mm and the crossing velocity is 580 m/sec . No correction estimate is included in the servo for point-ahead or for the $10 \mu\text{rad/sec}$ changing boresight error.

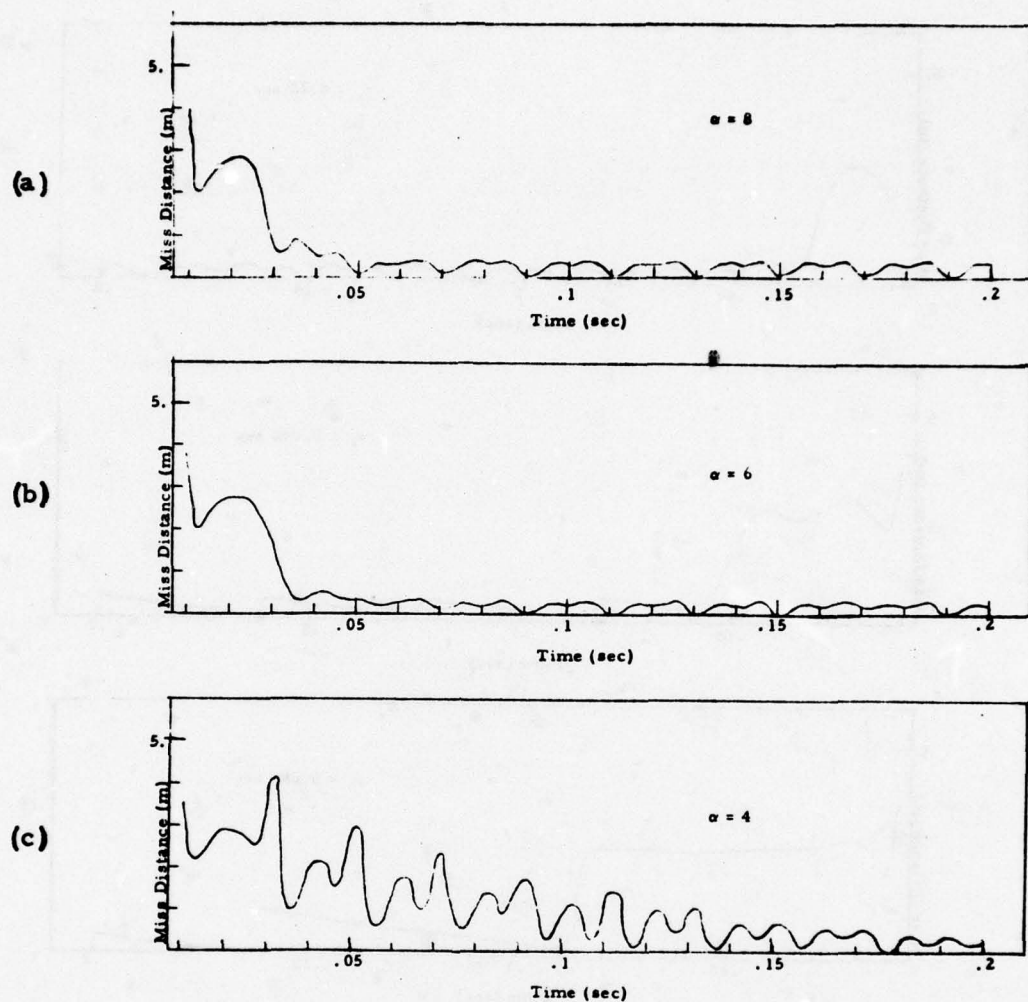


Figure 3.3 Laser/Target Miss Distance With Bias Update for Various Stability Factors.

The engagement and time-varying boresight error are identical to that of Fig. 2. The boresight error update rate is $\tau_b = 0.020$ sec. Stability factors of $\alpha = 8$, 6 , and 4 are shown in (a), (b), and (c), respectively. The best results appear to be provided with $\alpha = 6$. The results for $\alpha = 4$ indicate a marginal stability. Results for $\alpha = 3$ (not shown here) are clearly unstable.

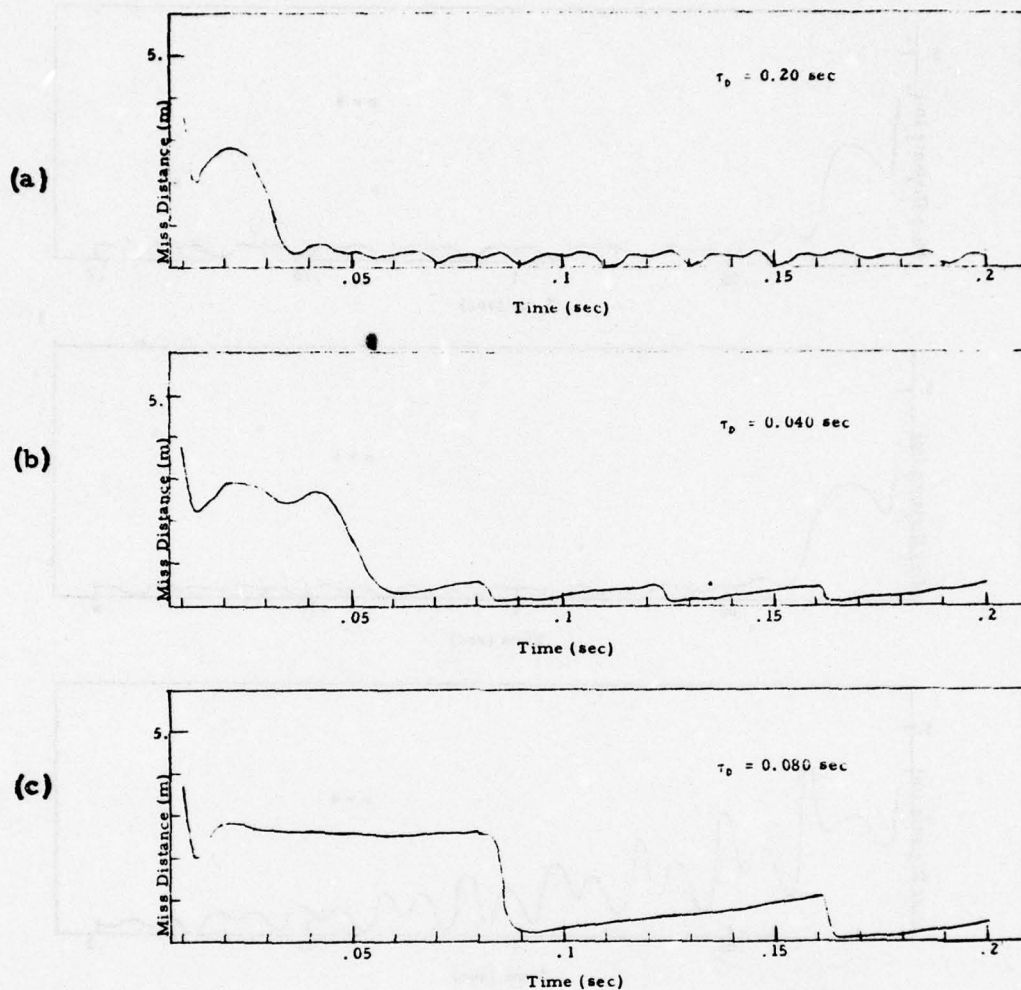


Figure 3.4 Laser/Target Miss Distance With Bias Update for Various Update Times.

The engagement and time-varying boresight error are identical to that of Fig. 2. The stability factor is $\alpha = 6$. Results for boresight error update rates of $\tau_b = 0.020$, 0.040 , and 0.080 sec are shown in (a), (b), and (c), respectively.

Table 3.1a

Outer Loop Bias Control of a Time-Dependent Boresight Error, With a
Servo Stability Factor of $\alpha = 8$, and a $\tau_b = 20$ msec Update Time

TIME (SEC.)	RANGE (METERS)	MISS DISTANCE (METERS)	THETA (RAD.)	PHI (RAD.)
0.005	1.0000E+06	2.1365E+04	1.013155	0.785400
0.010	1.0000E+06	3.5699E+00	1.013153	0.785404
0.015	1.0000E+06	2.3707E+00	1.013151	0.785406
0.020	1.0000E+06	2.7930E+00	1.013150	0.785409
0.025	1.0000E+06	2.6586E+00	1.013146	0.785415
0.030	1.0000E+06	6.3781E-01	1.013146	0.785417
0.035	1.0000E+06	8.6553E-01	1.013144	0.785420
0.040	1.0000E+06	4.5795E-01	1.013142	0.785427
0.045	1.0000E+06	5.7506E-01	1.013140	0.785426
0.050	1.0000E+06	8.7346E-02	1.013139	0.785429
0.055	1.0000E+06	3.4886E-01	1.013138	0.785432
0.060	1.0001E+06	3.4455E-01	1.013136	0.785435
0.065	1.0001E+06	4.1502E-01	1.013134	0.785438
0.070	1.0001E+06	8.5938E-02	1.013133	0.785441
0.075	1.0001E+06	3.0055E-01	1.013131	0.785444
0.080	1.0001E+06	3.3044E-01	1.013130	0.785446
0.085	1.0001E+06	3.9636E-01	1.013128	0.785449
0.090	1.0001E+06	8.7695E-02	1.013127	0.785452
0.095	1.0001E+06	3.1561E-01	1.013125	0.785455
0.100	1.0001E+06	3.3802E-01	1.013124	0.785458
0.105	1.0001E+06	4.0157E-01	1.013122	0.785461
0.110	1.0001E+06	7.8515E-02	1.013120	0.785464
0.115	1.0001E+06	3.2269E-01	1.013119	0.785467
0.120	1.0001E+06	3.2269E-01	1.013117	0.785470
0.125	1.0001E+06	3.9851E-01	1.013116	0.785472
0.130	1.0001E+06	8.7346E-02	1.013114	0.785475
0.135	1.0001E+06	3.2979E-01	1.013113	0.785478
0.140	1.0001E+06	3.2645E-01	1.013111	0.785481
0.145	1.0001E+06	4.0365E-01	1.013109	0.785484
0.150	1.0001E+06	9.6635E-02	1.013108	0.785487
0.155	1.0001E+06	3.7521E-01	1.013107	0.785490
0.160	1.0001E+06	3.7348E-01	1.013105	0.785493
0.165	1.0001E+06	4.2855E-01	1.013103	0.785495
0.170	1.0001E+06	9.3007E-02	1.013102	0.785498
0.175	1.0001E+06	3.7730E-01	1.013100	0.785501
0.180	1.0001E+06	3.7748E-01	1.013099	0.785504
0.185	1.0001E+06	4.2718E-01	1.013097	0.785507
0.190	1.0001E+06	9.6319E-02	1.013096	0.785510
0.195	1.0001E+06	3.2979E-01	1.013094	0.785513
0.200	1.0001E+06	3.5510E-01	1.013093	0.785516
0.205	1.0001E+06	4.2318E-01	1.013091	0.785518
0.210	1.0001E+06	6.3469E-02	1.013089	0.785521
0.215	1.0001E+06	3.2979E-01	1.013088	0.785524
0.220	1.0001E+06	3.7557E-01	1.013086	0.785527
0.225	1.0001E+06	3.9109E-01	1.013085	0.785530
0.230	1.0001E+06	7.7733E-02	1.013083	0.785533
0.235	1.0001E+06	3.2107E-01	1.013082	0.785536
0.240	1.0001E+06	3.2822E-01	1.013080	0.785539
0.245	1.0001E+06	4.1266E-01	1.013078	0.785541

0.250	1.0001E+06	8.3415E-02	1.013077	0.785544
0.255	1.0001E+06	3.2979E-01	1.013076	0.785547
0.260	1.0001E+06	3.3557E-01	1.013074	0.785550
0.265	1.0001E+06	4.0360E-01	1.013072	0.785553
0.270	1.0001E+06	6.7346E-02	1.013071	0.785556
0.275	1.0001E+06	3.2998E-01	1.013069	0.785559
0.280	1.0001E+06	3.3712E-01	1.013068	0.785562
0.285	1.0001E+06	4.0380E-01	1.013066	0.785564
0.290	1.0002E+06	7.7340E-02	1.013065	0.785567
0.295	1.0002E+06	3.2645E-01	1.013063	0.785570
0.300	1.0002E+06	3.4426E-01	1.013062	0.785573
0.305	1.0002E+06	4.1436E-01	1.013060	0.785576
0.310	1.0002E+06	8.7346E-02	1.013058	0.785579
0.315	1.0002E+06	3.1191E-01	1.013057	0.785582
0.320	1.0002E+06	3.3348E-01	1.013055	0.785585
0.325	1.0002E+06	4.0331E-01	1.013054	0.785587
0.330	1.0002E+06	8.4143E-02	1.013052	0.785590
0.335	1.0002E+06	3.0837E-01	1.013051	0.785593
0.340	1.0002E+06	3.3173E-01	1.013049	0.785596
0.345	1.0002E+06	4.0880E-01	1.013048	0.785599
0.350	1.0002E+06	8.9759E-02	1.013046	0.785602
0.355	1.0002E+06	3.1191E-01	1.013045	0.785605
0.360	1.0002E+06	3.3348E-01	1.013043	0.785608
0.365	1.0002E+06	4.0550E-01	1.013041	0.785610
0.370	1.0002E+06	8.7346E-02	1.013040	0.785613
0.375	1.0002E+06	3.1907E-01	1.013038	0.785616
0.380	1.0002E+06	3.1725E-01	1.013037	0.785619
0.385	1.0002E+06	4.0697E-01	1.013035	0.785622
0.390	1.0002E+06	1.1213E-01	1.013034	0.785625
0.395	1.0002E+06	3.4054E-01	1.013032	0.785628
0.400	1.0002E+06	3.4072E-01	1.013031	0.785631
0.405	1.0002E+06	4.2662E-01	1.013029	0.785633
0.410	1.0002E+06	9.3097E-02	1.013028	0.785636
0.415	1.0002E+06	3.3983E-01	1.013026	0.785639
0.420	1.0002E+06	3.3521E-01	1.013025	0.785642
0.425	1.0002E+06	4.2346E-01	1.013023	0.785645
0.430	1.0002E+06	9.1109E-02	1.013021	0.785648
0.435	1.0002E+06	3.3712E-01	1.013020	0.785651
0.440	1.0002E+06	3.4426E-01	1.013018	0.785654
0.445	1.0002E+06	4.1788E-01	1.013017	0.785656
0.450	1.0002E+06	8.4143E-02	1.013015	0.785660
0.455	1.0002E+06	3.3348E-01	1.013014	0.785662
0.460	1.0002E+06	3.4242E-01	1.013012	0.785665
0.465	1.0002E+06	4.3146E-01	1.013010	0.785669
0.470	1.0002E+06	8.1565E-02	1.013009	0.785671
0.475	1.0002E+06	3.1561E-01	1.013007	0.785674
0.480	1.0002E+06	3.3192E-01	1.013006	0.785677
0.485	1.0002E+06	4.1788E-01	1.013004	0.785680
0.490	1.0002E+06	8.5938E-02	1.013003	0.785683
0.495	1.0002E+06	3.2448E-01	1.013001	0.785685
0.500	1.0002E+06	3.2107E-01	1.013000	0.785688

Table 3.1b

Outer Loop Bias Control of a Time-Dependent Boresight Error, With a
Servo Stability Factor of $\alpha = 6$, and a $\tau_p = 20$ msec Update Time

TIME (SEC.)	RANGE (METERS)	MISS DISTANCE (METERS)	THETA (RAD.)	PHI (RAD.)
0.005	1.0000E+06	2.8853E+02	1.013155	0.785400
0.010	1.0000E+06	3.5699E+02	1.013153	0.785404
0.015	1.0000E+06	2.3707E+00	1.013151	0.785406
0.020	1.0000E+06	2.7930E+00	1.013150	0.785409
0.025	1.0000E+06	2.6586E+00	1.013146	0.785416
0.030	1.0000E+06	1.7319E+00	1.013145	0.785417
0.035	1.0000E+06	3.2041E-01	1.013143	0.785421
0.040	1.0000E+06	4.8223E-01	1.013142	0.785424
0.045	1.0000E+06	4.2375E-01	1.013141	0.785426
0.050	1.0000E+06	3.5673E-01	1.013139	0.785429
0.055	1.0000E+06	2.4569E-01	1.013138	0.785432
0.060	1.0001E+06	2.9984E-01	1.013136	0.785435
0.065	1.0001E+06	3.5295E-01	1.013134	0.785438
0.070	1.0001E+06	1.5109E-01	1.013132	0.785441
0.075	1.0001E+06	2.4219E-01	1.013131	0.785444
0.080	1.0001E+06	2.4382E-01	1.013130	0.785446
0.085	1.0001E+06	3.3146E-01	1.013128	0.785449
0.090	1.0001E+06	4.4879E-02	1.013127	0.785452
0.095	1.0001E+06	2.4569E-01	1.013125	0.785455
0.100	1.0001E+06	2.6540E-01	1.013124	0.785458
0.105	1.0001E+06	3.3901E-01	1.013122	0.785461
0.110	1.0001E+06	1.7469E-02	1.013120	0.785464
0.115	1.0001E+06	2.3307E-01	1.013119	0.785467
0.120	1.0001E+06	2.5122E-01	1.013117	0.785469
0.125	1.0001E+06	3.2822E-01	1.013116	0.785472
0.130	1.0001E+06	3.2212E-02	1.013114	0.785475
0.135	1.0001E+06	2.4619E-01	1.013113	0.785478
0.140	1.0001E+06	2.3503E-01	1.013111	0.785481
0.145	1.0001E+06	3.3348E-01	1.013109	0.785484
0.150	1.0001E+06	4.2072E-02	1.013108	0.785487
0.155	1.0001E+06	2.5122E-01	1.013106	0.785490
0.160	1.0001E+06	2.6192E-01	1.013105	0.785493
0.165	1.0001E+06	3.4965E-01	1.013103	0.785495
0.170	1.0001E+06	2.3439E-02	1.013102	0.785498
0.175	1.0001E+06	2.5219E-01	1.013100	0.785501
0.180	1.0001E+06	2.5327E-01	1.013099	0.785504
0.185	1.0001E+06	3.3748E-01	1.013097	0.785507
0.190	1.0001E+06	2.4703E-02	1.013096	0.785510
0.195	1.0001E+06	2.3863E-01	1.013094	0.785513
0.200	1.0001E+06	2.6192E-01	1.013093	0.785516
0.205	1.0001E+06	3.2663E-01	1.013091	0.785518
0.210	1.0001E+06	3.2212E-02	1.013089	0.785521
0.215	1.0001E+06	2.4432E-01	1.013088	0.785524
0.220	1.0001E+06	2.5122E-01	1.013086	0.785527
0.225	1.0001E+06	2.1561E-01	1.013085	0.785530
0.230	1.0001E+06	3.8273E-02	1.013083	0.785533
0.235	1.0001E+06	2.3940E-01	1.013082	0.785536
0.240	1.0001E+06	2.5460E-01	1.013080	0.785539
0.245	1.0001E+06	3.2803E-01	1.013078	0.785541

Table 1b (Continued)

0.250	1.0001E+06	3.2212E-02	1.013077	0.785544
0.255	1.0001E+06	2.3307E-01	1.013075	0.785547
0.260	1.0001E+06	2.4939E-01	1.013074	0.785550
0.265	1.0001E+06	3.1191E-01	1.013072	0.785553
0.270	1.0001E+06	3.2212E-02	1.013071	0.785556
0.275	1.0001E+06	2.3189E-01	1.013069	0.785559
0.280	1.0001E+06	2.4779E-01	1.013068	0.785562
0.285	1.0001E+06	3.2449E-01	1.013066	0.785564
0.290	1.0002E+06	4.0595E-02	1.013065	0.785567
0.295	1.0002E+06	2.3307E-01	1.013063	0.785570
0.300	1.0002E+06	2.6585E-01	1.013062	0.785573
0.305	1.0002E+06	3.2803E-01	1.013060	0.785576
0.310	1.0002E+06	3.9836E-02	1.013058	0.785579
0.315	1.0002E+06	2.3554E-01	1.013057	0.785582
0.320	1.0002E+06	2.3722E-01	1.013055	0.785585
0.325	1.0002E+06	3.2979E-01	1.013054	0.785587
0.330	1.0002E+06	2.9232E-02	1.013052	0.785590
0.335	1.0002E+06	2.5686E-01	1.013051	0.785593
0.340	1.0002E+06	2.6017E-01	1.013049	0.785596
0.345	1.0002E+06	3.3521E-01	1.013047	0.785599
0.350	1.0002E+06	3.9063E-02	1.013046	0.785602
0.355	1.0002E+06	2.4914E-01	1.013044	0.785605
0.360	1.0002E+06	2.4569E-01	1.013043	0.785608
0.365	1.0002E+06	3.3521E-01	1.013041	0.785610
0.370	1.0002E+06	2.5911E-02	1.013040	0.785613
0.375	1.0002E+06	2.5840E-01	1.013039	0.785616
0.380	1.0002E+06	2.2964E-01	1.013037	0.785619
0.385	1.0002E+06	3.4072E-01	1.013035	0.785622
0.390	1.0002E+06	5.2987E-02	1.013034	0.785625
0.395	1.0002E+06	2.6711E-01	1.013032	0.785628
0.400	1.0002E+06	2.8524E-01	1.013031	0.785631
0.405	1.0002E+06	3.5149E-01	1.013029	0.785633
0.410	1.0002E+06	3.4939E-02	1.013027	0.785636
0.415	1.0002E+06	2.3189E-01	1.013026	0.785639
0.420	1.0002E+06	2.4569E-01	1.013024	0.785642
0.425	1.0002E+06	3.1907E-01	1.013023	0.785645
0.430	1.0002E+06	4.5554E-02	1.013021	0.785648
0.435	1.0002E+06	2.4080E-01	1.013020	0.785651
0.440	1.0002E+06	2.5686E-01	1.013018	0.785654
0.445	1.0002E+06	3.2645E-01	1.013016	0.785656
0.450	1.0002E+06	2.8168E-02	1.013015	0.785659
0.455	1.0002E+06	2.3503E-01	1.013014	0.785662
0.460	1.0002E+06	2.5122E-01	1.013012	0.785665
0.465	1.0002E+06	3.4952E-01	1.013010	0.785668
0.470	1.0002E+06	3.2212E-02	1.013009	0.785671
0.475	1.0002E+06	2.3307E-01	1.013007	0.785674
0.480	1.0002E+06	2.5012E-01	1.013006	0.785677
0.485	1.0002E+06	3.2449E-01	1.013004	0.785679
0.490	1.0002E+06	3.5201E-02	1.013003	0.785682
0.495	1.0002E+06	2.3465E-01	1.013001	0.785685
0.500	1.0002E+06	2.5340E-01	1.013000	0.785688

Table 3.1c

Outer Loop Bias Control of a Time-Dependent Boresight Error, With a Servo Stability Factor of $\alpha = 4$, and a $\tau_D = 20$ msec Update Time

TIME (SEC.)	RANGE (METERS)	MISS DISTANCE (METERS)	THETA (RAD.)	PHI (RAD.)
0.005	1.0000E+06	2.8957E+02	1.013155	0.785403
0.010	1.0000E+06	3.5669E+00	1.013153	0.785404
0.015	1.0000E+06	2.3707E+00	1.013151	0.785406
0.020	1.0000E+06	2.7930E+00	1.013150	0.785409
0.025	1.0000E+06	2.6586E+00	1.013145	0.785418
0.030	1.0000E+06	3.9379E+00	1.013145	0.785418
0.035	1.0000E+06	1.0000E+00	1.013143	0.785422
0.040	1.0000E+06	1.9558E+00	1.013141	0.785425
0.045	1.0000E+06	1.7312E+00	1.013142	0.785423
0.050	1.0000E+06	2.8632E+00	1.013139	0.785428
0.055	1.0000E+06	7.6869E-01	1.013139	0.785430
0.060	1.0001E+06	1.4410E+00	1.013137	0.785434
0.065	1.0001E+06	1.2512E+00	1.013133	0.785440
0.070	1.0001E+06	2.1350E+00	1.013132	0.785441
0.075	1.0001E+06	6.2894E-01	1.013131	0.785445
0.080	1.0001E+06	1.1305E+00	1.013129	0.785447
0.085	1.0001E+06	1.0361E+00	1.013129	0.785448
0.090	1.0001E+06	1.6254E+00	1.013127	0.785452
0.095	1.0001E+06	4.3806E-01	1.013125	0.785454
0.100	1.0001E+06	8.1073E-01	1.013124	0.785457
0.105	1.0001E+06	7.2239E-01	1.013121	0.785462
0.110	1.0001E+06	1.2054E+00	1.013120	0.785464
0.115	1.0001E+06	3.9094E-01	1.013118	0.785467
0.120	1.0001E+06	6.6296E-01	1.013117	0.785470
0.125	1.0001E+06	6.3074E-01	1.013116	0.785471
0.130	1.0001E+06	9.1756E-01	1.013114	0.785475
0.135	1.0001E+06	2.7097E-01	1.013113	0.785478
0.140	1.0001E+06	4.7428E-01	1.013111	0.785481
0.145	1.0001E+06	4.2976E-01	1.013109	0.785484
0.150	1.0001E+06	6.1342E-01	1.013108	0.785487
0.155	1.0001E+06	2.6192E-01	1.013106	0.785490
0.160	1.0001E+06	3.8804E-01	1.013105	0.785493
0.165	1.0001E+06	4.2346E-01	1.013103	0.785495
0.170	1.0001E+06	4.7406E-01	1.013102	0.785498
0.175	1.0001E+06	1.6406E-01	1.013100	0.785501
0.180	1.0001E+06	2.2791E-01	1.013099	0.785504
0.185	1.0001E+06	2.6305E-01	1.013097	0.785507
0.190	1.0001E+06	2.9729E-01	1.013096	0.785510
0.195	1.0001E+06	2.0885E-01	1.013094	0.785513
0.200	1.0001E+06	2.5781E-01	1.013092	0.785516
0.205	1.0001E+06	3.2069E-01	1.013091	0.785518
0.210	1.0001E+06	2.4352E-01	1.013089	0.785521
0.215	1.0001E+06	1.5409E-01	1.013088	0.785524
0.220	1.0001E+06	1.9087E-01	1.013086	0.785527
0.225	1.0001E+06	2.2777E-01	1.013084	0.785530
0.230	1.0001E+06	1.7864E-01	1.013083	0.785533
0.235	1.0001E+06	1.7901E-01	1.013082	0.785536
0.240	1.0001E+06	2.1665E-01	1.013080	0.785539
0.245	1.0001E+06	2.7929E-01	1.013078	0.785541

Table 1c (Continued)

0.250	1.0001E+06	1.9311E-01	1.013077	0.785544
0.255	1.0001E+06	1.4427E-01	1.013075	0.785547
0.260	1.0001E+06	1.6499E-01	1.013074	0.785550
0.265	1.0001E+06	2.2125E-01	1.013072	0.785553
0.270	1.0001E+06	1.3666E-01	1.013071	0.785556
0.275	1.0001E+06	1.5703E-01	1.013069	0.785559
0.280	1.0001E+06	1.8037E-01	1.013068	0.785562
0.285	1.0001E+06	2.4544E-01	1.013066	0.785564
0.290	1.0002E+06	1.3189E-01	1.013065	0.785567
0.295	1.0002E+06	1.6973E-01	1.013063	0.785570
0.300	1.0002E+06	1.8652E-01	1.013062	0.785573
0.305	1.0002E+06	2.5674E-01	1.013060	0.785576
0.310	1.0002E+06	1.2377E-01	1.013058	0.785579
0.315	1.0002E+06	1.6181E-01	1.013057	0.785582
0.320	1.0002E+06	1.6350E-01	1.013055	0.785585
0.325	1.0002E+06	2.5049E-01	1.013054	0.785587
0.330	1.0002E+06	1.0276E-01	1.013052	0.785590
0.335	1.0002E+06	1.7712E-01	1.013051	0.785593
0.340	1.0002E+06	1.7626E-01	1.013049	0.785596
0.345	1.0002E+06	2.7388E-01	1.013047	0.785599
0.350	1.0002E+06	1.0246E-01	1.013046	0.785602
0.355	1.0002E+06	1.6937E-01	1.013044	0.785605
0.360	1.0002E+06	1.9057E-01	1.013043	0.785608
0.365	1.0002E+06	2.5531E-01	1.013041	0.785610
0.370	1.0002E+06	1.3056E-01	1.013040	0.785613
0.375	1.0002E+06	1.4864E-01	1.013038	0.785616
0.380	1.0002E+06	1.5488E-01	1.013037	0.785619
0.385	1.0002E+06	2.2548E-01	1.013035	0.785622
0.390	1.0002E+06	7.3703E-02	1.013034	0.785625
0.395	1.0002E+06	1.7487E-01	1.013032	0.785628
0.400	1.0002E+06	1.8053E-01	1.013031	0.785631
0.405	1.0002E+06	2.6905E-01	1.013029	0.785633
0.410	1.0002E+06	1.0511E-01	1.013027	0.785636
0.415	1.0002E+06	1.5429E-01	1.013026	0.785639
0.420	1.0002E+06	1.7258E-01	1.013024	0.785642
0.425	1.0002E+06	2.4244E-01	1.013023	0.785645
0.430	1.0002E+06	1.0597E-01	1.013021	0.785648
0.435	1.0002E+06	1.5992E-01	1.013020	0.785651
0.440	1.0002E+06	1.5992E-01	1.013018	0.785654
0.445	1.0002E+06	2.3307E-01	1.013016	0.785656
0.450	1.0002E+06	9.4075E-02	1.013015	0.785659
0.455	1.0002E+06	1.7258E-01	1.013013	0.785662
0.460	1.0002E+06	1.7487E-01	1.013012	0.785665
0.465	1.0002E+06	2.4269E-01	1.013010	0.785668
0.470	1.0002E+06	7.8515E-02	1.013009	0.785671
0.475	1.0002E+06	1.4946E-01	1.013007	0.785674
0.480	1.0002E+06	1.6573E-01	1.013006	0.785677
0.485	1.0002E+06	2.5864E-01	1.013004	0.785679
0.490	1.0002E+06	9.8202E-02	1.013003	0.785682
0.495	1.0002E+06	1.6937E-01	1.013001	0.785685
0.500	1.0002E+06	1.7712E-01	1.013000	0.785688

Table 3.1d

Outer Loop Bias Control of a Time-Dependent Boresight Error, With a
Servo Stability Factor of $\alpha = 3$, and a $\tau_0 = 20$ msec Update Time

TIME (SEC.)	RANGE (METERS)	MISS DISTANCE (METERS)	THETA (RAD.)	PHI (RAD.)
0.005	1.0000E+06	2.8856E+02	1.013155	0.785400
0.010	1.0000E+06	3.5649E+02	1.013153	0.785404
0.015	1.0000E+06	2.3707E+02	1.013151	0.785406
0.020	1.0000E+06	2.7930E+02	1.013150	0.785409
0.025	1.0000E+06	2.6586E+02	1.013143	0.785420
0.030	1.0000E+06	6.1292E+02	1.013144	0.785420
0.035	1.0000E+06	2.1982E+02	1.013142	0.785424
0.040	1.0000E+06	3.4805E+02	1.013140	0.785426
0.045	1.0000E+06	3.1561E+02	1.013144	0.785419
0.050	1.0000E+06	7.7688E+02	1.013140	0.785426
0.055	1.0000E+06	2.8121E+02	1.013140	0.785427
0.060	1.0001E+06	4.3947E+02	1.013138	0.785431
0.065	1.0001E+06	3.9727E+02	1.013129	0.785447
0.070	1.0001E+06	9.8432E+02	1.013131	0.785444
0.075	1.0001E+06	3.5922E+02	1.013128	0.785449
0.080	1.0001E+06	5.6414E+02	1.013127	0.785451
0.085	1.0001E+06	5.1172E+02	1.013134	0.785437
0.090	1.0001E+06	1.2584E+01	1.013129	0.785443
0.095	1.0001E+06	4.5593E+02	1.013129	0.785448
0.100	1.0001E+06	7.1655E+02	1.013127	0.785451
0.105	1.0001E+06	6.4613E+02	1.013114	0.785476
0.110	1.0001E+06	1.6044E+01	1.013117	0.785469
0.115	1.0001E+06	5.8679E+02	1.013114	0.785476
0.120	1.0001E+06	9.1912E+02	1.013113	0.785478
0.125	1.0001E+06	8.3342E+02	1.013126	0.785453
0.130	1.0001E+06	2.0531E+01	1.013118	0.785463
0.135	1.0001E+06	7.4585E+02	1.013119	0.785466
0.140	1.0001E+06	1.1683E+01	1.013117	0.785470
0.145	1.0001E+06	1.0572E+01	1.013096	0.785508
0.150	1.0001E+06	2.6124E+01	1.013103	0.785496
0.155	1.0001E+06	9.5521E+02	1.013098	0.785505
0.160	1.0001E+06	1.4943E+01	1.013098	0.785506
0.165	1.0001E+06	1.3518E+01	1.013120	0.785464
0.170	1.0001E+06	3.3389E+01	1.013108	0.785486
0.175	1.0001E+06	1.2154E+01	1.013110	0.785482
0.180	1.0001E+06	1.9028E+01	1.013108	0.785487
0.185	1.0001E+06	1.7201E+01	1.013076	0.785547
0.190	1.0001E+06	4.2553E+01	1.013087	0.785525
0.195	1.0001E+06	1.5538E+01	1.013081	0.785537
0.200	1.0001E+06	2.4314E+01	1.013081	0.785537
0.205	1.0001E+06	2.2013E+01	1.013118	0.785467
0.210	1.0001E+06	5.4327E+01	1.013100	0.785502
0.215	1.0001E+06	1.9771E+01	1.013105	0.785492
0.220	1.0001E+06	3.0981E+01	1.013101	0.785499
0.225	1.0001E+06	2.7989E+01	1.013050	0.785555
0.230	1.0001E+06	6.9279E+01	1.013070	0.785558
0.235	1.0001E+06	2.5278E+01	1.013060	0.785576
0.240	1.0001E+06	3.9588E+01	1.013061	0.785574
0.245	1.0001E+06	3.5802E+01	1.013123	0.785458

0.250	1.0001E+06	8.8479E+01	1.013094	0.785512
0.255	1.0001E+06	3.2242E+01	1.013103	0.785496
0.260	1.0001E+06	5.0492E+01	1.013098	0.785505
0.265	1.0001E+06	4.5635E+01	1.013016	0.785659
0.270	1.0001E+06	1.1267E+02	1.013049	0.785596
0.275	1.0001E+06	4.1165E+01	1.013034	0.785624
0.280	1.0001E+06	6.4465E+01	1.013037	0.785619
0.285	1.0001E+06	5.8294E+01	1.013138	0.785428
0.290	1.0002E+06	1.4410E+02	1.013092	0.785515
0.295	1.0002E+06	5.2499E+01	1.013107	0.785486
0.300	1.0002E+06	8.2237E+01	1.013100	0.785500
0.305	1.0002E+06	7.4346E+01	1.012968	0.785749
0.310	1.0002E+06	1.8388E+02	1.013023	0.785645
0.315	1.0002E+06	6.7055E+01	1.013000	0.785689
0.320	1.0002E+06	1.0499E+02	1.013006	0.785678
0.325	1.0002E+06	9.4959E+01	1.013171	0.785366
0.330	1.0002E+06	2.7469E+02	1.013097	0.785506
0.335	1.0002E+06	8.5505E+01	1.013123	0.785457
0.340	1.0002E+06	1.3392E+02	1.013112	0.785477
0.345	1.0002E+06	1.2109E+02	1.012896	0.785882
0.350	1.0002E+06	2.9941E+02	1.012989	0.785710
0.355	1.0002E+06	1.0915E+02	1.012952	0.785779
0.360	1.0002E+06	1.7054E+02	1.012962	0.785760
0.365	1.0002E+06	1.5458E+02	1.013232	0.785249
0.370	1.0002E+06	3.8215E+02	1.013113	0.785476
0.375	1.0002E+06	1.3925E+02	1.013156	0.785394
0.380	1.0002E+06	2.1910E+02	1.013140	0.785425
0.385	1.0002E+06	1.9719E+02	1.012791	0.786082
0.390	1.0002E+06	4.8760E+02	1.012941	0.785801
0.395	1.0002E+06	1.7776E+02	1.012882	0.785911
0.400	1.0002E+06	2.7838E+02	1.012899	0.785879
0.405	1.0002E+06	2.5175E+02	1.013340	0.785045
0.410	1.0002E+06	6.2238E+02	1.013146	0.785412
0.415	1.0002E+06	2.2678E+02	1.013217	0.785277
0.420	1.0002E+06	3.5521E+02	1.013192	0.785325
0.425	1.0002E+06	3.2116E+02	1.012626	0.786395
0.430	1.0002E+06	7.9411E+02	1.012870	0.785934
0.435	1.0002E+06	2.8950E+02	1.012775	0.786113
0.440	1.0002E+06	4.5335E+02	1.012804	0.786058
0.445	1.0002E+06	4.0994E+02	1.013522	0.784699
0.450	1.0002E+06	1.0136E+03	1.013208	0.785294
0.455	1.0002E+06	3.6935E+02	1.013325	0.785072
0.460	1.0002E+06	5.7849E+02	1.013265	0.785149
0.465	1.0002E+06	5.2308E+02	1.012364	0.786889
0.470	1.0002E+06	1.2932E+03	1.012762	0.786137
0.475	1.0002E+06	4.7145E+02	1.012609	0.786426
0.480	1.0002E+06	7.3824E+02	1.012656	0.786335
0.485	1.0002E+06	6.6759E+02	1.013828	0.784120
0.490	1.0002E+06	1.6507E+03	1.013317	0.785088
0.495	1.0002E+06	6.0142E+02	1.013509	0.784725
0.500	1.0002E+06	9.4206E+02	1.013443	0.784848

Table 3.2a

Outer Loop Bias Control of a Fixed Boresight Error, With a
Servo Stability Factor of $\alpha = 8$, and a $\tau_0 = 20$ msec Update
Time

TIME (SEC.)	RANGE (METERS)	MISS DISTANCE (METERS)	THETA (RAD.)	PHI (RAD.)
0.005	1.0000E+06	6.5445E+02	1.013155	0.785400
0.010	1.0000E+06	6.5091E+01	1.013153	0.785404
0.015	1.0000E+06	6.5233E+01	1.013151	0.785406
0.020	1.0000E+06	6.5177E+01	1.013150	0.785409
0.025	1.0000E+06	6.5187E+01	1.013090	0.785358
0.030	1.0000E+06	1.1979E+01	1.013113	0.785384
0.035	1.0000E+06	2.2716E+01	1.013102	0.785379
0.040	1.0000E+06	1.1545E+01	1.013104	0.785384
0.045	1.0000E+06	1.4481E+01	1.013091	0.785377
0.050	1.0000E+06	3.5733E-01	1.013094	0.785384
0.055	1.0000E+06	6.4042E+00	1.013091	0.785386
0.060	1.0001E+06	4.5552E+00	1.013090	0.785389
0.065	1.0001E+06	4.9590E+00	1.013085	0.785388
0.070	1.0001E+06	4.4709E-01	1.013085	0.785393
0.075	1.0001E+06	1.9452E+00	1.013083	0.785395
0.080	1.0001E+06	1.1906E+00	1.013081	0.785398
0.085	1.0001E+06	1.7719E+00	1.013079	0.785400
0.090	1.0001E+06	5.2987E-02	1.013078	0.785403
0.095	1.0001E+06	5.6602E-01	1.013076	0.785406
0.100	1.0001E+06	3.7132E-01	1.013075	0.785409
0.105	1.0001E+06	4.1773E-01	1.013073	0.785412
0.110	1.0001E+06	4.9411E-02	1.013071	0.785415
0.115	1.0001E+06	1.6701E-01	1.013070	0.785418
0.120	1.0001E+06	1.1822E-01	1.013068	0.785421
0.125	1.0001E+06	1.1771E-01	1.013067	0.785423
0.130	1.0001E+06	3.2212E-02	1.013065	0.785426
0.135	1.0001E+06	4.6219E-02	1.013064	0.785429
0.140	1.0001E+06	5.0024E-02	1.013062	0.785432
0.145	1.0001E+06	4.8159E-02	1.013061	0.785435
0.150	1.0001E+06	3.4054E-02	1.013059	0.785438
0.155	1.0001E+06	2.8152E-02	1.013058	0.785441
0.160	1.0001E+06	2.4705E-02	1.013056	0.785444
0.165	1.0001E+06	3.6644E-02	1.013055	0.785447
0.170	1.0001E+06	3.9876E-02	1.013053	0.785450
0.175	1.0001E+06	3.2212E-02	1.013052	0.785453
0.180	1.0001E+06	3.8273E-02	1.013050	0.785456
0.185	1.0001E+06	2.9232E-02	1.013049	0.785459
0.190	1.0001E+06	2.9232E-02	1.013047	0.785461
0.195	1.0001E+06	3.4739E-02	1.013046	0.785464
0.200	1.0001E+06	1.9137E-02	1.013044	0.785467
0.205	1.0001E+06	1.9137E-02	1.013043	0.785470
0.210	1.0001E+06	2.8158E-02	1.013041	0.785473
0.215	1.0001E+06	3.6644E-02	1.013040	0.785476
0.220	1.0001E+06	2.8158E-02	1.013038	0.785479
0.225	1.0001E+06	3.2212E-02	1.013037	0.785482
0.230	1.0001E+06	4.5554E-02	1.013035	0.785485
0.235	1.0001E+06	4.5554E-02	1.013034	0.785488
0.240	1.0001E+06	4.4879E-02	1.013032	0.785491
0.245	1.0001E+06	3.4054E-02	1.013031	0.785494

Table 2a (Continued)

Page 2

0.250	1.0001E+06	3.5801E-02	1.013029	0.785497
0.255	1.0001E+06	2.9232E-02	1.013028	0.785500
0.260	1.0001E+06	3.4939E-02	1.013026	0.785502
0.265	1.0001E+06	4.5554E-02	1.013025	0.785505
0.270	1.0001E+06	3.5801E-02	1.013023	0.785508
0.275	1.0001E+06	3.2212E-02	1.013022	0.785511
0.280	1.0001E+06	3.3146E-02	1.013020	0.785514
0.285	1.0001E+06	2.3438E-02	1.013019	0.785517
0.290	1.0002E+06	3.5801E-02	1.013017	0.785520
0.295	1.0002E+06	3.9836E-02	1.013016	0.785523
0.300	1.0002E+06	3.2212E-02	1.013014	0.785526
0.305	1.0002E+06	3.2212E-02	1.013013	0.785529
0.310	1.0002E+06	3.4939E-02	1.013011	0.785532
0.315	1.0002E+06	3.2212E-02	1.013010	0.785535
0.320	1.0002E+06	2.9232E-02	1.013008	0.785538
0.325	1.0002E+06	3.9063E-02	1.013007	0.785541
0.330	1.0002E+06	3.4054E-02	1.013005	0.785543
0.335	1.0002E+06	3.6644E-02	1.013004	0.785546
0.340	1.0002E+06	3.2212E-02	1.013002	0.785549
0.345	1.0002E+06	3.6644E-02	1.013001	0.785552
0.350	1.0002E+06	2.9232E-02	1.012999	0.785555
0.355	1.0002E+06	2.2097E-02	1.012998	0.785558
0.360	1.0002E+06	3.6644E-02	1.012996	0.785561
0.365	1.0002E+06	2.5911E-02	1.012995	0.785564
0.370	1.0002E+06	3.4939E-02	1.012993	0.785567
0.375	1.0002E+06	3.2212E-02	1.012992	0.785570
0.380	1.0002E+06	1.7469E-02	1.012990	0.785573
0.385	1.0002E+06	2.5911E-02	1.012989	0.785576
0.390	1.0002E+06	2.9232E-02	1.012987	0.785579
0.395	1.0002E+06	3.2212E-02	1.012986	0.785582
0.400	1.0002E+06	3.2212E-02	1.012984	0.785584
0.405	1.0002E+06	2.3438E-02	1.012983	0.785587
0.410	1.0002E+06	3.3146E-02	1.012981	0.785590
0.415	1.0002E+06	3.2212E-02	1.012980	0.785593
0.420	1.0002E+06	2.8168E-02	1.012978	0.785596
0.425	1.0002E+06	3.2212E-02	1.012977	0.785599
0.430	1.0002E+06	3.4054E-02	1.012975	0.785602
0.435	1.0002E+06	2.8168E-02	1.012974	0.785605
0.440	1.0002E+06	3.4054E-02	1.012972	0.785608
0.445	1.0002E+06	2.3438E-02	1.012971	0.785611
0.450	1.0002E+06	2.3438E-02	1.012969	0.785614
0.455	1.0002E+06	4.2072E-02	1.012968	0.785617
0.460	1.0002E+06	3.2212E-02	1.012966	0.785620
0.465	1.0002E+06	1.9137E-02	1.012965	0.785623
0.470	1.0002E+06	1.9137E-02	1.012963	0.785625
0.475	1.0002E+06	4.0595E-02	1.012962	0.785628
0.480	1.0002E+06	3.5801E-02	1.012960	0.785631
0.485	1.0002E+06	2.3438E-02	1.012959	0.785634
0.490	1.0002E+06	3.5801E-02	1.012957	0.785637
0.495	1.0002E+06	3.2212E-02	1.012956	0.785640
0.500	1.0002E+06	2.5911E-02	1.012954	0.785643

AD-A055 177

OPTICAL SCIENCES CO PLACENTIA CA
ADAPTIVE COMPENSATION TECHNIQUES.(U)

F/G 17/8

UNCLASSIFIED

MAY 78 D L FRIED, E J SCHONHEINZ, R B ASHER

F30602-77-C-0099

DR-105

RADC-TR-78-101

NL

2 OF 5
AD
A055177



Table 3.2b

Outer Loop Bias Control of a Fixed Boresight Error, With a
Servo Stability Factor of $\alpha = 6$, and a $\tau_0 = 20$ msec Update
Time

TIME (SEC.)	RANGE (METERS)	MISS DISTANCE (METERS)	THETA (RAD.)	PHI (RAD.)
0.005	1.0000E+06	2.8851E+02	1.013155	0.785403
0.010	1.0000E+06	6.5091E+01	1.013153	0.785404
0.015	1.0000E+06	6.5273E+01	1.013151	0.785406
0.020	1.0000E+06	6.5177E+01	1.013150	0.785409
0.025	1.0000E+06	6.5187E+01	1.013070	0.785340
0.030	1.0000E+06	3.7628E+01	1.013102	0.785374
0.035	1.0000E+06	8.5672E+00	1.013089	0.785366
0.040	1.0000E+06	6.7392E+00	1.013091	0.785372
0.045	1.0000E+06	2.4281E+00	1.013096	0.785381
0.050	1.0000E+06	6.9563E+00	1.013091	0.785381
0.055	1.0000E+06	2.3250E+00	1.013091	0.785385
0.060	1.0001E+06	3.9748E+00	1.013089	0.785388
0.065	1.0001E+06	3.4764E+00	1.013083	0.785386
0.070	1.0001E+06	2.6313E+00	1.013083	0.785391
0.075	1.0001E+06	1.1771E-01	1.013081	0.785393
0.080	1.0001E+06	8.0469E-01	1.013080	0.785397
0.085	1.0001E+06	5.4520E-01	1.013079	0.785400
0.090	1.0001E+06	6.7618E-01	1.013077	0.785403
0.095	1.0001E+06	1.0910E-01	1.013076	0.785406
0.100	1.0001E+06	2.9555E-01	1.013074	0.785409
0.105	1.0001E+06	2.4054E-01	1.013073	0.785411
0.110	1.0001E+06	2.2371E-01	1.013071	0.785415
0.115	1.0001E+06	2.5911E-02	1.013070	0.785417
0.120	1.0001E+06	7.6944E-02	1.013068	0.785420
0.125	1.0001E+06	7.0745E-02	1.013067	0.785423
0.130	1.0001E+06	7.4116E-02	1.013065	0.785426
0.135	1.0001E+06	4.0595E-02	1.013064	0.785429
0.140	1.0001E+06	3.3146E-02	1.013062	0.785432
0.145	1.0001E+06	4.0555E-02	1.013061	0.785435
0.150	1.0001E+06	3.5801E-02	1.013059	0.785438
0.155	1.0001E+06	3.6644E-02	1.013058	0.785441
0.160	1.0001E+06	3.9836E-02	1.013056	0.785444
0.165	1.0001E+06	4.4979E-02	1.013055	0.785447
0.170	1.0001E+06	3.2212E-02	1.013053	0.785450
0.175	1.0001E+06	3.2212E-02	1.013052	0.785453
0.180	1.0001E+06	2.4705E-02	1.013050	0.785456
0.185	1.0001E+06	2.7063E-02	1.013049	0.785459
0.190	1.0001E+06	3.4054E-02	1.013047	0.785461
0.195	1.0001E+06	3.5801E-02	1.013046	0.785464
0.200	1.0001E+06	2.7478E-02	1.013044	0.785467
0.205	1.0001E+06	2.5911E-02	1.013043	0.785470
0.210	1.0001E+06	3.3146E-02	1.013041	0.785473
0.215	1.0001E+06	3.2212E-02	1.013040	0.785476
0.220	1.0001E+06	2.5168E-02	1.013038	0.785479
0.225	1.0001E+06	2.2097E-02	1.013037	0.785482
0.230	1.0001E+06	3.6644E-02	1.013035	0.785485
0.235	1.0001E+06	4.6875E-02	1.013034	0.785488
0.240	1.0001E+06	2.5911E-02	1.013032	0.785491
0.245	1.0001E+06	3.6644E-02	1.013031	0.785494

Table 2b (Continued)

Page 2

0.250	1.0001E+06	3.4939E-02	1.013029	0.785497
0.255	1.0001E+06	2.9232E-02	1.013028	0.785500
0.260	1.0001E+06	3.6644E-02	1.013026	0.785502
0.265	1.0001E+06	2.3438E-02	1.013025	0.785505
0.270	1.0001E+06	2.7063E-02	1.013023	0.785508
0.275	1.0001E+06	3.2212E-02	1.013022	0.785511
0.280	1.0001E+06	3.6644E-02	1.013020	0.785514
0.285	1.0001E+06	2.8168E-02	1.013019	0.785517
0.290	1.0002E+06	4.6219E-02	1.013017	0.785520
0.295	1.0002E+06	1.9137E-02	1.013016	0.785523
0.300	1.0002E+06	3.2212E-02	1.013014	0.785526
0.305	1.0002E+06	3.6644E-02	1.013013	0.785529
0.310	1.0002E+06	3.6644E-02	1.013011	0.785532
0.315	1.0002E+06	3.2212E-02	1.013010	0.785535
0.320	1.0002E+06	2.9232E-02	1.013008	0.785538
0.325	1.0002E+06	2.3438E-02	1.013007	0.785541
0.330	1.0002E+06	2.8168E-02	1.013005	0.785543
0.335	1.0002E+06	3.6644E-02	1.013004	0.785546
0.340	1.0002E+06	2.9232E-02	1.013002	0.785549
0.345	1.0002E+06	1.9137E-02	1.013001	0.785552
0.350	1.0002E+06	3.7146E-02	1.012999	0.785555
0.355	1.0002E+06	3.4054E-02	1.012998	0.785558
0.360	1.0002E+06	2.9232E-02	1.012996	0.785561
0.365	1.0002E+06	2.3438E-02	1.012995	0.785564
0.370	1.0002E+06	3.7146E-02	1.012993	0.785567
0.375	1.0002E+06	3.6644E-02	1.012992	0.785570
0.380	1.0002E+06	2.9232E-02	1.012990	0.785573
0.385	1.0002E+06	2.2097E-02	1.012989	0.785576
0.390	1.0002E+06	3.9836E-02	1.012987	0.785579
0.395	1.0002E+06	3.2212E-02	1.012986	0.785582
0.400	1.0002E+06	3.2212E-02	1.012984	0.785584
0.405	1.0002E+06	3.8273E-02	1.012983	0.785587
0.410	1.0002E+06	2.9232E-02	1.012981	0.785590
0.415	1.0002E+06	3.6644E-02	1.012980	0.785593
0.420	1.0002E+06	4.2072E-02	1.012978	0.785596
0.425	1.0002E+06	3.2212E-02	1.012977	0.785599
0.430	1.0002E+06	5.0024E-02	1.012975	0.785602
0.435	1.0002E+06	2.8168E-02	1.012974	0.785605
0.440	1.0002E+06	3.2212E-02	1.012972	0.785608
0.445	1.0002E+06	1.9137E-02	1.012971	0.785611
0.450	1.0002E+06	2.3438E-02	1.012969	0.785614
0.455	1.0002E+06	4.0595E-02	1.012968	0.785617
0.460	1.0002E+06	3.5301E-02	1.012966	0.785620
0.465	1.0002E+06	2.5311E-02	1.012965	0.785623
0.470	1.0002E+06	3.9063E-02	1.012963	0.785625
0.475	1.0002E+06	4.0595E-02	1.012962	0.785628
0.480	1.0002E+06	1.9137E-02	1.012960	0.785631
0.485	1.0002E+06	1.7469E-02	1.012959	0.785634
0.490	1.0002E+06	4.0595E-02	1.012957	0.785637
0.495	1.0002E+06	2.9232E-02	1.012956	0.785640
0.500	1.0002E+06	2.8168E-02	1.012954	0.785643

Table 3.2c

Outer Loop Bias Control of a Fixed Boresight Error, With a
Servo Stability Factor of $\alpha = 4$, and a $\tau_p = 20$ msec Update
Time

TIME (SEC.)	RANGE (METERS)	MISS DISTANCE (METERS)	THETA (RAD.)	PHI (RAD.)
0.005	1.0000E+06	2.8850E+02	1.013155	0.785400
0.010	1.0000E+06	6.5091E+01	1.013153	0.785404
0.015	1.0000E+06	6.5273E+01	1.013151	0.785406
0.020	1.0000E+06	6.5177E+01	1.013150	0.785409
0.025	1.0000E+06	6.5107E+01	1.013031	0.785305
0.030	1.0000E+06	9.5051E+01	1.013080	0.785354
0.035	1.0000E+06	1.9761E+01	1.013060	0.785339
0.040	1.0000E+06	4.2081E+01	1.013064	0.785348
0.045	1.0000E+06	3.6242E+01	1.013137	0.785419
0.050	1.0000E+06	6.2436E+01	1.013103	0.785392
0.055	1.0000E+06	1.7488E+01	1.013114	0.785406
0.060	1.0001E+06	3.2186E+01	1.013108	0.785405
0.065	1.0001E+06	2.8234E+01	1.013050	0.785356
0.070	1.0001E+06	4.7261E+01	1.013073	0.785382
0.075	1.0001E+06	1.2941E+01	1.013062	0.785376
0.080	1.0001E+06	2.4138E+01	1.013064	0.785382
0.085	1.0001E+06	2.1142E+01	1.013105	0.785424
0.090	1.0001E+06	3.5474E+01	1.013085	0.785410
0.095	1.0001E+06	9.7265E+00	1.013090	0.785419
0.100	1.0001E+06	1.8134E+01	1.013087	0.785420
0.105	1.0001E+06	1.5892E+01	1.013053	0.785394
0.110	1.0001E+06	2.6637E+01	1.013066	0.785409
0.115	1.0001E+06	7.3115E+00	1.013059	0.785407
0.120	1.0001E+06	1.3635E+01	1.013059	0.785412
0.125	1.0001E+06	1.1928E+01	1.013092	0.785437
0.130	1.0001E+06	2.0045E+01	1.013070	0.785430
0.135	1.0001E+06	5.5049E+00	1.013072	0.785437
0.140	1.0001E+06	1.0254E+01	1.013069	0.785439
0.145	1.0001E+06	8.9817E+00	1.013050	0.785425
0.150	1.0001E+06	1.5066E+01	1.013056	0.785435
0.155	1.0001E+06	4.1229E+00	1.013052	0.785435
0.160	1.0001E+06	7.7162E+00	1.013051	0.785439
0.165	1.0001E+06	6.7469E+00	1.013063	0.785454
0.170	1.0001E+06	1.1352E+01	1.013056	0.785452
0.175	1.0001E+06	3.1302E+00	1.013057	0.785457
0.180	1.0001E+06	5.8047E+00	1.013054	0.785459
0.185	1.0001E+06	5.0255E+00	1.013043	0.785453
0.190	1.0001E+06	8.5157E+00	1.013046	0.785460
0.195	1.0001E+06	2.7346E+00	1.013042	0.785461
0.200	1.0001E+06	4.3464E+00	1.013041	0.785465
0.205	1.0001E+06	3.8100E+00	1.013048	0.785475
0.210	1.0001E+06	6.3816E+00	1.013043	0.785474
0.215	1.0001E+06	1.7453E+00	1.013042	0.785479
0.220	1.0001E+06	3.2510E+00	1.013041	0.785481
0.225	1.0001E+06	2.8547E+00	1.013033	0.785479
0.230	1.0001E+06	4.7752E+00	1.013034	0.785484
0.235	1.0001E+06	1.2992E+00	1.013032	0.785486
0.240	1.0001E+06	2.4779E+00	1.013031	0.785488
0.245	1.0001E+06	2.1750E+00	1.013033	0.785496

Table 2c (Continued)

0.250	1.0001E+06	3.5709E+00	1.013030	0.785497
0.255	1.0001E+06	9.9022E-01	1.013029	0.785501
0.260	1.0001E+06	1.8183E+00	1.013028	0.785504
0.265	1.0001E+06	1.6053E+00	1.013023	0.785504
0.270	1.0001E+06	2.6647E+00	1.013023	0.785508
0.275	1.0001E+06	7.2134E-01	1.013021	0.785510
0.280	1.0001E+06	1.3497E+00	1.013019	0.785513
0.285	1.0001E+06	1.1906E+00	1.013020	0.785519
0.290	1.0002E+06	1.9800E+00	1.013018	0.785520
0.295	1.0002E+06	5.3079E-01	1.013017	0.785524
0.300	1.0002E+06	1.0092E+00	1.013015	0.785527
0.305	1.0002E+06	8.8312E-01	1.013012	0.785528
0.310	1.0002E+06	1.4834E+00	1.013011	0.785531
0.315	1.0002E+06	4.0767E-01	1.013009	0.785534
0.320	1.0002E+06	7.6203E-01	1.013008	0.785537
0.325	1.0002E+06	6.6429E-01	1.013008	0.785541
0.330	1.0002E+06	1.1180E+00	1.013006	0.785544
0.335	1.0002E+06	3.0857E-01	1.013004	0.785547
0.340	1.0002E+06	5.7101E-01	1.013003	0.785550
0.345	1.0002E+06	5.0570E-01	1.013000	0.785552
0.350	1.0002E+06	8.2742E-01	1.012999	0.785555
0.355	1.0002E+06	2.7189E-01	1.012993	0.785558
0.360	1.0002E+06	4.2919E-01	1.012996	0.785561
0.365	1.0002E+06	3.7091E-01	1.012995	0.785564
0.370	1.0002E+06	6.2914E-01	1.012993	0.785567
0.375	1.0002E+06	1.8750E-01	1.012992	0.785570
0.380	1.0002E+06	3.1840E-01	1.012991	0.785573
0.385	1.0002E+06	2.8779E-01	1.012989	0.785575
0.390	1.0002E+06	4.6463E-01	1.012987	0.785579
0.395	1.0002E+06	1.1213E-01	1.012986	0.785581
0.400	1.0002E+06	2.7515E-01	1.012984	0.785584
0.405	1.0002E+06	2.1166E-01	1.012983	0.785588
0.410	1.0002E+06	3.4419E-01	1.012981	0.785590
0.415	1.0002E+06	1.1213E-01	1.012980	0.785593
0.420	1.0002E+06	1.7712E-01	1.012978	0.785596
0.425	1.0002E+06	1.5586E-01	1.012977	0.785599
0.430	1.0002E+06	2.5303E-01	1.012975	0.785602
0.435	1.0002E+06	7.2028E-02	1.012974	0.785605
0.440	1.0002E+06	1.3096E-01	1.012972	0.785608
0.445	1.0002E+06	1.1719E-01	1.012971	0.785611
0.450	1.0002E+06	1.9390E-01	1.012969	0.785614
0.455	1.0002E+06	7.7703E-02	1.012968	0.785617
0.460	1.0002E+06	1.0066E-01	1.012966	0.785620
0.465	1.0002E+06	8.7695E-02	1.012965	0.785622
0.470	1.0002E+06	1.4427E-01	1.012963	0.785625
0.475	1.0002E+06	5.1230E-02	1.012962	0.785628
0.480	1.0002E+06	8.3780E-02	1.012960	0.785631
0.485	1.0002E+06	7.1175E-02	1.012959	0.785634
0.490	1.0002E+06	1.2027E-01	1.012957	0.785637
0.495	1.0002E+06	4.2791E-02	1.012956	0.785640
0.500	1.0002E+06	6.0009E-02	1.012954	0.785643

Table 3.2d

Outer Loop Bias Control of a Fixed Boresight Error, With a
 Servo Stability Factor of $\alpha = 3$, and a $\tau_0 = 20$ msec Update
 Time

TIME (SEC.)	RANGE (METERS)	MISS DISTANCE (METERS)	THETA (RAD.)	PHI (RAD.)
0.005	1.0000E+06	2.8850E+02	1.013155	0.785400
0.010	1.0000E+06	6.5091E+01	1.013153	0.785404
0.015	1.0000E+06	6.5233E+01	1.013151	0.785406
0.020	1.0000E+06	6.5177E+01	1.013150	0.785409
0.025	1.0000E+06	6.5187E+01	1.012992	0.785269
0.030	1.0000E+06	1.4046E+02	1.013058	0.785334
0.035	1.0000E+06	4.8064E+01	1.013031	0.785313
0.040	1.0000E+06	7.7845E+01	1.013038	0.785324
0.045	1.0000E+06	7.0951E+01	1.013221	0.785495
0.050	1.0000E+06	1.7436E+02	1.013139	0.785425
0.055	1.0000E+06	6.3714E+01	1.013168	0.785456
0.060	1.0001E+06	9.9661E+01	1.013157	0.785449
0.065	1.0001E+06	9.0133E+01	1.012919	0.785236
0.070	1.0001E+06	2.2277E+02	1.013020	0.785333
0.075	1.0001E+06	8.1189E+01	1.012979	0.785300
0.080	1.0001E+06	1.2716E+02	1.012991	0.785315
0.085	1.0001E+06	1.1498E+02	1.013291	0.785594
0.090	1.0001E+06	2.8426E+02	1.013158	0.785477
0.095	1.0001E+06	1.0760E+02	1.013206	0.785525
0.100	1.0001E+06	1.6227E+02	1.013189	0.785513
0.105	1.0001E+06	1.4672E+02	1.012802	0.785164
0.110	1.0001E+06	3.6274E+02	1.012968	0.785320
0.115	1.0001E+06	1.3223E+02	1.012903	0.785265
0.120	1.0001E+06	2.0708E+02	1.012922	0.785287
0.125	1.0001E+06	1.8725E+02	1.013412	0.785739
0.130	1.0001E+06	4.6295E+02	1.013197	0.785547
0.135	1.0001E+06	1.6873E+02	1.013277	0.785624
0.140	1.0001E+06	2.6428E+02	1.013248	0.785602
0.145	1.0001E+06	3.3895E+02	1.012620	0.785032
0.150	1.0001E+06	5.9080E+02	1.012991	0.785284
0.155	1.0001E+06	2.1537E+02	1.012786	0.785192
0.160	1.0001E+06	3.7288E+02	1.012819	0.785227
0.165	1.0001E+06	3.0496E+02	1.013617	0.785962
0.170	1.0001E+06	7.5405E+02	1.013268	0.785646
0.175	1.0001E+06	2.7483E+02	1.013398	0.785770
0.180	1.0001E+06	4.7045E+02	1.013353	0.785733
0.185	1.0001E+06	3.8921E+02	1.012331	0.784302
0.190	1.0001E+06	9.6223E+02	1.012773	0.785211
0.195	1.0001E+06	3.5078E+02	1.012604	0.785060
0.200	1.0001E+06	5.4935E+02	1.012658	0.785113
0.205	1.0001E+06	4.9671E+02	1.013959	0.785309
0.210	1.0001E+06	1.2282E+03	1.013391	0.785793
0.215	1.0001E+06	4.4762E+02	1.013604	0.785993
0.220	1.0001E+06	7.0109E+02	1.013532	0.785931
0.225	1.0001E+06	6.3391E+02	1.011267	0.784412
0.230	1.0001E+06	1.5672E+03	1.012589	0.785076
0.235	1.0001E+06	5.7136E+02	1.012313	0.784629
0.240	1.0001E+06	8.9471E+02	1.012402	0.784914
0.245	1.0001E+06	8.0904E+02	1.014523	0.786260

Table 2d (Continued)

0.250	1.0001E+06	2.0006E+03	1.013599	0.786017
0.255	1.0001E+06	7.2897E+02	1.013947	0.786341
0.260	1.0001E+06	1.1418E+03	1.013830	0.786233
0.265	1.0001E+06	1.0324E+03	1.011120	0.783764
0.270	1.0001E+06	2.5522E+03	1.012297	0.784843
0.275	1.0001E+06	9.3059E+02	1.011849	0.784433
0.280	1.0001E+06	1.4572E+03	1.011994	0.784575
0.285	1.0001E+06	1.3176E+03	1.015448	0.787743
0.290	1.0002E+06	3.2585E+03	1.013944	0.786368
0.295	1.0002E+06	1.1871E+03	1.014512	0.786893
0.300	1.0002E+06	1.8596E+03	1.014323	0.786724
0.305	1.0002E+06	1.6814E+03	1.009909	0.782693
0.310	1.0002E+06	4.1561E+03	1.011829	0.784447
0.315	1.0002E+06	1.5158E+03	1.011099	0.783786
0.320	1.0002E+06	2.3732E+03	1.011337	0.784003
0.325	1.0002E+06	2.1460E+03	1.015961	0.789168
0.330	1.0002E+06	5.3078E+03	1.014915	0.786923
0.335	1.0002E+06	1.9371E+03	1.015440	0.787779
0.340	1.0002E+06	3.0287E+03	1.015133	0.787501
0.345	1.0002E+06	2.7383E+03	1.007944	0.780936
0.350	1.0002E+06	6.7675E+03	1.011073	0.783783
0.355	1.0002E+06	2.4691E+03	1.009885	0.782711
0.360	1.0002E+06	3.8650E+03	1.010274	0.783071
0.365	1.0002E+06	3.4952E+03	1.019430	0.791478
0.370	1.0002E+06	8.6467E+03	1.015452	0.787812
0.375	1.0002E+06	3.1475E+03	1.016958	0.789206
0.380	1.0002E+06	4.9326E+03	1.016459	0.788752
0.385	1.0002E+06	4.4595E+03	1.004747	0.778066
0.390	1.0002E+06	1.1018E+04	1.009851	0.782696
0.395	1.0002E+06	4.0224E+03	1.007914	0.780945
0.400	1.0002E+06	6.2944E+03	1.008549	0.781528
0.405	1.0002E+06	5.6927E+03	1.023452	0.795232
0.410	1.0002E+06	1.4028E+04	1.016926	0.789240
0.415	1.0002E+06	5.1241E+03	1.019436	0.791517
0.420	1.0002E+06	8.0333E+03	1.018624	0.790774
0.425	1.0002E+06	7.2623E+03	0.999536	0.773392
0.430	1.0002E+06	1.7974E+04	1.007869	0.780896
0.435	1.0002E+06	6.5540E+03	1.004707	0.778057
0.440	1.0002E+06	1.0251E+04	1.005743	0.779003
0.445	1.0002E+06	9.2719E+03	1.029995	0.801352
0.450	1.0002E+06	2.2958E+04	1.019493	0.791540
0.455	1.0002E+06	8.3395E+03	1.023472	0.795266
0.460	1.0002E+06	1.3083E+04	1.022151	0.794052
0.465	1.0002E+06	1.1326E+04	0.991025	0.765804
0.470	1.0002E+06	2.9180E+04	1.004652	0.777934
0.475	1.0002E+06	1.0692E+04	0.959482	0.773344
0.480	1.0002E+06	1.6692E+04	1.001173	0.774376
0.485	1.0002E+06	1.5102E+04	1.040618	0.811353
0.490	1.0002E+06	3.7425E+04	1.023563	0.795243
0.495	1.0002E+06	1.3566E+04	1.030041	0.801359
0.500	1.0002E+06	2.1305E+04	1.027891	0.799376

Table 3.3a

Outer Loop Bias Control of a Time-Dependent Boresight Error, With a
Servo Stability Factor of $\alpha = 6$, and a $\tau_0 = 20$ msec Update Time

This table is identical to Table 1b, and so is
not repeated here.

Table 3.3b

Outer Loop Bias Control of a Time-Dependent Boresight Error, With a Servo Stability Factor of $\alpha = 6$, and a $\tau_p = 40$ msec Update Time

TIME (SEC.)	RANGE (METERS)	MISS DISTANCE (METERS)	THETA (RAD.)	PHI (RAD.)
0.010	1.0000E+06	3.5649E+00	1.013153	0.785404
0.020	1.0000E+06	2.7930E+00	1.013150	0.785409
0.030	1.0000E+06	2.6835E+00	1.013147	0.785415
0.040	1.0000E+06	2.6655E+00	1.013144	0.785421
0.050	1.0000E+06	1.6452E+00	1.013139	0.785429
0.060	1.0001E+06	3.6217E-01	1.013136	0.785435
0.070	1.0001E+06	4.1044E-01	1.013133	0.785441
0.080	1.0001E+06	5.4693E-01	1.013130	0.785447
0.090	1.0001E+06	1.9184E-01	1.013127	0.785452
0.100	1.0001E+06	2.2111E-01	1.013124	0.785458
0.110	1.0001E+06	3.6048E-01	1.013121	0.785464
0.120	1.0001E+06	4.9318E-01	1.013118	0.785470
0.130	1.0001E+06	1.5468E-01	1.013114	0.785475
0.140	1.0001E+06	2.1036E-01	1.013111	0.785481
0.150	1.0001E+06	3.6752E-01	1.013108	0.785487
0.160	1.0001E+06	4.9126E-01	1.013105	0.785493
0.170	1.0001E+06	1.4106E-01	1.013102	0.785498
0.180	1.0001E+06	2.2670E-01	1.013099	0.785504
0.190	1.0001E+06	3.9078E-01	1.013096	0.785510
0.200	1.0001E+06	5.2530E-01	1.013093	0.785516
0.210	1.0001E+06	1.8455E-01	1.013089	0.785521
0.220	1.0001E+06	1.9562E-01	1.013086	0.785527
0.230	1.0001E+06	3.5673E-01	1.013083	0.785533
0.240	1.0001E+06	5.0546E-01	1.013080	0.785539
0.250	1.0001E+06	1.8003E-01	1.013077	0.785544
0.260	1.0001E+06	2.0101E-01	1.013074	0.785550
0.270	1.0001E+06	3.6752E-01	1.013071	0.785556
0.280	1.0001E+06	4.7688E-01	1.013068	0.785562
0.290	1.0002E+06	1.3755E-01	1.013065	0.785567
0.300	1.0002E+06	2.2791E-01	1.013062	0.785573
0.310	1.0002E+06	3.9078E-01	1.013059	0.785579
0.320	1.0002E+06	5.1693E-01	1.013056	0.785585
0.330	1.0002E+06	1.6276E-01	1.013052	0.785590
0.340	1.0002E+06	2.1791E-01	1.013049	0.785596
0.350	1.0002E+06	3.5852E-01	1.013046	0.785602
0.360	1.0002E+06	4.9712E-01	1.013043	0.785608
0.370	1.0002E+06	1.6332E-01	1.013040	0.785613
0.380	1.0002E+06	2.1166E-01	1.013037	0.785619
0.390	1.0002E+06	3.6926E-01	1.013034	0.785625
0.400	1.0002E+06	5.0643E-01	1.013031	0.785631
0.410	1.0002E+06	1.6276E-01	1.013027	0.785636
0.420	1.0002E+06	2.0655E-01	1.013024	0.785642
0.430	1.0002E+06	3.7459E-01	1.013021	0.785648
0.440	1.0002E+06	4.8532E-01	1.013018	0.785654
0.450	1.0003E+06	1.5249E-01	1.013015	0.785659
0.460	1.0002E+06	2.2215E-01	1.013012	0.785665
0.470	1.0002E+06	3.7459E-01	1.013009	0.785671
0.480	1.0002E+06	5.1474E-01	1.013006	0.785677
0.490	1.0002E+06	1.8504E-01	1.013003	0.785683

Table 3b (Continued)

0.500	1.0002E+06	2.2440E-01	1.013000	0.785689
0.510	1.0002E+06	3.7832E-01	1.012997	0.785694
0.520	1.0003E+06	4.9595E-01	1.012994	0.785700
0.530	1.0003E+06	1.5169E-01	1.012990	0.785706
0.540	1.0003E+06	2.2991E-01	1.012987	0.785711
0.550	1.0003E+06	3.9078E-01	1.012984	0.785717
0.560	1.0003E+06	5.1975E-01	1.012981	0.785723
0.570	1.0003E+06	1.6425E-01	1.012978	0.785729
0.580	1.0003E+06	2.2111E-01	1.012975	0.785734
0.590	1.0003E+06	3.7283E-01	1.012972	0.785740
0.600	1.0003E+06	4.9150E-01	1.012969	0.785746
0.610	1.0003E+06	1.4926E-01	1.012966	0.785752
0.620	1.0003E+06	2.2871E-01	1.012962	0.785757
0.630	1.0003E+06	3.7832E-01	1.012959	0.785763
0.640	1.0003E+06	5.1290E-01	1.012957	0.785769
0.650	1.0003E+06	1.7364E-01	1.012953	0.785775
0.660	1.0003E+06	2.1224E-01	1.012950	0.785780
0.670	1.0003E+06	3.6926E-01	1.012947	0.785786
0.680	1.0003E+06	4.8902E-01	1.012944	0.785792
0.690	1.0003E+06	1.4063E-01	1.012941	0.785798
0.700	1.0003E+06	2.3189E-01	1.012938	0.785803
0.710	1.0003E+06	3.9304E-01	1.012935	0.785809
0.720	1.0003E+06	5.1290E-01	1.012932	0.785815
0.730	1.0003E+06	1.6919E-01	1.012928	0.785821
0.740	1.0003E+06	2.2235E-01	1.012925	0.785826
0.750	1.0004E+06	3.7143E-01	1.012922	0.785832
0.760	1.0004E+06	4.8071E-01	1.012919	0.785838
0.770	1.0004E+06	1.3003E-01	1.012916	0.785844
0.780	1.0004E+06	2.4472E-01	1.012913	0.785850
0.790	1.0004E+06	4.0693E-01	1.012910	0.785855
0.800	1.0004E+06	5.1164E-01	1.012907	0.785861
0.810	1.0004E+06	1.5189E-01	1.012904	0.785867
0.820	1.0004E+06	2.2791E-01	1.012901	0.785873
0.830	1.0004E+06	3.8551E-01	1.012898	0.785878
0.840	1.0004E+06	5.0793E-01	1.012895	0.785884
0.850	1.0004E+06	1.5488E-01	1.012891	0.785890
0.860	1.0004E+06	2.2494E-01	1.012888	0.785896
0.870	1.0004E+06	3.6752E-01	1.012885	0.785901
0.880	1.0004E+06	4.9675E-01	1.012882	0.785907
0.890	1.0004E+06	1.6163E-01	1.012879	0.785913
0.900	1.0004E+06	2.1721E-01	1.012876	0.785919
0.910	1.0004E+06	3.7476E-01	1.012873	0.785924
0.920	1.0004E+06	5.0643E-01	1.012870	0.785930
0.930	1.0004E+06	1.6087E-01	1.012866	0.785936
0.940	1.0004E+06	2.1931E-01	1.012863	0.785942
0.950	1.0004E+06	3.7476E-01	1.012860	0.785947
0.960	1.0004E+06	4.9559E-01	1.012857	0.785953
0.970	1.0004E+06	1.4553E-01	1.012854	0.785959
0.980	1.0005E+06	2.2389E-01	1.012851	0.785965
0.990	1.0005E+06	3.8369E-01	1.012848	0.785971
1.000	1.0005E+06	5.1015E-01	1.012845	0.785976

Table 3.3c

Outer Loop Bias Control of a Time-Dependent Boresight Error, With a Servo Stability Factor of $\alpha = 6$, and a $\tau_D = 80$ msec Update Time

TIME (SEC.)	RANGE (METERS)	MISS DISTANCE (METERS)	THETA (RAD.)	BIAS (RAD.)
0.020	1.0000E+06	2.7230E+00	1.013150	0.785409
0.040	1.0000E+06	2.6655E+00	1.013144	0.785421
0.060	1.0001E+06	2.6790E+00	1.013139	0.785433
0.080	1.0001E+06	2.7293E+00	1.013132	0.785444
0.100	1.0001E+06	3.2747E-01	1.013123	0.785458
0.120	1.0001E+06	5.2122E-01	1.013117	0.785470
0.140	1.0001E+06	7.7190E-01	1.013111	0.785481
0.160	1.0001E+06	1.0253E+00	1.013105	0.785497
0.180	1.0001E+06	1.7764E-01	1.013099	0.785504
0.200	1.0001E+06	4.8595E-01	1.013093	0.785516
0.220	1.0001E+06	7.3740E-01	1.013087	0.785527
0.240	1.0001E+06	1.0220E+00	1.013081	0.785539
0.260	1.0001E+06	1.7591E-01	1.013074	0.785550
0.280	1.0001E+06	4.8425E-01	1.013068	0.785562
0.300	1.0002E+06	7.3833E-01	1.013062	0.785574
0.320	1.0002E+06	9.9676E-01	1.013056	0.785585
0.340	1.0002E+06	1.7712E-01	1.013049	0.785596
0.360	1.0002E+06	4.8045E-01	1.013043	0.785608
0.380	1.0002E+06	7.3408E-01	1.013037	0.785620
0.400	1.0002E+06	1.0113E+00	1.013031	0.785631
0.420	1.0002E+06	1.4448E-01	1.013024	0.785642
0.440	1.0002E+06	4.7739E-01	1.013018	0.785654
0.460	1.0002E+06	7.7067E-01	1.013012	0.785665
0.480	1.0002E+06	9.9215E-01	1.013006	0.785677
0.500	1.0002E+06	1.6901E-01	1.013000	0.785688
0.520	1.0003E+06	4.6437E-01	1.012994	0.785700
0.540	1.0003E+06	7.4087E-01	1.012988	0.785712
0.560	1.0003E+06	1.0091E+00	1.012982	0.785723
0.580	1.0003E+06	1.6200E-01	1.012975	0.785734
0.600	1.0003E+06	4.7354E-01	1.012969	0.785746
0.620	1.0003E+06	7.7773E-01	1.012963	0.785758
0.640	1.0003E+06	1.0006E+00	1.012957	0.785769
0.660	1.0003E+06	1.6499E-01	1.012950	0.785780
0.680	1.0003E+06	4.6614E-01	1.012944	0.785792
0.700	1.0003E+06	7.4194E-01	1.012938	0.785804
0.720	1.0003E+06	9.9335E-01	1.012932	0.785816
0.740	1.0003E+06	1.8104E-01	1.012925	0.785827
0.760	1.0004E+06	4.8071E-01	1.012919	0.785839
0.780	1.0004E+06	7.5762E-01	1.012913	0.785850
0.800	1.0004E+06	1.0002E+00	1.012907	0.785862
0.820	1.0004E+06	1.7286E-01	1.012901	0.785873
0.840	1.0004E+06	4.8595E-01	1.012895	0.785885
0.860	1.0004E+06	7.4256E-01	1.012889	0.785896
0.880	1.0004E+06	1.0056E+00	1.012883	0.785908
0.900	1.0004E+06	1.7063E-01	1.012876	0.785919
0.920	1.0004E+06	4.7753E-01	1.012870	0.785930
0.940	1.0004E+06	7.4357E-01	1.012864	0.785942
0.960	1.0004E+06	1.0053E+00	1.012858	0.785954
0.980	1.0005E+06	1.7217E-01	1.012851	0.785965

Table 3c (Continued)

Page 2

1.000	1.0005E+06	4.8242E-01	1.012845	0.785975
1.020	1.0005E+06	7.3823E-01	1.012839	0.785983
1.040	1.0005E+06	9.9746E-01	1.012833	0.786000
1.060	1.0005E+06	1.5507E-01	1.012826	0.786011
1.080	1.0005E+06	4.8475E-01	1.012820	0.786022
1.100	1.0005E+06	7.4449E-01	1.012814	0.786034
1.120	1.0005E+06	1.0129E+00	1.012809	0.786046
1.140	1.0005E+06	1.5273E-01	1.012802	0.786057
1.160	1.0005E+06	4.7354E-01	1.012796	0.786068
1.180	1.0005E+06	7.3976E-01	1.012790	0.786080
1.200	1.0005E+06	1.0011E+00	1.012784	0.786092
1.220	1.0006E+06	1.5296E-01	1.012777	0.786103
1.240	1.0006E+06	4.7393E-01	1.012771	0.786114
1.260	1.0006E+06	7.3264E-01	1.012765	0.786126
1.280	1.0006E+06	9.9793E-01	1.012759	0.786138
1.300	1.0006E+06	1.7832E-01	1.012752	0.786149
1.320	1.0006E+06	4.8438E-01	1.012746	0.786161
1.340	1.0006E+06	7.5729E-01	1.012740	0.786172
1.360	1.0006E+06	1.0026E+00	1.012734	0.786184
1.380	1.0006E+06	1.8138E-01	1.012727	0.786195
1.400	1.0006E+06	4.8627E-01	1.012721	0.786207
1.420	1.0006E+06	7.4825E-01	1.012715	0.786218
1.440	1.0007E+06	1.0205E+00	1.012709	0.786230
1.460	1.0007E+06	1.5048E-01	1.012703	0.786241
1.480	1.0007E+06	4.9150E-01	1.012697	0.786253
1.500	1.0007E+06	7.2551E-01	1.012691	0.786264
1.520	1.0007E+06	1.0056E+00	1.012685	0.786276
1.540	1.0007E+06	1.5942E-01	1.012678	0.786287
1.560	1.0007E+06	4.6966E-01	1.012672	0.786299
1.580	1.0007E+06	7.1765E-01	1.012666	0.786310
1.600	1.0007E+06	9.7897E-01	1.012660	0.786322
1.620	1.0007E+06	1.7764E-01	1.012653	0.786333
1.640	1.0007E+06	4.9313E-01	1.012647	0.786345
1.660	1.0007E+06	7.4906E-01	1.012641	0.786356
1.680	1.0008E+06	1.0252E+00	1.012635	0.786368
1.700	1.0008E+06	1.5109E-01	1.012628	0.786379
1.720	1.0008E+06	4.7354E-01	1.012622	0.786391
1.740	1.0008E+06	7.4449E-01	1.012616	0.786402
1.760	1.0008E+06	9.9117E-01	1.012610	0.786414
1.780	1.0008E+06	1.7332E-01	1.012604	0.786425
1.800	1.0008E+06	4.7554E-01	1.012598	0.786437
1.820	1.0008E+06	7.4490E-01	1.012592	0.786448
1.840	1.0008E+06	1.0047E+00	1.012586	0.786460
1.860	1.0008E+06	1.7966E-01	1.012579	0.786471
1.880	1.0008E+06	4.8045E-01	1.012573	0.786483
1.900	1.0008E+06	7.4338E-01	1.012567	0.786495
1.920	1.0009E+06	1.0011E+00	1.012561	0.786506
1.940	1.0009E+06	1.5149E-01	1.012554	0.786517
1.960	1.0009E+06	4.7315E-01	1.012548	0.786529
1.980	1.0009E+06	7.7408E-01	1.012542	0.786541
2.000	1.0009E+06	1.0125E+00	1.012536	0.786552

Appendix to Chapter 3

Computer Program Listing

This program is used to generate all of the simulation results presented in Tables 1-3 and Fig.'s 2-4. This program is closely related to that presented in Chapter 2 and uses the subroutines listed there.


```

DIMENSION RST(3), VS(3), RTZ(3), VT(3),%
DR(3), DV(3), LDV(3), D(3), DVSP(3), UT(3), UG(3), EPP(3),%
Z(3), XI(3), ETA(3), DS(3), UL(3), RTS(3), CLM(3), UDR(3),%
RTCLD(3), RSCLD(3), ULCLD(3), EB(2), GC(3), PLM(3),%
PARM(4), LTYPE(5,2)
NAMELIST /INPUT/ RST, VS, RTZ, VT, DS, GC, EB
DATA LTYPE / " V","EL","OC","IT","VY ",%
" P","CS","IT","IC","N "/,%
PARM / 2.0, 5.0, 4.0, 3.0 /

C      *** PROCESS FOR VELOCITY (LCOPCT=1) AND POSITION (LCOPCT=2) ***
DO 2999 LCOPCT=1,2

C      *** VARY BIAS SERVO PARAMETERS ***
DO 1999 IXPARM=1,4
TEMP = 1.0
NPRINT = 20
PI = 3.141592654
Z(1) = 0.
Z(2) = 0.
Z(3) = 1.
T = 0.
DT = 1.E-3
N = 0.

C-----
C-
C- SPECIFY/INITIALIZE BIAS SERVO PARAMETERS.
C-
C-----

NE = 60
EE(1) = 0.0
FACT = 2.0*(PI/PARM(IXPARM))
EE(2) = 0.0

C*****
C*
C* SPECIFY ENGAGEMENT PARAMETERS.
C*
C*****

```

```

RSZ(1) = 0.
RSZ(2) = 0.
RSZ(3) = 0.
VS(1) = 4.9E3
VS(2) = 7.1E2
VS(3) = 7.1E2
RTZ(1) = 6.E5
RTZ(2) = 6.E5
RTZ(3) = 5.29E5
VT(1) = 4.7E3
VT(2) = 1.21E3
VT(3) = 1.2E3

C **** SET EIAS-ERROR FOR VELOCITY OR FOR POSITION CALCULATION ****
IF (LOOPCT.FO.2) GO TO 5

C **** SET EIAS-ERROR FOR VELOCITY ****
DE(1) = 1.E-5
DE(2) = 1.E-5
GO TO 6

C **** SET EIAS-ERROR FOR POSITION ****
5 CONTINUE
DE(1)=5.E-5
DE(2)=5.E-5
6 CONTINUE
DE(3) = 0.0
GE(1)=1.
GE(2)=1.
GE(3)=0.

C*****
C*
C* CONVERT TO DIFFERENCE COORDINATES.
C*
C*****

CALL SUM (RTZ,RSZ,DE,-1)
CALL SUM (VT, VS, DV, -1)
CALL LVECT (DE, UDE, DRM, IF)
CALL LVECT (DV, UDV, DVM, IF)

C*****
C*
C* CALCULATE DISTANCE AT CLOSEST APPROACH.
C*
C*****

CALL DOT (UDE, UDV, DURV)

```

```

SF = DUFV*DRM
CALL SCMULT (SF, LCV, DVSE)
CALL SUM (DF, DVSE, 2, -1)
CALL LVECT (D, D, DM, IS)
PRINT 10, DM, DUFV, RST, VS, RTZ, VT, (LTYPE(IX, LCOPT), IX=1.5), %
      DE, PARM(IX, PARM), NP
PRINT 11
PRINT 12
10 FORMAT ("1", "CLOSEST APPROACH=", F10.3, " DOT PRODUCT =", %
      E10.3, " RSZ VECTOR =", F10.3, " VS VECTOR =", F10.3, %
      " RTZ VECTOR =", F10.3, " VT VECTOR =", F10.3, " CALCULATION", %
      " CS VECTOR =", F10.3, " PHASE-MARGIN FACTOR =", F5.1, %
      " NB INCFEM =", F5.1)
11 FORMAT("1", 5X, "TIME", 5X, "RANGE", 5X, "MISS DISTANCE", %
      5X, "THETA", 12X, "PHI")
12 FORMAT(5X, "(SEC.)", 5X, "(METERS)", 7X, "(METERS)", 9X, "(RAD.)", 9X, %
      "(RAD.)")

C*****
C*
C*      INITIALIZE SERVO/GIMBAL AND SET SERVO PARAMETERS.
C*
C*****

SGT=SQRT(LDR(1)*UDF(1)+UDF(2)*UDF(2))
THETAZ=ATAN2(SGT,UDF(3))
PHIZ = ATAN2(LDR(2), LDR(1))
SFREQ = 100.
GAIN = 27.9155*SFREQ*SFREQ
CLEAD=EXP(-DT*2*PI*SFREQ)
PHINT1 = 0.
PHINT2 = PHIZ
THINT1 = 0.
THINT2 = THETAZ
OTHER = 0.
OFHER = 0.
THETA = THINT2
PHI = PHINT2
CALL SPDEC (THETA, PHI, 1., UC)

C*****
C*
C*      INCREMENT CLOCK.
C*
C*****

100 N = N + 1
      T = T + DT

C*****
C*

```



```

C*      INCREMENT TARGET POSITION AND STORE.
C*      OBTAIN DELAYED TARGET POSITION.
C*
C*****

      CALL WSUM (1., DT, DP, DV, DR)
      CALL STACIN (1, DR)
      CALL LVECT(DP, LDR, DPM, IE)
      TTF = DPM/(3.58*DT)
      IF (TTF > 100) GO TO 100
      CALL STACCT (1, TTF, FTOLD)

C*****
C*
C*      COMPUTE TARGET TRACKING ERROR AS SEEN BY
C*      SENSOR ON THE GIMBALS (USING THE DELAYED
C*      TARGET POSITION).
C*
C*****

      CALL LVECT (PTOLD, UT, R, IE)
      CALL SUM (UT, LG, ERR, -1)
      CALL CROSS (Z, LG, XI)
      CALL LVECT (XI, XI, XIM, IE)
      CALL CROSS (UC, XI, ETA)
      CALL DOT (ERR, ETA, ERREL)
      ERREL = -1.*(ERREL+ER(1))
      CALL DOT (ERR, XI, ERRAZ)
      ERRAZ = ERRAZ+EE(2)

C*****
C*
C*      IMPLEMENT GIMBAL SERVO POINTING UPDATE.
C*
C*****

      ERRAZ = ERRAZ/SIN (THETA)
      Q1TH = (ERREL - CLEAD * OTHER)/(1. - CLEAD)
      Q1PH = (ERRAZ - CLEAD * OTHER)/(1. - CLEAD)
      OTHER = ERREL
      Q2TH = Q1TH * GAIN
      Q2PH = Q1PH * GAIN
      THINT1 = THINT1 + DT*Q2TH
      PHINT1 = PHINT1 + DT * Q2PH
      THINT2 = THINT2 + DT * THINT1
      PHINT2 = PHINT2 + DT * PHINT1
      THETA = THINT2

```

```

PHI = PHINT2
CALL SPHREC (THETA, PHI, 1., LG)

```

```

C*****
C*
C*      INTRODUCE LASER PORESIGHT ERROR.
C*
C*****

```

```

C      *** SET TEMP VAL TO T FOR VELOCITY CALCULATION, OR LEAVE IT
C      ***      AT 1.0 FOR POSITION CALCULATION      ****
IF (LOOPCT.EQ. 1) TEMP = T
T1 = THETA + DB(1) * TEMP
P1 = PHI + DB(2) * TEMP
CALL SPHREC(T1,P1,1.,UL)

```

```

C*****
C*
C*      CALCULATE LASER TARGET MISS DISTANCE.
C*
C*****

```

```

CALL STACIN (2,UL)
TTF2=2*TTF
CALL STACCT (2, TTF2, ULOLD)
CALL DOT (UT, ULOLD, DTL)
SF = -DTL*R
CALL WSLM (1., SF, ETOLD, ULOLD, DLM)
CALL LVECT (DLM, DLM, DLM, IE)

```

```

C-----
C-
C-      CALCULATE LASER POSITION ON TARGET AS IT WOULD BE
C-      SEEN ON SENSOR FOCAL PLANE, AND UPDATE BIAS SERVO
C-      OUTPUT.
C-----

```

```

NAB = N/NE
IF (NAB*NE.NF.N) GO TO 300
A = DLM/R
CALL SCMUL (A, DLM, PLM)
CALL DOT (PLM, ETA, FB1)
CALL DOT (PLM, XI, FB2)
EE(1) = EE(1)+FACT*FB1

```

```
EE(2) = EE(2)+FACT*ERR2  
300 CONTINUE
```

```
IF ((N/NPRINT)*NPRINT.NE.N) GO TO 100  
PRINT 200, T, S, OLMP, THETA, PHI  
200 FORMAT ( F10.3,5X, F10.4,5X, F10.4,5X, 0F10.6,5X, F10.6)
```

```
IF (N.LT. 2000) GO TO 100
```

```
C      **** END OF SERVO PARAMETER LOOP ****  
1999 CONTINUE  
C      **** END OF VELOCITY/POSITION MODE CALCULATION LOOP ****  
2999 CONTINUE
```

```
END
```


Chapter 4

Diffuse Backscatter

Focal Plane Statistics

for a

Laser Transmitter/Receiver

4.1 Introduction

We are interested here in determining the statistics of the receiver focal plane intensity for a transmitter/receiver system viewing the laser spot pattern which it projects onto some very rough target surface. In the transmitter/receiver configuration, by means of a beam splitter or a T/R switch, the same aperture serves the dual functions of 1) projecting an image of a monochromatic point source (i. e., a laser) located at the center of the focal plane onto the target, and 2) forming an image of the backscatter from the target on the focal plane.

We consider the target surface (normal) to be rotating (changing its orientation) with respect to the line-of-sight and, therefore, understand that, although the surface is randomly rough, there is a well-defined time-delay correlation of the surface height and thus of the induced phase shift at a point. Accordingly, we find it necessary to consider not only the spatial statistics of the signal across the focal plane, but the time delay/spatial statistics of the backscatter signal intensity in the focal plane. We shall assume that the statistics are adequately characterized by the first and second moments and accordingly shall restrict our attention to the computation of those two moments.

Our actual interest is in a system which utilizes a two-dimensional array of close-packed square detectors to determine the apparent location of the centroid of the backscatter pattern from the target. For the calculation of the effect of speckle statistics on this system, we need to know the temporal covariance of the signal intensity from any two of the detectors. Our approach to the calculation of this covariance is to first calculate the spatial-temporal covariance of the intensity in the focal plane. Then from this, we will calculate the covariance for the outputs of the individual detectors in the array. This latter calculation is rather straightforward

once we have an expression for the spatial-temporal covariance, but for convenience we postpone it to subsequent work, restricting our attention here to focal plane point statistics.

In the following section we shall discuss the geometry of the encounter, defining the various pertinent parameters. The section after that will be concerned with the spatial-temporal statistics and the mathematical treatment of the rough surface-induced phase shift. The subsequent section will present several of the more important mathematical and propagation formula. In the remaining sections we will present the calculation of the first and second moments of the focal plane point intensities.

4.2 Encounter Geometry

The encounter geometry is, for purposes of analysis, as indicated in Fig. 1. We consider everything to be defined relative to the transmitter/receiver aperture plane. We define position on this aperture plane by a two-dimensional vector, \vec{y} , with its origin at the center of the aperture. To define the target plane and the focal plane, we consider two planar surfaces at distances R and F , respectively, from the aperture plane. We use the two-dimensional vector \vec{x} to denote a position on the target surface, the two-dimensional vector \vec{y} to denote a position on the aperture plane, and the two-dimensional vector \vec{z} to denote a position on the focal plane. We shall assume that the range, R , is so much larger than the aperture diameter that the target surface is in the far-field of the aperture.

Referenced to the center of the aperture, the target position, \vec{x} , can be equated with the field angle.

$$\vec{\theta} = \vec{x}/R \quad . \quad (1)$$

Correspondingly, we equate the focal plane position, \vec{z} , with field angle

$$\vec{\vartheta} = -\vec{z}/F \quad . \quad (2)$$

Because of the time varying geometry of the engagement, the relationship between the line-of-sight and the physical target will be changing. This change corresponds to a rotation. For notational purposes it is convenient to define this rotation in terms of an incremental change in the surface normal unit vector. If $\hat{n}(t)$ denotes the unit normal* at time t ,

* A proper understanding of the meaning of \hat{n} and its relationship to the \vec{x} -plane requires some comment. We do not expect the target surface to actually conform to the \vec{x} -plane — the \vec{x} -plane being, by definition, perpendicular to the line-of-sight. Rather, we consider the actual target surface to be projected in accordance with the line-of-sight upon the \vec{x} -plane. It is this projection that we consider to

then at time $t + dt$, we may write

$$\hat{n}(t + dt) = \hat{n}(t) + \vec{\alpha}(t) dt, \quad (3)$$

with $\vec{\alpha}(t)$ denoting the rotation rate. Thus, if the random roughness of the target surface will introduce a random phase shift, $\phi_r(\vec{x}, t)$, into the radiation incident from along the line-of-sight, at \vec{x} , at time t , then at time $t + dt$, because of the rotation, it will produce a phase shift.

$$\phi_r(\vec{x}, t + dt) = \phi_r(\vec{x}, t) + \frac{4\pi}{\lambda} \vec{\alpha}(t) \cdot \vec{x} dt. \quad (4)$$

Here λ denotes the wavelength of the incident radiation.

We shall have no particular need, in this report, to consider the reason why $\vec{\alpha}$ has some particular value. For completeness, however, we note at this point that the value of $\vec{\alpha}$ will be determined by two factors. The first of these derives from actual rotation of the target. The cross-product of the target spin axis with a unit vector along the line-of-sight gives this contribution to $\vec{\alpha}$. The second factor contributing to $\vec{\alpha}$ arises from the motion of the target and sensor (i. e., aperture and focal plane assembly) with respect to each other. In as simple a pattern as a nonmaneuvering "fly-by" the relationship of the line-of-sight to the physical surface normal will change. This results in a factor contributing to the value of $\vec{\alpha}$.

(Continued from preceding page)

be the effective target surface. Thus, while in our analysis the effective target surface remains the \vec{x} -plane, despite actual rotation of the real target surface, we may talk of surface normal \hat{n} , corresponding to the actual target surface, and take account in our analysis of its rotation.

With the preceding definition of the encounter geometry now in hand, we turn our attention to the surface roughness statistics. We take this up in the next section.

4.3 Surface Roughness Statistics

Based on analysis which we have presented elsewhere*, we argue that the backscatter from a randomly rough target can be separated into two parts. The first of these, which we call the specular return, depends only on the target shape and its effective reflectivity. The effective reflectivity is a number less than unity, whose value is determined by one minus the absorption (and transmission) of the surface material times a number of the order of $\exp(-4k^2 \sigma^2)$ where σ^2 is the mean square target surface height variation and $k = 2\pi/\lambda$. The specular return appears to come from a perfectly polished target with this effective reflectivity. The specular return is not random. In general, it may be expected to be zero for a perfectly flat target (except very near normal incidence) and to vary only very slowly with change of target orientation for a compound curved target surface. The specular return is generally to be associated with a limited region on a compound curved surface, namely the region near where the surface normal is parallel to the line-of-sight. As the target/line-of-sight relative orientation changes, this region will shift on the target surface and correspondingly, the strength of the specular return will change in accordance with the changing radii of curvature at the specular region (and, of course, also in accordance with the change in the incident power density of the specular region).

The second part of the return from the rough target, which we refer to as the diffuse return, has been shown* to have a Rayleigh distributed random amplitude, and to originate from the entire illuminated region of the rough target surface, its average power being proportional to the

* D. L. Fried, "Statistics Of The Laser Radar Cross Section Of A Randomly Rough Target," J. Opt. Soc. Am. 66, 1150 (1976).

BRDF averaged over the entire target. This portion of the return appears to come from a target surface which induces a phase shift that is uniformly distributed between 0 and 2π . This insures that the correlation of the wavefunction scattered from two points, \vec{x} and \vec{x}' , that are far enough apart, will have zero value.

Arguing that we will always be considering fine grain surface roughness, we can show that for $\phi_R(\vec{x}', t)$ to be correlated, \vec{x} and \vec{x}' must be so close together that all propagation effects will be independent of the distinction between \vec{x} and \vec{x}' . This allows us to write

$$\langle \exp[i[\phi_R(\vec{x}, t) - \phi_R(\vec{x}', t)]] \rangle = \beta \delta(\vec{x} - \vec{x}') \quad , \quad (5)$$

where

$$\beta = \int d\vec{x}' \langle \exp[i[\phi_R(\vec{x}, t) - \phi_R(\vec{x}', t)]] \rangle \quad . \quad (6)$$

[We note here that we shall never actually attempt to evaluate β from Eq. (6).]

Making use of Eq. (4) we can extend Eq. (5) to the form

$$\langle \exp[i[\phi_R(\vec{x}, t) - \phi_R(\vec{x}', t')]] \rangle = \beta \delta(\vec{x} - \vec{x}') \times \exp\left[\frac{4\pi}{\lambda} \vec{\alpha} \cdot \vec{x}(t' - t)\right] \quad (7)$$

In writing this we have assumed that the rate of rotation, $\vec{\alpha}(t)$, is not a significant function of t , i.e., $\vec{\alpha}(t) \approx \vec{\alpha}(t')$, and accordingly, have dropped the t -dependence. As a further extension of Eq. (5) to a four-point function, we can write

$$\begin{aligned} & \langle \exp[i[\phi_R(\vec{x}, t) - \phi_R(\vec{x}', t') + \phi_R(\vec{x}'', t'') - \phi_R(\vec{x}''', t''')]] \rangle \\ &= \beta^2 \delta(\vec{x} - \vec{x}') \delta(\vec{x}'' - \vec{x}''') \exp\left\{\frac{4\pi}{\lambda} \vec{\alpha} \cdot [\vec{x}(t - t') \right. \\ & \quad \left. + \vec{x}''(t'' - t''')]\right\} \end{aligned}$$

(Continued)

$$\begin{aligned}
& + \beta^2 \delta(\vec{x} - \vec{x}''') \delta(\vec{x}'' - \vec{x}') \exp\left\{\frac{4\pi}{\lambda} i\vec{\alpha} \cdot \right. \\
& \left. \times [\vec{x}(t - t''') + \vec{x}''(t'' - t')]\right\} .
\end{aligned} \tag{8}$$

With these equations in hand, we may consider that we have adequately defined the statistics of the rough surface induced phase shift of the diffusely scattered wave. Similarly, having noted that the specular scattered wave is not random and varies only slowly, we may consider its characteristics adequately defined. Accordingly, we now turn our attention to the basic propagation formulations. We take this up in the next section.

4.4 Propagation Formulation

In the context of the scenario depicted by Fig. 1, we are interested in the propagation of (monochromatic) radiation from a point source located at the origin of the focal plane (i.e., the z -plane), through collimating optics in the aperture plane (i.e., the y -plane) where the optics focus it on the target, and thence out to the effective target surface (i.e., the \vec{x} -plane). The radiation incident on the effective target surface is back-scattered as two components, the specular part and the diffuse part. Simple geometric optics is sufficient for treatment of the specular part, and accordingly, we shall ignore it here, restricting our attention to the diffuse return. The random diffuse return backscattered from the target surface passes through the aperture plane and its optics and is then detected on the focal plane. Ultimately, we shall be interested in the statistics of the backscatter signal as detected by the elements of a detector array in the focal plane — but in this section we shall mainly develop an expression for the random amplitude at a point in the focal plane at some instant of time. Development of the statistics from this will be taken up in the next section.

We may write as our source wave-function, for a point source at the center of the focal plane

$$U_o(\vec{r}) = \frac{A}{r} \exp[i(kr - \omega t)] \quad , \quad (9)$$

where \vec{r} is a three-dimensional vector with its origin at the center of the focal plane. A is the amplitude of the wave-function, $k = 2\pi/\lambda$ is the optical wave-number, and $\omega = 2\pi c/\lambda$, where $c = 3 \times 10^8$ m/sec is the speed of light. If the aperture plane contains optics whose optical amplitude transmission is defined by the function $W_o(\vec{y})$ [where $0 \leq W_o(\vec{y}) \leq 1$], then the power transmitted by the optics will be

$$P_1 = \frac{1}{2}(A/F)^2 \int d\vec{y} [W_0(\vec{y})]^2, \quad (10)$$

based on the assumption that the relevant extent of the aperture is small enough that for all values of \vec{y} of interest

$$(F^2 + y^2)^{1/2} \approx F. \quad (11)$$

If the optics at position \vec{y} introduce a phase shift $\phi_r(\vec{y})$, then making use of the Fresnel-Kirchoff integral, we can write for the amplitude of the illumination at the target surface

$$v(\vec{x}) = -\frac{ikA}{4\pi} \int d\vec{y} W_0(\vec{y}) \frac{\exp\{ik[\mathcal{R}(\vec{x}, \vec{y}) + \mathcal{F}(\vec{y}, 0)] + i\phi_r(\vec{y})\}}{\mathcal{R}(\vec{x}, \vec{y}) \mathcal{F}(\vec{y}, 0)}, \quad (12)$$

where

$$\mathcal{R}(\vec{x}, \vec{y}) = (R^2 + |\vec{x} - \vec{y}|^2)^{1/2}, \quad (13)$$

$$\mathcal{F}(\vec{y}, \vec{z}) = (F^2 + |\vec{y} - \vec{z}|^2)^{1/2}. \quad (14)$$

Letting D denote the effective diameter of the optics, i.e., a measure of the largest value of \vec{y} for which W_0 is not negligibly small, and assuming that R is very much larger than D (the far field assumption mentioned earlier), and that F is much greater than D , i.e., that we are dealing with slow optics, we can write

$$\mathcal{R}(\vec{x}, \vec{y}) \approx R + \frac{x^2}{2R} + \frac{y^2}{2R} - \frac{\vec{x} \cdot \vec{y}}{R}, \quad (15)$$

$$\mathcal{F}(\vec{y}, \vec{z}) \approx F + \frac{y^2}{2F} + \frac{z^2}{2F} - \frac{\vec{y} \cdot \vec{z}}{F}. \quad (16)$$

Substituting Eq. (15) and (16) into Eq. (12), retaining all terms when substituting in the exponent since it will be multiplied by k , but retaining

only the leading term when substituting in the denominator, we get

$$\begin{aligned} \mathcal{V}(\vec{x}) = & -\frac{ikA}{4\pi} \int d\vec{y} W_0(\vec{y}) \exp\{ik[R + F + \frac{x^2}{2R} + \frac{y^2}{2} (R^{-1} + F^{-1}) \\ & - \frac{\vec{x} \cdot \vec{y}}{R}] + i\phi_f(\vec{y})\} (RF)^{-1} . \end{aligned} \quad (17)$$

The optics will cause the transmitted wave to be focused on the target at $\vec{x} = 0$ if the phase shift $\phi_f(\vec{y})$ has the value

$$\phi_f(\vec{y}) = -\frac{1}{2} ky^2 (R^{-1} + F^{-1}) , \quad (18)$$

which we shall assume to be the case. If we substitute Eq. (18) into Eq. (17) and simplify, we can write

$$\mathcal{V}(\vec{x}) = -\frac{ikA}{4\pi RF} \exp(ik\frac{x^2}{2R}) \int d\vec{y} W_0(\vec{y}) \exp[-iky \cdot (\vec{x}/R)] . \quad (19)$$

In obtaining Eq. (19), we have dropped a factor of $\exp[-ik(R+F)]$ as being of no consequence.

Making use of the Fresnel-Kirkhoff integral again, we can see that the backscatter signal amplitude of a point \vec{z} in the focal plane, at time t , due to the scattering at a point region $(\vec{x}, d\vec{x})$ on the target surface will be

$$\begin{aligned} dU(\vec{z}, t) = & -\frac{ik}{4\pi} \mathcal{V}(\vec{x}) \exp[i\phi_r(\vec{x}, t)] d\vec{x} \int d\vec{y} W_0(\vec{y}) \\ & \times \frac{\exp\{ik[\rho(\vec{x}, \vec{y}) + \mathcal{F}(\vec{y}, \vec{z})] + i\phi_f(\vec{y})\}}{\rho(\vec{x}, \vec{y}) \mathcal{F}(\vec{y}, \vec{z})} \end{aligned} \quad (20)$$

so that the total wave-function at \vec{z} due to all of the points on the target plane will be

$$U(\vec{z}) = -\frac{ik}{4\pi} \int d\vec{x} \mathcal{V}(\vec{x}) \exp[i\phi_R(\vec{x}, t)] \int d\vec{y} W_0(\vec{y}) \\ \times \frac{\exp\{ik [\mathcal{R}(\vec{x}, \vec{y}) + \mathcal{T}(\vec{y}, \vec{z})] + i\phi_r(\vec{y})\}}{\mathcal{R}(\vec{x}, \vec{y}) \mathcal{T}(\vec{y}, \vec{z})} \quad (21)$$

Again, making use of the approximations associated with Eq.'s (15) and (16), and substituting Eq. (18) into Eq. (21), we obtain the result that

$$U(\vec{z}, t) = -\frac{ik}{4\pi RF} \exp\left(ik \frac{z^2}{2R}\right) \iint d\vec{x} d\vec{y} \mathcal{V}(\vec{x}) \exp[i\phi_R(\vec{x}, t)] W_0(\vec{y}) \\ \times \exp\left[-ik \left(\frac{\vec{x} \cdot \vec{y}}{R} + \frac{\vec{y} \cdot \vec{z}}{F}\right)\right] \quad (22)$$

If we substitute Eq. (19) into Eq. (22), we can cast our result in the form

$$U(\vec{z}, t) = -\left(\frac{ik}{4\pi RF}\right)^2 A \exp\left(ik \frac{z^2}{2R}\right) \iiint d\vec{x} d\vec{y} d\vec{y}' W_0(\vec{y}) W_0(\vec{y}') \\ \times \exp\left\{ik \frac{x^2}{2R} + i\phi_R(\vec{x}, t) - ik \left[\frac{\vec{x} \cdot (\vec{y} + \vec{y}')}{R} + \frac{\vec{y} \cdot \vec{z}}{F}\right]\right\} \quad (23)$$

Eq. (23) represents our basic propagation results. It specifies the random backscattered amplitude in the focal plane at a point \vec{z} and time t , as a function of the random phase shift, $\phi_R(\vec{x}, t)$ on the target surface. With this result in hand we are now ready to proceed to the calculation of the focal plane backscatter signal point-intensity statistics. We take this up in the next section.

4.5 Point-Intensity Statistics

The random backscatter signal intensity at a time t and point z in the focal plane may be written as

$$I(\vec{z}, t) = \frac{1}{2} U^*(\vec{z}, t) U(\vec{z}, t) \quad (24)$$

If we substitute Eq. (23) into Eq. (24), and make multiple integrals out of the product of integrals, we obtain the expression

$$\begin{aligned} I(\vec{z}, t) = & \left(\frac{k}{4\pi R} \right)^4 \frac{P_T}{\mathcal{A} F^2} \iiint \iiint d\vec{x} d\vec{x}' d\vec{y} d\vec{y}' d\vec{y}'' d\vec{y}''' \\ & \times W_0(\vec{y}) W_0(\vec{y}') W_0(\vec{y}'') W_0(\vec{y}''') \\ & \times \exp \left\{ i k \frac{x^2 - x'^2}{2R} + i [\phi_R(\vec{x}, t) - \phi_R(\vec{x}', t)] \right. \\ & \left. - i k \left[\frac{\vec{x} \cdot (\vec{y} + \vec{y}') - \vec{x}' \cdot (\vec{y}'' + \vec{y}''')}{R} + \frac{(\vec{y} - \vec{y}''') \cdot \vec{z}}{F} \right] \right\} \quad (25) \end{aligned}$$

where P_T is the total transmitted power, as defined in Eq. (10), and \mathcal{A} is the effective aperture area, defined by the equation

$$\mathcal{A} = \int d\vec{y} [W_0(\vec{y})]^2 \quad (26)$$

The calculation of the average backscatter intensity, $\bar{I}(\vec{z}, t)$, where

$$\bar{I}(\vec{z}, t) = \langle I(\vec{z}, t) \rangle \quad (27)$$

is now a straightforward matter. [We recall that $\langle \rangle$ denote an ensemble average.] If we take the ensemble average of the right-hand-side of Eq. (25), commute the processes of integration and averaging, and then extract the

ϕ -dependent part of the exponential as a separate factor, which we make the only term enclosed in the angle brackets, we can then make use of Eq. (5) to allow us to write

$$\begin{aligned} \bar{I}(\vec{z}, t) = & \beta \left(\frac{k}{4\pi R} \right)^4 \frac{P_I}{Q_{F=2}} \iiint \iiint d\vec{x} d\vec{x}' d\vec{y} d\vec{y}' d\vec{y}'' d\vec{y}''' \\ & \times W_0(\vec{y}) W_0(\vec{y}') W_0(\vec{y}'') W_0(\vec{y}''') \delta(\vec{x} - \vec{x}') \\ & \times \exp \left\{ i k \left[\frac{\vec{x}^2 - \vec{x}'^2}{2R} - \frac{\vec{x} \cdot (\vec{y} + \vec{y}') - \vec{x}' \cdot (\vec{y}'' + \vec{y}''')}{R} - \frac{(\vec{y} - \vec{y}'') \cdot \vec{z}}{F} \right] \right\}. \quad (28) \end{aligned}$$

It is convenient at this point to replace the (\vec{y}, \vec{y}') and (\vec{y}'', \vec{y}''') pairs by sum and difference coordinates. We write

$$\vec{\sigma} = \frac{1}{2} (\vec{y} + \vec{y}''') \quad ; \quad \vec{\sigma}' = \frac{1}{2} (\vec{y}' + \vec{y}'') \quad , \quad (29)$$

$$\vec{\delta} = \vec{y} - \vec{y}'' \quad ; \quad \vec{\delta}' = \vec{y}' - \vec{y}''' \quad . \quad (30)$$

The Jacobians for the transformation of variables is unity and accordingly we may rewrite Eq. (28), performing the \vec{x}' -integration, as

$$\begin{aligned} \bar{I}(\vec{z}, t) = & \beta \left(\frac{k}{4\pi R} \right)^4 \frac{P_I}{Q_{F=2}} \iiint \iiint d\vec{\sigma} d\vec{\sigma}' d\vec{\delta} d\vec{\delta}' d\vec{x} \\ & \times W_0(\vec{\sigma} + \frac{1}{2}\vec{\delta}) W_0(\vec{\sigma} - \frac{1}{2}\vec{\delta}) W_0(\vec{\sigma}' + \frac{1}{2}\vec{\delta}') W_0(\vec{\sigma}' - \frac{1}{2}\vec{\delta}') \\ & \times \exp \left\{ - i k \left[\left(\frac{\vec{x}}{R} \right) \cdot (\vec{\delta} + \vec{\delta}') + \vec{\delta} \cdot \left(\frac{\vec{z}}{F} \right) \right] \right\} \quad . \quad (31) \end{aligned}$$

It is convenient, at this point, to define the aperture transmission overlap transform function, namely,

$$W_1(\vec{\delta}; \vec{\theta}) = \int d\vec{\sigma} W_0(\vec{\sigma} + \frac{1}{2}\vec{\delta}) W_0(\vec{\sigma} - \frac{1}{2}\vec{\delta}) \exp(-ik\vec{\theta} \cdot \vec{\sigma}), \quad (32)$$

which allows us to rewrite Eq. (31) in the form

$$\begin{aligned} \bar{I}(\vec{z}, t) = & \beta \left(\frac{k}{4\pi R} \right)^4 \frac{P_I}{\mathcal{A}F^2} \iiint d\vec{\delta} d\vec{\delta}' d\vec{x} W_1(\vec{\delta}, 0) W_1(\vec{\delta}', 0) \\ & \times \exp \left\{ -ik \left[\left(\frac{\vec{x}}{R} \right) \cdot (\vec{\delta} + \vec{\delta}') + \vec{\delta} \cdot \left(\frac{\vec{z}}{F} \right) \right] \right\}. \end{aligned} \quad (33)$$

For any well-behaved function, $g(\vec{r})$, where \vec{r} is a two-dimensional vector, it can be shown that

$$g(\vec{r}) = (2\pi)^{-2} \mu^2 \iint d\vec{r}' d\vec{r}'' g(\vec{r}') \exp [i\mu \vec{r}'' \cdot (\vec{r}' - \vec{r})], \quad (34)$$

which is really nothing more than the well-known fact that the repeated fourier integral recovers the starting function. Making use of Eq. (34) to simplify Eq. (33), we obtain the result that

$$\bar{I}(\vec{z}, t) = \beta \frac{k^2}{64\pi^2 R^2} \frac{P_I}{\mathcal{A}F^2} \int d\vec{\delta} W_1(\vec{\delta}; 0) W_1(-\vec{\delta}; 0) \exp(ik\vec{\delta} \cdot \vec{\mathcal{J}}), \quad (35)$$

where $\vec{\mathcal{J}}$ is as defined by Eq. (2). With this result in hand, we are now ready to turn our attention to the second moment statistics of focal plane irradiance.

We are interested in the covariance function for focal plane back-scatter intensity, namely,

$$C_I(\vec{z}, \vec{z}', t, t') = \langle [I(\vec{z}, t) - \bar{I}(\vec{z}, t)][I(\vec{z}', t') - \bar{I}(\vec{z}', t')] \rangle, \quad (36)$$

It is easy to see that

$$C_I(\vec{z}, \vec{z}', t, t') = \langle I(\vec{z}, t) I(\vec{z}', t') \rangle - \bar{I}(\vec{z}, t) \bar{I}(\vec{z}', t'), \quad (37)$$

and accordingly we now direct our attention to the evaluation of the second moment, $\langle I(\vec{z}, t) I(\vec{z}', t') \rangle$. Making use of Eq. (25), we can write

$$\begin{aligned} \langle I(\vec{z}, t) I(\vec{z}', t') \rangle &= \left(\frac{k}{4\pi R} \right)^8 \left(\frac{P_I}{\mathcal{Q}_{F-2}} \right)^2 \int \dots \int d\vec{x} \dots d\vec{x}'' \dots d\vec{y} \dots d\vec{y}'' \\ &\times W_0(\vec{y}) \dots W_0(\vec{y}'') \exp \left(i k \frac{\vec{x}^2 - \vec{x}'^2 + \vec{x}''^2 - \vec{x}'''^2}{2R} \right) \\ &\times \langle \exp \{ i [\phi_R(\vec{x}, t) - \phi_R(\vec{x}', t) + \phi_R(\vec{x}'', t') - \phi_R(\vec{x}''', t')] \} \rangle \\ &\times \exp \left[- i k \frac{\vec{x} \cdot (\vec{y} + \vec{y}') - \vec{x}' \cdot (\vec{y}'' + \vec{y}''') + \vec{x}'' \cdot (\vec{y}' + \vec{y}') - \vec{x}'' \cdot (\vec{y}' + \vec{y}'')}{R} \right] \\ &\times \exp \left[- i k \frac{(\vec{y} - \vec{y}'') \cdot \vec{z} + (\vec{y}' - \vec{y}''') \cdot \vec{z}'}{F} \right], \end{aligned} \quad (38)$$

where to facilitate evaluation of this expression, we have separated the exponential of the ϕ_R -dependencies and commuted the ensemble averaging and integration processes, so that the ensemble average brackets contained only the ϕ_R -dependent exponential. At this point, we make use of Eq. (8) to exploit the ϕ_R -statistics. This allows us to perform the \vec{x}' - and \vec{x}'' -integrations, obtaining

$$\begin{aligned} \langle I(\vec{z}, t) I(\vec{z}', t') \rangle &= \beta^2 \left(\frac{k}{4\pi R} \right)^8 \left(\frac{P_I}{\mathcal{Q}_{F-2}} \right)^2 \int \dots \int d\vec{x} d\vec{x}'' d\vec{y} \dots d\vec{y}'' \\ &\times W_0(\vec{y}) \dots W_0(\vec{y}'') \exp \left[- i k \frac{(\vec{y} - \vec{y}'') \cdot \vec{z} + (\vec{y}' - \vec{y}''') \cdot \vec{z}'}{F} \right] \\ &\times \left\{ \exp \left[- i k \frac{\vec{x} \cdot (\vec{y} + \vec{y}' - \vec{y}'' - \vec{y}''') + \vec{x}'' \cdot (\vec{y}' + \vec{y}' - \vec{y}' - \vec{y}''')}{R} \right] \right. \\ &\quad \left. + \exp \left[- i k \frac{\vec{x} \cdot (\vec{y} + \vec{y}' - \vec{y}' - \vec{y}''') + \vec{x}'' \cdot (\vec{y}' + \vec{y}' - \vec{y}'' - \vec{y}''')}{R} \right] \right\} \\ &\times \exp \left\{ \frac{4\pi}{\lambda} i \vec{\alpha} \cdot [\vec{x} (t - t') + \vec{x}'' (t' - t)] \right\} \}. \end{aligned} \quad (39)$$

Rather than proceed directly with the evaluation of this integral, we first note that if we consider only the first exponential term in the double curly brackets, we have a ten-fold integral which can be factored into the product of two essentially identical* five-fold integrals. Moreover, we note that each of these five-fold integrals corresponds exactly to what we get if we were to perform the \vec{x}' -integration in Eq. (28) directly (i. e., without any change of variables). This allows us to identify this ten-fold integral with the $\bar{I}(\vec{z}, t) \bar{I}(\vec{z}', t')$ product. In view of this fact, and taking note of Eq. (37), we can thus write in place of Eq. (39)

$$\begin{aligned}
 C_1(\vec{z}, \vec{z}', t, t') &= \beta^2 \left(\frac{k}{4\pi R} \right)^8 \left(\frac{P_c}{2F\epsilon} \right)^2 \int \dots \int d\vec{x} d\vec{x}' d\vec{y} \dots d\vec{y}^{v11} \\
 &\times W_0(\vec{y}) \dots W_0(\vec{y}^{v11}) \exp \left[-ik \frac{(\vec{y} - \vec{y}^{\sim}) \cdot \vec{z} + (\vec{y}^{1v} - \vec{y}^{v1}) \cdot \vec{z}'}{F} \right] \\
 &\times \exp \left[-ik \frac{\vec{x} \cdot (\vec{y} + \vec{y}' - \vec{y}^{v1} - \vec{y}^{v11}) + \vec{x}' \cdot (\vec{y}^{1v} + \vec{y}^v - \vec{y}^{\sim} - \vec{y}^{\sim})}{R} \right] \\
 &\times \exp [2ik(t-t') \vec{a} \cdot (\vec{x} - \vec{x}')] \quad . \quad (40)
 \end{aligned}$$

At this point, to proceed further with the analytic reduction, we need to make an extensive change of variables, to sum and difference coordinates.

We define

$$\vec{\sigma} = \frac{1}{2} (\vec{y} + \vec{y}^{\sim}) ; \quad \vec{\delta} = \vec{y} - \vec{y}^{\sim} , \quad (41)$$

$$\vec{\sigma}' = \frac{1}{2} (\vec{y}' + \vec{y}^{\sim}) ; \quad \vec{\delta}' = \vec{y}' - \vec{y}^{\sim} , \quad (42)$$

$$\vec{\sigma}^{\sim} = \frac{1}{2} (\vec{y}^{\sim} + \vec{y}^{v1}) ; \quad \vec{\delta}^{\sim} = \vec{y}^{\sim} - \vec{y}^{v1} , \quad (43)$$

$$\vec{\sigma}^{v1} = \frac{1}{2} (\vec{y}^v + \vec{y}^{v11}) ; \quad \vec{\delta}^{v1} = \vec{y}^v - \vec{y}^{v11} , \quad (44)$$

$$\vec{\sigma} = \frac{1}{2} (\vec{x} + \vec{x}') ; \quad \vec{\sigma} = \vec{x} - \vec{x}' . \quad (45)$$

* The integrals are exactly identical, except that (\vec{z}', t') appears in one, where (\vec{z}, t) appears in the other.

Noting that our results are only a function of $t-t'$, and not of t or t' separately, we define

$$\tau = t-t' \quad , \quad (46)$$

and replace $C_1(\vec{z}, \vec{z}', t, t')$ with $C_1(\vec{z}, \vec{z}'; \tau)$. Making use of the fact that for all of the transformations the Jacobian has unit value, we can write in place of Eq. (40)

$$\begin{aligned} C_1(\vec{z}, \vec{z}'; \tau) = & \beta^2 \left(\frac{k}{4\pi R} \right)^2 \left(\frac{P_r}{a} \right)^2 \int \dots \int d\vec{\mu} d\vec{\nu} d\vec{\sigma} \dots d\vec{\sigma}'' d\vec{\delta} \dots d\vec{\delta}'' \\ & \times W_0(\vec{\sigma} + \frac{1}{2}\vec{\delta}) W_0(\vec{\sigma} - \frac{1}{2}\vec{\delta}) W_0(\vec{\sigma}' + \frac{1}{2}\vec{\delta}') W_0(\vec{\sigma}' - \frac{1}{2}\vec{\delta}') \\ & \times W_0(\vec{\sigma}'' + \frac{1}{2}\vec{\delta}'') W_0(\vec{\sigma}'' - \frac{1}{2}\vec{\delta}'') W_0(\vec{\sigma}''' + \frac{1}{2}\vec{\delta}''') W_0(\vec{\sigma}''' - \frac{1}{2}\vec{\delta}''') \\ & \times \exp \left(-ik \frac{\vec{\delta} \cdot \vec{z} + \vec{\delta}'' \cdot \vec{z}'}{F} \right) \exp(2ik\tau \vec{\alpha} \cdot \vec{\nu}) \\ & \times \exp \left[-ik \frac{\vec{\mu} \cdot (\vec{\delta} + \vec{\delta}' + \vec{\delta}'' + \vec{\delta}''') + \vec{\nu} \cdot (\vec{\sigma} + \vec{\sigma}' - \vec{\sigma}'' - \vec{\sigma}''')}{R} \right] . \end{aligned} \quad (47)$$

In developing Eq. (47), we have made use of the fact that we can write

$$\begin{aligned} & \vec{x} \cdot (\vec{y} + \vec{y}' - \vec{y}'' - \vec{y}''') + \vec{x}'' \cdot (\vec{y}'' + \vec{y}'' - \vec{y}''' - \vec{y}''') \\ & = (\vec{\mu} + \frac{1}{2}\vec{\nu}) \cdot (\vec{y} + \vec{y}' - \vec{y}'' - \vec{y}''') + (\vec{\mu} - \frac{1}{2}\vec{\nu}) \cdot (\vec{y}'' + \vec{y}'' - \vec{y}''' - \vec{y}''') \\ & = \vec{\mu} \cdot (\vec{y} + \vec{y}' - \vec{y}'' - \vec{y}''') + \vec{y}'' + \vec{y}'' - \vec{y}''' - \vec{y}''' \\ & \quad + \frac{1}{2}\vec{\nu} \cdot (\vec{y} + \vec{y}' - \vec{y}'' - \vec{y}''') - \vec{y}'' - \vec{y}'' + \vec{y}''' + \vec{y}''' \\ & = \vec{\mu} \cdot (\vec{\delta} + \vec{\delta}' + \vec{\delta}'' + \vec{\delta}''') + \vec{\nu} \cdot (\vec{\sigma} + \vec{\sigma}' - \vec{\sigma}'' - \vec{\sigma}''') . \end{aligned} \quad (48)$$

Considering Eq. (32), we see that the $\vec{\sigma}$ -, $\vec{\sigma}'$ -, $\vec{\sigma}''$ -, and $\vec{\sigma}'''$ -integrations in Eq. (47) can all be performed. Thus we obtain the result that

$$\begin{aligned}
 C_1(\vec{z}, \vec{z}'; \tau) = & \beta^2 \left(\frac{k}{4\pi R} \right)^2 \left(\frac{P_1}{\mathcal{Q}F^2} \right)^2 \int \dots \int d\vec{\mu} d\vec{\nu} d\vec{\delta} \dots d\vec{\delta}''' \\
 & \times W_1(\vec{\delta}; \vec{\nu}/R) W_1(\vec{\delta}'; \vec{\nu}/R) W_1(\vec{\delta}''; -\vec{\nu}/R) W_1(\vec{\delta}'''; -\vec{\nu}/R) \\
 & \times \exp \left(-ik \frac{\vec{\delta} \cdot \vec{z} + \vec{\delta}''' \cdot \vec{z}'}{F} \right) \exp(2ik\tau \vec{\alpha} \cdot \vec{\nu}) \\
 & \times \exp \left[-ik \left(\frac{\vec{\mu}}{R} \right) \cdot (\vec{\delta} + \vec{\delta}' + \vec{\delta}'' + \vec{\delta}''') \right] .
 \end{aligned} \tag{49}$$

To further reduce this expression, we introduce, to replace the $(\vec{\delta}, \vec{\delta}', \vec{\delta}'', \vec{\delta}''')$ variables, the corresponding sum and difference coordinates, namely

$$\vec{p} = \frac{1}{2} (\vec{\delta} + \vec{\delta}') \quad ; \quad \vec{q} = \vec{\delta} - \vec{\delta}' \tag{50}$$

$$\vec{p}' = \frac{1}{2} (\vec{\delta}'' + \vec{\delta}''') \quad ; \quad \vec{q}' = \vec{\delta}'' - \vec{\delta}''' \tag{51}$$

Using these coordinates, we can rewrite Eq. (49) as

$$\begin{aligned}
 C_1(\vec{z}, \vec{z}'; \tau) = & \beta^2 \left(\frac{k}{4\pi R} \right)^2 \left(\frac{P_1}{\mathcal{Q}F^2} \right)^2 \int \dots \int d\vec{\mu} d\vec{\nu} d\vec{p} d\vec{p}' d\vec{q} d\vec{q}' \\
 & \times W_1(\vec{p} + \frac{1}{2}\vec{q}; \vec{\nu}/R) W_1(\vec{p} - \frac{1}{2}\vec{q}; \vec{\nu}/R) \\
 & \times W_1(\vec{p}' + \frac{1}{2}\vec{q}'; -\vec{\nu}/R) W_1(\vec{p}' - \frac{1}{2}\vec{q}'; -\vec{\nu}/R) \\
 & \times \exp \left[-ik \frac{(\vec{p} + \frac{1}{2}\vec{q}) \cdot \vec{z} + (\vec{p}' + \frac{1}{2}\vec{q}') \cdot \vec{z}'}{F} \right] \exp(2ik\tau \vec{\alpha} \cdot \vec{\nu}) \\
 & \times \exp \left[-2ik \left(\frac{\vec{\mu}}{R} \right) \cdot (\vec{p} + \vec{p}') \right] .
 \end{aligned} \tag{52}$$

If now, in analogy with Eq. (32), we define the W_2 -function by the expression

$$W_2(\vec{q}; \vec{\theta}; \vec{\phi}) = \int d\vec{p} W_1(\vec{p} + \frac{1}{2}\vec{q}; \vec{\theta}) W_1(\vec{p} - \frac{1}{2}\vec{q}; \vec{\theta}) \times \exp(-ik\vec{\phi} \cdot \vec{p}), \quad (53)$$

then we can rewrite Eq. (52) in the form

$$C_1(\vec{z}, \vec{z}'; \tau) = \beta^2 \left(\frac{k}{4\pi R}\right)^8 \left(\frac{P_I}{\sigma}\right)^2 \iiint d\vec{\mu} d\vec{\nu} d\vec{q} d\vec{q}' \times W_2\left(\vec{q}; \frac{\vec{\nu}}{R}; \frac{\vec{z}}{F} + 2\frac{\vec{\mu}}{R}\right) W_2\left(\vec{q}'; -\frac{\vec{\nu}}{R}; \frac{\vec{z}'}{F} + 2\frac{\vec{\mu}}{R}\right) \times \exp\left[-\frac{1}{2}ik\left(\vec{q} \cdot \frac{\vec{z}}{F} + \vec{q}' \cdot \frac{\vec{z}'}{F}\right) + 2ik\tau \vec{\alpha} \cdot \vec{\nu}\right]. \quad (54)$$

Making one more transformation to sum and difference coordinates, namely,

$$\vec{\Sigma} = \frac{1}{2}(\vec{q} + \vec{q}'); \quad \Delta = \vec{q} - \vec{q}', \quad (55)$$

and defining the W_3 -function by the expression

$$W_3(\vec{\Delta}; \vec{\theta}; \vec{\phi}, \vec{\phi}'; \vec{\psi}) = \int d\vec{\Sigma} W_2(\vec{\Sigma} + \frac{1}{2}\vec{\Delta}; \vec{\theta}; \vec{\phi}) W_2(\vec{\Sigma} - \frac{1}{2}\vec{\Delta}; -\vec{\theta}; \vec{\phi}') \times \exp(-ik\vec{\psi} \cdot \vec{\Sigma}), \quad (56)$$

we can rewrite Eq. (54) as

$$\begin{aligned}
 C_1(\vec{z}, \vec{z}'; \tau) = & \beta^2 \left(\frac{k}{4\pi R} \right)^2 \left(\frac{P_I}{\mathcal{Q}F-2} \right)^2 \iiint d\vec{\mu} d\vec{v} d\vec{\Sigma} d\vec{\Delta} \\
 & \times W_2\left(\vec{\Sigma} + \frac{1}{2}\vec{\Delta}; \frac{\vec{v}}{R}; \frac{\vec{z}}{F} + 2\frac{\vec{\mu}}{R}\right) W_2\left(\vec{\Sigma} - \frac{1}{2}\vec{\Delta}; -\frac{\vec{v}}{R}; \frac{\vec{z}'}{F} + 2\frac{\vec{\mu}}{R}\right) \\
 & \times \exp \left\{ -\frac{1}{2} i k \left[(\vec{\Sigma} + \frac{1}{2}\vec{\Delta}) \cdot \frac{\vec{z}}{F} + (\vec{\Sigma} - \frac{1}{2}\vec{\Delta}) \cdot \frac{\vec{z}'}{F} \right] \right\} \\
 & \times \exp (2 i k \tau \vec{\alpha} \cdot \vec{v}) \quad , \quad (57)
 \end{aligned}$$

which we can reduce to the form

$$\begin{aligned}
 C_1(\vec{z}, \vec{z}'; \tau) = & \beta^2 \left(\frac{k}{4\pi R} \right)^2 \left(\frac{P_I}{\mathcal{Q}F-2} \right)^2 \iiint d\vec{\mu} d\vec{v} d\vec{\Delta} \\
 & \times W_2\left(\vec{\Delta}; \frac{\vec{v}}{R}; \frac{\vec{z}}{F} + 2\frac{\vec{\mu}}{R}, \frac{\vec{z}}{F} + 2\frac{\vec{\mu}}{R}; \frac{1}{2}\left(\frac{\vec{z}}{F} + \frac{\vec{z}'}{F}\right)\right) \\
 & \times \exp \left[-\frac{1}{4} i k \vec{\Delta} \cdot \left(\frac{\vec{z}}{F} - \frac{\vec{z}'}{F} \right) + 2 i k \tau \vec{\alpha} \cdot \vec{v} \right] \quad . \quad (58)
 \end{aligned}$$

This is as far as we can proceed with the evaluation of the point statistics without some explicit expression for W_0 , from which we can evaluate W_1 , W_2 , and W_3 . In the next section we shall consider just such an explicit form for W_0 — but first, before closing this section, we note that our expression for \bar{I} , as given by Eq. (35), is susceptible to some further reduction in terms of the W_2 -function which we defined in Eq. (53). Comparing Eq.'s (35) and (53), and noting from Eq. (32) that $W_1(\vec{\delta}; \vec{\theta}) \equiv W_1(-\vec{\delta}; \vec{\theta})$, we see that we can write

$$I(\vec{z}, t) = \beta \frac{k^2}{64 \pi^2 R^2} \frac{P_I}{\mathcal{Q}F-2} W_2(0; 0; -\vec{\theta}) \quad . \quad (59)$$

With Eq. 's (58) and (59) in hand, we now take up, in the next section, the evaluation of these statistical quantities with W_0 having an explicit form.

corresponding to a circular aperture, with many transmission modes. The aperture and wave transmission outside the aperture, but inside the waveguide, would involve an with mathematically intricate expressions. To allow us to develop closed form results for the random parameter statistics, we shall assume that the aperture waveguide transmission function has a Gaussian (aper) with standard deviation σ . Thus we write

$$W_0(r) = \exp(-\frac{1}{2} \frac{r^2}{\sigma^2}) \quad (60)$$

With this form for W_0 , we shall be able to develop analytic expressions for \bar{W} , \bar{W}^2 , and \bar{W}^3 , which are the statistical functions \bar{W} and \bar{W}^2 . We start by noting that in accordance with Eq. (60), we can write

$$W_0(r) = \exp(-\frac{1}{2} \frac{r^2}{\sigma^2}) \quad (61)$$

$$W_0(r) = \exp(-\frac{1}{2} \frac{r^2}{\sigma^2}) \quad (62)$$

Making use of Eq. (60), we can then eq. (53) can be rewritten as

$$W_0(r) = \exp(-\frac{1}{2} \frac{r^2}{\sigma^2}) \quad (63)$$

We note that we can rewrite the exponent in Eq. (63) in the form

$$-\frac{1}{2} \frac{r^2}{\sigma^2} = -\frac{1}{2} \frac{r^2}{\sigma^2} \quad (64)$$

4.6 Evaluation With a Gaussian-Taper Aperture

It would be nice if we could evaluate Eq. 's (58) and (59) with W_0 corresponding to a circular aperture, with unity transmission inside the aperture and zero transmission outside the aperture. Unfortunately, this would involve us with mathematically intractable expressions. To allow us to develop closed form results for the random backscatter statistics, we shall assume that the aperture amplitude transmission function has a gaussian taper with standard deviation σ . Thus we write

$$W_0(\vec{y}) = \exp(-\frac{1}{2} y^2 / \sigma^2) \quad (60)$$

With this form for W_0 , we shall be able to develop analytic expressions for W_1 , W_2 , and W_3 , and thus for the statistical functions \bar{I} and C_1 .

We start by noting that in accordance with Eq. (26), we can write

$$\begin{aligned} A &= \int d\vec{y} \exp(-y^2 / \sigma^2) \\ &= 2\pi \int_0^\infty y dy \exp(-y^2 / \sigma^2) \\ &= \pi \sigma^2 \int_0^\infty d(y^2 / \sigma^2) \exp(-y^2 / \sigma^2) \\ &= \pi \sigma^2 \end{aligned} \quad (61)$$

Making use of Eq. (60), we see that Eq. (32) can be rewritten as

$$W_1(\vec{\delta}; \vec{\theta}) = \int d\vec{s} \exp \left[-\frac{1}{2} (|\vec{s} + \frac{1}{2}\vec{\delta}|^2 + |\vec{s} - \frac{1}{2}\vec{\delta}|^2) / \sigma^2 - i k \vec{\theta} \cdot \vec{s} \right] \quad (62)$$

We note that we can rewrite the exponent in Eq. (62) in the form

$$\begin{aligned} \phi &= -\frac{1}{2} \frac{|\vec{s} + \frac{1}{2}\vec{\delta}|^2 + |\vec{s} - \frac{1}{2}\vec{\delta}|^2}{\sigma^2} - i k \vec{\theta} \cdot \vec{s} \\ &= -\frac{2s^2 + \frac{1}{2}\delta^2 + 2ik\sigma^2 \vec{\theta} \cdot \vec{s}}{2\sigma^2} \end{aligned}$$

$$\begin{aligned}
&= - \frac{2(s^2 + ik \sigma^2 \vec{\theta} \cdot \vec{s} - \frac{1}{4} k^2 \sigma^4 \theta^2) + \frac{1}{2} k^2 \sigma^4 \theta^2 + \frac{1}{2} \delta^2}{2 \sigma^2} \\
&= - \frac{|\vec{s} + \frac{1}{2} ik \sigma^2 \vec{\theta}|^2}{\sigma^2} - \frac{1}{4} k^2 \sigma^2 \theta^2 - \frac{1}{4} (\delta/\sigma)^2 \quad . \quad (63)
\end{aligned}$$

By means of a simple change of the variable of integration, it can be shown that

$$\begin{aligned}
\int d\vec{s} \exp \left(- \frac{|\vec{s} + \frac{1}{2} ik \sigma^2 \vec{\theta}|^2}{\sigma^2} \right) &= \int d\vec{s} \exp \left(- \frac{s^2}{\sigma^2} \right) \\
&= 2\pi \int_0^\infty s ds \exp (-s^2/\sigma^2) \\
&= \pi \sigma^2 \int_0^\infty d(s^2/\sigma^2) \exp (-s^2/\sigma^2) \\
&= \pi \sigma^2 \quad , \quad (64)
\end{aligned}$$

so that it then follows that

$$W_1(\vec{\delta}; \vec{\theta}) = \pi \sigma^2 \exp \left(-\frac{1}{4} k^2 \sigma^2 \theta^2 - \frac{1}{4} \delta^2/\sigma^2 \right) \quad . \quad (65)$$

Starting with Eq. (53) and substituting in Eq. (65), we obtain for W_2 the expression

$$\begin{aligned}
W_2(\vec{q}; \vec{\theta}; \vec{\phi}) &= (\pi \sigma^2)^2 \int d\vec{p} \exp \left(-\frac{1}{2} k^2 \sigma^2 \theta^2 - \frac{1}{4} \frac{|\vec{p} + \frac{1}{2} \vec{q}|^2 + |\vec{p} - \frac{1}{2} \vec{q}|^2}{\sigma^2} \right. \\
&\quad \left. - ik \vec{\phi} \cdot \vec{p} \right) \quad . \quad (66)
\end{aligned}$$

The algebraic manipulations associated with Eq. 's (63) and (64) are applicable here, as in Eq. (62), and lead to the result that

$$W_2(\vec{q}; \vec{\theta}; \vec{\phi}) = 2 (\pi \sigma^2)^2 \exp \left[-\frac{1}{2} k^2 \sigma^2 (\theta^2 + \phi^2) - \frac{1}{8} q^2/\sigma^2 \right] \quad . \quad (67)$$

Proceeding in exactly the same way for the evaluation of W_3 , as given in Eq. (56), we obtain the result that

$$W_3(\vec{\Delta}; \vec{\theta}; \vec{\theta}', \vec{\theta}'') = 16 (\pi \sigma^2)^7 \exp \left[-\frac{1}{2} k^2 \sigma^2 (2\theta^2 + \theta'^2 + \theta''^2 + 2\theta\theta' + 2\theta\theta'') - \frac{1}{16} \Delta^2 / \sigma^2 \right]. \quad (68)$$

If we substitute Eq. 's (61) and (67) into Eq. (59), we get

$$\begin{aligned} \bar{I}(\vec{\theta}) &= \beta \frac{k^2}{64 \pi^2 R^2} \frac{P_r}{\pi \sigma^2 F^{-2}} 2 (\pi \sigma^2)^3 \exp \left(-\frac{1}{2} k^2 \sigma^2 \theta^2 \right) \\ &= \frac{\beta k^2 \sigma^4 P_r}{32 R^2 F^{-2}} \exp \left(-\frac{1}{2} k^2 \sigma^2 \theta^2 \right) \end{aligned} \quad (69)$$

where as a matter of convenience for later work we have rewritten the argument of \bar{I} as $\vec{\theta}$ instead of \vec{z} , and we have dropped the implied t -dependence in \bar{I} , since the right-hand-side is manifestly independent of t . (We recall from Eq. (2) that $\vec{\theta} = -\vec{z}/F$.)

Our basic problem at this point is to evaluate C_1 , as defined in Eq. (58), using the expression for W_3 given in Eq. (68). Substituting Eq. 's (61) and (68) into Eq. (58), we get

$$\begin{aligned} C_1(\vec{z}, \vec{z}'; \tau) &= \beta^2 \left(\frac{k}{4\pi R} \right)^8 \left(\frac{P_r}{\pi \sigma^2 F^{-2}} \right)^2 \iiint d\vec{\mu} d\vec{\nu} d\vec{\Delta} \\ &\quad \times 16 (\pi \sigma^2)^7 \exp \left\{ -\frac{1}{2} k^2 \sigma^2 \left[2 \left(\frac{\nu}{R} \right)^2 + \left| \frac{\vec{z}}{F} + 2 \frac{\vec{\mu}}{R} \right|^2 + \left| \frac{\vec{z}'}{F} + 2 \frac{\vec{\nu}}{R} \right|^2 \right. \right. \\ &\quad \left. \left. + \frac{1}{2} \left| \frac{\vec{z}}{F} + \frac{\vec{z}'}{F} \right|^2 \right] - \frac{1}{16} \Delta^2 / \sigma^2 \right\} \\ &\quad \times \exp \left[-\frac{1}{2} i k \vec{\Delta} \cdot \left(\frac{\vec{z}}{F} - \frac{\vec{z}'}{F} \right) + 2 i k \tau \vec{\alpha} \cdot \vec{\nu} \right] \\ &= \frac{\beta^2 k^8 \sigma^{10} P_r^2}{4096 \pi^3 R^3 F^{-4}} \exp \left(-\frac{1}{2} k^2 \sigma^2 \left| \frac{\vec{z}}{F} + \frac{\vec{z}'}{F} \right|^2 \right) \end{aligned}$$

$$\begin{aligned}
& \times \left\{ \int d\vec{r} \exp \left[-\frac{1}{8} k^2 \sigma^2 \left(\left| \frac{\vec{z}}{F} + 2 \frac{\vec{u}}{R} \right|^2 + \left| \frac{\vec{z}'}{F} + 2 \frac{\vec{u}}{R} \right|^2 \right) \right] \right\} \\
& \times \left\{ \int d\vec{v} \exp \left[-k^2 \sigma^2 \left(v/R \right)^2 + 2 i k \tau \vec{\alpha} \cdot \vec{v} \right] \right\} \\
& \times \left\{ \int d\vec{\Delta} \exp \left[-\frac{1}{16} \left(\frac{\Delta}{\sigma} \right)^2 - \frac{1}{4} i k \vec{\Delta} \cdot \left(\frac{\vec{z}}{F} - \frac{\vec{z}'}{F} \right) \right] \right\} \quad . \quad (70)
\end{aligned}$$

Each of the three integrals in Eq. (70) can be evaluated separately, in each case by completing the square. Thus we write

$$\begin{aligned}
\phi_1 &= -\frac{1}{16} \frac{\Delta^2}{\sigma^2} - \frac{1}{4} i k \vec{\Delta} \cdot \left(\frac{\vec{z}}{F} - \frac{\vec{z}'}{F} \right) \\
&= -\frac{1}{16} \left[\frac{\Delta^2}{\sigma^2} + 4 i k \vec{\Delta} \cdot (\vec{z}' - \vec{z}) - 4 k^2 \sigma^2 |\vec{z}' - \vec{z}|^2 + 4 k^2 \sigma^2 |\vec{z}' - \vec{z}|^2 \right] \\
&= -\frac{1}{16} \left| \frac{\Delta}{\sigma} + 2 i k \sigma (\vec{z}' - \vec{z}) \right|^2 - \frac{1}{4} k^2 \sigma^2 |\vec{z}' - \vec{z}|^2 \quad , \quad (71)
\end{aligned}$$

from which it follows that

$$\begin{aligned}
& \int d\vec{\Delta} \exp \left[-\frac{1}{16} \frac{\Delta^2}{\sigma^2} - \frac{1}{4} i k \vec{\Delta} \cdot \left(\frac{\vec{z}}{F} - \frac{\vec{z}'}{F} \right) \right] \\
&= \left\{ \int d\vec{\Delta} \exp \left[-\frac{1}{16} \left(\frac{\Delta}{\sigma} \right)^2 \right] \right\} \exp \left(-\frac{1}{4} k^2 \sigma^2 |\vec{z}' - \vec{z}|^2 \right) \\
&= 16 \pi \sigma^2 \exp \left(-\frac{1}{4} k^2 \sigma^2 |\vec{z}' - \vec{z}|^2 \right) \quad . \quad (72)
\end{aligned}$$

Similarly, we write

$$\phi_2 = -k^2 \sigma^2 \left(\frac{v}{R} \right)^2 + 2 i k \tau \vec{\alpha} \cdot \vec{v}$$

$$\begin{aligned}
&= -\left[k^2 \sigma^2 (\nu/R)^2 - 2 i k \tau \vec{\alpha} \cdot \vec{\nu} - \left(\frac{R\tau}{\sigma}\right)^2 \alpha^2 + \left(\frac{R\tau}{\sigma}\right)^2 \alpha^2\right] \\
&= -\left|\frac{k\sigma}{R} \vec{\nu} - i \frac{R\tau}{\sigma} \vec{\alpha}\right|^2 - \left(\frac{R\tau}{\sigma}\right)^2 \alpha^2
\end{aligned} \tag{73}$$

from which it follows that

$$\begin{aligned}
&\int d\vec{\nu} \exp \left\{ -k^2 \sigma^2 (\nu/R)^2 + 2 i k \tau \vec{\alpha} \cdot \vec{\nu} \right\} \\
&= \left\{ \int d\vec{\nu} \exp \left[-\left(\frac{k\sigma}{R}\right)^2 \nu^2 \right] \right\} \exp \left[-\left(\frac{R\tau}{\sigma}\right)^2 \alpha^2 \right] \\
&= \pi \left(\frac{R}{k\sigma}\right)^2 \exp \left[-\left(\frac{R\tau}{\sigma}\right)^2 \alpha^2 \right]
\end{aligned} \tag{74}$$

Finally, we write

$$\begin{aligned}
\phi_3 &= -\frac{1}{2} k^2 \sigma^2 \left(\left| \frac{\vec{z}}{F} + 2 \frac{\vec{\mu}}{R} \right|^2 + \left| \frac{\vec{z}'}{F} + 2 \frac{\vec{\mu}}{R} \right|^2 \right) \\
&= -\frac{1}{2} k^2 \sigma^2 \left[\frac{z^2}{F^2} + \frac{z'^2}{F^2} + 4 \left(\frac{\vec{z}}{F} + \frac{\vec{z}'}{F} \right) \cdot \frac{\vec{\mu}}{R} + 8 \frac{\mu^2}{R^2} \right] \\
&= -4 k^2 \sigma^2 \left\{ \left(\frac{\mu}{R} \right)^2 + \frac{1}{2} \frac{\vec{\mu}}{R} \cdot \left(\frac{\vec{z}}{F} + \frac{\vec{z}'}{F} \right) + \frac{1}{16} \left| \frac{\vec{z}}{F} + \frac{\vec{z}'}{F} \right|^2 \right. \\
&\quad \left. - \frac{1}{16} \left| \frac{\vec{z}}{F} - \frac{\vec{z}'}{F} \right|^2 + \frac{1}{8} \left[\left(\frac{z}{F} \right)^2 + \left(\frac{z'}{F} \right)^2 \right] \right\} \\
&= -4 k^2 \sigma^2 \left| \frac{\vec{\mu}}{R} + \frac{1}{4} \left(\frac{\vec{z}}{F} + \frac{\vec{z}'}{F} \right) \right|^2 + \frac{1}{4} k^2 \sigma^2 \left[\left(\frac{z}{F} \right)^2 + 2 \left[\left(\frac{z}{F} \right)^2 + 2 \left(\frac{\vec{z}}{F} \right) \cdot \left(\frac{\vec{z}'}{F} \right) \right. \right. \\
&\quad \left. \left. + \left(\frac{z'}{F} \right)^2 \right] - \frac{1}{2} k^2 \sigma^2 \left[\left(\frac{z}{F} \right)^2 + \left(\frac{z'}{F} \right)^2 \right] \right] \\
&= -4 k^2 \sigma^2 \left| \frac{\vec{\mu}}{R} + \frac{1}{4} \left(\frac{\vec{z}}{F} + \frac{\vec{z}'}{F} \right) \right|^2 - \frac{1}{4} k^2 \sigma^2 \left[\left(\frac{z}{F} \right)^2 - 2 \left(\frac{\vec{z}}{F} \right) \cdot \left(\frac{\vec{z}'}{F} \right) + \left(\frac{z'}{F} \right)^2 \right]
\end{aligned}$$

$$= -4 k^2 \sigma^2 \left| \frac{\vec{\mu}}{R} + \frac{1}{4} \left(\frac{\vec{z}}{F} + \frac{\vec{z}'}{F} \right) \right|^2 - \frac{1}{4} k^2 \sigma^2 \left| \frac{\vec{z}}{F} - \frac{\vec{z}'}{F} \right|^2 \quad (75)$$

from which, making use of Eq. (2), we can write

$$\begin{aligned} & \int d\vec{\mu} \exp \left[-\frac{1}{8} k^2 \sigma^2 \left(\left| \frac{\vec{z}}{F} + 2 \frac{\vec{\mu}}{R} \right|^2 + \left| \frac{\vec{z}'}{F} + \frac{\vec{\mu}}{R} \right|^2 \right) \right] \\ &= \left\{ \int d\vec{\mu} \exp \left[-4 k^2 \sigma^2 \left(\frac{\mu}{R} \right)^2 \right] \right\} \exp \left(-\frac{1}{4} k^2 \sigma^2 |\vec{\vartheta}' - \vec{\vartheta}|^2 \right) \\ &= \frac{1}{4} \pi \left(\frac{R}{k\sigma} \right)^2 \exp \left(-\frac{1}{4} k^2 \sigma^2 |\vec{\vartheta}' - \vec{\vartheta}|^2 \right) \end{aligned} \quad (76)$$

With these results in hand, namely Eq. 's (72), (74), and (76), we can now rewrite Eq. (70) as

$$\begin{aligned} C_1(\vec{z}, \vec{z}'; \tau) &= \frac{\beta^2 k^2 \sigma^{10} P_1^2}{4096 \pi^3 R^8 F^{-4}} \exp \left(-\frac{1}{4} k^2 \sigma^2 |\vec{\vartheta}' + \vec{\vartheta}|^2 \right) \\ &\times 16 \pi \sigma^2 \exp \left(-\frac{1}{4} k^2 \sigma^2 |\vec{\vartheta}' - \vec{\vartheta}|^2 \right) \\ &\times \pi \left(\frac{R}{k\sigma} \right)^2 \exp \left[-\left(\frac{R\tau\alpha}{\sigma} \right)^2 \right] \\ &\times \frac{1}{4} \pi \left(\frac{R}{k\sigma} \right)^2 \exp \left(-\frac{1}{4} k^2 \sigma^2 |\vec{\vartheta}' - \vec{\vartheta}|^2 \right) \\ &= \frac{\beta^2 k^4 \sigma^8 P_1^2}{1024 R^4 F^{-4}} \exp \left[-\frac{1}{4} k^2 \sigma^2 (|\vec{\vartheta}' + \vec{\vartheta}|^2 + 2 |\vec{\vartheta}' - \vec{\vartheta}|^2) \right] \\ &\times \exp \left[-(R\tau\alpha/\sigma)^2 \right] \end{aligned} \quad (77)$$

Making use of Eq. (69), we can rewrite Eq. (77) as

$$C_1(\vec{\vartheta}, \vec{\vartheta}'; \tau) = \bar{I}(\vec{\vartheta}) \bar{I}(\vec{\vartheta}') \exp \left(-\frac{1}{4} k^2 \sigma^2 |\vec{\vartheta}' - \vec{\vartheta}|^2 \right) \exp \left[-(R\tau\alpha/\sigma)^2 \right] \quad (78)$$

where, as a matter of future convenience, we have replaced the (\vec{z}, \vec{z}') arguments of C_1 by $(\vec{\vartheta}, \vec{\vartheta}')$ arguments.

Our basic results at this point are contained in Eq.'s (69) and (78). These give the point statistics of intensity fluctuations for the diffuse backscatter. We note that the point statistics have a normalized variance of unity. We take this as confirming the fact that the diffuse radiation is exponentially distributed, i. e., it corresponds to an electromagnetic field phasor with a gaussian random amplitude and a phase distributed uniformly over 0 to 2π . We shall use this insight into the signal statistics, together with the first and second moment values of Eq.'s (69) and (78) to define our simulation.

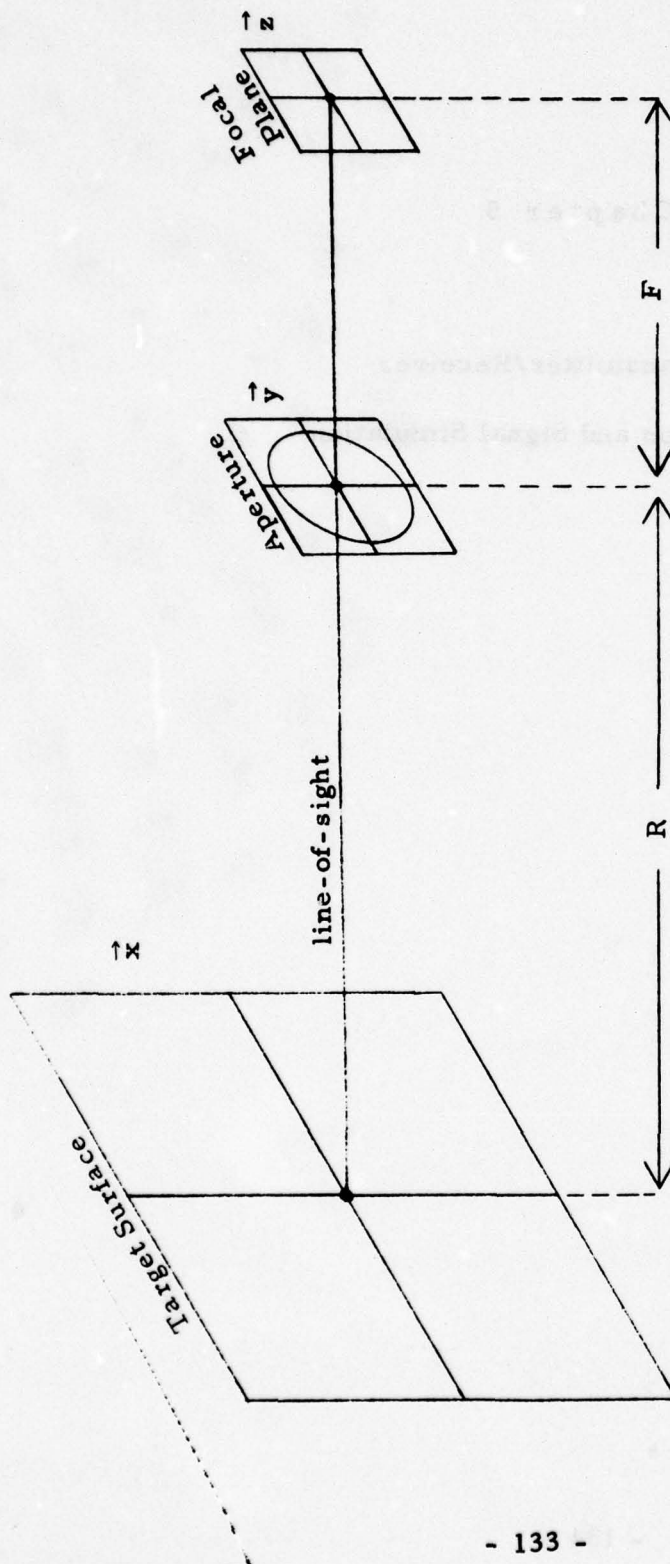


Figure 4.1 Engagement Geometry.

The randomly rough target surface is located at a range R from the transmitter/receiver aperture plane. The focal plane is located a distance F from the aperture plane. The two-dimensional vectors, \hat{x} , \hat{y} , \hat{z} , define positions on the target surface, the aperture plane, and the focal plane, respectively. The origins of these three coordinate systems are colinear, with the origin of the y coordinate system at the center of the aperture. The target surface can rotate (slowly) about an axis in the plane of the target surface, but otherwise the configuration is static.

Chapter 5

Laser Transmitter/Receiver

Sensor Definition and Signal Simulation

5.1 Introduction

In Chapter 4 we examined the focal plane statistics for the diffuse signal backscattered from a laser spot transmitted onto a rough surface. We developed expressions for the mean value, $\bar{I}(\vec{\vartheta})$, and the covariance, $C_1(\vec{\vartheta}, \vec{\vartheta}'; \tau)$ for the diffuse backscattered intensity at angular positions $\vec{\vartheta}$ and $\vec{\vartheta}'$ in the focal plane, with the origin of the $\vec{\vartheta}$ and $\vec{\vartheta}'$ coordinate systems corresponding to the nominal location of the laser spot as projected onto the focal plane. Here τ is the temporal separation of the time of the two measurements. Based on the assumption that the transmitter/receiver aperture had a gaussian taper with the amplitude transmission function being

$$W_0(\vec{y}) = \exp(-\frac{1}{2} y^2 / \sigma^2) \quad , \quad (1)$$

we showed there that the expected random backscatter signal power density at position $\vec{\vartheta}$ in the focal plane can be written as

$$\bar{I}(\vec{\vartheta}) = I_0 \exp[-\frac{1}{2} (k\sigma)^2 \vartheta^2] \quad , \quad (2)$$

where I_0 is a constant determined by various system and engagement parameters, and that the covariance of the power density at positions $\vec{\vartheta}$ and $\vec{\vartheta}'$ measured at instants separated by a period τ can be written as

$$C_1(\vec{\vartheta}, \vec{\vartheta}'; \tau) = \bar{I}(\vec{\vartheta}) \bar{I}(\vec{\vartheta}') \exp[-\frac{1}{2} (2^{-1/2} k\sigma)^2 |\vec{\vartheta} - \vec{\vartheta}'|^2] \\ \times \exp[-\frac{1}{2} (2^{1/2} R \alpha / \sigma)^2 \tau^2] \quad , \quad (3)$$

where α is a rotation rate, and R is the range to the rough surface target. Based on consideration of these results and of certain general

principles, it was argued that the diffuse return power density obeyed an exponential probability distribution.

In this report, starting with a consideration of these results, we shall first define a focal plane array to be used in sensing the backscatter return. We shall then develop information on the power density to be associated with the backscatter from a glint point. Using this, together with the diffuse return statistics, we shall then define the nature of the detector array output and define an algorithm for computer simulation of the array output.

5.2 Focal Plane Array Definition

We note from Eq. (3) that the spatial correlation range for the random backscattered signal power density on the focal plane has a correlation range of $2^{1/2}/(k\sigma)$. Accordingly, we argue that over a square region of size $[1/(k\sigma)]$ by $[1/(k\sigma)]$, the power density is essentially uniform at any instant, and has an average value at any instant equal to the value at that instant at the center of the element. Based on this consideration, we consider square detector elements of angular size Θ by Θ , where

$$\Theta = 1/(k\sigma) \quad , \quad (4)$$

to adequately finely sample the focal plane power density. Accordingly, we define a focal plane sensor array consisting of close packed square elements of angular size Θ by Θ . We consider the array to be four by four. This produces 16 outputs which we shall process to determine the location of the diffuse laser spot.

As a practical matter, in our simulation we shall assume that the output from each detector may be equated (to within a scaling factor) to the power density at the center of the detector element. For the 20×20 detector elements, the coordinates of the centers are

$$\vec{\mathcal{F}}_{i,j} = ((i-10.5)\Theta, (j-10.5)\Theta) \quad \begin{matrix} i = 1, 2, 3, \dots, 20 \\ j = 1, 2, 3, \dots, 20 \end{matrix} \quad (5)$$

where we use the notation $\vec{\mathcal{F}}_{i,j} = (\theta_x, \theta_y)$ to denote an angular vector with components θ_x and θ_y along the x-axis and y-axis. (We note that unlike our previous usage, here we use x and y to denote the two components of the focal plane/field-of-view two-dimensional coordinate system.)

To make our coordinate system explicit, we consider in writing Eq. (5) that the center of the array corresponds to the origin of the coordinate

system. Thus if the diffuse laser spot is centered at $\vec{\mathcal{F}}_0$, where

$$\begin{aligned}\vec{\mathcal{F}}_0 &= (\theta_{x,0}, \theta_{y,0}) \\ &= (\mu_0 \Theta, \nu_0 \Theta)\end{aligned}\quad (6)$$

then the average diffuse signal from each of the detectors in accordance with Eq. (2) will be

$$\bar{S}_0(i, j) = I_0 \exp \left[-\frac{1}{2} (k\sigma)^2 |\vec{\mathcal{F}}_0 - \vec{\mathcal{F}}_{i,j}|^2 \right] \quad (7)$$

The quantity I_0 represents I_0 times the appropriate scale factor to relate the power density at the center of the detector element to the detector signal. Making use of Eq. 's (4) and (5), we can rewrite Eq. (7) as

$$\bar{S}_0(i, j) = I_0 \exp \left(-\frac{1}{2} \{ [\mu_0 - (i - 10.5)]^2 + [\nu_0 - (j - 10.5)]^2 \} \right) \quad (8)$$

The covariance associated with the diffuse signal from the $(i, j)^{\text{th}}$ detector with respect to the $(i', j')^{\text{th}}$ detector can, in accordance with Eq. (3), be written as

$$\begin{aligned}C_0(i, j; i', j'; \tau) &= \bar{S}_0(i, j) \bar{S}_0(i', j') \\ &\times \exp \left\{ -\frac{1}{4} [(i - i')^2 + (j - j')^2] \right\} \\ &\times \exp \left[-\frac{1}{2} (\tau/T)^2 \right]\end{aligned}\quad (9)$$

where

$$T = \frac{\sigma}{2^{1/2} R \alpha} \quad (10)$$

is the correlation time.

With these expressions in hand, we now turn to a consideration of the expected focal plane power density to be associated with a glint point on the target. After this, we will be able to consider the problem of simulating the composite set of signals from the array of detectors.

5.3 Glint Return

We consider a glint point located at some position \vec{x}_g on the target. Based on the target surface curvature at that point and the strength of the laser spot (side-lobe) illumination of that point, the glint will appear as a point source of some amplitude, u_g . This amplitude does not vary with time, except perhaps as target rotation may shift the location of the glint point.* Using the formulation developed in the previous report, we can write for the amplitude of the glint-induced focal plane power density

$$U_g(\vec{z}) = -\frac{ik}{4\pi} u_g \int d\vec{y} W_0(\vec{y}) \times \frac{\exp\{ik[\mathcal{R}(\vec{x}_g, \vec{y}) + \mathcal{F}(\vec{y}, \vec{z})] + i\phi_r(\vec{y})\}}{\mathcal{R}(\vec{x}_g, \vec{y}) \mathcal{F}(\vec{y}, \vec{z})}, \quad (11)$$

where $W_0(\vec{y})$, the aperture amplitude transmission function, is given by the expression

$$W_0(\vec{y}) = \exp(-\frac{1}{2} y^2 / \sigma^2) \quad (12)$$

the path lengths, \mathcal{R} and \mathcal{F} , are given by the expressions

$$\mathcal{R}(\vec{x}_g, \vec{y}) \approx R + \frac{x_g^2}{2R} + \frac{y^2}{2R} - \frac{\vec{x}_g \cdot \vec{y}}{R} \quad (13)$$

$$\mathcal{F}(\vec{y}, \vec{z}) \approx F + \frac{y^2}{2F} + \frac{z^2}{2F} - \frac{\vec{y} \cdot \vec{z}}{F} \quad (14)$$

where R and F are the range to the target and the optics focal length,

* A glint point is a point where the target surface is normal to the line-of-sight. Accordingly, rotation of the target relative to the line-of-sight can shift the location of the glint point on the target and thus can also change the curvature at the glint point — as a consequence, changing the amplitude, u_g , of the return.

respectively, and ϕ_r , the optics induced phase shift at the aperture, which results in the target's being in focus at the focal plane, is given by the expression

$$\phi_r(\vec{y}) = -\frac{1}{2} k y^2 (R^{-1} + F^{-1}) \quad (15)$$

Making use of Eq. 's (13), (14), and (15), we can rewrite Eq. (11) as

$$U_g(\vec{z}) = -\frac{ik}{4\pi} \mathcal{U}_g \int d\vec{y} W_0(\vec{y}) \frac{\exp \left[ik \frac{x_g^2}{2R} - \vec{y} \cdot \left(\frac{\vec{x}_g}{R} + \frac{\vec{z}}{F} \right) + \frac{z^2}{2F} + R + F \right]}{RF} \quad (16)$$

The glint-induced focal plane power density can be written as

$$I_g(\vec{\vartheta}) = \frac{1}{2} |U_g(\vec{z})|^2 \quad (17)$$

(where $\vec{\vartheta} = -\vec{z}/F$ is the angular coordinate associated with focal plane position), which using Eq. (16) can be rewritten as

$$I_g(\vec{\vartheta}) = \left(\frac{k}{4\pi} \right)^2 \left(\frac{1}{2} |\mathcal{U}_g|^2 \right) \iint d\vec{y} d\vec{y}' W_0(\vec{y}) W_0(\vec{y}') \times \frac{\exp \left[ik (\vec{y} - \vec{y}') \cdot \left(\frac{\vec{x}_g}{R} - \vec{\vartheta} \right) \right]}{R^2 F^2} \quad (18)$$

Recalling from our previous work that

$$W_1(\vec{\delta}) = \int d\vec{s} W_0(\vec{s} + \frac{1}{2}\vec{\delta}) W_0(\vec{s} - \frac{1}{2}\vec{\delta}) \quad (19)$$

and transforming to sum and difference coordinates in the double integral of Eq. (18), we obtain the result that

$$I_g(\vec{\vartheta}) = \left(\frac{k}{4\pi R F} \right)^2 \left(\frac{1}{2} |\mathcal{U}_g|^2 \right) \int d\vec{s} W_1(\vec{\delta}) \exp \left[ik \vec{\delta} \cdot \left(\frac{\vec{x}_g}{R} - \vec{\vartheta} \right) \right] \quad (20)$$

Making use of Eq. (12), we can easily show that

$$W_1(\vec{\delta}) = \pi \sigma^2 \exp(-\frac{1}{4} \delta^2 / \sigma^2) \quad , \quad (21)$$

so that Eq. (20) can be rewritten as

$$I_0(\vec{\vartheta}) = \pi \sigma^2 \left(\frac{k}{4\pi RF} \right)^2 \left(\frac{1}{2} |\mathcal{U}_0|^2 \right) \int d\vec{\delta} \exp \left[-\frac{1}{4} (\delta/\sigma)^2 \right. \\ \left. + i k \vec{\delta} \cdot (\vec{\vartheta}_0 - \vec{\vartheta}) \right] \quad , \quad (22)$$

where $\vec{\vartheta}_0 = \vec{x}_0/R$ is the angle associated with the location of the glint point.

Completing the square in the exponent, we can write

$$\begin{aligned} \delta &= -\frac{1}{4} (\delta/\sigma)^2 + i k \vec{\delta} \cdot (\vec{\vartheta}_0 - \vec{\vartheta}) \\ &= -\frac{1}{4} \left[(\delta/\sigma)^2 - 4 i k \vec{\delta} \cdot (\vec{\vartheta}_0 - \vec{\vartheta}) - 4 (k\sigma)^2 |\vec{\vartheta}_0 - \vec{\vartheta}|^2 + 4 (k\sigma)^2 |\vec{\vartheta}_0 - \vec{\vartheta}|^2 \right] \\ &= -\frac{1}{4} \left| (\delta/\sigma) - 2 i k \sigma (\vec{\vartheta}_0 - \vec{\vartheta}) \right|^2 - (k\sigma)^2 |\vec{\vartheta}_0 - \vec{\vartheta}|^2 \end{aligned} \quad (23)$$

This allows us to rewrite Eq. (22) with a constant added to the variable of integration, as

$$I_0(\vec{\vartheta}) = \pi \sigma^2 \left(\frac{k}{4\pi RF} \right)^2 \left(\frac{1}{2} |\mathcal{U}_0|^2 \right) \exp \left[- (k\sigma)^2 |\vec{\vartheta}_0 - \vec{\vartheta}|^2 \right] \\ \times \int d\vec{\delta} \exp \left[-\frac{1}{4} (\delta/\sigma)^2 \right] \quad . \quad (24)$$

Since

$$\begin{aligned} \int d\vec{\delta} \exp \left[-\frac{1}{4} (\delta/\sigma)^2 \right] &= 2\pi \int_0^\infty \delta d\delta \exp \left[-\frac{1}{4} (\delta/\sigma)^2 \right] \\ &= 4\pi \sigma^2 \int_0^\infty d\left[\frac{1}{4} (\delta/\sigma)^2 \right] \exp \left[-\frac{1}{4} (\delta/\sigma)^2 \right] \\ &= 4\pi \sigma^2 \end{aligned} \quad (25)$$

then it follows from Eq. (24) that

$$I_g(\vec{\vartheta}) = I_g(0) \exp [-(k\sigma)^2 |\vec{\vartheta}_g - \vec{\vartheta}|^2] , \quad (26)$$

where

$$I_g(0) = \left(\frac{k\sigma}{2RF} \right)^2 \left(\frac{1}{2} |\mathcal{U}_g|^2 \right) . \quad (27)$$

Taking note of the fact that $I_g(\vec{\vartheta})$ varies only rather slowly over the area of a detector element, compared to its value at the center of the element, we argue the practicality of using the value at the center of the detector as a measure of the glint-induced detector signal. Thus we write for the glint-induced detector signal for the $(i, j)^{\text{th}}$ detector

$$\begin{aligned} S_g(i, j) &= I_g \exp [-(k\sigma)^2 |\vec{\vartheta}_g - \vec{\vartheta}_{1,j}|^2] \\ &= I_g \exp \left(-\{ [\mu_g - (i-10.5)]^2 + [v_g - (j-10.5)]^2 \} \right) , \end{aligned} \quad (28)$$

where I_g is related to $I_g(0)$ by the detector area integration factor, and (μ_g, v_g) denote the glint point location in units of Θ according to the relationship

$$\vec{\vartheta}_g \equiv (\mu_g \Theta, v_g \Theta) . \quad (29)$$

With Eq. 's (7), (9), and (28) in hand, we are now ready to consider the task of generating signals simulating the detector output. This is treated in the next section.

5.4 Array Output Simulation

We desire a simulation which will produce a set of sample values for the output of each of the 20×20 elements in the array. We denote these output values by $\mathcal{J}(i, j; n)$, where (i, j) denote the detector element, and n denotes the time, t , according to the equation

$$t = n \Delta t \quad . \quad (30)$$

We shall arbitrarily choose

$$\Delta t = T/4 \quad , \quad (31)$$

where T , according to Eq. (10), is the correlation time for the diffuse radiation. We recognize that this choice of Δt may not match the requirements of a larger, more extensive simulation, but argue that in accordance with Eq. (9), the correlation of the randomly fluctuating diffuse signal is good enough over the period, Δt , that interpolation to a finer time scale should be straightforward, and accordingly we plan to run the signal generation simulation considering only the time increment, Δt .

We now take note of the fact that the diffuse signal power density apparently obeys an exponential distribution, so that, because of the high correlation of the diffuse signal over a single detector element, we can consider the diffuse contribution to the detector output to also obey an exponential distribution. This, in turn, implies that the actual random variables are two orthogonal independent gaussianly distributed random variables, one of the orthogonal components being in phase with the glint and the other 90° out of phase. Thus we would associate with $\mathcal{J}(i, j; n)$ the two independent gaussian random amplitudes, $A_{\parallel}(i, j; n)$ and $A_{\perp}(i, j; n)$, with the glint return associated with the amplitude $A_g(i, j; n)$. The random diffuse signal would be $\frac{1}{2}[A_{\parallel}(i, j; n)]^2 + \frac{1}{2}[A_{\perp}(i, j; n)]^2$, to be equated with \bar{S}_0 and C_0 , and the glint signal would be $\frac{1}{2}[A_g(i, j; n)]^2$, to be associated

with S_0 . However, because of interference between the diffuse and glint returns, which in practice results in a composite signal obeying Rician statistics, we would write for the detector output

$$s(i, j; n) = \frac{1}{2} [A_{\parallel}(i, j; n) + A_0(i, j; n)]^2 + \frac{1}{2} [A_{\perp}(i, j; n)]^2 \quad (32)$$

Our simulation problem thus reduces to choosing A_{\parallel} , A_{\perp} , and A_0 so that

$$\begin{aligned} S_0(i, j) &= I_0 \exp \left(-\{[\mu_0 - (i - 10.5)]^2 + [\nu_0 - (j - 10.5)]^2\} \right) \\ &= \frac{1}{2} [A_0(i, j; n)]^2 \end{aligned} \quad (33)$$

$$\begin{aligned} \bar{S}_0(i, j) &= I_0 \exp \left(-\frac{1}{2} \{[\mu_0 - (i - 10.5)]^2 + [\nu_0 - (j - 10.5)]^2\} \right) \\ &= \frac{1}{2} \{ \langle [A_{\parallel}(i, j; n)]^2 \rangle + \langle [A_{\perp}(i, j; n)]^2 \rangle \} \end{aligned} \quad (34)$$

and

$$C_0(i, j, i', j'; n) = \bar{S}_0(i, j) \bar{S}_0(i', j') \exp \left\{ -\frac{1}{2} [(i - i')^2 + (j - j')^2] - \frac{1}{32} n^2 \right\} \quad (35)$$

with the additional condition that

$$\langle [A_{\parallel}(i, j; n)]^2 \rangle = \langle [A_{\perp}(i, j; n)]^2 \rangle \quad (36)$$

Our basic problem is the satisfaction of Eq. (35), particularly the exponential portion of the right-hand side. To accomplish this, we consider two three-dimensional arrays of gaussian random numbers, $r_{\parallel}(i, j; n)$ and $r_{\perp}(i, j; n)$, each having zero mean and unity standard deviation, and each element being independent of all other elements. Thus we can write

$$\langle r_{\parallel}(i, j; n) r_{\parallel}(i', j'; n') \rangle = \delta(i, i') \delta(j, j') \delta(n, n') \quad , \quad (37)$$

$$\langle r_{\perp}(i, j; n) r_{\perp}(i', j'; n') \rangle = \delta(i, i') \delta(j, j') \delta(n, n') \quad , \quad (38)$$

$$\langle r_{\parallel}(i, j; n) r_{\perp}(i', j'; n') \rangle = 0 \quad , \quad (39)$$

where the $\delta(i, i')$ -like terms are Kronecker deltas, equal to unity if the two arguments are identical, and equal to zero otherwise. We form as a weighted sum over these random arrays the terms

$$\begin{aligned} \tilde{A}_{\parallel}(i, j; n) &= \sum_{i', j', n'} r_{\parallel}(i-i', j-j'; n-n') \\ &\times \exp \left[-\frac{1}{4} (i'^2 + j'^2 + \frac{1}{8} n'^2) \right] \quad , \end{aligned} \quad (40)$$

and

$$\begin{aligned} \tilde{A}_{\perp}(i, j; n) &= \sum_{i', j', n'} r_{\perp}(i-i', j-j'; n-n') \\ &\times \exp \left[-\frac{1}{4} (i'^2 + j'^2 + \frac{1}{8} n'^2) \right] \quad . \end{aligned} \quad (41)$$

If we define the quantity $\tilde{\mathcal{A}}_0(i, j; n)$ by the expression

$$\tilde{\mathcal{A}}_0(i, j; n) = \frac{1}{2} [\tilde{A}_{\parallel}(i, j; n)]^2 + \frac{1}{2} [\tilde{A}_{\perp}(i, j; n)]^2 \quad , \quad (42)$$

then making use of Eq. 's (40) and (41), we can write

$$\begin{aligned} \tilde{\mathcal{A}}_0(i, j; n) &= \frac{1}{2} \sum_{\substack{p, q, m \\ p', q', m'}} \left\{ \exp \left[-\frac{1}{4} (p^2 + p'^2 + q^2 + q'^2 + \frac{1}{8} m^2 + \frac{1}{8} m'^2) \right] \right. \\ &\times [r_{\parallel}(i-p, j-q; n-m) r_{\parallel}(i-p', j-q'; n-m') \\ &\left. + r_{\perp}(i-p, j-q; n-m) r_{\perp}(i-p', j-q'; n-m')] \right\} \quad . \end{aligned} \quad (43)$$

We note that the average value can be written as

$$\begin{aligned}
 \langle \tilde{\mathcal{L}}_0(i, j; n) \rangle &= \frac{1}{2} \sum_{p, p', q, q', m, m'} \{ \exp [-\frac{1}{2} (p^2 + p'^2 + q^2 + q'^2 + \frac{1}{8} m^2 + \frac{1}{8} m'^2)] \\
 &\quad \times 2 \delta(p, p') \delta(q, q') \delta(m, m') \} \\
 &= \sum_{p, q, m} \exp [-\frac{1}{2} (p^2 + q^2 + \frac{1}{8} m^2)] \quad . \quad (44)
 \end{aligned}$$

Treating the summation as sufficiently fine scaled with respect to the exponential function that it can be replaced by an integration, we can write in place of Eq. (44)

$$\begin{aligned}
 \langle \tilde{\mathcal{L}}_0(i, j; n) \rangle &= \int_{-\infty}^{+\infty} \int_{-\infty}^{+\infty} \int_{-\infty}^{+\infty} dp \, dq \, dm \exp [-\frac{1}{2} (p^2 + q^2 + \frac{1}{8} m^2)] \\
 &= \int_{-\infty}^{+\infty} \int_{-\infty}^{+\infty} \int_{-\infty}^{+\infty} dp \, dq \, dm \exp \{ -\frac{1}{2} [p^2 + q^2 + (m/2^{3/2})^2] \} \\
 &= (2\pi)^{1/2} (2\pi)^{1/2} (2\pi \cdot 2^3)^{1/2} \\
 &= 8\pi^{3/2} \quad . \quad (45)
 \end{aligned}$$

Thus if we write

$$\begin{aligned}
 \mathcal{L}_0(i, j; n) &= \frac{1}{8} \pi^{-3/2} I_0 \exp \left(-\frac{1}{2} \{ [\mu_0 - (i-2.5)]^2 + [\nu_0 - (j-2.5)]^2 \} \right) \\
 &\quad \times \tilde{\mathcal{L}}_0(i, j; n) \quad , \quad (46)
 \end{aligned}$$

then manifestly Eq. (34) will be satisfied if we use $\mathcal{L}_0(i, j; n)$ to denote the

diffuse signal produced from the $(i, j)^{\text{th}}$ detector at time $n\Delta t$.

To consider whether this will also satisfy Eq. (35), we define the covariance function

$$\begin{aligned} \tilde{C}_0(i, j; i', j'; n) = & \langle [\mathcal{J}_0(i, j; N) - \langle \mathcal{J}_0(i, j; N) \rangle] \\ & \times [\mathcal{J}_0(i', j'; N-n) - \langle \mathcal{J}_0(i', j'; N-n) \rangle] \rangle \end{aligned} \quad (47)$$

Making use of Eq. (45), this can be recast in the form

$$\tilde{C}_0(i, j; i', j'; n) = \langle \tilde{\mathcal{J}}_0(i, j; N) \tilde{\mathcal{J}}_0(i', j'; N-n) \rangle - 64 \pi^3 \quad (48)$$

If we substitute Eq. (43) into Eq. (48), we obtain the result that

$$\begin{aligned} \tilde{C}_0(i, j; i', j'; n) + 64 \pi^3 = & \frac{1}{4} \sum_{\substack{p, p', p'', p''' \\ q, q', q'', q''' \\ m, m', m'', m'''}} \left\{ \exp \left\{ -\frac{1}{4} [p^2 + p'^2 + p''^2 + p'''^2 \right. \right. \\ & + q^2 + q'^2 + q''^2 + q'''^2 + \frac{1}{8} (m^2 + m'^2 + m''^2 + m'''^2)] \left. \right\} \\ & \times \{ \langle r_{\parallel}(i-p, j-q; N-m) r_{\parallel}(i-p', j-q'; N-m') \\ & \times r_{\parallel}(i'-p'', j'-q''; N-n-m'') r_{\parallel}(i'-p''', j'-q'''; N-n-m''') \rangle \\ & + 2 \langle r_{\parallel}(i-p, j-q; N-m) r_{\parallel}(i-p', j-q'; N-m') \\ & \times r_{\perp}(i'-p'', j'-q''; N-n-m'') r_{\perp}(i'-p''', j'-q'''; N-n-m''') \rangle \\ & + \langle r_{\perp}(i-p, j-q; N-m) r_{\perp}(i-p', j-q'; N-m') \\ & \times r_{\perp}(i'-p'', j'-q''; N-n-m'') r_{\perp}(i'-p''', j'-q'''; N-n-m''') \rangle \} \} \quad (49) \end{aligned}$$

The first and third ensemble averages in Eq. (49) give rise to the following Kronecker delta functions, namely

$$\begin{aligned} & \delta(p, p') \delta(p'', p''') \delta(q, q') \delta(q'', q''') \delta(m, m') \delta(m'', m''') \\ & + \delta(p - i + i', p'') \delta(p' - i + i', p''') \delta(q - j + j', q'') \delta(q' - j + j', q''') \\ & \times \delta(m - n, m'') \delta(m' - n, m''') \\ & + \delta(p - i + i', p''') \delta(p' - i + i', p'') \delta(q - j + j', q''') \delta(q' - j + j', q'') \\ & \times \delta(m - n, m''') \delta(m' - n, m'') \end{aligned}$$

while the second ensemble average gives rise to the much less complex Kronecker delta function, namely

$$\delta(p, p') \delta(p'', p'') \delta(q, q') \delta(q'', q'') \delta(m, m') \delta(m'', m'') .$$

If we insert these Kronecker delta functions into Eq. (49) in place of the ensemble averages, and carry out the six trivial summations, we obtain the result that

$$\begin{aligned} \tilde{C}_p(i, j; i', j'; n) + 64 \pi^3 = & \frac{1}{4} \sum_{\substack{p, p', q, q', m, m' \\ p'', q'', m''}} \left\{ 4 \exp \left\{ -\frac{1}{2} [p^2 + p'^2 + q^2 + q'^2 + \frac{1}{8} (m^2 - m'^2)] \right\} \right. \\ & + 2 \exp \left\{ -\frac{1}{4} [p^2 + p'^2 + (p - i + i')^2 + (p' - i + i')^2 \right. \\ & \quad \left. + q^2 + q'^2 + (q - j + j')^2 + (q' - j + j')^2 \right. \\ & \quad \left. + \frac{1}{8} m^2 + \frac{1}{8} m'^2 + \frac{1}{8} (m - n)^2 + \frac{1}{8} (m' - n)^2] \right\} \\ & + 2 \exp \left\{ -\frac{1}{4} [p^2 + p'^2 + (p - i + i')^2 + (p' - i + i')^2 \right. \\ & \quad \left. + q^2 + q'^2 + (q - j + j')^2 + (q' - j + j')^2 \right. \end{aligned}$$

$$+ \frac{1}{8} m^2 + \frac{1}{8} m'^2 + \frac{1}{8} (m-n)^2 + \frac{1}{8} (m'-n)^2] \} \quad (50)$$

We note that the multiple sum over the first exponential in Eq. (50) can be rewritten as the product of two equivalent sums, each identical to the final form of Eq. (44). Hence, considering Eq. (45), we see that the double sum over the first exponential in Eq. (50) can be replaced by $64 \pi^3$, cancelling the $64 \pi^3$ on the left-hand-side of that equation. We further note that the two other exponentials in Eq. (50) are identical, and moreover note that the multiple sum can be split into the product of two identical parts. Thus we get from Eq. (50)

$$\tilde{C}_0(i, j; i', j'; n) = \left\{ \sum_{p, q, m} \exp \left\{ -\frac{1}{4} [p^2 + (p-i+i')^2 + q^2 + (q-j+j')^2 + \frac{1}{8} m^2 + \frac{1}{8} (m-n)^2] \right\} \right\}^2 \quad (51)$$

Completing the squares in the exponent of Eq. (51), we write

$$\begin{aligned} p^2 + (p-i+i')^2 &= 2 p^2 - 2 p(i-i') + (i-i')^2 \\ &= 2 [p^2 - p(i-i') + \frac{1}{4} (i-i')^2 - \frac{1}{4} (i-i')^2] + (i-i')^2 \\ &= 2 [p - \frac{1}{2} (i-i')]^2 + \frac{1}{2} (i-i')^2 \end{aligned} \quad (52)$$

$$q^2 + (q-j+j')^2 = 2 [q - \frac{1}{2} (j-j')]^2 + \frac{1}{2} (j-j')^2 \quad (53)$$

$$m^2 + (m-n)^2 = 2 (m - \frac{1}{2} n)^2 + \frac{1}{2} n^2 \quad (54)$$

Again arguing that we can approximate the summation by an integration, and making use of Eq. 's (52), (53), and (54), we can rewrite Eq. (51) as

$$\begin{aligned} \tilde{C}_0(i, j; i', j'; n) = & \left\{ \exp \left\{ -\frac{1}{4} \left[\frac{1}{2} (i-i')^2 + \frac{1}{2} (j-j')^2 + \frac{1}{16} n^2 \right] \right\} \right. \\ & \times \int_{-\infty}^{+\infty} \int_{-\infty}^{+\infty} \int_{-\infty}^{+\infty} dp \, dq \, dn \exp \left\{ -\frac{1}{2} \left[p - \frac{1}{2} (i-i') \right]^2 \right. \\ & \left. \left. - \frac{1}{2} \left[q - \frac{1}{2} (j-j') \right]^2 - \frac{1}{16} (m - \frac{1}{2} n)^2 \right] \right\} \right\}^2. \end{aligned} \quad (55)$$

The triple integral in Eq. (55) can be cast in a form identical to Eq. (45), indicating that it can be replaced by $8\pi^{3/2}$. Thus we obtain, in place of Eq. (55), the expression

$$\tilde{C}_0(i, j; i', j'; n) = 64\pi^3 \exp \left\{ -\frac{1}{4} \left[(i-i')^2 + (j-j')^2 \right] - \frac{1}{32} n^2 \right\} \quad (56)$$

Comparing this expression with Eq. (35), we see that with the normalization implied by Eq. (46), the expression for $\mathcal{J}_0(i, j; n)$ defined there would behave exactly as we would wish the diffuse return alone to behave.

To incorporate the glint contribution and take proper account of normalization, we would work with the detector signals $\mathcal{J}(i, j; n)$ as defined by Eq. (32). The normalization will be achieved by letting A_{\parallel} , A_{\perp} , and A_g have the following values

$$\begin{aligned} A_{\parallel}(i, j; n) = & \left(\frac{I_0}{8\pi^{3/2}} \right)^{1/2} \exp \left(-\frac{1}{4} \left\{ [\mu_0 - (i - 10.5)]^2 + [\nu_0 - (j - 10.5)]^2 \right\} \right) \\ & \times \tilde{A}_{\parallel}(i, j; n), \end{aligned} \quad (57)$$

$$A_{\perp}(i, j; n) = \left(\frac{I_0}{8\pi^{3/2}} \right)^{1/2} \exp \left(-\frac{1}{2} \{ [\mu_0 - (i-10.5)]^2 + [\nu_0 - (j-10.5)]^2 \} \right) \times \tilde{A}_{\perp}(i, j; n) \quad (58)$$

$$A_0(i, j; n) = (2I_0)^{1/2} \exp \left(-\frac{1}{2} \{ [\mu_0 - (i-10.5)]^2 + [\nu_0 - (j-10.5)]^2 \} \right) \quad (59)$$

Eq.'s (32), (40), (41), (57), (58), and (59) completely define the basis for generation of the time-varying outputs of the 16 detectors, in conformance with expected spatial-temporal statistics, except that Eq.'s (40) and (41), involving as they do infinite summations, are not practical for a simulation. To get around this problem, we note that the exponentials provide a basis for rapid truncation of the series. If we restrict the summations to $i' = -5$ to $+5$, $j' = -5$ to $+5$, and $n' = -16$ to $+16$, we would be dropping terms whose weighting factors are equal to 1×10^{-4} or less. Accordingly, we write, in place of Eq.'s (40) and (41),

$$\tilde{A}_{\parallel}(i, j; n) = \sum_{i'=-5}^5 \sum_{j'=-5}^5 \sum_{n'=-16}^{16} r_{\parallel}(i-i', j-j'; n-n') \times \exp \left[-\frac{1}{2} (i'^2 + j'^2 + \frac{1}{8} n'^2) \right] \quad (60)$$

$$\tilde{A}_{\perp}(i, j; n) = \sum_{i'=-5}^5 \sum_{j'=-5}^5 \sum_{n'=-16}^{16} r_{\perp}(i-i', j-j'; n-n') \times \exp \left[-\frac{1}{2} (i'^2 + j'^2 + \frac{1}{8} n'^2) \right] \quad (61)$$

We note that since i and j are restricted to the range 1 to 20, $i-i'$ and $j-j'$ are each restricted to the range -4 to 25 (a total of 30 elements by 30 elements). The range of n is from zero to infinity, and thus the

range of $n-n'$ is from -16 to infinity. To simplify the computation of the $\tilde{A}_{\parallel}(i, j; n)$ and $\tilde{A}_{\perp}(i, j; n)$ terms, we suggest the computation of the intermediate terms

$$\tilde{B}_{\parallel}(p, q; n) = \sum_{n'=-16}^{16} r_{\parallel}(p, q; n-n') \exp\left(-\frac{1}{32} n'^2\right), \quad (62)$$

$$\tilde{B}_{\perp}(p, q; n) = \sum_{n'=-16}^{16} r_{\perp}(p, q; n-n') \exp\left(-\frac{1}{32} n'^2\right). \quad (63)$$

Then we can write

$$\tilde{A}_{\parallel}(i, j; n) = \sum_{i', j'=-5}^5 \tilde{B}_{\parallel}(i-i', j-j'; n) \exp\left[-\frac{1}{4}(i'^2 + j'^2)\right], \quad (64)$$

$$\tilde{A}_{\perp}(i, j; n) = \sum_{i', j'=-5}^5 \tilde{B}_{\perp}(i-i', j-j'; n) \exp\left[-\frac{1}{4}(i'^2 + j'^2)\right]. \quad (65)$$

In the computer simulation, we would start by generating a string of 33 values of r_{\parallel} and of r_{\perp} for each of the $(30)^2$ values of (p, q) between $(-4$ and $25)$ by $(-4$ and $25)$. We would assign those 33 values to "time slots," $n-n'$, numbered -16 to $+16$. We would then evaluate each of the $(30)^2$ corresponding values of \tilde{B}_{\parallel} and \tilde{B}_{\perp} using Eq. 's (62) and (63) with $n = 0$. These $(30)^2$ values of \tilde{B}_{\parallel} and of \tilde{B}_{\perp} would then be substituted into Eq. 's (64) and (65) for i and j taking the $(20)^2$ values from $(1$ to $20)$ by $(1$ to $20)$. Using Eq. 's (57), (58), and (59), and then Eq. (32), we would generate the $(20)^2$ values of $\mathcal{A}(i, j; n)$ for that time instant.

To advance to the next time instant, we would shift the $(30)^2$ values of r_{\parallel} and of r_{\perp} one time slot, i. e., $(30)^2 \times 33$ values would have to be shifted. Of these, $(30)^2$ would be shifted out of the $(-16 \text{ to } 16)$ array at one end, and a new set of $(30)^2$ random values would have to be supplied at the other end. With these values of r_{\parallel} and r_{\perp} , we could then repeat the procedure of the preceding paragraph (still retaining $n = 0$ in Eq.'s (62) and (63). The end product would be a new set of $(20)^2$ detector signals corresponding to the output a time Δt later. This procedure can now be continuously cycled to generate the time-dependent sequence of outputs.

Chapter 6

Simulation of Random Laser Backscatter

6.1 Introduction

In this chapter, we wish to take up the problem of simulating the random laser backscatter signal as it would be sensed in a high energy laser weapon satellite-to-satellite engagement. We assume a shared aperture transmitter/receiver with a two-dimensional receiver focal plane array and a gaussian tapered aperture. At the target, we assume an extensive, diffusely scattering surface with a single glint point, not necessarily located at the intended aimpoint. We assume that the weapon system is able to sense the apparent position of the aimpoint, and that some sort of servo control system adjusts the pointing of the transmitter/receiver with respect to this position. This, in conjunction with target motion, servo design considerations, laser bias (and bias estimates), and the effect of the speed-of-light round-trip transit time delay, results in a laser miss distance (or position of the laser spot on the target) and the associated laser backscatter signal. This position of the laser spot on the target is well-defined, but unfortunately is not necessarily the desired aimpoint.

With the engagement situation thus defined, we wish to establish a basis for calculation of the randomly fluctuating laser backscatter signal. The demonstration of a valid simulation of the detector signals in this case is the subject of this chapter.

The theoretical basis for such a simulation was generated in the two previous chapters. In fact, in the latter of these reports, the general principles for the simulation and the supporting equations for the simulation

were explicitly developed. With one minor change to allow treatment of a larger detector array than was treated there, we will be able to use those results here in their original form.

The kinematics of the engagement, including the high bandwidth servo control, have been modeled in Chapter 2. We shall use the simulation program developed there as the overall structure on which we shall "build" the current simulation, using that simulation to provide all of the angular and spatial position information and all line-of-sight orientation data, as well as accommodating the speed-of-light round-trip transit time delay effects.

In the next section, we will briefly review the features of this kinematics simulation and along with that define the optical system parameters. The section after that will review the philosophy of simulation of the random laser backscatter signal generation and present the pertinent formulas. The section after that will describe the pertinent aspects of the full computer simulation. The final section will present some sample runs and discuss special features in these results.

It is to be remembered that this simulation, like all those that have preceded it, is just a building block leading to a complete simulation of closed loop laser pointing bias control system. The simulation we are presenting in this report does not attempt this bias control function. However, the backscatter signal it provides will be the basis for estimating the pointing error (even in the presence of a glint point), and thus will allow us, in the next chapter, to demonstrate the full closed-loop laser pointing bias control function.

6.2 System and Engagement Parameters

Our engagement is specified in terms of a set of coordinates and velocities for the target satellite and for the laser weapon satellite — each defined in a hypothetical "absolute" (rectangular) inertial coordinate space. To accommodate relativistic effects, we shift to an inertial coordinate system fixed in the laser weapon satellite. In this coordinate system, the target satellite appears at some range, moving with some uniform linear velocity. The laser weapon system senses the apparent position of the target aimpoint and commands the gimbals so that the shared aperture optics see the aimpoint as appearing at or very near the center of the receiver's field-of-view.

The apparent position of the target aimpoint is, however, not the "current" actual position, but rather the position of the target aimpoint a time R/c ago. Here, R is the range, and c is the speed of light. This is accomplished in the simulation with a push-down data stack that stores previous target position data. Each time that apparent target position information is required, the data stack is assessed to see where the target was a time R/c ago, and this is used to calculate the apparent target position. Each simulation time increment, the actual target position is updated and the information is placed at the top of the push-down data stack.

Using the difference between the apparent target position and the direction defined by the center of the receiver's field-of-view as the tracking error, the servo system calculates a gimbal pointing correction and the gimbal orientation is appropriately updated. This gimbal orientation is combined with any applicable laser bias to define the deviation of the transmitted laser beam. This transmitted laser beam direction information is entered into a second push-down stack.

To determine the nature of the backscattered laser signal at any instant, the two push-down data stacks are assessed at time R/c ago for

the target position information, and at time $2 R/c$ ago for the transmitted laser beam direction. (These time delays exactly account for the speed-of-light transit time delays involved.) With this information, we can calculate where the laser beam struck the target relative to the aimpoint.

Knowing where the laser beam was incident on the target at the time when the backscatter signal which we are now receiving was produced, and knowing where the target aimpoint appears in the receiver's field-of-view, we can then calculate the position in the receiver's field-of-view where the laser would appear to be striking the target surface. To the extent that the diffuse scattering of the laser beam from the target surface indicates the laser position, this will be the center of the location of the diffuse scattering as seen in the receiver's field-of-view.

In addition to this diffuse scattering, there may also be some laser backscatter signal associated with a glint point on the target. The glint point position is specified in terms of its position relative to the target aimpoint. Knowing this displacement and knowing the (R/c) delayed position of the target aimpoint, we can then calculate the position of the glint point as seen by the shared aperture sensor. The strength of the glint-induced portion of the backscattered laser signal is dependent on some inherent measure of the glint region multiplied by the laser flux density falling on the glint point. This laser flux density can be calculated from the difference between the apparent positions of the glint point and the point where the laser beam (center) strikes the target, each as seen by the shared aperture receiver.

The shared aperture optics correspond to a gaussian tapered transmission telescope aperture. By means of some sort of T/R switch, this telescope is used both to transmit a laser beam and to receive radiation from the target. The telescope adjustment is assumed to be such that the

laser beam (which, in its transmitted form, has the same gaussian taper) is focused on the target. Similarly, this telescope adjustment causes a focused image of the target to fall on the receiver focal plane. The receiver can be considered to consist of two focal planes dividing the received signal via a dichroic beamsplitter. One of these two focal planes senses the target image and from this determines the target aimpoint position and the tracking error. Exactly how this focal plane is organized, how it functions, and even the matter of what wavelengths it operates at are matters of no concern to us here. We simply assume that it is capable of producing target aimpoint information, and that it is perfectly registered, via the dichroic beamsplitter, with the second focal plane.

The second focal plane is the one we shall be particularly concerned with. It senses the backscattered laser signal, and it is from the information that it produces that we shall ultimately attempt to determine the laser position on the target. Hereafter, when we speak of the shared aperture receiver focal plane, we shall have this unit in mind. The focal plane consists of a square array, 20×20 of square elements. The center of this array corresponds to the center of the shared aperture sensor's field-of-view.

The shared aperture has a gaussian taper such that its amplitude transmission function varies as $\exp(-\frac{1}{2} y^2/\sigma^2)$. Thus σ is a measure of the radius of the aperture. (If we were to define the aperture in terms of the e^{-1} intensity levels, the aperture diameter would be 2σ .) Operating with a laser wavelength λ , and optical wave number $k = 2\pi/\lambda$, we may take $(k\sigma)^{-1}$ as a measure of the aperture's diffraction spread. The individual detector elements are defined as having an angular subtense equal to $(k\sigma)^{-1}$, thus matching their resolution fairly closely to that of the laser beam transmission process.

The two-dimensional detector array is assumed to be organized along the previously introduced $\hat{\xi}$ and $\hat{\eta}$ axes. (These axes are defined to be unit vectors each perpendicular to the direction of \hat{u}_g , the unit vector that defines the centerline of the receiver's field-of-view. They are mutually perpendicular and $\hat{\xi}$ is also perpendicular to the gimbal system polar axis, \hat{z} .) For convenience, we shall measure apparent angular position in focal plane array coordinates, (μ, ν) . With a 20×20 detector array, the center of the sensor field-of-view (corresponding to the gimbal orientation unit vector, \hat{u}_g) lies at the intersection between the 10th and 11th detectors, horizontally and vertically. Thus the (μ, ν) coordinates of the center of the detector just above and to the right of the array center is $(\frac{1}{2}, \frac{1}{2})$, while that of the center of the detector just above and to the left of the array center is $(-\frac{1}{2}, \frac{1}{2})$. If the angle vector $\vec{\theta} = (\vartheta_{\xi}, \vartheta_{\eta})$ denotes the angular position of a point in space relative to the center of the sensor's field-of-view, then the (μ, ν) -coordinates of that point's image would be $(k_{\sigma} \vartheta_{\xi}, k_{\sigma} \vartheta_{\eta})$.

We have previously shown that if $\vec{\theta}$ is the angular separation between the apparent position of the point where the laser beam strikes the target, and some position defined by a point of interest on the focal plane, then the diffuse laser backscatter intensity will vary as $\exp[-\frac{1}{2}(k_{\sigma})^2 |\vec{\theta}|^2]$. If we let (μ_0, ν_0) denote the apparent position where the center of the (delayed) laser beam strikes the target, and let I_0 be a measure of the diffuse backscatter peak intensity, then the diffuse intensity of a focal plane position (μ, ν) will be

$$I_0(\mu, \nu) = I_0 \exp \left\{ -\frac{1}{2} [(\mu - \mu_0)^2 + (\nu - \nu_0)^2] \right\} \quad (1)$$

Though we have not previously worked it out in detail, it is easy to show* that the laser beam power density at the target falls off $\exp \{ -[k\sigma/R]x^2 \}$. Recognizing that (x/R) represents an angle, in this case the angular separation between the laser spot center and the position of the glint point, we can write for the glint strength

$$I_g = I_{g,0} \exp \{ -[(\mu_0 - \mu_g)^2 + (\nu_0 - \nu_g)^2] \} \quad (2)$$

where (μ_g, ν_g) denotes the position in the focal plane of the image of the glint point. The quantity, $I_{g,0}$ is a measure of the combined glint strength (proportional to the product of the local radii of curvature) and the laser power density. It represents a peak possible value of glint strength, corresponding to when the laser beam center is coincident with the glint point. The actual glint strength at any time is really I_g , as given by Eq. (2). The glint return appears to come from a point source (as distinct from the extended source for the diffuse return) and so at the laser backscatter sensor focal plane, the intensity at focal plane positions (μ, ν) is

$$I_g(\mu, \nu) = I_g \exp \{ -[(\mu - \mu_g)^2 + (\nu - \nu_g)^2] \} \quad (3)$$

* This can be accomplished by considering Eq.'s (19) and (60) of Chapter 4. With appropriate substitution, we find that the laser amplitude at position \vec{x} on the target, at range R is proportional to

$$\int d\vec{y} \exp [-ik\vec{y} \cdot (\vec{x}/R)] \exp (-\frac{1}{2} y^2 / \sigma^2) \quad .$$

Noting that when we complete the square

$$\frac{y^2}{\sigma^2} + 2i \frac{k}{R} \vec{x} \cdot \vec{y} = \left(\frac{\vec{y}}{\sigma} + \frac{k\sigma}{R} \vec{x} \right)^2 + \left(\frac{k\sigma}{R} \vec{x} \right)^2 \quad ,$$

we see that the amplitude is proportional to $\exp \left[-\frac{1}{2} \left(\frac{k\sigma}{R} \vec{x} \right)^2 \right]$.

From this, it follows that the intensity is proportional to $\exp \left[- \left(\frac{k\sigma}{R} \vec{x} \right)^2 \right]$.

Making use of Eq.'s (1), (2), and (3), we see that if we can calculate the apparent position of the laser spot (at the place where it strikes the target) and of the glint point, each in terms of where it appears on the focal plane, then we can calculate the glint and diffuse backscatter intensities at any point in the focal plane. The calculation of the apparent positions of the glint point and of the diffuse spot center follow in a straightforward manner from our previous modeling of the basic engagement and gimbal servo in Chapter 2.

We let the gimbal orientation unit vector, which defines the direction associated with the centerline of the backscatter sensor's field-of-view, be denoted by \hat{u}_g , and let the target aimpoint position be defined by a range vector, \vec{r}_t . If \vec{d}_g is a vector denoting the displacement between the target aimpoint and the glint point, then the unit vector defining the direction from the shared aperture receiver to the glint point will be

$$\hat{u}_{gl} = \frac{\vec{r}_t + \vec{d}_g}{|\vec{r}_t + \vec{d}_g|} \quad (4)$$

Similarly, if \vec{d}_{lm} is a vector denoting the distance by which the laser beam missed the target aimpoint, then the unit vector defining the direction from the shared aperture receiver to the point where the laser spot struck the target (to produce the diffuse return) will be

$$\hat{u}_d = \frac{\vec{r}_t + \vec{d}_{lm}}{|\vec{r}_t + \vec{d}_{lm}|} \quad (5)$$

The backscatter sensor's focal plane coordinates are defined by the two unit vectors $\hat{\xi}$ and $\hat{\eta}$, corresponding to the focal plane μ and ν coordinates, respectively. Thus we can calculate the focal plane coordinates of the apparent position of the glint point as

$$\mu_g = (\hat{u}_{gl} - \hat{u}_g) \cdot \hat{\xi} \quad , \quad (6a)$$

$$\nu_g = (\hat{u}_{gl} - \hat{u}_g) \cdot \hat{\eta} \quad . \quad (6b)$$

Similarly, for the apparent position of the center of the laser spot on the target, we can write

$$\mu_o = (\hat{u}_o - \hat{u}_g) \cdot \hat{\xi} \quad , \quad (7a)$$

$$\nu_o = (\hat{u}_o - \hat{u}_g) \cdot \hat{\eta} \quad . \quad (7b)$$

With Eq. 's (6) and (7) to tell us where the glint and diffuse return sources would appear to be centered on the backscatter sensor's focal plane, and with Eq. 's (1), (2), and (3) to tell us how the two types of back-scattered energy are distributed about their centers, we are now ready to consider the problem of detailed simulation of the randomly fluctuating backscatter return. We take up the problem of how to generate a simulation of this random return in the next two sections. In the next section, we review the statistical properties we require of our simulated backscatter return. The section after that explains how we accomplished the simulation.

6.3 Synopsis of the Required Backscatter Statistics

From our previous work, we know that the laser backscatter signal intensity incident on any point (any detector) in the sensor focal plane will obey a Rician distribution, and that this Rician distribution can be considered to be composed of two components added coherently. Of the two components, the first has a non-random intensity and corresponds to the glint return, as defined by Eq. (3). The other component has an intensity that fluctuates randomly, in accordance with a Rayleigh distribution. Its average intensity is as defined by Eq. (1).

Since a Rayleigh distributed random variable with intensity $I_b(\mu, \nu)$ corresponds to a pair of independent random amplitudes, A_{\parallel} and A_{\perp} , each with a zero mean gaussian distribution and standard deviations σ_A

$$\sigma_A = \langle (A_{\parallel})^2 \rangle^{1/2} = \langle (A_{\perp})^2 \rangle^{1/2} \quad , \quad (8)$$

such that

$$\sigma_A = [I_b(\mu, \nu)]^{1/2} \quad . \quad (9)$$

We may view the glint return as being due to a constant amplitude, A_g , which gives rise to the glint intensity $I_g(\mu, \nu)$ according to the equation

$$I_g(\mu, \nu) = \frac{1}{2} [A_g(\mu, \nu)]^2 \quad . \quad (10)$$

Then the Rician distribution random intensity, I , is simulated by forming the gaussian random variable, A_{\parallel} and A_{\perp} , and then writing

$$I(\mu, \nu) = \frac{1}{2} \{ [A_{\parallel}(\mu, \nu) + A_g(\mu, \nu)]^2 + [A_{\perp}(\mu, \nu)]^2 \} \quad . \quad (11)$$

Our problem thus reduces to finding a way to generate the gaussian variables A_{\parallel} and A_{\perp} .

The generation of these two random variables is complicated by the fact that not only must they each be a gaussian random variable, but that they must also each, separately, conform to certain spatial and temporal covariance considerations. To accommodate these constraints, we have previously found it convenient to introduce the quantities \tilde{A}_{\parallel} and \tilde{A}_{\perp} , and generate a full two-dimensional time-varying array of these quantities, a pair for each of the 20×20 detectors in the sensor focal plane array. Each of these pairs will have zero mean value and the same standard deviation. If the standard deviation is $\tilde{\sigma}$, i.e.,

$$\tilde{\sigma} = \langle (\tilde{A}_{\parallel})^2 \rangle^{1/2} = \langle (\tilde{A}_{\perp})^2 \rangle^{1/2}, \quad (12)$$

then we would write

$$A_{\parallel} = (\sigma_A / \tilde{\sigma}) \tilde{A}_{\parallel}, \quad (13)$$

$$A_{\perp} = (\sigma_A / \tilde{\sigma}) \tilde{A}_{\perp}. \quad (14)$$

It is, of course, to be understood that not only are \tilde{A}_{\parallel} , \tilde{A}_{\perp} , and A_{\parallel} , A_{\perp} two-dimensional, 20×20 , time-varying arrays, but that σ_A as used in Eq. 's (13) and (14) is also a two-dimensional, 20×20 , (but not time-varying) array.

To discuss the spatial-temporal statistics of \tilde{A}_{\parallel} and \tilde{A}_{\perp} , it is convenient to first make explicit the spatial and temporal dependence. Measuring focal plane position in units of $(k\sigma)^{-1}$, i.e., in the (μ, ν) coordinate system, and measuring time in units of

$$T_4 = \frac{1}{4} \frac{\sigma}{2^{1/2} R \alpha}, \quad (15)$$

i. e., denoting the time t by

$$n = t/T_4, \quad (16)$$

where α in Eq. (15) is the angular rate of rotation of the target surface normal with respect to the line-of-sight from the laser to the target, we would write the diffuse intensity as $I_b(\mu, \nu; n)$. We have shown in Chapter 5 that the spatial temporal covariance function for the diffuse intensity should be

$$\begin{aligned} C_b(\mu, \mu', \nu, \nu'; n, n') &= \langle [I_b(\mu, \nu; n) - \langle I_b(\mu, \nu; n) \rangle] \\ &\quad \times [I_b(\mu', \nu'; n') - \langle I_b(\mu', \nu'; n') \rangle] \rangle \\ &\quad \times \exp \left\{ -\frac{1}{2} [(\mu - \mu')^2 + (\nu - \nu')^2] \right\} \\ &= I_b(\mu, \nu) I_b(\mu', \nu') \exp \left[-\frac{1}{32} (n - n')^2 \right], \end{aligned} \quad (17)$$

where $I_b(\mu, \nu)$ is to be understood as the mean value of the diffuse intensity at focal plane position (μ, ν) — as specified by Eq. (1). Our task in developing the spatial-temporal random variables $\tilde{A}_{\parallel}(\mu, \nu; n)$ and $\tilde{A}_{\perp}(\mu, \nu; n)$ is to insure that if we write

$$I_b(\mu, \nu; n) = \frac{1}{2} \left(\frac{\sigma_A}{\sigma} \right)^2 \{ [\tilde{A}_{\parallel}(\mu, \nu; n)]^2 + [\tilde{A}_{\perp}(\mu, \nu; n)]^2 \}, \quad (18)$$

then $I_b(\mu, \nu; n)$ will have the statistics required by Eq. (17), with $\tilde{A}_{\parallel}(\mu, \nu; n)$ and $\tilde{A}_{\perp}(\mu, \nu; n)$ each having a zero mean value, being statistically independent, and having the same statistical nature. In the next section, we show how this can be done.

6.4 Generation of the \tilde{A} -Quantities

As suggested in an earlier report, in view of the gaussian nature of the spatial and the temporal correlation functions in Eq. (17), we wish to develop results for \tilde{A} which have nearly equivalent gaussian correlation functions. We showed that this could be accomplished if we generated a spatial-temporal array of statistically independent zero mean, unit variance gaussian random variables, $r_{\parallel}(\mu, \nu; n)$ and $r_{\perp}(\mu, \nu; n)$, and formed the sums

$$\begin{aligned} \tilde{A}_{\parallel}(\mu, \nu; n) = & \sum_{\mu'} \sum_{\nu'} \sum_{n'} r_{\parallel}(\mu', \nu'; n') \\ & \times \exp \left\{ -\frac{1}{4} [(\mu - \mu')^2 + (\nu - \nu')^2] - \frac{1}{32} (n - n')^2 \right\} \end{aligned} \quad (19)$$

$$\begin{aligned} \tilde{A}_{\perp}(\mu, \nu; n) = & \sum_{\mu'} \sum_{\nu'} \sum_{n'} r_{\perp}(\mu', \nu'; n') \\ & \times \exp \left\{ -\frac{1}{4} [(\mu - \mu')^2 + (\nu - \nu')^2] - \frac{1}{32} (n - n')^2 \right\} \end{aligned} \quad (20)$$

where the sums on μ' , ν' , and n' are each from $-\infty$ to $+\infty$. It can be shown that this definition of the \tilde{A} 's will result in Eq. (17) being satisfied. It is thus basically no more difficult to generate the set of spatially-temporally correlated gaussian random variables \tilde{A}_{\parallel} and \tilde{A}_{\perp} than it is to generate the statistically independent set of gaussian random variables r_{\parallel} and r_{\perp} — for which there are standard computer procedures.

Taking note of Eq. (12), we can evaluate $\tilde{\sigma}^2$ by making use of the fact that the r 's are zero mean, unit variance, and statistically independent. From these facts, it follows that

$$\tilde{\sigma}^2 = \sum_{\mu'} \sum_{\nu'} \sum_{n'} \exp \left\{ -\frac{1}{2} [(\mu - \mu')^2 + (\nu - \nu')^2] - \frac{1}{16} (n - n')^2 \right\} . \quad (21)$$

Approximating these infinite summations by integrations, so that the three same sums turn into three gaussian integrations, each from $-\infty$ to $+\infty$, which we can perform with trivial effort, we get

$$\begin{aligned} \tilde{\sigma}^2 &\approx (2\pi)^{1/2} (2\pi)^{1/2} (16\pi)^{1/2} \\ &= 8\pi^{3/2} . \end{aligned} \quad (22)$$

Thus, combining Eq.'s (1), (9), and (22), we can rewrite Eq.'s (13) and (14) as

$$A_{\parallel}(\mu, \nu, n) = \left(\frac{I_b}{8\pi^{3/2}} \right)^{1/2} \exp \left\{ -\frac{1}{4} [(\mu - \mu_0)^2 + (\nu - \nu_0)^2] \right\} \tilde{A}_{\parallel}(\mu, \nu; n) , \quad (23)$$

$$A_{\perp}(\mu, \nu; n) = \left(\frac{I_b}{8\pi^{3/2}} \right)^{1/2} \exp \left\{ -\frac{1}{4} [(\mu - \mu_0)^2 + (\nu - \nu_0)^2] \right\} \tilde{A}_{\perp}(\mu, \nu; n) . \quad (24)$$

As a practical matter, it is reasonable to limit the summations in Eq. (19) and (20) to a range of ± 5 around μ and ν for the μ' and ν' -summations, respectively, and to ± 16 around n for the n' -summation. Compared to a peak exponential weighting factor of unity, the terms thus dropped all have weighting factors less than $\exp \left[-\frac{1}{4} (\pm 5)^2 \right] = 1.93 \times 10^{-3}$, or than $\exp \left[-\frac{1}{32} (\pm 16)^2 \right] = 3.35 \times 10^{-4}$. With these truncated summations, it is convenient to rewrite Eq.'s (19) and (20) as

$$\begin{aligned} \tilde{A}_{\parallel}(\mu, \nu; n) &= \sum_{\mu'=-5}^5 \sum_{\nu'=-5}^5 \sum_{n'=-16}^{16} r_{\parallel}(\mu - \mu', \nu - \nu'; n - n') \\ &\times \exp \left\{ -\frac{1}{4} [(\mu')^2 + (\nu')^2] - \frac{1}{32} (n')^2 \right\} , \end{aligned} \quad (25)$$

$$\begin{aligned} \tilde{A}_1(\mu, \nu; n) = & \sum_{\mu'=-5}^5 \sum_{\nu'=-5}^5 \sum_{n'=-16}^{16} r_{\perp}(\mu-\mu', \nu-\nu'; n-n') \\ & \times \exp \left\{ -\frac{1}{4} [(\mu')^2 + (\nu')^2] - \frac{1}{32} (n')^2 \right\} . \end{aligned} \quad (26)$$

Eq.'s (25) and (26) are directly suggestive of a method of generating the \tilde{A} 's in a computer program in a time-varying manner.

If we desire a 20×20 array of values of the \tilde{A} , we start with a three-dimensional storage array $(20 + 2 \times 5) \times (20 + 2 \times 5) \times (1 + 2 \times 16) = 30 \times 30 \times 33$ in size. Consider this array to be organized as a "push-down" stack, i.e., at each time increment we push the values stored in the array down one level in the 33 dimension. The data stored in the bottom level, i.e., the 33rd level, is pushed out while new data is introduced in the first level. There are two push-down stacks, one filled with the r_{\parallel} -values and the other with the r_{\perp} -values. Each time cycle, i.e., every time the actual clock time in the simulation increased by T_4 , the data stacks would each be pushed down one and new sets of 30×30 gaussian random values would be added at the top of each stack. With the data thus stored in the stack, it is a straightforward matter to then implement Eq.'s (25) and (26) to calculate the \tilde{A} -values. The fact that mostly the same r -values are used, with (slightly) different weighting factors, to calculate the various \tilde{A} -values insures the desired spatial correlation. The fact that mostly the same r -values will also be used after the push-down process to calculate the \tilde{A} -values at different times, again with (slightly) different weighting factors, results in the desired temporal correlation.

Our computer simulations for the generation of the \tilde{A} -values, and thus for the random backscatter signals, are defined by the programs listed in the appendix. In these programs, we have found it convenient to

- 171 -

6.5 Sample Results

To exercise the random laser backscatter signal generation program and subroutines listed in the appendix, we ran a series of engagements and took as computer outputs the 20×20 array of random intensities generated by the backscattered laser signal on the receiver focal plane array. In all cases, the shared aperture size corresponded to $\sigma = 1.0 \text{ m}$, and the laser wavelength was $\lambda = 1.0 \times 10^{-6} \text{ m}$ (i.e., $k = 6.28 \times 10^6$). In the first three cases, we considered a target starting at 1.0 Mm range and closing at a rate of $1 \times 10^4 \text{ m/sec}$, with a crossing velocity of 50 m/sec . The tracking data, which we list in Table 1, is the same for all three cases. The tracker utilizes an $f_s = 100 \text{ Hz}$ servo bandwidth.

As can be seen, by about time $t = 0.030 \text{ sec}$ after tracking starts, the tracking error has settled in to very near its asymptotic value. (The very small, apparently random, tracking error variations beyond this time are almost entirely due to computer round-off errors.) This time for the apparent tracking error to settle to its asymptotic value can be considered to be composed of three parts. First, there is a time R/c after time $t = 0.0$ before the track error sensor gets any target position data. Second, there is a time of the order of $2/f_s$ for the servo transients to die out. Third, there is a time $2R/c$ that must elapse before the effect of fully stable tracking can be seen at the receiver as a stable laser miss distance. Thus the total time delay is

$$T_0 = 3R/c + 2/f_s \quad . \quad (27)$$

Until this much time has elapsed, the laser spot will "wander" over the target and there is no particular interest in the statistics of the backscattered laser intensity pattern.

With a crossing velocity of $V_{\perp} = 50.0 \text{ m/sec}$ and a range of $R = 1.0 \times 10^6 \text{ m}$ for a perfectly stabilized target, the target surface will

rotate with respect to the line-of-sight with an angular rate

$$\alpha = V_{\perp}/R = 5.0 \times 10^{-6} \text{ rad/sec} \quad , \quad (28)$$

so that in accordance with Eq. (15), the quarter correlation time, * T_4 , is

$$\begin{aligned} T_4 &= \frac{1}{4 \cdot 21^{1/2} \times 1.0 \times 10^3 \times 5 \times 10^{-6}} \\ &= 3.5355 \times 10^{-3} \text{ sec} \quad . \end{aligned} \quad (29)$$

Accordingly, in Tables 2, 3, and 4, we took printouts of the 20×20 array every four milliseconds. Results are shown for the time interval from $t > T_0$ to $t = 0.1 \text{ sec}$.

Backscatter signal results are shown in Tables 2, 3, 4 (and 5, 6) as ten plus the logarithm (to the base ten) of the intensity, but with all negative values set to zero.

$$\text{Printed Value} = \begin{cases} 10 + \log_{10} [I(\mu, \nu; n)] & , \\ \quad \text{if } I(\mu, \nu; n) \geq 1.0 \times 10^{-10} \\ 0 & , \text{ if } I(\mu, \nu; n) < 1.0 \times 10^{-10} \end{cases} \quad (30)$$

The difference between the data in Tables 2, 3, and 4 concerns the specified glint point strength, $I_{g,0}$. In all cases $I_0 = 1.0$. For Table 2, $I_{g,0} = 0.0$; for Table 3, $I_{g,0} = 100$; and for Table 4, $I_{g,0} = 10,000$. In all three cases, the glint point was taken as being coincident with the aimpoint.

Tables 5 and 6 correspond to essentially the same case as Table 2, i.e., $I_{g,0} = 0.0$, except that the crossing velocities are $V_{\perp} = 100 \text{ m/sec}$

* The correlation time is more properly taken to be $4 T_4$, rather than simply T_4 .

and 200 m/sec , respectively. Accordingly, the values of T_d are 1.7678×10^{-3} sec and 0.8839 sec , respectively. To properly show the temporal dependence in Table 4, we show the detector array output every two milliseconds, and in Table 5, we show the output every one millisecond. Although data was generated for the entire period from $t \geq 0.03$ sec to $t = 0.10$ sec , in each case we show only the first 18 pages of output.

In each of the pages of Tables 2, 3, 4, 5, and 6, we have drawn a pair of crossed lines to define the $\hat{\xi}$ - and $\hat{\eta}$ -axes on the focal plane, with the intersection of the lines defining the center of the focal plane. (The horizontal line corresponds to the $\hat{\xi}$ -axis.) The position of the laser spot is shown by the shaded ellipses (in all cases on the left half of the page). The open ellipsis indicates the position of the target aimpoint and of the glint point location, when appropriate. (In all cases, this is on the right half of the page.)

Interpretation of the data in Tables 2-6 is straightforward. The presence of the glint point is clearly manifested by the very large signal return in the vicinity of the glint point location in Tables 3 and 4. The average value in each case is in good agreement with that defined by Eq. (2). (There are small fluctuations due, in part, to the added random return and, in part, to a small amount of laser spot jitter associated with computer round-off error in the tracking process.) The results listed in Tables 2 to 6 can be shown to satisfy the statistical considerations we have previously presented.

With this ability to accurately simulate the laser backscatter signal as seen by the receiver detector array, we are now ready to take up the problem of determining the laser spot position from the backscatter signal and closing a boresight error control servo loop with this information. We shall take this up in the next chapter.

Table 6.1

Target Tracking Kinematics

These results correspond to the engagement of Tables 2, 3, and 4,

$R_0 = 1.0 \text{ Mm}$, $V_{\text{CLOSING}} = 1.0 \times 10^4 \text{ m/sec}$, $V_L = 50 \text{ m/sec}$.

TIME (SEC.)	RANGE (METERS)	MISS DISTANCE (METERS)	THETA (RAD.)	FREQ (RAD.)
0.004	1.0000E+06	1.0000E+06	1.570796	1.57079627
0.005	1.0000E+06	1.0000E+06	1.570796	1.57079617
0.006	1.0000E+06	1.0000E+06	1.570796	1.57079610
0.007	1.0000E+06	1.0000E+06	1.570796	1.57079604
0.008	1.0001E+06	1.0001E+06	1.570796	1.57079597
0.009	1.0001E+06	8.8935E+05	1.570796	1.57079591
0.010	1.0001E+06	2.9793E-01	1.570796	1.57079585
0.011	1.0001E+06	2.7342E-01	1.570796	1.57079578
0.012	1.0001E+06	2.4891E-01	1.570796	1.57079572
0.013	1.0001E+06	2.2440E-01	1.570796	1.57079566
0.014	1.0001E+06	2.0486E-01	1.570796	1.57079560
0.015	1.0001E+06	2.0017E-01	1.570796	1.57079554
0.016	1.0001E+06	2.1041E-01	1.570796	1.57079548
0.017	1.0001E+06	2.2565E-01	1.570796	1.57079542
0.018	1.0002E+06	2.3094E-01	1.570796	1.57079536
0.019	1.0002E+06	2.3622E-01	1.570796	1.57079530
0.020	1.0002E+06	2.4151E-01	1.570796	1.57079524
0.021	1.0002E+06	2.4679E-01	1.570796	1.57079518
0.022	1.0002E+06	2.4713E-01	1.570796	1.57079512
0.023	1.0002E+06	2.3763E-01	1.570796	1.57079506
0.024	1.0002E+06	2.2788E-01	1.570796	1.57079500
0.025	1.0002E+06	2.2320E-01	1.570796	1.57079494
0.026	1.0002E+06	2.2848E-01	1.570796	1.57079488
0.027	1.0002E+06	2.3375E-01	1.570796	1.57079482
0.028	1.0003E+06	2.3903E-01	1.570796	1.57079476
0.029	1.0003E+06	2.3937E-01	1.570796	1.57079470
0.030	1.0003E+06	2.3481E-01	1.570796	1.57079464
0.031	1.0003E+06	2.3514E-01	1.570796	1.57079458
0.032	1.0003E+06	2.3032E-01	1.570796	1.57079452
0.033	1.0003E+06	2.3559E-01	1.570796	1.57079446
0.034	1.0003E+06	2.3592E-01	1.570796	1.57079440
0.035	1.0003E+06	2.3122E-01	1.570796	1.57079434
0.036	1.0003E+06	2.3155E-01	1.570796	1.57079428
0.037	1.0003E+06	2.2635E-01	1.570796	1.57079422
0.038	1.0004E+06	2.3212E-01	1.570796	1.57079416
0.039	1.0004E+06	2.3739E-01	1.570796	1.57079410
0.040	1.0004E+06	2.3772E-01	1.570796	1.57079404
0.041	1.0004E+06	2.3301E-01	1.570796	1.57079398
0.042	1.0004E+06	2.3334E-01	1.570796	1.57079392
0.043	1.0004E+06	2.2863E-01	1.570796	1.57079386
0.044	1.0004E+06	2.3789E-01	1.570796	1.57079380
0.045	1.0004E+06	2.3422E-01	1.570796	1.57079374
0.046	1.0004E+06	2.2950E-01	1.570796	1.57079368
0.047	1.0004E+06	2.3489E-01	1.570796	1.57079362
0.048	1.0005E+06	2.3509E-01	1.570796	1.57079356
0.049	1.0005E+06	2.3076E-01	1.570796	1.57079350
0.050	1.0005E+06	2.3562E-01	1.570796	1.57079344
0.051	1.0005E+06	2.3595E-01	1.570796	1.57079338
0.052	1.0005E+06	2.3122E-01	1.570796	1.57079332

0.053	1.0005E+06	2.3647E-01	1.570796	1.57079375
0.054	1.0005E+06	2.3681E-01	1.570796	1.57079370
0.055	1.0005E+06	2.3206E-01	1.570796	1.57079364
0.056	1.0005E+06	2.3240E-01	1.570796	1.57079360
0.057	1.0005E+06	2.2765E-01	1.570796	1.57079354
0.058	1.0006E+06	2.3290E-01	1.570796	1.57079349
0.059	1.0006E+06	2.3815E-01	1.570796	1.57079345
0.060	1.0006E+06	2.3848E-01	1.570796	1.57079339
0.061	1.0006E+06	2.3376E-01	1.570796	1.57079335
0.062	1.0006E+06	2.3448E-01	1.570796	1.57079330
0.063	1.0006E+06	2.2973E-01	1.570796	1.57079326
0.064	1.0006E+06	2.3473E-01	1.570796	1.57079320
0.065	1.0006E+06	2.3489E-01	1.570796	1.57079314
0.066	1.0006E+06	2.3312E-01	1.570796	1.57079309
0.067	1.0006E+06	2.3576E-01	1.570796	1.57079305
0.068	1.0007E+06	2.3573E-01	1.570796	1.57079301
0.069	1.0007E+06	2.3093E-01	1.570796	1.57079294
0.070	1.0007E+06	2.3126E-01	1.570796	1.57079290
0.071	1.0007E+06	2.2649E-01	1.570796	1.57079285
0.072	1.0007E+06	2.3172E-01	1.570796	1.57079279
0.073	1.0007E+06	2.3695E-01	1.570796	1.57079275
0.074	1.0007E+06	2.3729E-01	1.570796	1.57079269
0.075	1.0007E+06	2.3731E-01	1.570796	1.57079265
0.076	1.0007E+06	2.3774E-01	1.570796	1.57079261
0.077	1.0007E+06	2.3807E-01	1.570796	1.57079254
0.078	1.0008E+06	2.3328E-01	1.570796	1.57079250
0.079	1.0008E+06	2.3762E-01	1.570796	1.57079245
0.080	1.0008E+06	2.2883E-01	1.570796	1.57079239
0.081	1.0008E+06	2.3405E-01	1.570796	1.57079235
0.082	1.0008E+06	2.3439E-01	1.570796	1.57079230
0.083	1.0008E+06	2.2959E-01	1.570796	1.57079224
0.084	1.0008E+06	2.3481E-01	1.570796	1.57079220
0.085	1.0008E+06	2.3515E-01	1.570796	1.57079214
0.086	1.0008E+06	2.3034E-01	1.570796	1.57079209
0.087	1.0009E+06	2.3556E-01	1.570796	1.57079205
0.088	1.0009E+06	2.3590E-01	1.570796	1.57079200
0.089	1.0009E+06	2.3109E-01	1.570796	1.57079194
0.090	1.0009E+06	2.3156E-01	1.570796	1.57079190
0.091	1.0009E+06	2.2661E-01	1.570796	1.57079185
0.092	1.0009E+06	2.3122E-01	1.570796	1.57079180
0.093	1.0009E+06	2.3704E-01	1.570796	1.57079174
0.094	1.0009E+06	2.3737E-01	1.570796	1.57079169
0.095	1.0009E+06	2.3655E-01	1.570796	1.57079165
0.096	1.0009E+06	2.3774E-01	1.570796	1.57079160
0.097	1.0009E+06	2.3810E-01	1.570796	1.57079155
0.098	1.0010E+06	2.2938E-01	1.570796	1.57079150
0.099	1.0010E+06	2.2370E-01	1.570796	1.57079145
0.100	1.0010E+06	2.2877E-01	1.570796	1.57079139
0.101	1.0010E+06	2.3193E-01	1.570796	1.57079135

Table 6.2

Laser Backscatter Detector Array Outputs
For $V_{\perp} = 50$ m/sec and $I_{g,0} = 0.0$

Results are shown as a 20×20 array (corresponding to the detector array), every 4 m/sec. The actual laser spot position as imaged on the array is indicated by μ_0, ν_0 . The glint point position corresponds to the aim-point and is shown as μ_g, ν_g . The entries are spaced a distance $\Delta\mu = 1.0$ and/or $\Delta\nu = 1.0$ apart with the four central detectors at $(\mu, \nu) = (-0.5, -0.5), (-0.5, 0.5), (0.5, -0.5),$ and $(0.5, 0.5)$ [corresponding to lower left, upper left, lower right, and upper right corners, respectively]. The horizontal line corresponds to the $\hat{\xi}$ -axis on the focal plane and the vertical to the $\hat{\eta}$ -axis. Their intersection defines $(\mu, \nu) = (0, 0)$. The shaded ellipses indicates the laser spot position while the open ellipses shows the aim-point position.

[illegible]

AD-A055 177

OPTICAL SCIENCES CO PLACENTIA CA
ADAPTIVE COMPENSATION TECHNIQUES.(U)

F/G 17/8

MAY 78 D L FRIED, E J SCHONHEINZ, R B ASHER

F30602-77-C-0099

UNCLASSIFIED

DR-105

RADC-TR-78-101

NL

3 OF 5
AD
A055177



[illegible][illegible]

[illegible][illegible]

[illegible]

[illegible]

[illegible][illegible]

TIME =	0.0385 (=2)	(MUC = -1.212)	MUC = -0.012	(MUC = 0.269)	MUC = -0.008
0.00	0.00	0.00	0.00	0.00	0.00
0.01	0.00	0.00	0.00	0.00	0.00
0.02	0.00	0.00	0.00	0.00	0.00
0.03	0.00	0.00	0.00	0.00	0.00
0.04	0.00	0.00	0.00	0.00	0.00
0.05	0.00	0.00	0.00	0.00	0.00
0.06	0.00	0.00	0.00	0.00	0.00
0.07	0.00	0.00	0.00	0.00	0.00
0.08	0.00	0.00	0.00	0.00	0.00
0.09	0.00	0.00	0.00	0.00	0.00
0.10	0.00	0.00	0.00	0.00	0.00
0.11	0.00	0.00	0.00	0.00	0.00
0.12	0.00	0.00	0.00	0.00	0.00
0.13	0.00	0.00	0.00	0.00	0.00
0.14	0.00	0.00	0.00	0.00	0.00
0.15	0.00	0.00	0.00	0.00	0.00
0.16	0.00	0.00	0.00	0.00	0.00
0.17	0.00	0.00	0.00	0.00	0.00
0.18	0.00	0.00	0.00	0.00	0.00
0.19	0.00	0.00	0.00	0.00	0.00
0.20	0.00	0.00	0.00	0.00	0.00
0.21	0.00	0.00	0.00	0.00	0.00
0.22	0.00	0.00	0.00	0.00	0.00
0.23	0.00	0.00	0.00	0.00	0.00
0.24	0.00	0.00	0.00	0.00	0.00
0.25	0.00	0.00	0.00	0.00	0.00
0.26	0.00	0.00	0.00	0.00	0.00
0.27	0.00	0.00	0.00	0.00	0.00
0.28	0.00	0.00	0.00	0.00	0.00
0.29	0.00	0.00	0.00	0.00	0.00
0.30	0.00	0.00	0.00	0.00	0.00
0.31	0.00	0.00	0.00	0.00	0.00
0.32	0.00	0.00	0.00	0.00	0.00
0.33	0.00	0.00	0.00	0.00	0.00
0.34	0.00	0.00	0.00	0.00	0.00
0.35	0.00	0.00	0.00	0.00	0.00
0.36	0.00	0.00	0.00	0.00	0.00
0.37	0.00	0.00	0.00	0.00	0.00
0.38	0.00	0.00	0.00	0.00	0.00
0.39	0.00	0.00	0.00	0.00	0.00
0.40	0.00	0.00	0.00	0.00	0.00
0.41	0.00	0.00	0.00	0.00	0.00
0.42	0.00	0.00	0.00	0.00	0.00
0.43	0.00	0.00	0.00	0.00	0.00
0.44	0.00	0.00	0.00	0.00	0.00
0.45	0.00	0.00	0.00	0.00	0.00
0.46	0.00	0.00	0.00	0.00	0.00
0.47	0.00	0.00	0.00	0.00	0.00
0.48	0.00	0.00	0.00	0.00	0.00
0.49	0.00	0.00	0.00	0.00	0.00
0.50	0.00	0.00	0.00	0.00	0.00
0.51	0.00	0.00	0.00	0.00	0.00
0.52	0.00	0.00	0.00	0.00	0.00
0.53	0.00	0.00	0.00	0.00	0.00
0.54	0.00	0.00	0.00	0.00	0.00
0.55	0.00	0.00	0.00	0.00	0.00
0.56	0.00	0.00	0.00	0.00	0.00
0.57	0.00	0.00	0.00	0.00	0.00
0.58	0.00	0.00	0.00	0.00	0.00
0.59	0.00	0.00	0.00	0.00	0.00
0.60	0.00	0.00	0.00	0.00	0.00
0.61	0.00	0.00	0.00	0.00	0.00
0.62	0.00	0.00	0.00	0.00	0.00
0.63	0.00	0.00	0.00	0.00	0.00
0.64	0.00	0.00	0.00	0.00	0.00
0.65	0.00	0.00	0.00	0.00	0.00
0.66	0.00	0.00	0.00	0.00	0.00
0.67	0.00	0.00	0.00	0.00	0.00
0.68	0.00	0.00	0.00	0.00	0.00
0.69	0.00	0.00	0.00	0.00	0.00
0.70	0.00	0.00	0.00	0.00	0.00
0.71	0.00	0.00	0.00	0.00	0.00
0.72	0.00	0.00	0.00	0.00	0.00
0.73	0.00	0.00	0.00	0.00	0.00
0.74	0.00	0.00	0.00	0.00	0.00
0.75	0.00	0.00	0.00	0.00	0.00
0.76	0.00	0.00	0.00	0.00	0.00
0.77	0.00	0.00	0.00	0.00	0.00
0.78	0.00	0.00	0.00	0.00	0.00
0.79	0.00	0.00	0.00	0.00	0.00
0.80	0.00	0.00	0.00	0.00	0.00
0.81	0.00	0.00	0.00	0.00	0.00
0.82	0.00	0.00	0.00	0.00	0.00
0.83	0.00	0.00	0.00	0.00	0.00
0.84	0.00	0.00	0.00	0.00	0.00
0.85	0.00	0.00	0.00	0.00	0.00
0.86	0.00	0.00	0.00	0.00	0.00
0.87	0.00	0.00	0.00	0.00	0.00
0.88	0.00	0.00	0.00	0.00	0.00
0.89	0.00	0.00	0.00	0.00	0.00
0.90	0.00	0.00	0.00	0.00	0.00
0.91	0.00	0.00	0.00	0.00	0.00
0.92	0.00	0.00	0.00	0.00	0.00
0.93	0.00	0.00	0.00	0.00	0.00
0.94	0.00	0.00	0.00	0.00	0.00
0.95	0.00	0.00	0.00	0.00	0.00
0.96	0.00	0.00	0.00	0.00	0.00
0.97	0.00	0.00	0.00	0.00	0.00
0.98	0.00	0.00	0.00	0.00	0.00
0.99	0.00	0.00	0.00	0.00	0.00
1.00	0.00	0.00	0.00	0.00	0.00

[illegible]

[illegible]

Table 6.3

Laser Backscatter Detector Array Outputs

For $V_{\perp} = 50$ m/sec and $I_{e,0} = 100$.

Results are shown as a 20×20 array (corresponding to the detector array) every 4 m/sec. The actual laser spot position as imaged on the array is indicated by μ_0, ν_0 . The glint point position corresponds to the aim-point and is shown as μ_a, ν_a . The entries are spaced a distance $\Delta\mu = 1.0$ and/or $\Delta\nu = 1.0$ apart with the four central detectors at $(\mu, \nu) = (-0.5, -0.5), (-0.5, 0.5), (0.5, -0.5)$, and $(0.5, 0.5)$ [corresponding to lower left, upper left, lower right, and upper right corners, respectively]. The horizontal line corresponds to the $\hat{\xi}$ - axis on the focal plane and the vertical to the $\hat{\eta}$ - axis. Their intersection defines $(\mu, \nu) = (0, 0)$. The shaded ellipses indicates the laser spot position while the open ellipses shows the aim-point (as well as the glint point), position.

[illegible][illegible]

[illegible]

[illegible]

TIME	0.05(S)	(μ = -1.124)	(μ = -0.012)	(μ = 0.328)	(μ = 0.306)
0.00	0.00	0.00	0.00	0.00	0.00
0.01	0.00	0.00	0.00	0.00	0.00
0.02	0.00	0.00	0.00	0.00	0.00
0.03	0.00	0.00	0.00	0.00	0.00
0.04	0.00	0.00	0.00	0.00	0.00
0.05	0.00	0.00	0.00	0.00	0.00
0.06	0.00	0.00	0.00	0.00	0.00
0.07	0.00	0.00	0.00	0.00	0.00
0.08	0.00	0.00	0.00	0.00	0.00
0.09	0.00	0.00	0.00	0.00	0.00
0.10	0.00	0.00	0.00	0.00	0.00
0.11	0.00	0.00	0.00	0.00	0.00
0.12	0.00	0.00	0.00	0.00	0.00
0.13	0.00	0.00	0.00	0.00	0.00
0.14	0.00	0.00	0.00	0.00	0.00
0.15	0.00	0.00	0.00	0.00	0.00
0.16	0.00	0.00	0.00	0.00	0.00
0.17	0.00	0.00	0.00	0.00	0.00
0.18	0.00	0.00	0.00	0.00	0.00
0.19	0.00	0.00	0.00	0.00	0.00
0.20	0.00	0.00	0.00	0.00	0.00
0.21	0.00	0.00	0.00	0.00	0.00
0.22	0.00	0.00	0.00	0.00	0.00
0.23	0.00	0.00	0.00	0.00	0.00
0.24	0.00	0.00	0.00	0.00	0.00
0.25	0.00	0.00	0.00	0.00	0.00
0.26	0.00	0.00	0.00	0.00	0.00
0.27	0.00	0.00	0.00	0.00	0.00
0.28	0.00	0.00	0.00	0.00	0.00
0.29	0.00	0.00	0.00	0.00	0.00
0.30	0.00	0.00	0.00	0.00	0.00
0.31	0.00	0.00	0.00	0.00	0.00
0.32	0.00	0.00	0.00	0.00	0.00
0.33	0.00	0.00	0.00	0.00	0.00
0.34	0.00	0.00	0.00	0.00	0.00
0.35	0.00	0.00	0.00	0.00	0.00
0.36	0.00	0.00	0.00	0.00	0.00
0.37	0.00	0.00	0.00	0.00	0.00
0.38	0.00	0.00	0.00	0.00	0.00
0.39	0.00	0.00	0.00	0.00	0.00
0.40	0.00	0.00	0.00	0.00	0.00
0.41	0.00	0.00	0.00	0.00	0.00
0.42	0.00	0.00	0.00	0.00	0.00
0.43	0.00	0.00	0.00	0.00	0.00
0.44	0.00	0.00	0.00	0.00	0.00
0.45	0.00	0.00	0.00	0.00	0.00
0.46	0.00	0.00	0.00	0.00	0.00
0.47	0.00	0.00	0.00	0.00	0.00
0.48	0.00	0.00	0.00	0.00	0.00
0.49	0.00	0.00	0.00	0.00	0.00
0.50	0.00	0.00	0.00	0.00	0.00
0.51	0.00	0.00	0.00	0.00	0.00
0.52	0.00	0.00	0.00	0.00	0.00
0.53	0.00	0.00	0.00	0.00	0.00
0.54	0.00	0.00	0.00	0.00	0.00
0.55	0.00	0.00	0.00	0.00	0.00
0.56	0.00	0.00	0.00	0.00	0.00
0.57	0.00	0.00	0.00	0.00	0.00
0.58	0.00	0.00	0.00	0.00	0.00
0.59	0.00	0.00	0.00	0.00	0.00
0.60	0.00	0.00	0.00	0.00	0.00
0.61	0.00	0.00	0.00	0.00	0.00
0.62	0.00	0.00	0.00	0.00	0.00
0.63	0.00	0.00	0.00	0.00	0.00
0.64	0.00	0.00	0.00	0.00	0.00
0.65	0.00	0.00	0.00	0.00	0.00
0.66	0.00	0.00	0.00	0.00	0.00
0.67	0.00	0.00	0.00	0.00	0.00
0.68	0.00	0.00	0.00	0.00	0.00
0.69	0.00	0.00	0.00	0.00	0.00
0.70	0.00	0.00	0.00	0.00	0.00
0.71	0.00	0.00	0.00	0.00	0.00
0.72	0.00	0.00	0.00	0.00	0.00
0.73	0.00	0.00	0.00	0.00	0.00
0.74	0.00	0.00	0.00	0.00	0.00
0.75	0.00	0.00	0.00	0.00	0.00
0.76	0.00	0.00	0.00	0.00	0.00
0.77	0.00	0.00	0.00	0.00	0.00
0.78	0.00	0.00	0.00	0.00	0.00
0.79	0.00	0.00	0.00	0.00	0.00
0.80	0.00	0.00	0.00	0.00	0.00
0.81	0.00	0.00	0.00	0.00	0.00
0.82	0.00	0.00	0.00	0.00	0.00
0.83	0.00	0.00	0.00	0.00	0.00
0.84	0.00	0.00	0.00	0.00	0.00
0.85	0.00	0.00	0.00	0.00	0.00
0.86	0.00	0.00	0.00	0.00	0.00
0.87	0.00	0.00	0.00	0.00	0.00
0.88	0.00	0.00	0.00	0.00	0.00
0.89	0.00	0.00	0.00	0.00	0.00
0.90	0.00	0.00	0.00	0.00	0.00
0.91	0.00	0.00	0.00	0.00	0.00
0.92	0.00	0.00	0.00	0.00	0.00
0.93	0.00	0.00	0.00	0.00	0.00
0.94	0.00	0.00	0.00	0.00	0.00
0.95	0.00	0.00	0.00	0.00	0.00
0.96	0.00	0.00	0.00	0.00	0.00
0.97	0.00	0.00	0.00	0.00	0.00
0.98	0.00	0.00	0.00	0.00	0.00
0.99	0.00	0.00	0.00	0.00	0.00
1.00	0.00	0.00	0.00	0.00	0.00

[illegible][illegible]

193/194

Page 7

[illegible]

[illegible]

- 197 -

[illegible]

Table 6.4

Laser Backscatter Detector Array Outputs

For $V_{\perp} = 50$ m/sec and $I_{a,0} = 10,000$.

Results are shown as a 20×20 array (corresponding to the detector array) every 4 m/sec. The actual laser spot position as imaged on the array is indicated by μ_0, ν_0 . The glint point position corresponds to the aim-point and is shown as μ_g, ν_g . The entries are spaced a distance $\Delta\mu = 1.0$ and/or $\Delta\nu = 1.0$ apart with the four central detectors at $(\mu, \nu) = (-0.5, -0.5), (-0.5, 0.5), (0.5, -0.5)$, and $(0.5, 0.5)$ [corresponding to lower left, upper left, lower right, and upper right corners, respectively]. The horizontal line corresponds to the $\hat{\xi}$ -axis on the focal plane and the vertical to the $\hat{\eta}$ -axis. Their intersection defines $(\mu, \nu) = (0, 0)$. The shaded ellipses indicates the laser spot position while the open ellipses shows the aim-point (as well as the glint point), position.

[illegible]

TIME =	0.036(45.5)	(MUC = -1.100)	MUD = -0.012	(MUC = 0.299)	MUC = -0.0061
0.00	0.00	3.00	0.00	0.00	0.00
0.01	0.00	3.00	0.00	0.00	0.00
0.02	0.00	3.00	0.00	0.00	0.00
0.03	0.00	3.00	0.00	0.00	0.00
0.04	0.00	3.00	0.00	0.00	0.00
0.05	0.00	3.00	0.00	0.00	0.00
0.06	0.00	3.00	0.00	0.00	0.00
0.07	0.00	3.00	0.00	0.00	0.00
0.08	0.00	3.00	0.00	0.00	0.00
0.09	0.00	3.00	0.00	0.00	0.00
0.10	0.00	3.00	0.00	0.00	0.00
0.11	0.00	3.00	0.00	0.00	0.00
0.12	0.00	3.00	0.00	0.00	0.00
0.13	0.00	3.00	0.00	0.00	0.00
0.14	0.00	3.00	0.00	0.00	0.00
0.15	0.00	3.00	0.00	0.00	0.00
0.16	0.00	3.00	0.00	0.00	0.00
0.17	0.00	3.00	0.00	0.00	0.00
0.18	0.00	3.00	0.00	0.00	0.00
0.19	0.00	3.00	0.00	0.00	0.00
0.20	0.00	3.00	0.00	0.00	0.00
0.21	0.00	3.00	0.00	0.00	0.00
0.22	0.00	3.00	0.00	0.00	0.00
0.23	0.00	3.00	0.00	0.00	0.00
0.24	0.00	3.00	0.00	0.00	0.00
0.25	0.00	3.00	0.00	0.00	0.00
0.26	0.00	3.00	0.00	0.00	0.00
0.27	0.00	3.00	0.00	0.00	0.00
0.28	0.00	3.00	0.00	0.00	0.00
0.29	0.00	3.00	0.00	0.00	0.00
0.30	0.00	3.00	0.00	0.00	0.00
0.31	0.00	3.00	0.00	0.00	0.00
0.32	0.00	3.00	0.00	0.00	0.00
0.33	0.00	3.00	0.00	0.00	0.00
0.34	0.00	3.00	0.00	0.00	0.00
0.35	0.00	3.00	0.00	0.00	0.00
0.36	0.00	3.00	0.00	0.00	0.00
0.37	0.00	3.00	0.00	0.00	0.00
0.38	0.00	3.00	0.00	0.00	0.00
0.39	0.00	3.00	0.00	0.00	0.00
0.40	0.00	3.00	0.00	0.00	0.00
0.41	0.00	3.00	0.00	0.00	0.00
0.42	0.00	3.00	0.00	0.00	0.00
0.43	0.00	3.00	0.00	0.00	0.00
0.44	0.00	3.00	0.00	0.00	0.00
0.45	0.00	3.00	0.00	0.00	0.00
0.46	0.00	3.00	0.00	0.00	0.00
0.47	0.00	3.00	0.00	0.00	0.00
0.48	0.00	3.00	0.00	0.00	0.00
0.49	0.00	3.00	0.00	0.00	0.00
0.50	0.00	3.00	0.00	0.00	0.00
0.51	0.00	3.00	0.00	0.00	0.00
0.52	0.00	3.00	0.00	0.00	0.00
0.53	0.00	3.00	0.00	0.00	0.00
0.54	0.00	3.00	0.00	0.00	0.00
0.55	0.00	3.00	0.00	0.00	0.00
0.56	0.00	3.00	0.00	0.00	0.00
0.57	0.00	3.00	0.00	0.00	0.00
0.58	0.00	3.00	0.00	0.00	0.00
0.59	0.00	3.00	0.00	0.00	0.00
0.60	0.00	3.00	0.00	0.00	0.00
0.61	0.00	3.00	0.00	0.00	0.00
0.62	0.00	3.00	0.00	0.00	0.00
0.63	0.00	3.00	0.00	0.00	0.00
0.64	0.00	3.00	0.00	0.00	0.00
0.65	0.00	3.00	0.00	0.00	0.00
0.66	0.00	3.00	0.00	0.00	0.00
0.67	0.00	3.00	0.00	0.00	0.00
0.68	0.00	3.00	0.00	0.00	0.00
0.69	0.00	3.00	0.00	0.00	0.00
0.70	0.00	3.00	0.00	0.00	0.00
0.71	0.00	3.00	0.00	0.00	0.00
0.72	0.00	3.00	0.00	0.00	0.00
0.73	0.00	3.00	0.00	0.00	0.00
0.74	0.00	3.00	0.00	0.00	0.00
0.75	0.00	3.00	0.00	0.00	0.00
0.76	0.00	3.00	0.00	0.00	0.00
0.77	0.00	3.00	0.00	0.00	0.00
0.78	0.00	3.00	0.00	0.00	0.00
0.79	0.00	3.00	0.00	0.00	0.00
0.80	0.00	3.00	0.00	0.00	0.00
0.81	0.00	3.00	0.00	0.00	0.00
0.82	0.00	3.00	0.00	0.00	0.00
0.83	0.00	3.00	0.00	0.00	0.00
0.84	0.00	3.00	0.00	0.00	0.00
0.85	0.00	3.00	0.00	0.00	0.00
0.86	0.00	3.00	0.00	0.00	0.00
0.87	0.00	3.00	0.00	0.00	0.00
0.88	0.00	3.00	0.00	0.00	0.00
0.89	0.00	3.00	0.00	0.00	0.00
0.90	0.00	3.00	0.00	0.00	0.00
0.91	0.00	3.00	0.00	0.00	0.00
0.92	0.00	3.00	0.00	0.00	0.00
0.93	0.00	3.00	0.00	0.00	0.00
0.94	0.00	3.00	0.00	0.00	0.00
0.95	0.00	3.00	0.00	0.00	0.00
0.96	0.00	3.00	0.00	0.00	0.00
0.97	0.00	3.00	0.00	0.00	0.00
0.98	0.00	3.00	0.00	0.00	0.00
0.99	0.00	3.00	0.00	0.00	0.00
1.00	0.00	3.00	0.00	0.00	0.00

[illegible]

[illegible][illegible]

- 203 -

[illegible][illegible]

[illegible][illegible]

[illegible][illegible]

[illegible]

[illegible][illegible]

Table 6.5

Laser Backscatter Detector Array Outputs

For $V_1 = 100$ m/sec and $I_{a,0} = 0.0$

Results are shown as a 20×20 array (corresponding to the detector array) every 2 m/sec. The actual laser spot position as imaged on the array is indicated by μ_0, ν_0 . The glint point position corresponds to the aim-point and is shown as μ_g, ν_g . The entries are spaced a distance $\Delta\mu = 1.0$ and/or $\Delta\nu = 1.0$ apart with the four central detectors at $(\mu, \nu) = (-0.5, -0.5), (-0.5, 0.5), (0.5, -0.5)$, and $(0.5, 0.5)$ [corresponding to lower left, upper left, lower right, and upper right corners, respectively]. The horizontal line corresponds to the $\hat{\xi}$ - axis on the focal plane and the vertical to the $\hat{\eta}$ - axis. Their intersection defines $(\mu, \nu) = (0.0)$. The shaded ellipses indicates the laser spot position while the open ellipses shows the aim-point position.

TIME =	0-0.030(S-C)	(MUL = -2.256,	MUJ = -0.012)	(MUG = 0.698,	MUG = -0.008)
0-0.00	0.00	0.00	0.00	0.00	0.00
0-0.01	0.00	0.00	0.00	0.00	0.00
0-0.02	0.00	0.00	0.00	0.00	0.00
0-0.03	0.00	0.00	0.00	0.00	0.00
0-0.04	0.00	0.00	0.00	0.00	0.00
0-0.05	0.00	0.00	0.00	0.00	0.00
0-0.06	0.00	0.00	0.00	0.00	0.00
0-0.07	0.00	0.00	0.00	0.00	0.00
0-0.08	0.00	0.00	0.00	0.00	0.00
0-0.09	0.00	0.00	0.00	0.00	0.00
0-0.10	0.00	0.00	0.00	0.00	0.00
0-0.11	0.00	0.00	0.00	0.00	0.00
0-0.12	0.00	0.00	0.00	0.00	0.00
0-0.13	0.00	0.00	0.00	0.00	0.00
0-0.14	0.00	0.00	0.00	0.00	0.00
0-0.15	0.00	0.00	0.00	0.00	0.00
0-0.16	0.00	0.00	0.00	0.00	0.00
0-0.17	0.00	0.00	0.00	0.00	0.00
0-0.18	0.00	0.00	0.00	0.00	0.00
0-0.19	0.00	0.00	0.00	0.00	0.00
0-0.20	0.00	0.00	0.00	0.00	0.00
0-0.21	0.00	0.00	0.00	0.00	0.00
0-0.22	0.00	0.00	0.00	0.00	0.00
0-0.23	0.00	0.00	0.00	0.00	0.00
0-0.24	0.00	0.00	0.00	0.00	0.00
0-0.25	0.00	0.00	0.00	0.00	0.00
0-0.26	0.00	0.00	0.00	0.00	0.00
0-0.27	0.00	0.00	0.00	0.00	0.00
0-0.28	0.00	0.00	0.00	0.00	0.00
0-0.29	0.00	0.00	0.00	0.00	0.00
0-0.30	0.00	0.00	0.00	0.00	0.00
0-0.31	0.00	0.00	0.00	0.00	0.00
0-0.32	0.00	0.00	0.00	0.00	0.00
0-0.33	0.00	0.00	0.00	0.00	0.00
0-0.34	0.00	0.00	0.00	0.00	0.00
0-0.35	0.00	0.00	0.00	0.00	0.00
0-0.36	0.00	0.00	0.00	0.00	0.00
0-0.37	0.00	0.00	0.00	0.00	0.00
0-0.38	0.00	0.00	0.00	0.00	0.00
0-0.39	0.00	0.00	0.00	0.00	0.00
0-0.40	0.00	0.00	0.00	0.00	0.00
0-0.41	0.00	0.00	0.00	0.00	0.00
0-0.42	0.00	0.00	0.00	0.00	0.00
0-0.43	0.00	0.00	0.00	0.00	0.00
0-0.44	0.00	0.00	0.00	0.00	0.00
0-0.45	0.00	0.00	0.00	0.00	0.00
0-0.46	0.00	0.00	0.00	0.00	0.00
0-0.47	0.00	0.00	0.00	0.00	0.00
0-0.48	0.00	0.00	0.00	0.00	0.00
0-0.49	0.00	0.00	0.00	0.00	0.00
0-0.50	0.00	0.00	0.00	0.00	0.00
0-0.51	0.00	0.00	0.00	0.00	0.00
0-0.52	0.00	0.00	0.00	0.00	0.00
0-0.53	0.00	0.00	0.00	0.00	0.00
0-0.54	0.00	0.00	0.00	0.00	0.00
0-0.55	0.00	0.00	0.00	0.00	0.00
0-0.56	0.00	0.00	0.00	0.00	0.00
0-0.57	0.00	0.00	0.00	0.00	0.00
0-0.58	0.00	0.00	0.00	0.00	0.00
0-0.59	0.00	0.00	0.00	0.00	0.00
0-0.60	0.00	0.00	0.00	0.00	0.00
0-0.61	0.00	0.00	0.00	0.00	0.00
0-0.62	0.00	0.00	0.00	0.00	0.00
0-0.63	0.00	0.00	0.00	0.00	0.00
0-0.64	0.00	0.00	0.00	0.00	0.00
0-0.65	0.00	0.00	0.00	0.00	0.00
0-0.66	0.00	0.00	0.00	0.00	0.00
0-0.67	0.00	0.00	0.00	0.00	0.00
0-0.68	0.00	0.00	0.00	0.00	0.00
0-0.69	0.00	0.00	0.00	0.00	0.00
0-0.70	0.00	0.00	0.00	0.00	0.00
0-0.71	0.00	0.00	0.00	0.00	0.00
0-0.72	0.00	0.00	0.00	0.00	0.00
0-0.73	0.00	0.00	0.00	0.00	0.00
0-0.74	0.00	0.00	0.00	0.00	0.00
0-0.75	0.00	0.00	0.00	0.00	0.00
0-0.76	0.00	0.00	0.00	0.00	0.00
0-0.77	0.00	0.00	0.00	0.00	0.00
0-0.78	0.00	0.00	0.00	0.00	0.00
0-0.79	0.00	0.00	0.00	0.00	0.00
0-0.80	0.00	0.00	0.00	0.00	0.00
0-0.81	0.00	0.00	0.00	0.00	0.00
0-0.82	0.00	0.00	0.00	0.00	0.00
0-0.83	0.00	0.00	0.00	0.00	0.00
0-0.84	0.00	0.00	0.00	0.00	0.00
0-0.85	0.00	0.00	0.00	0.00	0.00
0-0.86	0.00	0.00	0.00	0.00	0.00
0-0.87	0.00	0.00	0.00	0.00	0.00
0-0.88	0.00	0.00	0.00	0.00	0.00
0-0.89	0.00	0.00	0.00	0.00	0.00
0-0.90	0.00	0.00	0.00	0.00	0.00
0-0.91	0.00	0.00	0.00	0.00	0.00
0-0.92	0.00	0.00	0.00	0.00	0.00
0-0.93	0.00	0.00	0.00	0.00	0.00
0-0.94	0.00	0.00	0.00	0.00	0.00
0-0.95	0.00	0.00	0.00	0.00	0.00
0-0.96	0.00	0.00	0.00	0.00	0.00
0-0.97	0.00	0.00	0.00	0.00	0.00
0-0.98	0.00	0.00	0.00	0.00	0.00
0-0.99	0.00	0.00	0.00	0.00	0.00
0-1.00	0.00	0.00	0.00	0.00	0.00

[illegible]

Year	0.034(5.1)	(MUC = -2.237)	MUC = -0.012	(MUC = 0.621)	MUC = -0.306
0.00	0.00	0.00	0.00	0.00	0.00
0.10	0.00	0.00	0.00	0.00	0.00
0.20	0.00	0.00	0.00	0.00	0.00
0.30	0.00	0.00	0.00	0.00	0.00
0.40	0.00	0.00	0.00	0.00	0.00
0.50	0.00	0.00	0.00	0.00	0.00
0.60	0.00	0.00	0.00	0.00	0.00
0.70	0.00	0.00	0.00	0.00	0.00
0.80	0.00	0.00	0.00	0.00	0.00
0.90	0.00	0.00	0.00	0.00	0.00
1.00	0.00	0.00	0.00	0.00	0.00
1.10	0.00	0.00	0.00	0.00	0.00
1.20	0.00	0.00	0.00	0.00	0.00
1.30	0.00	0.00	0.00	0.00	0.00
1.40	0.00	0.00	0.00	0.00	0.00
1.50	0.00	0.00	0.00	0.00	0.00
1.60	0.00	0.00	0.00	0.00	0.00
1.70	0.00	0.00	0.00	0.00	0.00
1.80	0.00	0.00	0.00	0.00	0.00
1.90	0.00	0.00	0.00	0.00	0.00
2.00	0.00	0.00	0.00	0.00	0.00
2.10	0.00	0.00	0.00	0.00	0.00
2.20	0.00	0.00	0.00	0.00	0.00
2.30	0.00	0.00	0.00	0.00	0.00
2.40	0.00	0.00	0.00	0.00	0.00
2.50	0.00	0.00	0.00	0.00	0.00
2.60	0.00	0.00	0.00	0.00	0.00
2.70	0.00	0.00	0.00	0.00	0.00
2.80	0.00	0.00	0.00	0.00	0.00
2.90	0.00	0.00	0.00	0.00	0.00
3.00	0.00	0.00	0.00	0.00	0.00
3.10	0.00	0.00	0.00	0.00	0.00
3.20	0.00	0.00	0.00	0.00	0.00
3.30	0.00	0.00	0.00	0.00	0.00
3.40	0.00	0.00	0.00	0.00	0.00
3.50	0.00	0.00	0.00	0.00	0.00
3.60	0.00	0.00	0.00	0.00	0.00
3.70	0.00	0.00	0.00	0.00	0.00
3.80	0.00	0.00	0.00	0.00	0.00
3.90	0.00	0.00	0.00	0.00	0.00
4.00	0.00	0.00	0.00	0.00	0.00
4.10	0.00	0.00	0.00	0.00	0.00
4.20	0.00	0.00	0.00	0.00	0.00
4.30	0.00	0.00	0.00	0.00	0.00
4.40	0.00	0.00	0.00	0.00	0.00
4.50	0.00	0.00	0.00	0.00	0.00
4.60	0.00	0.00	0.00	0.00	0.00
4.70	0.00	0.00	0.00	0.00	0.00
4.80	0.00	0.00	0.00	0.00	0.00
4.90	0.00	0.00	0.00	0.00	0.00
5.00	0.00	0.00	0.00	0.00	0.00
5.10	0.00	0.00	0.00	0.00	0.00
5.20	0.00	0.00	0.00	0.00	0.00
5.30	0.00	0.00	0.00	0.00	0.00
5.40	0.00	0.00	0.00	0.00	0.00
5.50	0.00	0.00	0.00	0.00	0.00
5.60	0.00	0.00	0.00	0.00	0.00
5.70	0.00	0.00	0.00	0.00	0.00
5.80	0.00	0.00	0.00	0.00	0.00
5.90	0.00	0.00	0.00	0.00	0.00
6.00	0.00	0.00	0.00	0.00	0.00
6.10	0.00	0.00	0.00	0.00	0.00
6.20	0.00	0.00	0.00	0.00	0.00
6.30	0.00	0.00	0.00	0.00	0.00
6.40	0.00	0.00	0.00	0.00	0.00
6.50	0.00	0.00	0.00	0.00	0.00
6.60	0.00	0.00	0.00	0.00	0.00
6.70	0.00	0.00	0.00	0.00	0.00
6.80	0.00	0.00	0.00	0.00	0.00
6.90	0.00	0.00	0.00	0.00	0.00
7.00	0.00	0.00	0.00	0.00	0.00
7.10	0.00	0.00	0.00	0.00	0.00
7.20	0.00	0.00	0.00	0.00	0.00
7.30	0.00	0.00	0.00	0.00	0.00
7.40	0.00	0.00	0.00	0.00	0.00
7.50	0.00	0.00	0.00	0.00	0.00
7.60	0.00	0.00	0.00	0.00	0.00
7.70	0.00	0.00	0.00	0.00	0.00
7.80	0.00	0.00	0.00	0.00	0.00
7.90	0.00	0.00	0.00	0.00	0.00
8.00	0.00	0.00	0.00	0.00	0.00
8.10	0.00	0.00	0.00	0.00	0.00
8.20	0.00	0.00	0.00	0.00	0.00
8.30	0.00	0.00	0.00	0.00	0.00
8.40	0.00	0.00	0.00	0.00	0.00
8.50	0.00	0.00	0.00	0.00	0.00
8.60	0.00	0.00	0.00	0.00	0.00
8.70	0.00	0.00	0.00	0.00	0.00
8.80	0.00	0.00	0.00	0.00	0.00
8.90	0.00	0.00	0.00	0.00	0.00
9.00	0.00	0.00	0.00	0.00	0.00
9.10	0.00	0.00	0.00	0.00	0.00
9.20	0.00	0.00	0.00	0.00	0.00
9.30	0.00	0.00	0.00	0.00	0.00
9.40	0.00	0.00	0.00	0.00	0.00
9.50	0.00	0.00	0.00	0.00	0.00
9.60	0.00	0.00	0.00	0.00	0.00
9.70	0.00	0.00	0.00	0.00	0.00
9.80	0.00	0.00	0.00	0.00	0.00
9.90	0.00	0.00	0.00	0.00	0.00
10.00	0.00	0.00	0.00	0.00	0.00

TIME =	0.676(5.2)	(MUS = -2.208,	MUS = -3.312)	(MUS = 0.676,	MUS = -0.306)
0.00	1.00	1.00	1.00	1.00	1.00
0.10	0.99	0.99	0.99	0.99	0.99
0.20	0.98	0.98	0.98	0.98	0.98
0.30	0.97	0.97	0.97	0.97	0.97
0.40	0.96	0.96	0.96	0.96	0.96
0.50	0.95	0.95	0.95	0.95	0.95
0.60	0.94	0.94	0.94	0.94	0.94
0.70	0.93	0.93	0.93	0.93	0.93
0.80	0.92	0.92	0.92	0.92	0.92
0.90	0.91	0.91	0.91	0.91	0.91
1.00	0.90	0.90	0.90	0.90	0.90
1.10	0.89	0.89	0.89	0.89	0.89
1.20	0.88	0.88	0.88	0.88	0.88
1.30	0.87	0.87	0.87	0.87	0.87
1.40	0.86	0.86	0.86	0.86	0.86
1.50	0.85	0.85	0.85	0.85	0.85
1.60	0.84	0.84	0.84	0.84	0.84
1.70	0.83	0.83	0.83	0.83	0.83
1.80	0.82	0.82	0.82	0.82	0.82
1.90	0.81	0.81	0.81	0.81	0.81
2.00	0.80	0.80	0.80	0.80	0.80
2.10	0.79	0.79	0.79	0.79	0.79
2.20	0.78	0.78	0.78	0.78	0.78
2.30	0.77	0.77	0.77	0.77	0.77
2.40	0.76	0.76	0.76	0.76	0.76
2.50	0.75	0.75	0.75	0.75	0.75
2.60	0.74	0.74	0.74	0.74	0.74
2.70	0.73	0.73	0.73	0.73	0.73
2.80	0.72	0.72	0.72	0.72	0.72
2.90	0.71	0.71	0.71	0.71	0.71
3.00	0.70	0.70	0.70	0.70	0.70
3.10	0.69	0.69	0.69	0.69	0.69
3.20	0.68	0.68	0.68	0.68	0.68
3.30	0.67	0.67	0.67	0.67	0.67
3.40	0.66	0.66	0.66	0.66	0.66
3.50	0.65	0.65	0.65	0.65	0.65
3.60	0.64	0.64	0.64	0.64	0.64
3.70	0.63	0.63	0.63	0.63	0.63
3.80	0.62	0.62	0.62	0.62	0.62
3.90	0.61	0.61	0.61	0.61	0.61
4.00	0.60	0.60	0.60	0.60	0.60
4.10	0.59	0.59	0.59	0.59	0.59
4.20	0.58	0.58	0.58	0.58	0.58
4.30	0.57	0.57	0.57	0.57	0.57
4.40	0.56	0.56	0.56	0.56	0.56
4.50	0.55	0.55	0.55	0.55	0.55
4.60	0.54	0.54	0.54	0.54	0.54
4.70	0.53	0.53	0.53	0.53	0.53
4.80	0.52	0.52	0.52	0.52	0.52
4.90	0.51	0.51	0.51	0.51	0.51
5.00	0.50	0.50	0.50	0.50	0.50
5.10	0.49	0.49	0.49	0.49	0.49
5.20	0.48	0.48	0.48	0.48	0.48
5.30	0.47	0.47	0.47	0.47	0.47
5.40	0.46	0.46	0.46	0.46	0.46
5.50	0.45	0.45	0.45	0.45	0.45
5.60	0.44	0.44	0.44	0.44	0.44
5.70	0.43	0.43	0.43	0.43	0.43
5.80	0.42	0.42	0.42	0.42	0.42
5.90	0.41	0.41	0.41	0.41	0.41
6.00	0.40	0.40	0.40	0.40	0.40
6.10	0.39	0.39	0.39	0.39	0.39
6.20	0.38	0.38	0.38	0.38	0.38
6.30	0.37	0.37	0.37	0.37	0.37
6.40	0.36	0.36	0.36	0.36	0.36
6.50	0.35	0.35	0.35	0.35	0.35
6.60	0.34	0.34	0.34	0.34	0.34
6.70	0.33	0.33	0.33	0.33	0.33
6.80	0.32	0.32	0.32	0.32	0.32
6.90	0.31	0.31	0.31	0.31	0.31
7.00	0.30	0.30	0.30	0.30	0.30
7.10	0.29	0.29	0.29	0.29	0.29
7.20	0.28	0.28	0.28	0.28	0.28
7.30	0.27	0.27	0.27	0.27	0.27
7.40	0.26	0.26	0.26	0.26	0.26
7.50	0.25	0.25	0.25	0.25	0.25
7.60	0.24	0.24	0.24	0.24	0.24
7.70	0.23	0.23	0.23	0.23	0.23
7.80	0.22	0.22	0.22	0.22	0.22
7.90	0.21	0.21	0.21	0.21	0.21
8.00	0.20	0.20	0.20	0.20	0.20
8.10	0.19	0.19	0.19	0.19	0.19
8.20	0.18	0.18	0.18	0.18	0.18
8.30	0.17	0.17	0.17	0.17	0.17
8.40	0.16	0.16	0.16	0.16	0.16
8.50	0.15	0.15	0.15	0.15	0.15
8.60	0.14	0.14	0.14	0.14	0.14
8.70	0.13	0.13	0.13	0.13	0.13
8.80	0.12	0.12	0.12	0.12	0.12
8.90	0.11	0.11	0.11	0.11	0.11
9.00	0.10	0.10	0.10	0.10	0.10
9.10	0.09	0.09	0.09	0.09	0.09
9.20	0.08	0.08	0.08	0.08	0.08
9.30	0.07	0.07	0.07	0.07	0.07
9.40	0.06	0.06	0.06	0.06	0.06
9.50	0.05	0.05	0.05	0.05	0.05
9.60	0.04	0.04	0.04	0.04	0.04
9.70	0.03	0.03	0.03	0.03	0.03
9.80	0.02	0.02	0.02	0.02	0.02
9.90	0.01	0.01	0.01	0.01	0.01
10.00	0.00	0.00	0.00	0.00	0.00

[illegible][illegible]

[illegible]

Table 5 - Continued

[illegible]

TIME =	0.046(SEC)	(MUD = -2.295°	MUD = -0.012°	(MUG = 0.632,	MUG = -0.336)
0.3C	0.00	0.00	0.00	0.00	0.00
0.4C	0.00	0.00	0.00	0.00	0.00
0.5C	0.00	0.00	0.00	0.00	0.00
0.6C	0.00	0.00	0.00	0.00	0.00
0.7C	0.00	0.00	0.00	0.00	0.00
0.8C	0.00	0.00	0.00	0.00	0.00
0.9C	0.00	0.00	0.00	0.00	0.00
1.0C	0.00	0.00	0.00	0.00	0.00
1.1C	0.00	0.00	0.00	0.00	0.00
1.2C	0.00	0.00	0.00	0.00	0.00
1.3C	0.00	0.00	0.00	0.00	0.00
1.4C	0.00	0.00	0.00	0.00	0.00
1.5C	0.00	0.00	0.00	0.00	0.00
1.6C	0.00	0.00	0.00	0.00	0.00
1.7C	0.00	0.00	0.00	0.00	0.00
1.8C	0.00	0.00	0.00	0.00	0.00
1.9C	0.00	0.00	0.00	0.00	0.00
2.0C	0.00	0.00	0.00	0.00	0.00
2.1C	0.00	0.00	0.00	0.00	0.00
2.2C	0.00	0.00	0.00	0.00	0.00
2.3C	0.00	0.00	0.00	0.00	0.00
2.4C	0.00	0.00	0.00	0.00	0.00
2.5C	0.00	0.00	0.00	0.00	0.00
2.6C	0.00	0.00	0.00	0.00	0.00
2.7C	0.00	0.00	0.00	0.00	0.00
2.8C	0.00	0.00	0.00	0.00	0.00
2.9C	0.00	0.00	0.00	0.00	0.00
3.0C	0.00	0.00	0.00	0.00	0.00
3.1C	0.00	0.00	0.00	0.00	0.00
3.2C	0.00	0.00	0.00	0.00	0.00
3.3C	0.00	0.00	0.00	0.00	0.00
3.4C	0.00	0.00	0.00	0.00	0.00
3.5C	0.00	0.00	0.00	0.00	0.00
3.6C	0.00	0.00	0.00	0.00	0.00
3.7C	0.00	0.00	0.00	0.00	0.00
3.8C	0.00	0.00	0.00	0.00	0.00
3.9C	0.00	0.00	0.00	0.00	0.00
4.0C	0.00	0.00	0.00	0.00	0.00
4.1C	0.00	0.00	0.00	0.00	0.00
4.2C	0.00	0.00	0.00	0.00	0.00
4.3C	0.00	0.00	0.00	0.00	0.00
4.4C	0.00	0.00	0.00	0.00	0.00
4.5C	0.00	0.00	0.00	0.00	0.00
4.6C	0.00	0.00	0.00	0.00	0.00
4.7C	0.00	0.00	0.00	0.00	0.00
4.8C	0.00	0.00	0.00	0.00	0.00
4.9C	0.00	0.00	0.00	0.00	0.00
5.0C	0.00	0.00	0.00	0.00	0.00
5.1C	0.00	0.00	0.00	0.00	0.00
5.2C	0.00	0.00	0.00	0.00	0.00
5.3C	0.00	0.00	0.00	0.00	0.00
5.4C	0.00	0.00	0.00	0.00	0.00
5.5C	0.00	0.00	0.00	0.00	0.00
5.6C	0.00	0.00	0.00	0.00	0.00
5.7C	0.00	0.00	0.00	0.00	0.00
5.8C	0.00	0.00	0.00	0.00	0.00
5.9C	0.00	0.00	0.00	0.00	0.00
6.0C	0.00	0.00	0.00	0.00	0.00
6.1C	0.00	0.00	0.00	0.00	0.00
6.2C	0.00	0.00	0.00	0.00	0.00
6.3C	0.00	0.00	0.00	0.00	0.00
6.4C	0.00	0.00	0.00	0.00	0.00
6.5C	0.00	0.00	0.00	0.00	0.00
6.6C	0.00	0.00	0.00	0.00	0.00
6.7C	0.00	0.00	0.00	0.00	0.00
6.8C	0.00	0.00	0.00	0.00	0.00
6.9C	0.00	0.00	0.00	0.00	0.00
7.0C	0.00	0.00	0.00	0.00	0.00
7.1C	0.00	0.00	0.00	0.00	0.00
7.2C	0.00	0.00	0.00	0.00	0.00
7.3C	0.00	0.00	0.00	0.00	0.00
7.4C	0.00	0.00	0.00	0.00	0.00
7.5C	0.00	0.00	0.00	0.00	0.00
7.6C	0.00	0.00	0.00	0.00	0.00
7.7C	0.00	0.00	0.00	0.00	0.00
7.8C	0.00	0.00	0.00	0.00	0.00
7.9C	0.00	0.00	0.00	0.00	0.00
8.0C	0.00	0.00	0.00	0.00	0.00
8.1C	0.00	0.00	0.00	0.00	0.00
8.2C	0.00	0.00	0.00	0.00	0.00
8.3C	0.00	0.00	0.00	0.00	0.00
8.4C	0.00	0.00	0.00	0.00	0.00
8.5C	0.00	0.00	0.00	0.00	0.00
8.6C	0.00	0.00	0.00	0.00	0.00
8.7C	0.00	0.00	0.00	0.00	0.00
8.8C	0.00	0.00	0.00	0.00	0.00
8.9C	0.00	0.00	0.00	0.00	0.00
9.0C	0.00	0.00	0.00	0.00	0.00
9.1C	0.00	0.00	0.00	0.00	0.00
9.2C	0.00	0.00	0.00	0.00	0.00
9.3C	0.00	0.00	0.00	0.00	0.00
9.4C	0.00	0.00	0.00	0.00	0.00
9.5C	0.00	0.00	0.00	0.00	0.00
9.6C	0.00	0.00	0.00	0.00	0.00
9.7C	0.00	0.00	0.00	0.00	0.00
9.8C	0.00	0.00	0.00	0.00	0.00
9.9C	0.00	0.00	0.00	0.00	0.00
10.0C	0.00	0.00	0.00	0.00	0.00
10.1C	0.00	0.00	0.00	0.00	0.00
10.2C	0.00	0.00	0.00	0.00	0.00
10.3C	0.00	0.00	0.00	0.00	0.00
10.4C	0.00	0.00	0.00	0.00	0.00
10.5C	0.00	0.00	0.00	0.00	0.00
10.6C	0.00	0.00	0.00	0.00	0.00
10.7C	0.00	0.00	0.00	0.00	0.00
10.8C	0.00	0.00	0.00	0.00	0.00
10.9C	0.00	0.00	0.00	0.00	0.00
11.0C	0.00	0.00	0.00	0.00	0.00
11.1C	0.00	0.00	0.00	0.00	0.00
11.2C	0.00	0.00	0.00	0.00	0.00
11.3C	0.00	0.00	0.00	0.00	0.00
11.4C	0.00	0.00	0.00	0.00	0.00
11.5C	0.00	0.00	0.00	0.00	0.00
11.6C	0.00	0.00	0.00	0.00	0.00
11.7C	0.00	0.00	0.00	0.00	0.00
11.8C	0.00	0.00	0.00	0.00	0.00
11.9C	0.00	0.00	0.00	0.00	0.00
12.0C	0.00	0.00	0.00	0.00	0.00
12.1C	0.00	0.00	0.00	0.00	0.00
12.2C	0.00	0.00	0.00	0.00	0.00
12.3C	0.00	0.00	0.00	0.00	0.00
12.4C	0.00	0.00	0.00	0.00	0.00
12.5C	0.00	0.00	0.00	0.00	0.00
12.6C	0.00	0.00	0.00	0.00	0.00
12.7C	0.00	0.00	0.00	0.00	0.00
12.8C	0.00	0.00	0.00	0.00	0.00
12.9C	0.00	0.00	0.00	0.00	0.00
13.0C	0.00	0.00	0.00	0.00	0.00
13.1C	0.00	0.00	0.00	0.00	0.00
13.2C	0.00	0.00	0.00	0.00	0.00
13.3C	0.00	0.00	0.00	0.00	0.00
13.4C	0.00	0.00	0.00	0.00	0.00
13.5C	0.00	0.00	0.00	0.00	0.00
13.6C	0.00	0.00	0.00	0.00	0.00
13.7C	0.00	0.00	0.00	0.00	0.00
13.8C	0.00	0.00	0.00	0.00	0.00
13.9C	0.00	0.00	0.00	0.00	0.00
14.0C	0.00	0.00	0.00	0.00	0.00
14.1C	0.00	0.00	0.00	0.00	0.00
14.2C	0.00	0.00	0.00	0.00	0.00
14.3C	0.00	0.00	0.00	0.00	0.00
14.4C	0.00	0.00	0.00	0.00	0.00
14.5C	0.00	0.00	0.00	0.00	0.00
14.6C	0.00	0.00	0.00	0.00	0.00
14.7C	0.00	0.00	0.00	0.00	0.00
14.8C	0.00	0.00	0.00	0.00	0.00
14.9C	0.00	0.00	0.00	0.00	0.00
15.0C	0.00	0.00	0.00	0.00	0.00
15.1C	0.00	0.00	0.00	0.00	0.00
15.2C	0.00	0.00	0.00	0.00	0.00
15.3C	0.00	0.00	0.00	0.00	0.00
15.4C	0.00	0.00	0.00	0.00	0.00
15.5C	0.00	0.00	0.00	0.00	0.00
15.6C	0.00	0.00	0.00	0.00	0.00
15.7C	0.00	0.00	0.00	0.00	0.00
15.8C	0.00	0.00	0.00	0.00	0.00
15.9C	0.00	0.00	0.00	0.00	0.00
16.0C	0.00	0.00	0.00	0.00	0.00
16.1C	0.00	0.00	0.00	0.00	0.00
16.2C	0.00	0.00	0.00	0.00	0.00
16.3C	0.00	0.00	0.00	0.00	0.00
16.4C	0.00	0.00	0.00	0.00	0.00
16.5C	0.00	0.00	0.00	0.00	0.00
16.6C	0.00	0.00	0.00	0.00	0.00
16.7C	0.00	0.00	0.00	0.00	0.00
16.8C	0.00	0.00	0.00	0.00	0.00
16.9C	0.00	0.00	0.00	0.00	0.00
17.0C	0.00	0.00	0.00	0.00	0.00
17.1C	0.00	0.00	0.00	0.00	0.00
17.2C	0.00	0.00	0.00	0.00	0.00
17.3C	0.00	0.00	0.00	0.00	0.00
17.4C	0.00	0.00	0.00	0.00	0.00
17.5C	0.00	0.00	0.00	0.00	0.00
17.6C	0.00	0.00	0.00	0.00	0.00
17.7C	0.00	0.00	0.00	0.00	0.00
17.8C	0.00	0.00	0.00	0.00	0.00
17.9C	0.00	0.00	0.00	0.00	0.00
18.0C	0.00	0.00	0.00	0.00	0.00
18.1C	0.00	0.00	0.00	0.00	0.00
18.2C	0.00	0.00	0.00	0.00	0.00
18.3C	0.00	0.00	0.00	0.00	0.00
18.4C	0.00	0.00	0.00	0.00	0.00
18.5C	0.00	0.00	0.00	0.00	0.00
18.6C	0.00	0.00	0.00	0.00	0.00
18.7C	0.00	0.00	0.00	0.00	0.00
18.8C	0.00	0.00	0.00	0.00	0.00
18.9C	0.00	0.00	0.00	0.00	0.00
19.0C	0.00	0.00	0.00	0.00	0.00
19.1C	0.00	0.00	0.00	0.00	0.00
19.2C	0.00	0.00	0.00	0.00	0.00
19.3C	0.00	0.00	0.00	0.00	0.00
19.4C	0.00	0.00	0.00	0.00	0.00
19.5C	0.00	0.00	0.00	0.00	0.00
19.6C	0.00	0.00	0.00	0.00	0.00
19.7C	0.00	0.00	0.00	0.00	0.00
19.8C	0.00	0.00	0.00	0.00	0.00
19.9C	0.00	0.00	0.00	0.00	0.00
20.0C	0.00	0.00	0.00	0.00	0.00
20.1C	0.00	0.00	0.00	0.00	0.00
20.2C	0.00	0.00	0.00	0.00	0.00
20.3C	0.00	0.00	0.00	0.00	0.00
20.4C	0.00	0.00	0.00	0.00	0.00
20.5C	0.00	0.00	0.00	0.00	0.00
20.6C	0.00	0.00	0.00	0.00	0.00
20.7C	0.00	0.00	0.00	0.00	0.00
20.8C	0.00	0.00	0.00	0.00	0.00
20.9C	0.00	0.00	0.00	0.00	0.00
21.0C	0.00	0.00	0.00	0.00	0.00
21.1C	0.00	0.00	0.00	0.00	0.00
21.2C	0.00	0.00	0.00	0.00	0.00
21.3C</					

[illegible]

TIME =	C.05211.00	(MUC = -2.261,	MUC = -0.012)	(MUC = 0.649,	MUC = -0.036)
0.00	0.00	0.00	0.00	0.00	0.00
0.10	0.00	0.00	0.00	0.00	0.00
0.20	0.00	0.00	0.00	0.00	0.00
0.30	0.00	0.00	0.00	0.00	0.00
0.40	0.00	0.00	0.00	0.00	0.00
0.50	0.00	0.00	0.00	0.00	0.00
0.60	0.00	0.00	0.00	0.00	0.00
0.70	0.00	0.00	0.00	0.00	0.00
0.80	0.00	0.00	0.00	0.00	0.00
0.90	0.00	0.00	0.00	0.00	0.00
1.00	0.00	0.00	0.00	0.00	0.00
1.10	0.00	0.00	0.00	0.00	0.00
1.20	0.00	0.00	0.00	0.00	0.00
1.30	0.00	0.00	0.00	0.00	0.00
1.40	0.00	0.00	0.00	0.00	0.00
1.50	0.00	0.00	0.00	0.00	0.00
1.60	0.00	0.00	0.00	0.00	0.00
1.70	0.00	0.00	0.00	0.00	0.00
1.80	0.00	0.00	0.00	0.00	0.00
1.90	0.00	0.00	0.00	0.00	0.00
2.00	0.00	0.00	0.00	0.00	0.00
2.10	0.00	0.00	0.00	0.00	0.00
2.20	0.00	0.00	0.00	0.00	0.00
2.30	0.00	0.00	0.00	0.00	0.00
2.40	0.00	0.00	0.00	0.00	0.00
2.50	0.00	0.00	0.00	0.00	0.00
2.60	0.00	0.00	0.00	0.00	0.00
2.70	0.00	0.00	0.00	0.00	0.00
2.80	0.00	0.00	0.00	0.00	0.00
2.90	0.00	0.00	0.00	0.00	0.00
3.00	0.00	0.00	0.00	0.00	0.00
3.10	0.00	0.00	0.00	0.00	0.00
3.20	0.00	0.00	0.00	0.00	0.00
3.30	0.00	0.00	0.00	0.00	0.00
3.40	0.00	0.00	0.00	0.00	0.00
3.50	0.00	0.00	0.00	0.00	0.00
3.60	0.00	0.00	0.00	0.00	0.00
3.70	0.00	0.00	0.00	0.00	0.00
3.80	0.00	0.00	0.00	0.00	0.00
3.90	0.00	0.00	0.00	0.00	0.00
4.00	0.00	0.00	0.00	0.00	0.00
4.10	0.00	0.00	0.00	0.00	0.00
4.20	0.00	0.00	0.00	0.00	0.00
4.30	0.00	0.00	0.00	0.00	0.00
4.40	0.00	0.00	0.00	0.00	0.00
4.50	0.00	0.00	0.00	0.00	0.00
4.60	0.00	0.00	0.00	0.00	0.00
4.70	0.00	0.00	0.00	0.00	0.00
4.80	0.00	0.00	0.00	0.00	0.00
4.90	0.00	0.00	0.00	0.00	0.00
5.00	0.00	0.00	0.00	0.00	0.00
5.10	0.00	0.00	0.00	0.00	0.00
5.20	0.00	0.00	0.00	0.00	0.00
5.30	0.00	0.00	0.00	0.00	0.00
5.40	0.00	0.00	0.00	0.00	0.00
5.50	0.00	0.00	0.00	0.00	0.00
5.60	0.00	0.00	0.00	0.00	0.00
5.70	0.00	0.00	0.00	0.00	0.00
5.80	0.00	0.00	0.00	0.00	0.00
5.90	0.00	0.00	0.00	0.00	0.00
6.00	0.00	0.00	0.00	0.00	0.00
6.10	0.00	0.00	0.00	0.00	0.00
6.20	0.00	0.00	0.00	0.00	0.00
6.30	0.00	0.00	0.00	0.00	0.00
6.40	0.00	0.00	0.00	0.00	0.00
6.50	0.00	0.00	0.00	0.00	0.00
6.60	0.00	0.00	0.00	0.00	0.00
6.70	0.00	0.00	0.00	0.00	0.00
6.80	0.00	0.00	0.00	0.00	0.00
6.90	0.00	0.00	0.00	0.00	0.00
7.00	0.00	0.00	0.00	0.00	0.00
7.10	0.00	0.00	0.00	0.00	0.00
7.20	0.00	0.00	0.00	0.00	0.00
7.30	0.00	0.00	0.00	0.00	0.00
7.40	0.00	0.00	0.00	0.00	0.00
7.50	0.00	0.00	0.00	0.00	0.00
7.60	0.00	0.00	0.00	0.00	0.00
7.70	0.00	0.00	0.00	0.00	0.00
7.80	0.00	0.00	0.00	0.00	0.00
7.90	0.00	0.00	0.00	0.00	0.00
8.00	0.00	0.00	0.00	0.00	0.00
8.10	0.00	0.00	0.00	0.00	0.00
8.20	0.00	0.00	0.00	0.00	0.00
8.30	0.00	0.00	0.00	0.00	0.00
8.40	0.00	0.00	0.00	0.00	0.00
8.50	0.00	0.00	0.00	0.00	0.00
8.60	0.00	0.00	0.00	0.00	0.00
8.70	0.00	0.00	0.00	0.00	0.00
8.80	0.00	0.00	0.00	0.00	0.00
8.90	0.00	0.00	0.00	0.00	0.00
9.00	0.00	0.00	0.00	0.00	0.00
9.10	0.00	0.00	0.00	0.00	0.00
9.20	0.00	0.00	0.00	0.00	0.00
9.30	0.00	0.00	0.00	0.00	0.00
9.40	0.00	0.00	0.00	0.00	0.00
9.50	0.00	0.00	0.00	0.00	0.00
9.60	0.00	0.00	0.00	0.00	0.00
9.70	0.00	0.00	0.00	0.00	0.00
9.80	0.00	0.00	0.00	0.00	0.00
9.90	0.00	0.00	0.00	0.00	0.00
10.00	0.00	0.00	0.00	0.00	0.00

[illegible][illegible]

[illegible][illegible]

72

[illegible][illegible]

Table 6.6

Laser Backscatter Detector Array Outputs

For $V_{\perp} = 200$ m/sec and $I_{0,0} = 0.0$

Results are shown as a 20×20 array (corresponding to the detector array) every 1 m/sec. The actual laser spot position as imaged on the array is indicated by μ_0, ν_0 . The glint point position corresponds to the aim-point and is shown as μ_a, ν_a . The entries are spaced a distance $\Delta\mu = 1.0$ and/or $\Delta\nu = 1.0$ apart with the four central detectors at $(\mu, \nu) = (-0.5, -0.5), (-0.5, 0.5), (0.5, -0.5)$, and $(0.5, 0.5)$ [corresponding to lower left, upper left, lower right, and upper right corners, respectively]. The horizontal line corresponds to the $\hat{\xi}$ -axis on the focal plane and the vertical to the $\hat{\eta}$ -axis. Their intersection defines $(\mu, \nu) = (0.0)$. The shaded ellipses indicates the laser spot position while the open ellipses shows the aim-point position.

[illegible][illegible]

TIME =	G.012(S.C)					(MUO = -6.618)					(MUG = -0.012)					(MUG = 1.219)					(MUG = -0.036)																																																																																																																																																																																																																																																																																																																																																																																																																																																																																																																																																																																																																																																																																																																																																																																																																																																																																																																																																	
0.00	0.00	0.00	0.00	0.00	0.00	0.00	0.00	0.00	0.00	0.00	0.00	0.00	0.00	0.00	0.00	0.00	0.00	0.00	0.00	0.00	0.00	0.00	0.00	0.00	0.00	0.00	0.00	0.00	0.00	0.00	0.00	0.00	0.00	0.00	0.00	0.00	0.00	0.00	0.00	0.00	0.00	0.00	0.00	0.00	0.00	0.00	0.00	0.00	0.00	0.00	0.00	0.00	0.00	0.00	0.00	0.00	0.00	0.00	0.00	0.00	0.00	0.00	0.00	0.00	0.00	0.00	0.00	0.00	0.00	0.00	0.00	0.00	0.00	0.00	0.00	0.00	0.00	0.00	0.00	0.00	0.00	0.00	0.00	0.00	0.00	0.00	0.00	0.00	0.00	0.00	0.00	0.00	0.00	0.00	0.00	0.00	0.00	0.00	0.00	0.00	0.00	0.00	0.00	0.00	0.00	0.00	0.00	0.00	0.00	0.00	0.00	0.00	0.00	0.00	0.00	0.00	0.00	0.00	0.00	0.00	0.00	0.00	0.00	0.00	0.00	0.00	0.00	0.00	0.00	0.00	0.00	0.00	0.00	0.00	0.00	0.00	0.00	0.00	0.00	0.00	0.00	0.00	0.00	0.00	0.00	0.00	0.00	0.00	0.00	0.00	0.00	0.00	0.00	0.00	0.00	0.00	0.00	0.00	0.00	0.00	0.00	0.00	0.00	0.00	0.00	0.00	0.00	0.00	0.00	0.00	0.00	0.00	0.00	0.00	0.00	0.00	0.00	0.00	0.00	0.00	0.00	0.00	0.00	0.00	0.00	0.00	0.00	0.00	0.00	0.00	0.00	0.00	0.00	0.00	0.00	0.00	0.00	0.00	0.00	0.00	0.00	0.00	0.00	0.00	0.00	0.00	0.00	0.00	0.00	0.00	0.00	0.00	0.00	0.00	0.00	0.00	0.00	0.00	0.00	0.00	0.00	0.00	0.00	0.00	0.00	0.00	0.00	0.00	0.00	0.00	0.00	0.00	0.00	0.00	0.00	0.00	0.00	0.00	0.00	0.00	0.00	0.00	0.00	0.00	0.00	0.00	0.00	0.00	0.00	0.00	0.00	0.00	0.00	0.00	0.00	0.00	0.00	0.00	0.00	0.00	0.00	0.00	0.00	0.00	0.00	0.00	0.00	0.00	0.00	0.00	0.00	0.00	0.00	0.00	0.00	0.00	0.00	0.00	0.00	0.00	0.00	0.00	0.00	0.00	0.00	0.00	0.00	0.00	0.00	0.00	0.00	0.00	0.00	0.00	0.00	0.00	0.00	0.00	0.00	0.00	0.00	0.00	0.00	0.00	0.00	0.00	0.00	0.00	0.00	0.00	0.00	0.00	0.00	0.00	0.00	0.00	0.00	0.00	0.00	0.00	0.00	0.00	0.00	0.00	0.00	0.00	0.00	0.00	0.00	0.00	0.00	0.00	0.00	0.00	0.00	0.00	0.00	0.00	0.00	0.00	0.00	0.00	0.00	0.00	0.00	0.00	0.00	0.00	0.00	0.00	0.00	0.00	0.00	0.00	0.00	0.00	0.00	0.00	0.00	0.00	0.00	0.00	0.00	0.00	0.00	0.00	0.00	0.00	0.00	0.00	0.00	0.00	0.00	0.00	0.00	0.00	0.00	0.00	0.00	0.00	0.00	0.00	0.00	0.00	0.00	0.00	0.00	0.00	0.00	0.00	0.00	0.00	0.00	0.00	0.00	0.00	0.00	0.00	0.00	0.00	0.00	0.00	0.00	0.00	0.00	0.00	0.00	0.00	0.00	0.00	0.00	0.00	0.00	0.00	0.00	0.00	0.00	0.00	0.00	0.00	0.00	0.00	0.00	0.00	0.00	0.00	0.00	0.00	0.00	0.00	0.00	0.00	0.00	0.00	0.00	0.00	0.00	0.00	0.00	0.00	0.00	0.00	0.00	0.00	0.00	0.00	0.00	0.00	0.00	0.00	0.00	0.00	0.00	0.00	0.00	0.00	0.00	0.00	0.00	0.00	0.00	0.00	0.00	0.00	0.00	0.00	0.00	0.00	0.00	0.00	0.00	0.00	0.00	0.00	0.00	0.00	0.00	0.00	0.00	0.00	0.00	0.00	0.00	0.00	0.00	0.00	0.00	0.00	0.00	0.00	0.00	0.00	0.00	0.00	0.00	0.00	0.00	0.00	0.00	0.00	0.00	0.00	0.00	0.00	0.00	0.00	0.00	0.00	0.00	0.00	0.00	0.00	0.00	0.00	0.00	0.00	0.00	0.00	0.00	0.00	0.00	0.00	0.00	0.00	0.00	0.00	0.00	0.00	0.00	0.00	0.00	0.00	0.00	0.00	0.00	0.00	0.00	0.00	0.00	0.00	0.00	0.00	0.00	0.00	0.00	0.00	0.00	0.00	0.00	0.00	0.00	0.00	0.00	0.00	0.00	0.00	0.00	0.00	0.00	0.00	0.00	0.00	0.00	0.00	0.00	0.00	0.00	0.00	0.00	0.00	0.00	0.00	0.00	0.00	0.00	0.00	0.00	0.00	0.00	0.00	0.00	0.00	0.00	0.00	0.00	0.00	0.00	0.00	0.00	0.00	0.00	0.00	0.00	0.00	0.00	0.00	0.00	0.00	0.00	0.00	0.00	0.00	0.00	0.00	0.00	0.00	0.00	0.00	0.00	0.00	0.00	0.00	0.00	0.00	0.00	0.00	0.00	0.00	0.00	0.00	0.00	0.00	0.00	0.00	0.00	0.00	0.00	0.00	0.00	0.00	0.00	0.00	0.00	0.00	0.00	0.00	0.00	0.00	0.00	0.00	0.00	0.00	0.00	0.00	0.00	0.00	0.00	0.00	0.00	0.00	0.00	0.00	0.00	0.00	0.00	0.00	0.00	0.00	0.00	0.00	0.00	0.00	0.00	0.00	0.00	0.00	0.00	0.00	0.00	0.00	0.00	0.00	0.00	0.00	0.00	0.00	0.00	0.00	0.00	0.00	0.00	0.00	0.00	0.00	0.00	0.00	0.00	0.00	0.00	0.00	0.00	0.00	0.00	0.00	0.00	0.00	0.00	0.00	0.00	0.00	0.00	0.00	0.00	0.00	0.00	0.00	0.00	0.00	0.00	0.00	0.00	0.00	0.00	0.00	0.00	0.00	0.00	0.00	0.00	0.00	0.00	0.00	0.00	0.00	0.00	0.00	0.00	0.00	0.00	0.00	0.00	0.00	0.00	0.00	0.00	0.00	0.00	0.00	0.00	0.00	0.00	0.00	0.00	0.00	0.00	0.00	0.00	0.00	0.00	0.00	0.00	0.00	0.00	0.00	0.00	0.00	0.00	0.00	0.00	0.00	0.00	0.00	0.00	0.00	0.00	0.00	0.00	0.00	0.00	0.00	0.00	0.00	0.00	0.00	0.00	0.00	0.00	0.00	0.00	0.00	0.00	0.00	0.00	0.00	0.00	0.00	0.00	0.00	0.00	0.00	0.00	0.00	0.00	0.00	0.00	0.00	0.00	0.00	0.00	0.00	0.00	0.00	0.00	0.00	0.00	0.00	0.00	0.00	0.00	0.00	0.00	0.00	0.00	0.00	0.00	0.00	0.00	0.00	0.00	0.00	0.00	0.00	0.00	0.00	0.00	0.00	0.00	0.00	0.00	0.00	0.00	0.00	0.00	0.00	0.00	0.00	0.00	0.00	0.00	0.00	0.00	0.00	0.00	0.00	0.00	0.00	0.00	0.00	0.00	0.00	0.00	0.00	0.00	0.00	0.00	0.00	0.00	0.00	0.00	0.00	0.00	0.00	0.00	0.00	0.00	0.00	0.00	0.00	0.00	0.00	0.00	0.00	0.00	0.00	0.00	0.00	0.00	0.00	0.00	0.00	0.00	0.00	0.00	0.00	0.00	0.00	0.00	0.00	0.00	0.00	0.00	0.00	0.00	0.00	0.00	0.00	0.00	0.00	0.00	0.00	0.00	0.00	0.00	0.00	0.00	0.00	0.00	0.00	0.00	0.00	0.00	0.00	0.00	0.00	0.00	0.00	0.00	0.00	0.00	0.00	0.00	0.00	0.00	0.00	0.00	0.00	0.00	0.00	0.00	0.00	0.00	0.00	0.00	

[illegible]

[illegible][illegible]

[illegible][illegible]

[illegible][illegible]

[illegible][illegible]

[illegible][illegible]

[illegible][illegible]

[illegible][illegible]

Appendix to Chapter 6

COMPUTER PROGRAM LISTINGS

MAIN PROGRAM

ACT10A.FORTRAN

```

REAL ID,IG,MUD,NUG,MUG,NUG,IGZ,IG1
DIMENSION RSZ(3),VS(3),RTZ(3),VT(3),AT2(20,20),S(20,20),Z
  DR(3),DV(3),UDV(3),D(3),DVSF(3),UT(3),UG(3),ERR(3),Z
  Z(3),XI(3),ETA(3),DE(3),UL(3),RTS(3),OLM(3),UDR(3),Z
  PTOLO(3),PSOLD(3),ULOLD(3),EB(2),GD(3),AT1(20,20)
NAMELIST /INPUT/ RSZ, VS, RTZ, VT, DR, GD, EB
NPRINT = 4
PI = 3.141592654
Z(1) = 0.
Z(2) = 0.
Z(3) = 1.
T = 0.
DT = 1.E-3
N = 0.

```

```

C-----
C-
C-      SET OPTICAL SYSTEM PARAMETERS.
C-
C-----

```

```

      IGZ = 0.
      ID = 1.
      SIGMA = 1.
      WL = 1.0E-6
      DETW = 1./((2*PI/WL)*SIGMA)

```

```

C*****
C*
C*      SPECIFY ENGAGEMENT PARAMETERS.
C*
C*****

```

```

      RSZ(1) = 0.
      RSZ(2) = 0.
      RSZ(3) = 0.
      VS(1) = 0.
      VS(2) = 0.
      VS(3) = 0.
      RTZ(1) = 0.
      RTZ(2) = 1.E6
      RTZ(3) = 0.
      VT(1) = 50.0
      VT(2) = 1.E4
      VT(3) = 0.
      DE(1) = 0.

```

```

DB(2) = 0.
EB(1) = 0.
EB(2) = 0.
GB(1) = 0.
GB(2) = 0.
GB(3) = 0.

```

```

C*****
C*
C*      CONVERT TO DIFFERENCE COORDINATES.
C*
C*****

```

```

CALL SUM (RTZ,RSZ,DT,-1)
CALL SUM (VT,VS,DV,-1)
CALL UVECT (DR,UR,DRM,16)
CALL UVECT (DV,UDV,DVM,16)

```

```

C*****
C*
C*      CALCULATE DISTANCE AT CLOSEST APPROACH.
C*
C*****

```

```

CALL DOT (UDR,UDV,DURV)
SF = DURV*DRM
CALL SCHULT (SF,UDV,DURV)
CALL SUM (DR,DVSF,D,-1)
CALL UVECT (D,D,DM,16)
PRINT 10,DM,DURV,DRM,VS,RTZ,VT,DR,100,10,GB(1),GB(2),GB(3)
10 FORMAT ("1","CLOSEST APPROACH=","E10.3//",DOT PRODUCT ="",
  E10.3//",RSZ VECTOR ="",E10.3//",VS VECTOR ="",E10.3//",
  " RTZ VECTOR ="",E10.3//",VT VECTOR ="",E10.3//",DR VECTOR ="",
  E10.3//",100 ="",E10.3//",10 ="",E10.3//",GB ="",E10.3)

```

```

C*****
C*
C*      INITIALIZE SERVO/ANALOG AND SET SERVO PARAMETERS.
C*
C*****

```

```

SQT=SQRT(UDR(1)*UDR(1)+UDR(2)*UDR(2))
THETAZ=ATAN2(SQT,UDR(1))
PHIZ = ATAN2(UDR(2),UDR(1))
SPEED = 100.
GAIN = 27.9155*SPEED*SPEED
CLEAD=EXP(-DT*2*PI*SPEED)
PHINT1 = 0.
PHINT2 = PHIZ
THINT1 = 0.
THINT2 = THETAZ

```



```

OTHER = 0.
OPHER = 0.
THETA = THINT2
PHI = PHINT2
CALL SPHREC (THETA, PHI, 1., UG)
TTF = DRH/(3.E8*DT)
TDELAY = 3.*TTF+2./(SFREQ*DT)

```

```

C-----
C-
C-      SET UP RANDOM ARRAY CONTROL/GENERATION PARAMETERS
C-      AND OBTAIN INITIAL VALUES OF A-TILDE'S.
C-----

```

```

F = 1
FPR = 1
ALPHA = DVH*SQRT(1.-DURV*DURV)/DPM
T4 = 0.707107*SIGMA/(4.*DPM*ALPHA)
T1 = TDELAY*DT
CALL RINT(F, T1, T4, A*1, AT2)

```

```

C*****
C*
C*      INCREMENT CLOCK.
C*
C*****

```

```

100 N = N + 1
T = T + DT

```

```

C*****
C*
C*      INCREMENT TARGET POSITION AND STORE.
C*      OBTAIN DELAYED TARGET POSITION.
C*
C*****

```

```

CALL USUM (1., DT, DR, DV, DP)
CALL STACIN (1, DR)
CALL UVECT(DR, UDR, DPM, IE)
TTF = DRH/(3.E8*DT)
IF (N.LT.TTF) GO TO 100
CALL STACCT (1, TTF, STOLD)

```

```

C*****
C*
C*      COMPUTE TARGET TRACKING ERROR AS SEEN BY SENSOR ON
C*      THE GIMBALS (USING THE DELAYED TARGET POSITION).
C*
C*****

```

```

CALL UVECT (RTOLD, UT, R, IF)
CALL SUM (UT,UG, ERR, -1)
CALL CROSS (Z, UG, XI)
CALL UVECT (XI, XI, XI4, IF)
CALL CROSS (UG, XI, ETA)
CALL DOT (ERR, ETA, ERREL)
ERRREL=-ERRREL+ER(1)
CALL DOT (ERP, XI, ERRAZ)
ERRAZ=ERRAZ+ER(2)

```

```

C*****
C*
C*      IMPLEMENT GIMBAL SERVO POINTING UPDATE.
C*
C*****

```

```

ERRAZ = ERRAZ/SIN (THETA)
Q1TH = (ERREL - CLEAD * OTHER)/(1. - CLEAD)
Q1PH = (ERRAZ - CLEAD * OTHER)/(1. - CLEAD)
OTHER = ERREL
OTHER = ERRAZ
Q2TH = Q1TH * GAIN
Q2PH = Q1PH * GAIN
THINT1 = THINT1 + DT*Q2TH
PHINT1 = PHINT1 + DT * Q2PH
THINT2 = THINT2 + DT * THINT1
PHINT2 = PHINT2 + DT * PHINT1
THETA = THINT2
PHI = PHINT2
CALL SPHREC (THETA, PHI, 1., UG)

```

```

C-----
C-
C-      CALCULATE GLINT POSITION ON SENSOR FOCAL PLANE.
C-
C-----

```

```

CALL MUNUC(UG,RTOLD,CD,DETW,XI,ETA,MUG,NUG)

```

```

C*****
C*
C*      INTRODUCE LASER FORESIGHT ERROR.
C*
C*****

```

```

T1= THETA+DB(1)
P1=PHI+DB(2)
CALL SPHREC(T1,P1,1.,UL)

```

84

```

C-----
C*
C*      CALCULATE LASER TARGET MISS DISTANCE.
C*
C-----

```

```

      CALL STACIN (2,UL)
      IF (N.LT.TDELAY) GO TO 100
      TTF2 = 2*TTF
      CALL STACOT (2, TTF2, ULOLD)
      CALL DOT (UT, ULOLD, DTL)
      SF = -DTL/R
      CALL USUM (1., SF, RTOLD, ULOLD, DLM)

```

```

C-----
C-
C-      CALCULATE LASER POSITION ON TARGET AS SEEN
C-      ON SENSOR FOCAL PLANE AND GLINT INTENSITY.
C-      CALCULATE THE ARRAY OF FOCAL PLANE SIGNAL
C-      INTENSITIES.
C-
C-----

```

```

      CALL MUNUC(UG,RTOLD,DLM,DFTW,XI,ETA,MUD,MUD)
      X = MUG-MUD
      Y = NUG-MUD
      IG = 0
      IG1 = X*X+Y*Y
      IF (IG1.LT.76) IG=IGZ*EXP(-IG1)
      CALL SIG(F,MUD,MUD,MUG,NUG,ID,IG,T,T4,S)
      IF ((N/NPRINT)*NPRINT.NE.N) GO TO 100
      FPR = FPR+1
      IF (FPR.EQ.2) FPR = 0
      IF (FPR.EQ.1) GO TO 300
      PRINT 301
301  FORMAT ("1")
300  PRINT 302,T,MUD,MUD,MUG,NUG
302  FORMAT (5X,"TIME =",F10.3,"(SEC)",15X,"(MUD =",F8.3,"  NUD =",F8.3,")",8X,"(MUG =",F9.3,"  NUG =",F8.3,")" /)
      IF (N.GT.100) GO TO 210
      DO 205 J=1,20
      DO 205 I=1,20
      IF ( S(I,J) .LT. 1.E-10 ) S(I,J)=1.E-10
205  CONTINUE
      PRINT 220, ((ALOG10(S(I,J))+10, I=1,20), J=1,20)
220  FORMAT (20(1X, 20F6.2//))
210  CONTINUE
      IF (N.LE.100) GO TO 100

```

END

SUBROUTINE SIG

SIG.FORTRAN

```
C-----
C-
C-   CALCULATE SIGNAL STRENGTH FOR EACH DETECTOR POSITION.
C-
C-----
```

```
SUBROUTINE SIG(F,MUF,NUG,MUG,NUG,ID,IG,T,T4,2)
REAL MUG,NUG,MUG,NUG,ID,IG,MUGI,MUGJ,MUDI,NLDJ
DIMENSION S(20,20),AT1(20,20),AT2(20,20)
```

```
C-----
C-
C-   INITIALIZE CLINT/DIFFUSE POSITIONS AND SIGNAL
C-   STRENGTH PARAMETERS.
C-
C-----
```

```
R=0
CC=SQRT(ID/44.54**2)
CC=SQRT(2.*IG)
CALL RINT(F,T,T4,AT1,AT2)
DO 100 I=1,20
DO 101 J=1,20
MUGI=MUG-(I-10.5)
NLDJ=NUG-(J-10.5)
MUDI=MUG-(I-10.5)
NLDJ=NUG-(J-10.5)
ED = 0
AC = 0
D1 = 0
D2 = 0
```

```
C-----
C-
C-   CALCULATE SIGNAL STRENGTH FOR EACH DETECTOR.
C-
C-----
```

```
IF (CC.NE.0) D1 = (MUDI*MUGI+NLDJ*NUGJ)/2
IF (CC.NE.0) D2 = (MUGI*MUGI+NLDJ*NUGJ)/2
IF (D1.LT.23) ED=CC*EXP(-D1)
IF (D2.LT.23) AC=CC*EXP(-D2)
AD1=ED*AT1(I,J)
AD2=ED*AT2(I,J)
101 B(I,J)=0.5*((AD1+AC)*(AD1+AC)+AT2*AD2)
100 CONTINUE
```

SUBROUTINE 20

RETURN
END

SUBROUTINE RINT

RINT.FORTRAN

```

C-----
C-
C-   INTERPOLATE A-TILDE'S.
C-
C-----

SUBROUTINE RINT(F,T,T4,AT1,AT2)
  DIMENSION AT1(20,20),AT2(20,20),ATPAR(20,20),ATPERP(20,20),%
  ATROLD(20,20),ATPCLD(20,20)
  COMMON /RINT/ TNEW,ATPAR,ATPERP,ATROLD,ATPCLD

C-----
C-
C-   GENERATE A-TILDE'S FOR F = 1.
C-
C-----

  IF (F.EQ.0.) GO TO 200
  CALL RINC(F,ATPAR,ATPERP)
  TNEW=T
  RETURN
200 CONTINUE

C-----
C-
C-   CALCULATE INTERPOLATED A-TILDE'S FOR F = 0.
C-
C-----

  IF (T-TNEW.LT.0.) GO TO 400
  DO 300 I=1,20
  DO 301 J=1,20
    ATROLD(I,J)=ATPAR(I,J)
  301 ATPCLD(I,J)=ATPERP(I,J)
  300 CONTINUE
  CALL RINC(F,ATPAR,ATPERP)
  TNEW=TNEW+T4
  GO TO 200
400 CONTINUE
  C1=(TNEW-T)/T4
  C2=1-C1
  DO 500 I=1,20
  DO 501 J=1,20
    AT1(I,J)=ATROLD(I,J)*C1+ATPAR(I,J)*C2
  501 AT2(I,J)=ATPCLD(I,J)*C1+ATPERP(I,J)*C2
  500 CONTINUE

```


THIRTY EIGHTH

RETURN
END

SUBROUTINE RINC

RINC.FORTRAN

```

C-----
C-
C-   CALCULATE AND INCREMENT A-TILOS'S.
C-
C-----

SUBROUTINE RINC(F,ATPAR,ATPERP)
DIMENSION RPAP(30,30,33),RPERP(30,30,33),P1(900),P2(900),X
CT(33),CKY(11,11),RPAR(30,30),RPERP(30,30),ATPAR(20,20),X
ATPERP(20,20)
COMMON/RINC/RPAR,RPERP,CT,CKY
IF(F.EQ.0.) GO TO 700

C-----
C-
C-   CALCULATE WEIGHTING COEFFICIENTS.
C-
C-----

      DO 100 I=-16.16
100 CT(I+17)=EXP(-I*I/2.)
      DO 110 I=-5.5
      DO 111 J=-5.5
111 CKY(I+5,J+6)=EXP(-(I*I+J*J)/4.)
110 CONTINUE

C-----
C-
C-   PREPARE TWO ARRAYS OF 30X30X32 ELEMENTS EACH.
C-
C-----

      DO 200 I=2.33
      CALL RANDOM_SNORMAL_SEQ (P1,900)
      CALL RANDOM_SNORMAL_SEQ (P2,900)
      DO 210 J=1.33
      DO 211 K=1.33
      L=30*(J-1)+K
      RPAR(J,K,I)=P1(L)
211 RPERP(J,K,I)=P2(L)
210 CONTINUE
200 CONTINUE
300 CONTINUE

```

```

C-----
C-
C-   SHIFT ARRAYS DOWN ONE AND ADD A 30X30 RANDOM ARRAY
C-   TO FORM A NEW 30X30X33 ARRAY.
C-
C-----

```

```

      DO 400 I=1.32
      DO 410 J=1.30
      DO 411 K=1.30
      RPAR(J,K,I)=RPAR(J,K,I+1)
411  RPERP(J,K,I)=RPERP(J,K,I+1)
410  CONTINUE
400  CONTINUE
      CALL RANDOM_SNORMAL_SEO (R1.900)
      CALL RANDOM_SNORMAL_SEO (R2.900)
      DO 500 J=1.30
      DO 501 K=1.30
      L=30*(J-1)+K
      RPAR(J,K,33)=R1(L)
501  RPERP(J,K,33)=R2(L)
500  CONTINUE

```

```

C-----
C-
C-   FORM THE WEIGHTED SUM OF ELEMENTS ALONG THE 33 DIMENSION.
C-
C-----

```

```

      DO 600 J=1.30
      DO 601 K=1.30
      BPAR(J,K)=0.
      BPERP(J,K)=0.
      DO 610 I=1.33
      BPAR(J,K)=BPAR(J,K)+CT(I)*RPAR(J,K,I)
610  BPERP(J,K)=BPERP(J,K)+CT(I)*RPERP(J,K,I)
601  CONTINUE
600  CONTINUE

```

```

C-----
C-
C-   FORM THE WEIGHTED SUMS OF ELEVEN ELEMENTS ALONG THE
C-   30X30 DIMENSION.
C-
C-----

```

```

      DO 700 J=1.20
      DO 701 K=1.20
      ATPAR(J,K)=0.
      ATPERP(J,K)=0.

```



```

00 710 J1=1.11
00 711 K1=1.11
      ATPAP(J,K)=ATPAR(J,K)+CXV(J1,K1)*BPAP(J-J1+11,K-K1+11)
711 ATPERF(J,K)=ATPERP(J,K)+CXV(J1,K1)*BPERP(J-J1+11,K-K1+11)
710 CONTINUE
701 CONTINUE
700 CONTINUE
      RETURN

```

```

END

```

SUBROUTINE MUNU

MUNU.FORTRAN

C-----
C-
C- CALCULATE GLINT/DIFFUSE POSITIONS ON FOCAL PLANE.
C-
C-----

```
SUBROUTINE MUNU(UG,RTOLD,D,DETH,XI,ETA,MU,NU)
DIMENSION UG(3),RTOLD(3),D(3),XI(3),ETA(3),R(3)
REAL MU,NU
CALL SUM(RTOLD,D,R,+1)
CALL UVECT(R,R,RM,IE)
CALL SUM(R,LG,R,-1)
CALL DOT(R,XI,MU)
CALL DOT(R,ETA,NU)
ML=MU/DETH
NL=NU/DETH
RETURN
END
```

Chapter 7

Outer Loop Laser Boresight Error Control

By

Sensing The Backscatter Signal

7.1 Introduction

In the preceding chapters, we developed a theory to describe the statistics of the random laser backscatter from a laser irradiated target with both diffuse reflection and glint point reflection, and developed a computer program to simulate the randomly fluctuating backscatter intensity on a 20×20 focal plane detector array. In other chapters we developed a computer model to allow simulation of a satellite-to-satellite space engagement between a high energy laser pointer/tracker shared aperture system, and a target satellite. This allowed demonstration of the laser pointing process, and demonstrated the effects of laser bias error and of the speed-of-light round-trip transit time delay effect in determining the miss laser distance relative to the aim-point on the target. We assumed that the target aim-point was well defined and could be sensed by the imaging portion of the shared aperture.

The target tracking was entirely local, based on the sensed aim-point position, so that a high servo bandwidth (100 Hz, type 2 servo) could be achieved, and the target tracking was very stable though the laser miss distance was, in general, quite substantial. To zero the laser miss distance we exploited the fact that if target image tracking was stable, then the miss distance would change only very slowly. This allowed us to formulate the concept of an outer loop bias control that would sense the laser miss distance and allow that information to adjust the image tracker demodulation process in the high bandwidth local tracker loop. This could be adjusted to cause the true miss distance to go to zero. This process involves a round-trip transit time delay from the shared aperture laser transmitter to the target and then back to the shared aperture receiver, and so this outer loop bias control was

necessarily low bandwidth — but so long as the bias type errors only changed very slowly, this low bandwidth was entirely adequate. In a previous report, assuming that the shared aperture received could precisely determine the apparent laser miss distance, we showed how this bias control outer servo loop could be implemented and developed a computer simulation to model the low bandwidth outer servo loop (on top of the high band target aim-point tracking loop) , and were able to demonstrate the achievement of a negligibly small laser miss distance.

Our present concern is to show that the laser miss distance can be determined from the random laser backscatter signal with enough accuracy to allow good control of the laser miss distance. In particular, we are concerned with the effect of any possible glint point in the immediate vicinity of the aim-point. We assume that by some mechanism the laser boresight error has been controlled well enough so that the laser strikes the target* , but that because of the possible presence of a glint point, the center of gravity of the laser radiation as formed on an image of the backscatter compared to the location of the aim-point on the image, can not be used to tell what the laser miss distance is. Our approach here is to take advantage of the fact that the diffuse return, which is a good indicator of the laser spot position, fluctuates (randomly) in time while the glint return will be constant in time (so long as the laser spot is nearly stationary on the target) , so that we can distinguish between the two

* A possible method of getting the laser beam to strike the target in the presence of a large initial laser boresight error would be to deliberately scan the beam in a raster pattern around the nominal target position. The timing of the receipt of the backscatter signal (indicating that the laser was on the target), in conjunction with (approximate) knowledge of the round-trip delay time, and of the raster scan rate will allow the pointing control system to determine the boresight error well enough to get the laser on the target.

parts of the backscatter signal. This allows us to use the calculated center-of-gravity of the diffuse return to determine the laser spot position on the target and thus the laser miss distance with respect to the aim-point.

In this chapter we shall first present the details of the rather simple theory that allows us to separate the diffuse from the glint returns. In the section after that we will present a computer simulation program, drawing on our previous work, that will attempt to separate the diffuse from the glint reform and calculate the laser spot position, in the presence of a nearby glint point. We shall see from the results presented, that even in the presence of a very strong nearby glint point, an accurate laser spot position determination can be made. In the final section we shall modify this simulation to use the estimated laser spot position to allow laser miss distance control, and shall show that it is, in general, possible to drive the miss distance to a fraction of a spot diameter.

7.2 Separation of Diffuse and Glint Returns

From the theoretical results developed previously we know that the statistics of the laser backscatter signal falling on any point (any single detector), in the focal plane of the shared aperture (backscatter) receiver are described by considering the signal to be composed of three amplitude components $\mathcal{U}_g(t)$, $\mathcal{U}_{\parallel}(t)$, and $\mathcal{U}_{\perp}(t)$, which we can write as

$$\mathcal{U}_g(t) = A_g \exp \left[(2\pi i c t / \lambda) + i \phi_0 \right] \quad (1)$$

$$\mathcal{U}_{\parallel}(t) = A_{\parallel}(t) \exp \left[(2\pi i c t / \lambda) + i \phi_0 \right] \quad (2)$$

$$\mathcal{U}_{\perp}(t) = A_{\perp}(t) \exp \left[(2\pi i c t / \lambda) + (\tfrac{1}{2} \pi i) + i \phi_0 \right] \quad (3)$$

Here ϕ_0 is an arbitrary phase factor, $c = 3 \times 10^8$ m/sec is the speed of light, and λ is the laser wavelength. The glint amplitude, A_g , is constant. The two amplitudes $A_{\parallel}(t)$ and $A_{\perp}(t)$ are statistically independent, time varying gaussian random variable, which we associate with the diffuse scattering processes, and which would be present with this same amplitude, whether or not the glint return were present.

The time dependence of $A_{\parallel}(t)$ and of $A_{\perp}(t)$ are very slow compared with the optical frequency time dependence of $\exp(2\pi i c t / \lambda)$. The signal intensity due to these three components will be

$$I_s(t) = \tfrac{1}{2} [\mathcal{U}(t)]^* \mathcal{U}(t), \quad (4)$$

where

$$u(t) = u_0(t) + u_{\parallel}(t) + u_{\perp}(t). \quad (5)$$

The intensity that we would expect from the diffuse return, [i. e., $I_s(t)$ when there is no glint return], can be written as

$$I_0(t) = \frac{1}{2} [u_{\parallel}(t) + u_{\perp}(t)]^2. \quad (6)$$

We would like to determine the mean value of $I_0(t)$, i. e. \bar{I}_0 from the time varying nature of $I_s(t)$. We shall show in what follows that we can determine \bar{I}_0 from the mean and variance of $I_s(t)$, i. e. from \bar{I}_s and Var_s . First, we define

$$\bar{I}_0 = \langle I_0(t) \rangle, \quad (7)$$

$$\bar{I}_s = \langle I_s(t) \rangle, \quad (8)$$

$$\text{Var}_s = \langle [I_s(t) - \bar{I}_s]^2 \rangle, \quad (9)$$

where the angle brackets have the meaning of an ensemble averaging process. If we can calculate \bar{I}_0 from the quantities \bar{I}_s and Var_s , which we can measure* from the focal plane signal $I_s(t)$, we can then estimate the apparent laser spot position by taking a weighted average of the calculated values of \bar{I}_0 over the focal plane. This

* Our estimation of \bar{I}_s and Var_s will, in the system simulation, be based on the assumption that temporal averaging can be equated with ensemble averaging, and that we have an adequate temporal data base. In practice, we shall always be significantly limited by the fact that our temporal data base is very short.

will give us the nominal centroid of the diffuse return portion of the laser backscatter image and thus the nominal location of the laser spot on the target image.

Combining Eq. 's (1), (2), (3), (4), and (5) it can be shown that

$$I_s(t) = \frac{1}{2} \{ [A_0 + A_{\parallel}(t)]^2 + [A_{\perp}(t)]^2 \}. \quad (10)$$

Proceeding similarly but making use of Eq. 's (2), (3), and (6) we get

$$I_0(t) = \frac{1}{2} \{ [A_{\parallel}(t)]^2 + [A_{\perp}(t)]^2 \}. \quad (11)$$

Making use of the fact that $A_{\parallel}(t)$ and $A_{\perp}(t)$ are each gaussian random variable with zero mean and the same standard deviation, which we denote by σ_A , so that we can write

$$\sigma_A^2 = \langle [A_{\parallel}(t)]^2 \rangle, \quad (12a)$$

$$\sigma_A^2 = \langle [A_{\perp}(t)]^2 \rangle, \quad (12b)$$

then it is easy to obtain from a combination of Eq. 's (7), (11), and (12), that

$$\bar{I}_0 = \sigma_A^2. \quad (13)$$

In order to evaluate \bar{I}_s we must first note that since $A_{\parallel}(t)$ is a zero mean random variable, then

$$\langle A_{\parallel}(t) \rangle = 0. \quad (14)$$

Thus when we seek to evaluate \bar{I}_s from Eq.'s (8), (10), and (12), we get

$$\begin{aligned} \bar{I}_s &= \frac{1}{2} \{ [A_G^2 + 2 A_G \langle A_{\parallel}(t) \rangle + \sigma_A^2] + \sigma_A^2 \} \\ &= \frac{1}{2} A_G^2 + \sigma_A^2. \end{aligned} \quad (15)$$

In carrying out an evaluation of Var_s , starting from Eq.'s (9), and (10), we obtain

$$\begin{aligned} \text{Var}_s &= \frac{1}{4} \langle \{ [A_G + A_{\parallel}(t)]^2 + [A_{\perp}(t)]^2 - 2\bar{I}_s \}^2 \rangle \\ &= \frac{1}{4} \langle \{ [A_G + A_{\parallel}(t)]^4 + 2 [A_G + A_{\parallel}(t)]^2 [A_{\perp}(t)]^2 \\ &\quad + [A_{\perp}(t)]^4 \} \\ &\quad - \langle \{ [A_G + A_{\parallel}(t)]^2 + [A_{\perp}(t)]^2 + [A_{\perp}(t)]^2 \} \rangle \bar{I}_s + \bar{I}_s^2 \rangle \\ &= \frac{1}{4} \langle \{ [A_G + A_{\parallel}(t)]^4 + 2 [A_G + A_{\parallel}(t)]^2 [A_{\perp}(t)]^2 \\ &\quad + [A_{\perp}(t)]^4 \} - \bar{I}_s^2 \rangle. \end{aligned} \quad (16)$$

From the statistical independence of $A_{\parallel}(t)$ and $A_{\perp}(t)$ it follows that

$$\langle [A_{\parallel}(t)]^2 [A_{\perp}(t)]^2 \rangle = \langle [A_{\parallel}(t)]^2 \rangle \langle [A_{\perp}(t)]^2 \rangle, \quad (17)$$

while from the fact that $A_{\parallel}(t)$ and $A_{\perp}(t)$ are each zero mean gaussian random variables it follows that

$$\langle [A_{\parallel}(t)]^4 \rangle = 3 \langle [A_{\parallel}(t)]^2 \rangle^2, \quad (18a)$$

$$\langle [A_{\perp}(t)]^4 \rangle = 3 \langle [A_{\perp}(t)]^2 \rangle^2, \quad (18b)$$

$$\langle [A_{\parallel}(t)]^3 \rangle = 0. \quad (19)$$

Making use of Eq. 's (14), (17), (18), and (19) we can reduce Eq. (16) to the form

$$\begin{aligned} \text{Var}_s &= \frac{1}{4} \{ A_0^4 + 6 A_0^2 \langle [A_{\parallel}(t)]^2 \rangle + 3 \langle [A_{\parallel}(t)]^2 \rangle^2 \\ &\quad + 2 A_0^2 \langle [A_{\perp}(t)]^2 \rangle + 2 \langle [A_{\parallel}(t)]^2 \rangle \langle [A_{\perp}(t)]^2 \rangle \\ &\quad + 3 \langle [A_{\perp}(t)]^2 \rangle^2 \} - \bar{I}_s^2 \\ &= \frac{1}{4} [A_0^4 + 8 A_0^2 \sigma_A^2 + 8 (\sigma_A^2)^2] - \left(\frac{1}{2} A_0^2 + \sigma_A^2 \right)^2 \\ &= A_0^2 \sigma_A^2 + (\sigma_A^2)^2. \end{aligned} \quad (20)$$

Making use of Eq. (13) we can rewrite Eq. 's (15), and (20) as

$$\bar{I}_s = \frac{1}{2} A_0^2 + \bar{I}_0, \quad (21)$$

$$\text{Var}_s = (A_0^2 + \bar{I}_0) \bar{I}_0. \quad (22)$$

Our problem now reduces to solving this set of simultaneous quadratic equations for \bar{I}_0 in terms of \bar{I}_s and Var_s .

Proceeding in a straightforward manner, we obtain from Eq. (21)

$$A_0^2 = 2 (\bar{I}_s - \bar{I}_0) . \quad (23)$$

Substituting this into Eq. (22) we get

$$\text{Var}_s = (2 \bar{I}_s - \bar{I}_0) \bar{I}_0 , \quad (24)$$

which we recast in the standard quadratic equation form as

$$\bar{I}_0^2 - 2 \bar{I}_0 \bar{I}_s + \text{Var}_s = 0 . \quad (25)$$

The solution to this equation is

$$\bar{I}_0 = \frac{2 \bar{I}_s \pm [(-2 \bar{I}_s)^2 - 4 \text{Var}_s]^{1/2}}{2} . \quad (26)$$

The plus/minus sign, however, must be restricted to the positive value if \bar{I}_0 is to be less than \bar{I}_s , which we know it must be to maintain the glint intensity ($\frac{1}{2} A_0^2$) as a non-negative quantity. Thus we write

$$\bar{I}_0 = \bar{I}_s - [(\bar{I}_s)^2 - \text{Var}_s]^{1/2} . \quad (27)$$

With this equation we can calculate \bar{I}_0 from the measured mean and variance of the detector signals. With this result in hand, we are ready to proceed with our estimation of the laser spot position from the fluctuating laser backscatter image. We treat this matter in the next section.

7.3 Laser Spot Position Estimation

Using the computer simulation program developed in a previous report, and making use of Eq. (27), we are now ready to consider simulation of the laser spot position estimation problem. Because we have assumed that the glint return is constant, and since we will be using temporal averaging in place of ensemble averaging it is necessary that the laser spot be nearly stationary on the target for the period of our backscatter fluctuation measurement. Accordingly, we have assumed that backscatter signal variability measurements should not start till after two times the inverse of the servo bandwidth. In our simulation, with a 100 Hz servo bandwidth, this corresponds to 0.020 sec. Furthermore, to allow for round-trip transit time effects, a total time of 0.0066 sec, we should wait 0.0266 sec. As a measure of caution, and to allow for a simulation start-up delay of 0.0033 sec, in our simulations we have chosen to allow a total of 0.030 sec before we start to collect backscatter signal fluctuation statistics.

In Tables 1a to 1l, which we generated with the program listed in Appendix I, we show the true and estimated positions of the laser spot in terms of the focal plane coordinates μ_D , ν_D , for various glint point positions. Results are shown every millisecond starting at 0.031 sec and continuing to 0.101 sec. For the engagement simulated the glint point strength was taken to have $I_{g,0} = 1 \times 10^3$, i.e., if the laser spot were exactly centered on the glint point, the strength of the glint return would be 1000 times the strength of the diffuse return. The engagement simulation, like many of those we have ran previously involved a target at $R = 1.0$ Mm range, closing at 1.0×10^4 m/sec, and with a crossing velocity of 50. m/sec. The shared aperture system had a gaussian amplitude transmission taper with a standard deviation of $\sigma = 1.0$ m. The laser wavelength is $\lambda = 1.0 \times 10^{-6}$ m.

Under these engagement conditions the laser spot on the target has a gaussian intensity taper with a standard deviation of $\sigma_1 = 0.1125$ m, and a corresponding "diameter" of $2\sigma_1 = 0.225$ m. The focal plane array has detector elements whose angular subtense is $(k\sigma)^{-1} = 0.159$ μ rad, which is equivalent to 0.159 m on the target. This is about two-thirds of the laser spot diameter. The backscatter statistics will fluctuate with a characteristic period of $T_4 = 0.003536$ sec, and a correlation time of $4T_4 = 0.01414$ sec.

The question of how long we have to wait to get reasonably accurate statistics is perhaps best judged by comparison of the estimated and true values of (μ_0, ν_0) in Tables 1a to 1l. To facilitate our visualization of this data, in Fig.'s 1a and 1b we show the estimated laser spot coordinates as a function of the glint point position for the estimate formed after 30 msec (i.e. at $t = 0.060$ sec), and after 70 msec (i.e. at $t = 0.100$ sec). There does not appear to be a clear distinction between the two sets of values. Accordingly, considering the need to form the estimate as quickly as possible, we propose to use the estimate formed after 30 msec, i.e. after only two correlation times.

There are two things we should note about our results. First, there does not appear to be any significant pulling of the estimated laser spot position towards the glint point. This can be seen directly from a study of Fig. 1a where we see that the set of estimated positions follows the actual position much more closely than it does the glint point position. In a sense this can also be seen indirectly from a comparison between Fig.'s 1a and 1b, from which we see that in the direction in which glint pulling was significant, there was no more spread or bias than for the direction for which glint pulling does not exist. In Fig. 2 we show the relative strength of the glint return compared to the diffuse return for various glint point positions. As can be seen, for the cases we have

considered, the glint strength is generally very much larger than the diffuse return strength.

The second feature of our results that we should note from Fig. 's 1a and 1b concerns the spread in the estimated position. The errors are virtually all less than one laser spot radius. The distribution of errors is entirely compatible with the concept of Rayleigh noise inherent in the diffuse laser spot and the use of such a short measurement period. Accordingly, we expect that if we could have allowed a measurement period that were many times the backscatter signal correlation time, (as would naturally be the case if the target had a higher crossing velocity), then the spread in the estimates of the laser spot position would be much smaller. In any case, the significant point is that the errors are apparently always of the order of, or less than the laser spot radius.

With this validation of our technique for estimation of the laser spot position, even in the presence of a strong glint point, we are now ready to proceed to the task of closing the boresight error control loop. We shall take this up in the next section using the same approximately two correlation-times measurement period that seemed to work well enough here.

7.4 Boresight Error Control Simulation

In order to demonstrate that we could combine all of the previously developed features into one closed loop boresight error control operation, the computer program listed in Appendix II was prepared. In this computer simulation the inner loop 100 Hz bandwidth image tracking servo has its boresight error corrected by a periodically updated boresight error estimate, using the first order periodic update servo concept developed in a previous report. In the simulation, the boresight error is estimated from a determination of the laser spot position made by observing the fluctuating part of the laser backscatter image, as described in the previous sections. For our simulation, based on a target at a range of 1.0 Mm, with a crossing velocity of 50. msec, we used a 30 msec observation period and a 30 msec gimbal update slew and settle time.

Results are shown in Table 2a for a glint point 0.25 m from the aim-point, so that with the laser spot on the aim-point the glint return is about 85 times the strength of the diffuse return. As can be seen, this configuration is able to reduce the initial boresight error of 0.43 m, i.e. about 2 laser spot diameters ($0.43 \mu\text{rad}$) to a value of the order of one-half a spot diameter or less. In Tables 2b(1) to 2b(4), we show a series of nearly equivalent runs except that in this case the glint spot is 0.35 m from the aim-point, so its backscatter strength is about 8 times the diffuse scattering signal level. Here again, it is seen, from the data in these Tables, and their representation in Fig.'s 3a to 3d, that the initial 2 laser spot diameter miss distance can be reduced to the order of one-half a spot diameter.

These results can be considered a demonstration of the concept that laser spot position can be determined even in the presence of strong glint from the fluctuating part of the backscatter signal. It is probably also

worth noting that the Rayleigh statistics of the backscatter signal, which limited the accuracy of the laser spot position determination, would have a less deleterious effect if the targets crossing velocity were higher, or if the target surface were subject to some minor vibrations. This would reduce the backscatter correlation time and thus improve the quality of our averaging processes.

But almost certainly, the key achievement of this work is the demonstration of the very important concept that high servo bandwidth tracking can be combined with round-trip pointing error sensing to control boresight errors, even in the case of a space engagement at very long ranges ! Extension of this general concept to more complex control aspects of a high energy laser space engagement should be straightforward. We expect to be able to apply an extension of the principles we have demonstrated here, to the problem of adaptive optics control with a high local servo bandwidth, but with a low bandwidth outer loop to control errors in the local wavefront distortion sensor system !

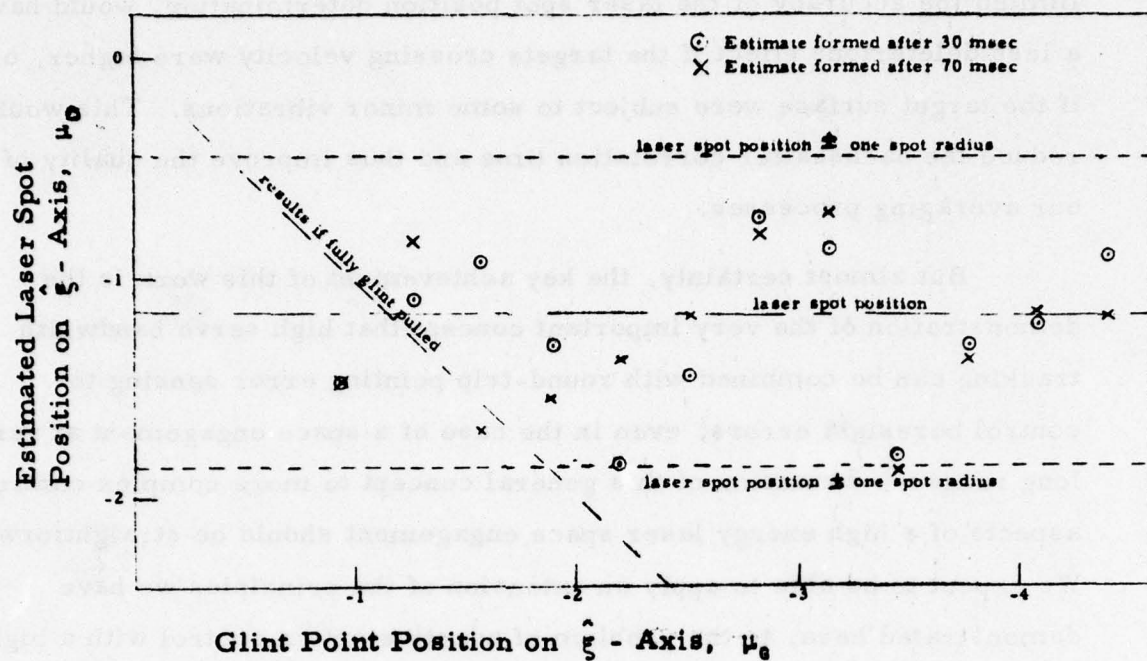


Figure 7.1a Estimated Laser Spot Position Along $\hat{\xi}$ - Axis.

The results correspond to the data in Tables 1a to 1l .
 Fig. 2 shows the glint strength as a function of μ_θ for this data.

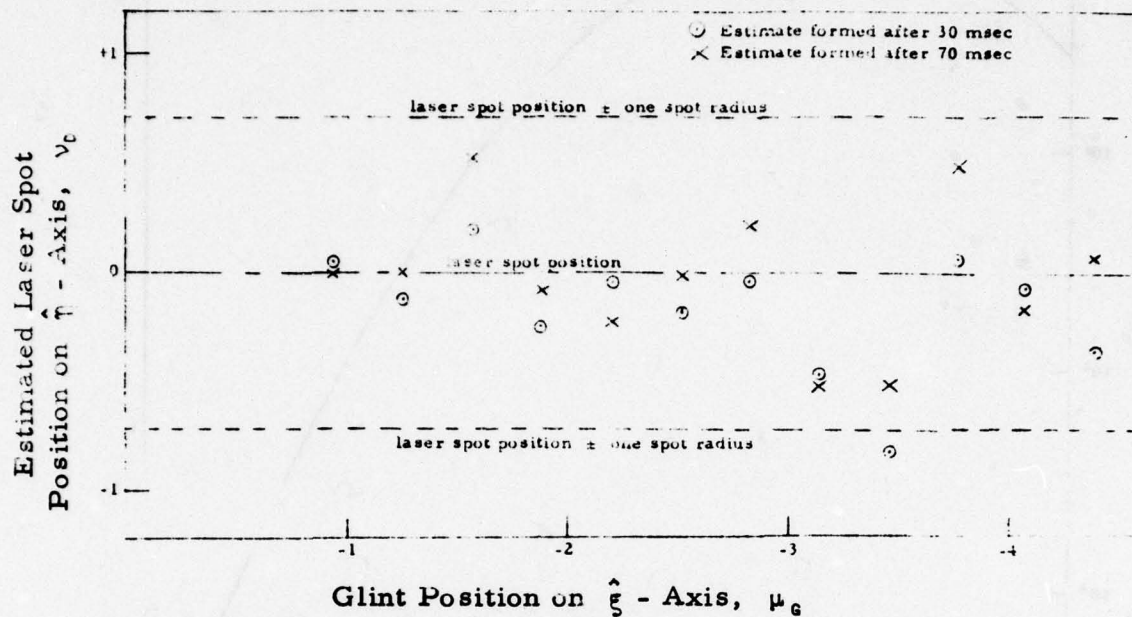


Figure 7.1b Estimated Laser Spot Position Along $\hat{\eta}$ - Axis.

The results correspond to the data in Tables 1a to 1l. Fig. 2 shows the glint strength as a function of μ_c for this data.

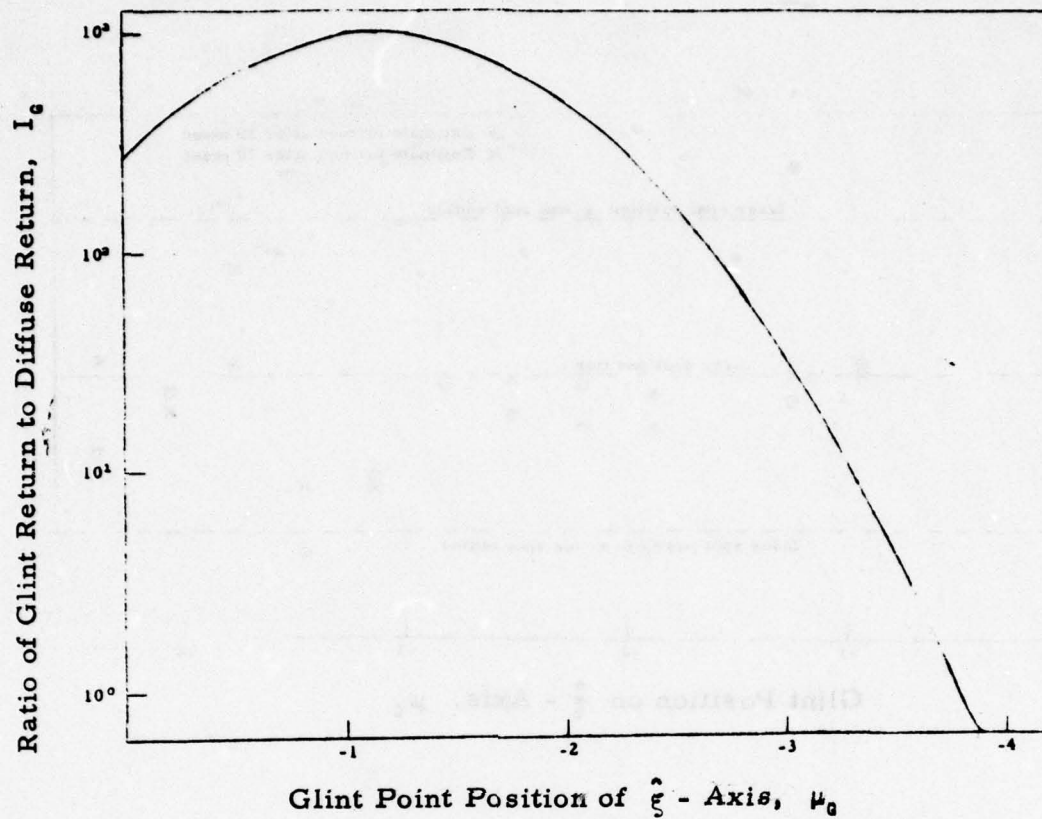


Figure 7.2 Relative Glint Strength.

For these results, which correspond to the cases giving rise to the data in Fig.'s 1a and 1b, the laser spot was at $(\mu_0, \nu_0) = (-1.15, 0.0)$, while the glint point is at $(\mu_g, \nu_g) = (\mu_g, 0.0)$.

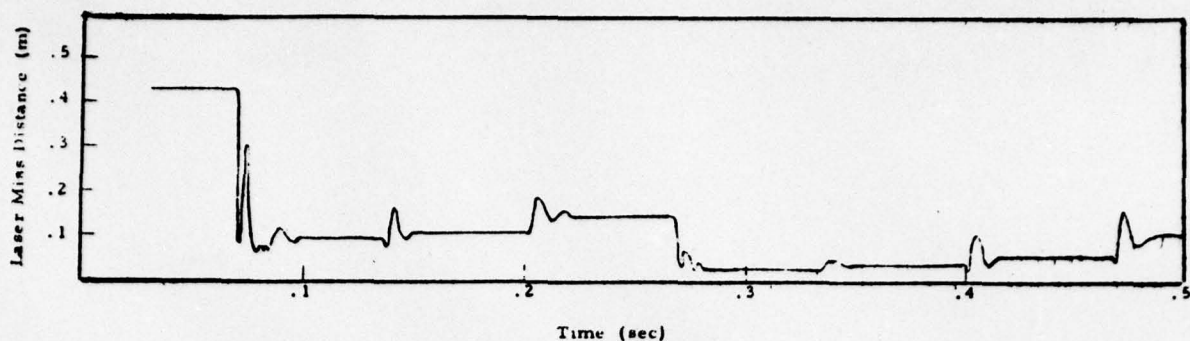


Figure 7.3a Closed Loop Boresight Error Control: Data from Table 2b (1)

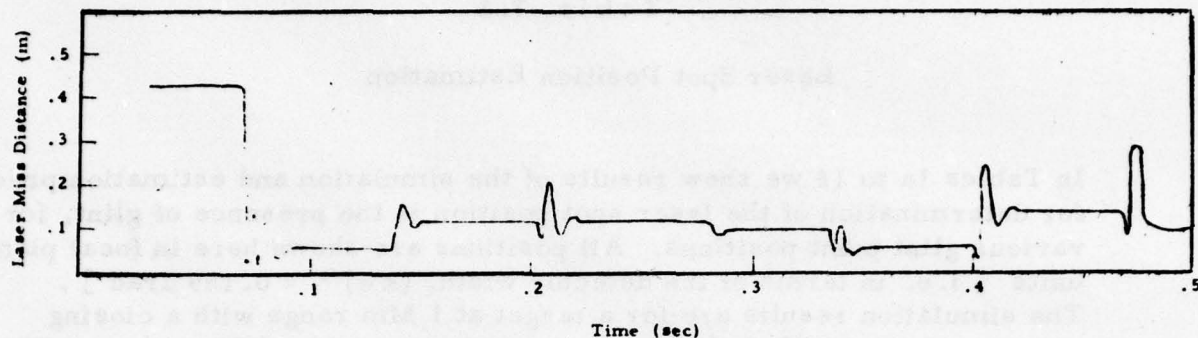


Figure 7.3b Closed Loop Boresight Error Control: Data from Table 2b (2)

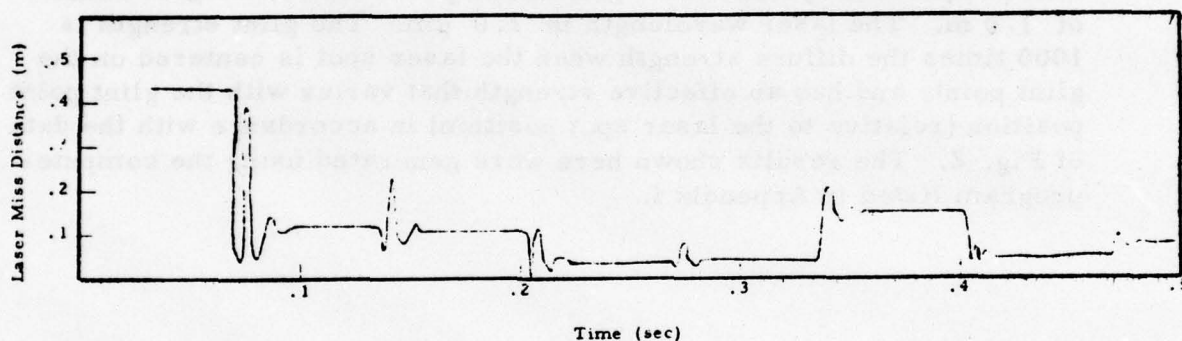


Figure 7.3c Closed Loop Boresight Error Control: Data from Table 2b (3)

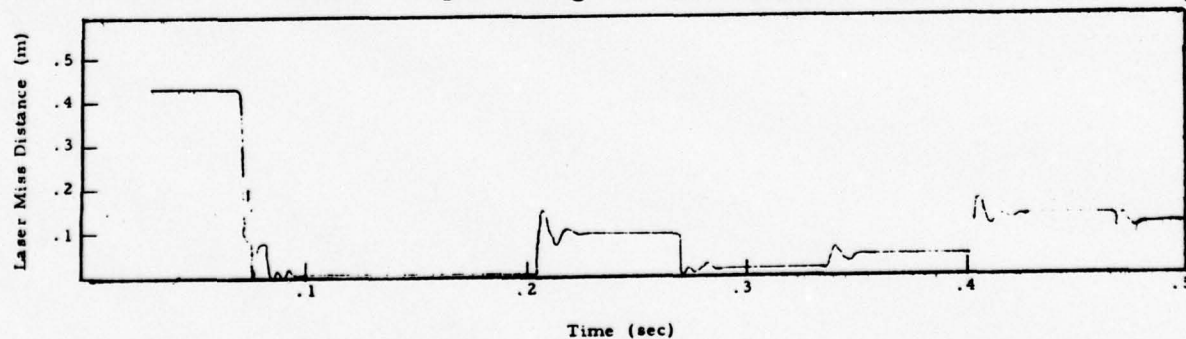


Figure 7.3d Closed Loop Boresight Error Control: Data from Table 2b (4)

Table 7.1

Laser Spot Position Estimation

In Tables 1a to 1l we show results of the simulation and estimation process for determination of the laser spot position in the presence of glint, for various glint point positions. All positions are shown here in focal plane units [i.e. in terms of the detector width, $(k \sigma)^{-1} = 0.159 \mu\text{rad}$]. The simulation results are for a target at 1 Mm range with a closing velocity of $1. \times 10^4$ m/sec and a crossing velocity of 50. m/sec. The shared aperture system has a gaussian taper with a one sigma radius of 1.0 m. The laser wavelength is $1.0 \mu\text{m}$. The glint strength is 1000 times the diffuse strength when the laser spot is centered on the glint point, and has an effective strength that varies with the glint point position (relative to the laser spot position) in accordance with the data of Fig. 2. The results shown here were generated using the computer program listed in Appendix I.

Table 1a

TIME	PUC		NUG		PUG	NUG
	EST	TRUE	EST	TRUE		
C.C31	-1.54	-1.16	-0.53	-0.00	-0.54	0.00
C.C32	-1.33	-1.16	-0.50	-0.00	-0.54	0.00
C.C33	-1.02	-1.16	-0.51	-0.00	-0.54	-0.00
C.C34	-0.82	-1.15	-0.79	0.00	-0.54	-0.00
C.C35	-0.79	-1.15	-0.60	0.00	-0.54	-0.00
C.C36	-0.80	-1.15	-0.48	0.00	-0.54	-0.00
C.C37	-0.79	-1.15	-0.43	0.00	-0.54	-0.00
C.C38	-0.79	-1.15	-0.40	0.00	-0.54	-0.00
C.C39	-0.78	-1.15	-0.40	-0.00	-0.54	0.00
C.C40	-0.77	-1.15	-0.41	-0.00	-0.54	0.00
C.C41	-0.77	-1.15	-0.42	-0.00	-0.54	0.00
C.C42	-0.77	-1.15	-0.41	-0.00	-0.54	0.00
C.C43	-0.79	-1.15	-0.39	-0.00	-0.54	0.00
C.C44	-0.81	-1.15	-0.37	-0.00	-0.54	0.00
C.C45	-0.84	-1.15	-0.33	0.00	-0.54	-0.00
C.C46	-0.89	-1.15	-0.29	0.00	-0.54	-0.00
C.C47	-0.94	-1.15	-0.24	0.00	-0.54	-0.00
C.C48	-1.00	-1.15	-0.19	0.00	-0.54	-0.00
C.C49	-1.05	-1.15	-0.14	0.00	-0.54	-0.00
C.C50	-1.11	-1.15	-0.10	0.00	-0.54	0.00
C.C51	-1.16	-1.15	-0.06	-0.00	-0.54	0.00
C.C52	-1.22	-1.15	-0.03	-0.00	-0.54	0.00
C.C53	-1.27	-1.15	-0.01	-0.00	-0.54	0.00
C.C54	-1.31	-1.15	0.02	-0.00	-0.54	0.00
C.C55	-1.35	-1.15	0.03	-0.00	-0.54	0.00
C.C56	-1.38	-1.15	0.05	0.00	-0.54	-0.00
C.C57	-1.41	-1.15	0.05	0.00	-0.54	-0.00
C.C58	-1.43	-1.15	0.06	0.00	-0.54	-0.00
C.C59	-1.45	-1.15	0.06	0.00	-0.54	-0.00
C.C60	-1.47	-1.15	0.05	0.00	-0.54	-0.00
C.C61	-1.48	-1.15	0.05	0.00	-0.54	-0.00
C.C62	-1.48	-1.15	0.04	-0.00	-0.54	0.00
C.C63	-1.49	-1.15	0.03	-0.00	-0.54	0.00
C.C64	-1.49	-1.15	0.02	-0.00	-0.54	0.00
C.C65	-1.48	-1.15	0.01	-0.00	-0.54	0.00
C.C66	-1.48	-1.15	0.00	-0.00	-0.54	0.00
C.C67	-1.47	-1.15	-0.01	0.00	-0.54	-0.00
C.C68	-1.47	-1.15	-0.02	0.00	-0.54	-0.00
C.C69	-1.46	-1.15	-0.03	0.00	-0.54	-0.00
C.C70	-1.45	-1.15	-0.05	0.00	-0.54	-0.00
C.C71	-1.44	-1.15	-0.06	0.00	-0.54	-0.00
C.C72	-1.43	-1.15	-0.07	0.00	-0.54	-0.00
C.C73	-1.42	-1.15	-0.08	-0.00	-0.54	0.00
C.C74	-1.41	-1.15	-0.09	-0.00	-0.54	0.00
C.C75	-1.40	-1.15	-0.10	-0.00	-0.54	0.00
C.C76	-1.39	-1.15	-0.11	-0.00	-0.54	0.00
C.C77	-1.38	-1.15	-0.12	-0.00	-0.54	0.00
C.C78	-1.37	-1.15	-0.13	-0.00	-0.54	0.00

Table 1a - Continued

Page 2

C.C79	-1.36	-1.15	-C.14	0.00	-C.54	-0.00
C.C80	-1.35	-1.15	-C.15	0.00	-C.54	-0.00
C.C81	-1.34	-1.15	-C.16	0.00	-C.54	-0.00
C.C82	-1.34	-1.15	-C.16	0.00	-C.54	-0.00
C.C83	-1.33	-1.15	-C.17	0.00	-C.54	-0.00
C.C84	-1.33	-1.15	-C.17	-0.00	-C.54	0.00
C.C85	-1.33	-1.15	-C.18	-0.00	-C.54	0.00
C.C86	-1.32	-1.15	-C.18	-0.00	-C.54	0.00
C.C87	-1.32	-1.15	-C.18	-0.00	-C.54	0.00
C.C88	-1.33	-1.15	-C.17	-0.00	-C.54	0.00
C.C89	-1.33	-1.15	-C.17	-0.00	-C.54	0.00
C.C90	-1.34	-1.15	-C.16	0.00	-C.54	-0.00
C.C91	-1.34	-1.15	-C.15	0.00	-C.54	-0.00
C.C92	-1.35	-1.15	-C.14	0.00	-C.54	-0.00
C.C93	-1.36	-1.15	-C.13	0.00	-C.54	-0.00
C.C94	-1.38	-1.15	-C.12	0.00	-C.54	-0.00
C.C95	-1.39	-1.15	-C.10	0.00	-C.54	-0.00
C.C96	-1.40	-1.15	-C.C9	-0.00	-C.54	0.00
C.C97	-1.42	-1.15	-C.C7	-0.00	-C.54	0.00
C.C98	-1.43	-1.15	-C.C5	-0.00	-C.54	0.00
C.C99	-1.45	-1.15	-C.C3	-0.00	-C.54	0.00
C.100	-1.46	-1.15	-C.C1	-0.00	-C.54	0.00
C.101	-1.48	-1.15	C.C1	0.00	-C.54	-0.00

Table 1b

TYPE	PUC		AUC		PUG	NUG
	EST	TRUE	EST	TRUE		
C.C31	-0.85	-1.16	C.C5	-0.00	-1.25	0.00
C.C32	-0.85	-1.16	C.C6	-0.00	-1.25	0.00
C.C33	-1.04	-1.16	C.C6	-0.00	-1.25	-0.00
C.C34	-1.12	-1.15	C.C6	0.00	-1.26	-0.00
C.C35	-1.17	-1.15	C.C5	0.00	-1.26	-0.00
C.C36	-1.20	-1.15	C.C4	0.00	-1.26	-0.00
C.C37	-1.21	-1.15	C.C3	0.00	-1.26	-0.00
C.C38	-1.21	-1.15	C.C2	0.00	-1.26	-0.00
C.C39	-1.20	-1.15	C.C1	-0.00	-1.26	0.00
C.C40	-1.19	-1.15	-C.C1	-0.00	-1.26	0.00
C.C41	-1.17	-1.15	-C.C2	-0.00	-1.26	0.00
C.C42	-1.16	-1.15	-C.C3	-0.00	-1.26	0.00
C.C43	-1.15	-1.15	-C.C4	-0.00	-1.26	0.00
C.C44	-1.15	-1.15	-C.C5	-0.00	-1.26	0.00
C.C45	-1.14	-1.15	-C.C6	0.00	-1.26	-0.00
C.C46	-1.14	-1.15	-C.C7	0.00	-1.26	-0.00
C.C47	-1.14	-1.15	-C.C7	0.00	-1.26	-0.00
C.C48	-1.14	-1.15	-C.C8	0.00	-1.26	-0.00
C.C49	-1.13	-1.15	-C.C9	0.00	-1.26	-0.00
C.C50	-1.13	-1.15	-C.C9	0.00	-1.26	0.00
C.C51	-1.13	-1.15	-C.10	-0.00	-1.26	0.00
C.C52	-1.13	-1.15	-C.10	-0.00	-1.26	0.00
C.C53	-1.12	-1.15	-C.11	-0.00	-1.26	0.00
C.C54	-1.12	-1.15	-C.11	-0.00	-1.26	0.00
C.C55	-1.12	-1.15	-C.12	-0.00	-1.26	0.00
C.C56	-1.11	-1.15	-C.12	0.00	-1.26	-0.00
C.C57	-1.11	-1.15	-C.12	0.00	-1.26	-0.00
C.C58	-1.10	-1.15	-C.12	0.00	-1.26	-0.00
C.C59	-1.10	-1.15	-C.12	0.00	-1.26	-0.00
C.C60	-1.09	-1.15	-C.12	0.00	-1.26	-0.00
C.C61	-1.09	-1.15	-C.12	0.00	-1.26	-0.00
C.C62	-1.08	-1.15	-C.12	-0.00	-1.26	0.00
C.C63	-1.07	-1.15	-C.12	-0.00	-1.26	0.00
C.C64	-1.07	-1.15	-C.12	-0.00	-1.26	0.00
C.C65	-1.06	-1.15	-C.12	-0.00	-1.26	0.00
C.C66	-1.05	-1.15	-C.12	-0.00	-1.26	0.00
C.C67	-1.04	-1.15	-C.11	0.00	-1.26	-0.00
C.C68	-1.03	-1.15	-C.11	0.00	-1.26	-0.00
C.C69	-1.03	-1.15	-C.11	0.00	-1.26	-0.00
C.C70	-1.02	-1.15	-C.10	0.00	-1.26	-0.00
C.C71	-1.01	-1.15	-C.10	0.00	-1.26	-0.00
C.C72	-1.00	-1.15	-C.10	0.00	-1.26	-0.00
C.C73	-0.99	-1.15	-C.C9	-0.00	-1.26	0.00
C.C74	-0.98	-1.15	-C.C9	-0.00	-1.26	0.00
C.C75	-0.98	-1.15	-C.C8	-0.00	-1.26	0.00
C.C76	-0.97	-1.15	-C.C8	-0.00	-1.26	0.00
C.C77	-0.96	-1.15	-C.C7	-0.00	-1.26	0.00
C.C78	-0.95	-1.15	-C.C7	-0.00	-1.26	0.00

C.C79	-C.95	-1.15	-C.C6	0.00	-1.26	-0.00
C.C80	-C.94	-1.15	-C.C6	0.00	-1.26	-0.00
C.C81	-C.93	-1.15	-C.C5	0.00	-1.26	-0.00
C.C82	-C.92	-1.15	-C.C5	0.00	-1.26	-0.00
C.C83	-C.92	-1.15	-C.C4	0.00	-1.26	-0.00
C.C84	-C.91	-1.15	-C.C4	-0.00	-1.26	0.00
C.C85	-C.90	-1.15	-C.C3	-0.00	-1.26	0.00
C.C86	-C.90	-1.15	-C.C3	-0.00	-1.26	0.00
C.C87	-C.89	-1.15	-C.C2	-0.00	-1.26	0.00
C.C88	-C.88	-1.15	-C.C2	-0.00	-1.26	0.00
C.C89	-C.88	-1.15	-C.C2	-0.00	-1.26	0.00
C.C90	-C.87	-1.15	-C.C1	0.00	-1.26	-0.00
C.C91	-C.87	-1.15	-C.C1	0.00	-1.26	-0.00
C.C92	-C.86	-1.15	-C.C1	0.00	-1.26	-0.00
C.C93	-C.85	-1.15	-C.C1	0.00	-1.26	-0.00
C.C94	-C.85	-1.15	-C.C0	0.00	-1.26	-0.00
C.C95	-C.84	-1.15	-C.C0	0.00	-1.26	-0.00
C.C96	-C.84	-1.15	-C.C0	-0.00	-1.26	0.00
C.C97	-C.83	-1.15	C.C0	-0.00	-1.26	0.00
C.C98	-C.83	-1.15	C.C0	-0.00	-1.26	0.00
C.C99	-C.82	-1.15	C.C0	-0.00	-1.26	0.00
C.100	-C.82	-1.15	C.C0	-0.00	-1.26	0.00
C.101	-C.81	-1.15	C.C0	0.00	-1.26	-0.00

Table 1c

TYPE	PUC		NUC		PUC	NUG
	EST	TRUE	EST	TRUE		
C.C31	-0.97	-1.16	C.22	-0.00	-1.57	0.00
C.C32	-0.97	-1.16	C.27	-0.00	-1.57	0.00
C.C33	-0.97	-1.16	C.33	-0.00	-1.57	-0.00
C.C34	-0.97	-1.15	C.39	0.00	-1.57	-0.00
C.C35	-0.97	-1.15	C.43	0.00	-1.57	-0.00
C.C36	-0.96	-1.15	C.46	0.00	-1.57	-0.00
C.C37	-0.96	-1.15	C.49	0.00	-1.57	-0.00
C.C38	-0.96	-1.15	C.50	0.00	-1.57	-0.00
C.C39	-0.96	-1.15	C.49	-0.00	-1.57	0.00
C.C40	-0.95	-1.15	C.46	-0.00	-1.57	0.00
C.C41	-0.95	-1.15	C.43	-0.00	-1.57	0.00
C.C42	-0.95	-1.15	C.40	-0.00	-1.57	0.00
C.C43	-0.94	-1.15	C.38	-0.00	-1.57	0.00
C.C44	-0.94	-1.15	C.35	-0.00	-1.57	0.00
C.C45	-0.93	-1.15	C.33	0.00	-1.57	-0.00
C.C46	-0.93	-1.15	C.31	0.00	-1.57	-0.00
C.C47	-0.93	-1.15	C.30	0.00	-1.57	-0.00
C.C48	-0.92	-1.15	C.28	0.00	-1.57	-0.00
C.C49	-0.92	-1.15	C.26	0.00	-1.57	-0.00
C.C50	-0.92	-1.15	C.25	0.00	-1.57	0.00
C.C51	-0.92	-1.15	C.23	-0.00	-1.57	0.00
C.C52	-0.91	-1.15	C.22	-0.00	-1.57	0.00
C.C53	-0.91	-1.15	C.21	-0.00	-1.57	0.00
C.C54	-0.91	-1.15	C.20	-0.00	-1.57	0.00
C.C55	-0.91	-1.15	C.19	-0.00	-1.57	0.00
C.C56	-0.91	-1.15	C.19	0.00	-1.57	-0.00
C.C57	-0.91	-1.15	C.19	0.00	-1.57	-0.00
C.C58	-0.91	-1.15	C.19	0.00	-1.57	-0.00
C.C59	-0.92	-1.15	C.19	0.00	-1.57	-0.00
C.C60	-0.92	-1.15	C.20	0.00	-1.57	-0.00
C.C61	-0.93	-1.15	C.21	0.00	-1.57	-0.00
C.C62	-0.94	-1.15	C.23	-0.00	-1.57	0.00
C.C63	-0.95	-1.15	C.25	-0.00	-1.57	0.00
C.C64	-0.97	-1.15	C.27	-0.00	-1.57	0.00
C.C65	-0.99	-1.15	C.30	-0.00	-1.57	0.00
C.C66	-1.01	-1.15	C.33	-0.00	-1.57	0.00
C.C67	-1.04	-1.15	C.36	0.00	-1.57	-0.00
C.C68	-1.07	-1.15	C.39	0.00	-1.57	-0.00
C.C69	-1.11	-1.15	C.42	0.00	-1.57	-0.00
C.C70	-1.15	-1.15	C.45	0.00	-1.57	-0.00
C.C71	-1.19	-1.15	C.48	0.00	-1.57	-0.00
C.C72	-1.23	-1.15	C.51	0.00	-1.57	-0.00
C.C73	-1.28	-1.15	C.54	-0.00	-1.57	0.00
C.C74	-1.32	-1.15	C.56	-0.00	-1.57	0.00
C.C75	-1.36	-1.15	C.59	-0.00	-1.57	0.00
C.C76	-1.40	-1.15	C.61	-0.00	-1.57	0.00

Table 1c - Continued

Page 2

C.077	-1.44	-1.15	C.63	-0.00	-1.57	0.00
C.078	-1.48	-1.15	C.64	-0.00	-1.57	0.00
C.079	-1.51	-1.15	C.65	0.00	-1.57	-0.00
C.080	-1.55	-1.15	C.67	0.00	-1.57	-0.00
C.081	-1.58	-1.15	C.67	0.00	-1.57	-0.00
C.082	-1.61	-1.15	C.68	0.00	-1.57	-0.00
C.083	-1.63	-1.15	C.69	0.00	-1.57	-0.00
C.084	-1.66	-1.15	C.69	-0.00	-1.57	0.00
C.085	-1.68	-1.15	C.69	-0.00	-1.57	0.00
C.086	-1.69	-1.15	C.69	-0.00	-1.57	0.00
C.087	-1.71	-1.15	C.69	-0.00	-1.57	0.00
C.088	-1.72	-1.15	C.69	-0.00	-1.57	0.00
C.089	-1.74	-1.15	C.68	-0.00	-1.57	0.00
C.090	-1.75	-1.15	C.67	0.00	-1.57	-0.00
C.091	-1.75	-1.15	C.66	0.00	-1.57	-0.00
C.092	-1.76	-1.15	C.65	0.00	-1.57	-0.00
C.093	-1.76	-1.15	C.64	0.00	-1.57	-0.00
C.094	-1.76	-1.15	C.63	0.00	-1.57	-0.00
C.095	-1.75	-1.15	C.61	0.00	-1.57	-0.00
C.096	-1.75	-1.15	C.59	-0.00	-1.57	0.00
C.097	-1.74	-1.15	C.58	-0.00	-1.57	0.00
C.098	-1.72	-1.15	C.56	-0.00	-1.57	0.00
C.099	-1.71	-1.15	C.54	-0.00	-1.57	0.00
C.100	-1.69	-1.15	C.52	-0.00	-1.57	0.00
C.101	-1.66	-1.15	C.50	0.00	-1.57	-0.00

Table 1d

TIME	PUC		NUG		PUC	NUG
	EST	TRUE	EST	TRUE		
C.C31	-1.61	-1.16	C.17	-0.00	-1.68	0.00
C.C32	-1.54	-1.16	C.18	-0.00	-1.68	0.00
C.C33	-1.79	-1.16	C.10	-0.00	-1.68	-0.00
C.C34	-0.98	-1.15	-C.07	0.00	-1.68	-0.00
C.C35	-0.89	-1.15	-C.14	0.00	-1.68	-0.00
C.C36	-0.90	-1.15	-C.15	0.00	-1.68	-0.00
C.C37	-0.89	-1.15	-C.15	0.00	-1.69	-0.00
C.C38	-0.83	-1.15	-C.14	0.00	-1.69	-0.00
C.C39	-0.87	-1.15	-C.13	-0.00	-1.68	0.00
C.C40	-0.84	-1.15	-C.12	-0.00	-1.68	0.00
C.C41	-0.81	-1.15	-C.12	-0.00	-1.68	0.00
C.C42	-0.79	-1.15	-C.12	-0.00	-1.68	0.00
C.C43	-0.77	-1.15	-C.12	-0.00	-1.69	0.00
C.C44	-0.76	-1.15	-C.13	-0.00	-1.68	0.00
C.C45	-0.77	-1.15	-C.14	0.00	-1.68	-0.00
C.C46	-0.79	-1.15	-C.15	0.00	-1.68	-0.00
C.C47	-0.81	-1.15	-C.15	0.00	-1.68	-0.00
C.C48	-0.84	-1.15	-C.18	0.00	-1.68	-0.00
C.C49	-0.87	-1.15	-C.19	0.00	-1.68	-0.00
C.C50	-0.91	-1.15	-C.20	0.00	-1.68	0.00
C.C51	-0.95	-1.15	-C.21	-0.00	-1.68	0.00
C.C52	-0.98	-1.15	-C.22	-0.00	-1.68	0.00
C.C53	-1.02	-1.15	-C.23	-0.00	-1.68	0.00
C.C54	-1.06	-1.15	-C.24	-0.00	-1.68	0.00
C.C55	-1.10	-1.15	-C.24	-0.00	-1.68	0.00
C.C56	-1.14	-1.15	-C.25	0.00	-1.68	-0.00
C.C57	-1.18	-1.15	-C.25	0.00	-1.68	-0.00
C.C58	-1.22	-1.15	-C.25	0.00	-1.68	-0.00
C.C59	-1.26	-1.15	-C.25	0.00	-1.68	-0.00
C.C60	-1.30	-1.15	-C.24	0.00	-1.68	-0.00
C.C61	-1.33	-1.15	-C.24	0.00	-1.68	-0.00
C.C62	-1.36	-1.15	-C.24	-0.00	-1.68	0.00
C.C63	-1.39	-1.15	-C.23	-0.00	-1.68	0.00
C.C64	-1.42	-1.15	-C.22	-0.00	-1.68	0.00
C.C65	-1.45	-1.15	-C.21	-0.00	-1.68	0.00
C.C66	-1.47	-1.15	-C.20	-0.00	-1.68	0.00
C.C67	-1.48	-1.15	-C.19	0.00	-1.68	-0.00
C.C68	-1.51	-1.15	-C.18	0.00	-1.68	-0.00
C.C69	-1.54	-1.15	-C.18	0.00	-1.68	-0.00
C.C70	-1.57	-1.15	-C.16	0.00	-1.68	-0.00
C.C71	-1.59	-1.15	-C.15	0.00	-1.68	-0.00
C.C72	-1.61	-1.15	-C.14	0.00	-1.68	-0.00
C.C73	-1.63	-1.15	-C.13	-0.00	-1.68	0.00
C.C74	-1.65	-1.15	-C.12	-0.00	-1.68	0.00
C.C75	-1.66	-1.15	-C.12	-0.00	-1.68	0.00
C.C76	-1.67	-1.15	-C.11	-0.00	-1.68	0.00

C.C77	-1.68	-1.15	-C.11	-0.00	-1.68	0.00
C.C78	-1.68	-1.15	-C.11	-0.00	-1.68	0.00
C.C79	-1.69	-1.15	-C.11	0.00	-1.68	-0.00
C.C80	-1.69	-1.15	-C.11	0.00	-1.68	-0.00
C.C81	-1.69	-1.15	-C.10	0.00	-1.68	-0.00
C.C82	-1.69	-1.15	-C.10	0.00	-1.68	-0.00
C.C83	-1.68	-1.15	-C.11	0.00	-1.68	-0.00
C.C84	-1.67	-1.15	-C.11	-0.00	-1.68	0.00
C.C85	-1.67	-1.15	-C.10	-0.00	-1.68	0.00
C.C86	-1.67	-1.15	-C.10	-0.00	-1.68	0.00
C.C87	-1.67	-1.15	-C.09	-0.00	-1.68	0.00
C.C88	-1.67	-1.15	-C.09	-0.00	-1.68	0.00
C.C89	-1.67	-1.15	-C.08	-0.00	-1.68	0.00
C.C90	-1.67	-1.15	-C.08	0.00	-1.68	-0.00
C.C91	-1.66	-1.15	-C.07	0.00	-1.68	-0.00
C.C92	-1.65	-1.15	-C.07	0.00	-1.68	-0.00
C.C93	-1.65	-1.15	-C.07	0.00	-1.68	-0.00
C.C94	-1.64	-1.15	-C.06	0.00	-1.68	-0.00
C.C95	-1.62	-1.15	-C.06	0.00	-1.68	-0.00
C.C96	-1.61	-1.15	-C.06	-0.00	-1.68	0.00
C.C97	-1.60	-1.15	-C.06	-0.00	-1.68	0.00
C.C98	-1.58	-1.15	-C.07	-0.00	-1.68	0.00
C.C99	-1.57	-1.15	-C.07	-0.00	-1.68	0.00
C.100	-1.55	-1.15	-C.08	-0.00	-1.68	0.00
C.101	-1.54	-1.15	-C.08	0.00	-1.68	-0.00

Table 1e

TIME	PUC		AUC		PUC	NUG
	EST	TRUE	EST	TRUE		
C.C31	-1.84	-1.16	C.C1	-0.00	-2.20	0.00
C.C32	-1.78	-1.16	-C.C1	-0.00	-2.20	0.00
C.C33	-1.81	-1.16	-C.C6	-0.00	-2.20	-0.00
C.C34	-1.79	-1.15	-C.14	0.00	-2.20	-0.00
C.C35	-1.84	-1.15	-C.19	0.00	-2.20	-0.00
C.C36	-1.13	-1.15	-C.24	0.00	-2.20	-0.00
C.C37	-1.01	-1.15	-C.28	0.00	-2.20	-0.00
C.C38	-C.90	-1.15	-C.31	0.00	-2.20	-0.00
C.C39	-1.00	-1.15	-C.27	-0.00	-2.20	0.00
C.C40	-1.22	-1.15	-C.19	-0.00	-2.20	0.00
C.C41	-1.22	-1.15	-C.13	-0.00	-2.20	0.00
C.C42	-1.57	-1.15	-C.C9	-0.00	-2.20	0.00
C.C43	-1.65	-1.15	-C.C7	-0.00	-2.20	0.00
C.C44	-1.71	-1.15	-C.C5	-0.00	-2.20	0.00
C.C45	-1.74	-1.15	-C.C5	0.00	-2.20	-0.00
C.C46	-1.77	-1.15	-C.C4	0.00	-2.20	-0.00
C.C47	-1.79	-1.15	-C.C4	0.00	-2.20	-0.00
C.C48	-1.81	-1.15	-C.C3	0.00	-2.20	-0.00
C.C49	-1.82	-1.15	-C.C3	0.00	-2.20	-0.00
C.C50	-1.83	-1.15	-C.C3	0.00	-2.20	0.00
C.C51	-1.84	-1.15	-C.C3	-0.00	-2.20	0.00
C.C52	-1.84	-1.15	-C.C3	-0.00	-2.20	0.00
C.C53	-1.84	-1.15	-C.C3	-0.00	-2.20	0.00
C.C54	-1.84	-1.15	-C.C3	-0.00	-2.20	0.00
C.C55	-1.84	-1.15	-C.C3	-0.00	-2.20	0.00
C.C56	-1.84	-1.15	-C.C3	0.00	-2.20	-0.00
C.C57	-1.84	-1.15	-C.C3	0.00	-2.20	-0.00
C.C58	-1.84	-1.15	-C.C3	0.00	-2.20	-0.00
C.C59	-1.83	-1.15	-C.C3	0.00	-2.20	-0.00
C.C60	-1.83	-1.15	-C.C4	0.00	-2.20	-0.00
C.C61	-1.83	-1.15	-C.C4	0.00	-2.20	-0.00
C.C62	-1.82	-1.15	-C.C4	-0.00	-2.20	0.00
C.C63	-1.82	-1.15	-C.C5	-0.00	-2.20	0.00
C.C64	-1.82	-1.15	-C.C5	-0.00	-2.20	0.00
C.C65	-1.81	-1.15	-C.C6	-0.00	-2.20	0.00
C.C66	-1.81	-1.15	-C.C7	-0.00	-2.20	0.00
C.C67	-1.81	-1.15	-C.C7	0.00	-2.20	-0.00
C.C68	-1.80	-1.15	-C.C8	0.00	-2.20	-0.00
C.C69	-1.80	-1.15	-C.C9	0.00	-2.20	-0.00
C.C70	-1.79	-1.15	-C.10	0.00	-2.20	-0.00
C.C71	-1.78	-1.15	-C.11	0.00	-2.20	-0.00
C.C72	-1.77	-1.15	-C.12	0.00	-2.20	-0.00
C.C73	-1.76	-1.15	-C.14	-0.00	-2.20	0.00
C.C74	-1.75	-1.15	-C.15	-0.00	-2.20	0.00
C.C75	-1.74	-1.15	-C.16	-0.00	-2.20	0.00
C.C76	-1.73	-1.15	-C.18	-0.00	-2.20	0.00
C.C77	-1.72	-1.15	-C.19	-0.00	-2.20	0.00
C.C78	-1.70	-1.15	-C.20	-0.00	-2.20	0.00

Table 1e - Continued

Page 2

C.C75	-1.69	-1.15	-C.21	0.00	-2.20	-0.00
C.C80	-1.67	-1.15	-C.22	0.00	-2.20	-0.00
C.C81	-1.66	-1.15	-C.23	0.00	-2.20	-0.00
C.C82	-1.64	-1.15	-C.24	0.00	-2.20	-0.00
C.C83	-1.63	-1.15	-C.24	0.00	-2.20	-0.00
C.C84	-1.61	-1.15	-C.25	-0.00	-2.20	0.00
C.C85	-1.59	-1.15	-C.25	-0.00	-2.20	0.00
C.C86	-1.58	-1.15	-C.25	-0.00	-2.20	0.00
C.C87	-1.56	-1.15	-C.26	-0.00	-2.20	0.00
C.C88	-1.54	-1.15	-C.26	-0.00	-2.20	0.00
C.C89	-1.53	-1.15	-C.26	-0.00	-2.20	0.00
C.C90	-1.51	-1.15	-C.25	0.00	-2.20	-0.00
C.C91	-1.49	-1.15	-C.25	0.00	-2.20	-0.00
C.C92	-1.48	-1.15	-C.25	0.00	-2.20	-0.00
C.C93	-1.46	-1.15	-C.24	0.00	-2.20	-0.00
C.C94	-1.45	-1.15	-C.24	0.00	-2.20	-0.00
C.C95	-1.44	-1.15	-C.24	0.00	-2.20	-0.00
C.C96	-1.42	-1.15	-C.23	-0.00	-2.20	0.00
C.C97	-1.41	-1.15	-C.23	-0.00	-2.20	0.00
C.C98	-1.40	-1.15	-C.23	-0.00	-2.20	0.00
C.C99	-1.39	-1.15	-C.22	-0.00	-2.20	0.00
C.100	-1.38	-1.15	-C.22	-0.00	-2.20	0.00
C.101	-1.37	-1.15	-C.22	0.00	-2.20	-0.00

Table 1f

TYPE	PUC		NUC		PUC	NUG
	EST	TRUE	EST	TRUE		
C.C31	-1.15	-1.16	C.E0	-0.00	-2.51	0.00
C.C32	-0.86	-1.16	C.E5	-0.00	-2.51	0.00
C.C33	-1.14	-1.16	C.E6	-0.00	-2.51	-0.00
C.C34	-1.57	-1.15	C.E4	0.00	-2.51	-0.00
C.C35	-1.80	-1.15	C.E1	0.00	-2.51	-0.00
C.C36	-1.90	-1.15	-C.E5	0.00	-2.51	-0.00
C.C37	-1.93	-1.15	-C.E7	0.00	-2.51	-0.00
C.C38	-1.91	-1.15	-C.E9	0.00	-2.51	-0.00
C.C39	-1.87	-1.15	-C.E9	-0.00	-2.51	0.00
C.C40	-1.81	-1.15	-C.E9	-0.00	-2.51	0.00
C.C41	-1.75	-1.15	-C.E9	-0.00	-2.51	0.00
C.C42	-1.69	-1.15	-C.E7	-0.00	-2.51	0.00
C.C43	-1.64	-1.15	-C.E6	-0.00	-2.51	0.00
C.C44	-1.59	-1.15	-C.E6	-0.00	-2.51	0.00
C.C45	-1.56	-1.15	-C.E6	0.00	-2.51	-0.00
C.C46	-1.53	-1.15	-C.E6	0.00	-2.51	-0.00
C.C47	-1.50	-1.15	-C.E6	0.00	-2.51	-0.00
C.C48	-1.48	-1.15	-C.E6	0.00	-2.51	-0.00
C.C49	-1.47	-1.15	-C.E7	0.00	-2.51	-0.00
C.C50	-1.45	-1.15	-C.E7	0.00	-2.51	0.00
C.C51	-1.44	-1.15	-C.E8	-0.00	-2.51	0.00
C.C52	-1.43	-1.15	-C.E9	-0.00	-2.51	0.00
C.C53	-1.43	-1.15	-C.E0	-0.00	-2.51	0.00
C.C54	-1.43	-1.15	-C.E1	-0.00	-2.51	0.00
C.C55	-1.42	-1.15	-C.E2	-0.00	-2.51	0.00
C.C56	-1.42	-1.15	-C.E3	0.00	-2.51	-0.00
C.C57	-1.43	-1.15	-C.E4	0.00	-2.51	-0.00
C.C58	-1.43	-1.15	-C.E5	0.00	-2.51	-0.00
C.C59	-1.43	-1.15	-C.E7	0.00	-2.51	-0.00
C.C60	-1.44	-1.15	-C.E8	0.00	-2.51	-0.00
C.C61	-1.44	-1.15	-C.E9	0.00	-2.51	-0.00
C.C62	-1.44	-1.15	-C.E0	-0.00	-2.51	0.00
C.C63	-1.45	-1.15	-C.E2	-0.00	-2.51	0.00
C.C64	-1.45	-1.15	-C.E3	-0.00	-2.51	0.00
C.C65	-1.44	-1.15	-C.E4	-0.00	-2.51	0.00
C.C66	-1.44	-1.15	-C.E5	-0.00	-2.51	0.00
C.C67	-1.43	-1.15	-C.E5	0.00	-2.51	-0.00
C.C68	-1.41	-1.15	-C.E6	0.00	-2.51	-0.00
C.C69	-1.39	-1.15	-C.E6	0.00	-2.51	-0.00
C.C70	-1.37	-1.15	-C.E6	0.00	-2.51	-0.00
C.C71	-1.35	-1.15	-C.E6	0.00	-2.51	-0.00
C.C72	-1.32	-1.15	-C.E5	0.00	-2.51	-0.00
C.C73	-1.30	-1.15	-C.E4	-0.00	-2.51	0.00
C.C74	-1.27	-1.15	-C.E4	-0.00	-2.51	0.00
C.C75	-1.25	-1.15	-C.E3	-0.00	-2.51	0.00
C.C76	-1.23	-1.15	-C.E2	-0.00	-2.51	0.00

Table 1f - Continued

Page 2

C.C77	-1.20	-1.15	-C.21	-0.00	-2.51	0.00
C.C78	-1.18	-1.15	-C.20	-0.00	-2.51	0.00
C.C79	-1.16	-1.15	-C.19	0.00	-2.51	-0.00
C.C80	-1.14	-1.15	-C.18	0.00	-2.51	-0.00
C.C81	-1.12	-1.15	-C.16	0.00	-2.51	-0.00
C.C82	-1.10	-1.15	-C.15	0.00	-2.51	-0.00
C.C83	-1.08	-1.15	-C.14	0.00	-2.51	-0.00
C.C84	-1.07	-1.15	-C.14	-0.00	-2.51	0.00
C.C85	-1.06	-1.15	-C.13	-0.00	-2.51	0.00
C.C86	-1.05	-1.15	-C.12	-0.00	-2.51	0.00
C.C87	-1.04	-1.15	-C.11	-0.00	-2.51	0.00
C.C88	-1.04	-1.15	-C.10	-0.00	-2.51	0.00
C.C89	-1.03	-1.15	-C.09	-0.00	-2.51	0.00
C.C90	-1.03	-1.15	-C.08	0.00	-2.51	-0.00
C.C91	-1.04	-1.15	-C.08	0.00	-2.51	-0.00
C.C92	-1.04	-1.15	-C.07	0.00	-2.51	-0.00
C.C93	-1.05	-1.15	-C.06	0.00	-2.51	-0.00
C.C94	-1.07	-1.15	-C.05	0.00	-2.51	-0.00
C.C95	-1.08	-1.15	-C.04	0.00	-2.51	-0.00
C.C96	-1.10	-1.15	-C.04	-0.00	-2.51	0.00
C.C97	-1.12	-1.15	-C.03	-0.00	-2.51	0.00
C.C98	-1.13	-1.15	-C.02	-0.00	-2.51	0.00
C.C99	-1.15	-1.15	-C.01	-0.00	-2.51	0.00
C.100	-1.17	-1.15	-C.01	-0.00	-2.51	0.00
C.101	-1.20	-1.15	-C.00	0.00	-2.51	-0.00

Table 1g

TIME	PUC		NUC		PUC	NUG
	EST	TRUE	EST	TRUE		
C.C31	-2.11	-1.16	C.29	-0.00	-2.82	0.00
C.C32	-1.66	-1.16	C.40	-0.00	-2.82	0.00
C.C33	-1.23	-1.16	C.46	-0.00	-2.82	-0.00
C.C34	-1.06	-1.15	C.38	0.00	-2.83	-0.00
C.C35	-1.08	-1.15	C.25	0.00	-2.83	-0.00
C.C36	-1.11	-1.15	C.17	0.00	-2.83	-0.00
C.C37	-1.11	-1.15	C.13	0.00	-2.83	-0.00
C.C38	-1.08	-1.15	C.08	0.00	-2.83	-0.00
C.C39	-1.04	-1.15	C.03	-0.00	-2.83	0.00
C.C40	-1.00	-1.15	-C.01	-0.00	-2.83	0.00
C.C41	-0.97	-1.15	-C.05	-0.00	-2.83	0.00
C.C42	-0.94	-1.15	-C.09	-0.00	-2.83	0.00
C.C43	-0.91	-1.15	-C.12	-0.00	-2.83	0.00
C.C44	-0.90	-1.15	-C.15	-0.00	-2.83	0.00
C.C45	-0.88	-1.15	-C.17	0.00	-2.83	-0.00
C.C46	-0.88	-1.15	-C.17	0.00	-2.83	-0.00
C.C47	-0.88	-1.15	-C.17	0.00	-2.83	-0.00
C.C48	-0.87	-1.15	-C.17	0.00	-2.83	-0.00
C.C49	-0.87	-1.15	-C.15	0.00	-2.83	-0.00
C.C50	-0.86	-1.15	-C.13	0.00	-2.83	0.00
C.C51	-0.85	-1.15	-C.11	-0.00	-2.83	0.00
C.C52	-0.84	-1.15	-C.08	-0.00	-2.83	0.00
C.C53	-0.83	-1.15	-C.06	-0.00	-2.83	0.00
C.C54	-0.82	-1.15	-C.04	-0.00	-2.83	0.00
C.C55	-0.80	-1.15	-C.02	-0.00	-2.83	0.00
C.C56	-0.79	-1.15	-C.00	0.00	-2.83	-0.00
C.C57	-0.78	-1.15	C.01	0.00	-2.83	-0.00
C.C58	-0.76	-1.15	C.02	0.00	-2.83	-0.00
C.C59	-0.74	-1.15	C.03	0.00	-2.83	-0.00
C.C60	-0.71	-1.15	C.03	0.00	-2.83	-0.00
C.C61	-0.71	-1.15	C.05	0.00	-2.83	-0.00
C.C62	-0.72	-1.15	C.07	-0.00	-2.83	0.00
C.C63	-0.72	-1.15	C.08	-0.00	-2.83	0.00
C.C64	-0.72	-1.15	C.09	-0.00	-2.83	0.00
C.C65	-0.72	-1.15	C.11	-0.00	-2.83	0.00
C.C66	-0.72	-1.15	C.12	-0.00	-2.83	0.00
C.C67	-0.72	-1.15	C.13	0.00	-2.83	-0.00
C.C68	-0.72	-1.15	C.15	0.00	-2.83	-0.00
C.C69	-0.72	-1.15	C.16	0.00	-2.83	-0.00
C.C70	-0.71	-1.15	C.17	0.00	-2.83	-0.00
C.C71	-0.71	-1.15	C.13	0.00	-2.83	-0.00
C.C72	-0.71	-1.15	C.20	0.00	-2.83	-0.00

C.C73	-C.71	-1.15	C.21	-0.00	-2.83	0.00
C.C74	-C.70	-1.15	C.22	-0.00	-2.83	0.00
C.C75	-C.70	-1.15	C.24	-0.00	-2.83	0.00
C.C76	-C.69	-1.15	C.25	-0.00	-2.83	0.00
C.C77	-C.68	-1.15	C.26	-0.00	-2.83	0.00
C.C78	-C.68	-1.15	C.27	-0.00	-2.83	0.00
C.C79	-C.67	-1.15	C.29	0.00	-2.83	-0.00
C.C80	-C.67	-1.15	C.31	0.00	-2.83	-0.00
C.C81	-C.67	-1.15	C.31	0.00	-2.83	-0.00
C.C82	-C.67	-1.15	C.31	0.00	-2.83	-0.00
C.C83	-C.67	-1.15	C.31	0.00	-2.83	-0.00
C.C84	-C.67	-1.15	C.30	-0.00	-2.83	0.00
C.C85	-C.67	-1.15	C.30	-0.00	-2.83	0.00
C.C86	-C.68	-1.15	C.29	-0.00	-2.83	0.00
C.C87	-C.68	-1.15	C.29	-0.00	-2.83	0.00
C.C88	-C.69	-1.15	C.29	-0.00	-2.83	0.00
C.C89	-C.69	-1.15	C.28	-0.00	-2.83	0.00
C.C90	-C.70	-1.15	C.28	0.00	-2.83	-0.00
C.C91	-C.71	-1.15	C.28	0.00	-2.83	-0.00
C.C92	-C.71	-1.15	C.29	0.00	-2.83	-0.00
C.C93	-C.72	-1.15	C.29	0.00	-2.83	-0.00
C.C94	-C.73	-1.15	C.29	0.00	-2.83	-0.00
C.C95	-C.74	-1.15	C.26	0.00	-2.83	-0.00
C.C96	-C.75	-1.15	C.25	-0.00	-2.83	0.00
C.C97	-C.76	-1.15	C.24	-0.00	-2.83	0.00
C.C98	-C.78	-1.15	C.23	-0.00	-2.83	0.00
C.C99	-C.79	-1.15	C.22	-0.00	-2.82	0.00
C.100	-C.80	-1.15	C.21	-0.00	-2.82	0.00
C.101	-C.82	-1.15	C.20	0.00	-2.82	-0.00

Table 1h

TIME	PUC		NUC		PUC	NLG
	EST	TRUE	EST	TRUE		
C.C 31	-1.52	-1.16	C.16	-0.00	-3.14	0.00
C.C 32	-1.53	-1.16	C.18	-0.00	-3.14	0.00
C.C 33	-1.32	-1.16	C.17	-0.00	-3.14	-0.00
C.C 34	-1.27	-1.15	C.12	0.00	-3.14	-0.00
C.C 35	-1.28	-1.15	C.07	0.00	-3.14	-0.00
C.C 36	-1.29	-1.15	C.03	0.00	-3.14	-0.00
C.C 37	-1.28	-1.15	C.01	0.00	-3.14	-0.00
C.C 38	-1.26	-1.15	-C.02	0.00	-3.14	-0.00
C.C 39	-1.22	-1.15	-C.05	-0.00	-3.14	0.00
C.C 40	-1.19	-1.15	-C.07	-0.00	-3.14	0.00
C.C 41	-1.17	-1.15	-C.10	-0.00	-3.14	0.00
C.C 42	-1.14	-1.15	-C.12	-0.00	-3.14	0.00
C.C 43	-1.12	-1.15	-C.15	-0.00	-3.14	0.00
C.C 44	-1.10	-1.15	-C.17	-0.00	-3.14	0.00
C.C 45	-1.08	-1.15	-C.20	0.00	-3.14	-0.00
C.C 46	-1.07	-1.15	-C.22	0.00	-3.14	-0.00
C.C 47	-1.05	-1.15	-C.25	0.00	-3.14	-0.00
C.C 48	-1.03	-1.15	-C.27	0.00	-3.14	-0.00
C.C 49	-1.01	-1.15	-C.29	0.00	-3.14	-0.00
C.C 50	-1.00	-1.15	-C.32	0.00	-3.14	0.00
C.C 51	-0.98	-1.15	-C.34	-0.00	-3.14	0.00
C.C 52	-0.97	-1.15	-C.36	-0.00	-3.14	0.00
C.C 53	-0.95	-1.15	-C.37	-0.00	-3.14	0.00
C.C 54	-0.94	-1.15	-C.39	-0.00	-3.14	0.00
C.C 55	-0.92	-1.15	-C.41	-0.00	-3.14	0.00
C.C 56	-0.91	-1.15	-C.42	0.00	-3.14	-0.00
C.C 57	-0.90	-1.15	-C.43	0.00	-3.14	-0.00
C.C 58	-0.89	-1.15	-C.44	0.00	-3.14	-0.00
C.C 59	-0.87	-1.15	-C.45	0.00	-3.14	-0.00
C.C 60	-0.86	-1.15	-C.46	0.00	-3.14	-0.00
C.C 61	-0.85	-1.15	-C.46	0.00	-3.14	-0.00
C.C 62	-0.85	-1.15	-C.47	-0.00	-3.14	0.00
C.C 63	-0.84	-1.15	-C.48	-0.00	-3.14	0.00
C.C 64	-0.83	-1.15	-C.48	-0.00	-3.14	0.00
C.C 65	-0.83	-1.15	-C.49	-0.00	-3.14	0.00
C.C 66	-0.82	-1.15	-C.49	-0.00	-3.14	0.00
C.C 67	-0.82	-1.15	-C.49	0.00	-3.14	-0.00
C.C 68	-0.82	-1.15	-C.50	0.00	-3.14	-0.00
C.C 69	-0.82	-1.15	-C.50	0.00	-3.14	-0.00
C.C 70	-0.82	-1.15	-C.50	0.00	-3.14	-0.00
C.C 71	-0.82	-1.15	-C.50	0.00	-3.14	-0.00
C.C 72	-0.82	-1.15	-C.51	0.00	-3.14	-0.00
C.C 73	-0.82	-1.15	-C.51	-0.00	-3.14	0.00
C.C 74	-0.82	-1.15	-C.51	-0.00	-3.14	0.00
C.C 75	-0.82	-1.15	-C.51	-0.00	-3.14	0.00
C.C 76	-0.82	-1.15	-C.51	-0.00	-3.14	0.00
C.C 77	-0.82	-1.15	-C.51	-0.00	-3.14	0.00
C.C 78	-0.82	-1.15	-C.51	-0.00	-3.14	0.00

AD-A055 177

OPTICAL SCIENCES CO PLACENTIA CA
ADAPTIVE COMPENSATION TECHNIQUES.(U)

F/G 17/8

MAY 78 D L FRIED, E J SCHONHEINZ, R B ASHER

F30602-77-C-0099

UNCLASSIFIED

DR-105

RADC-TR-78-101

NL

4 OF 5
AD
A055177



C.C75	-C.E2	-1.15	-C.E1	0.00	-3.14	-0.00
C.C80	-C.E2	-1.15	-C.E2	0.00	-3.14	-0.00
C.C81	-C.E3	-1.15	-C.E3	0.00	-3.14	-0.00
C.C82	-C.E3	-1.15	-C.E4	0.00	-3.14	-0.00
C.C83	-C.E4	-1.15	-C.E6	0.00	-3.14	-0.00
C.C84	-C.E3	-1.15	-C.E6	-0.00	-3.14	0.00
C.C85	-C.E2	-1.15	-C.E6	-0.00	-3.14	0.00
C.C86	-C.E1	-1.15	-C.E6	-0.00	-3.14	0.00
C.C87	-C.79	-1.15	-C.E6	-0.00	-3.14	0.00
C.C88	-C.79	-1.15	-C.E6	-0.00	-3.14	0.00
C.C89	-C.78	-1.15	-C.E6	-0.00	-3.14	0.00
C.C90	-C.78	-1.15	-C.E6	0.00	-3.14	-0.00
C.C91	-C.77	-1.15	-C.E7	0.00	-3.14	-0.00
C.C92	-C.77	-1.15	-C.E7	0.00	-3.14	-0.00
C.C93	-C.74	-1.15	-C.E5	0.00	-3.14	-0.00
C.C94	-C.72	-1.15	-C.E5	0.00	-3.14	-0.00
C.C95	-C.71	-1.15	-C.E4	0.00	-3.14	-0.00
C.C96	-C.71	-1.15	-C.E4	-0.00	-3.14	0.00
C.C97	-C.70	-1.15	-C.E3	-0.00	-3.14	0.00
C.C98	-C.70	-1.15	-C.E3	-0.00	-3.14	0.00
C.C99	-C.70	-1.15	-C.E2	-0.00	-3.14	0.00
C.100	-C.70	-1.15	-C.E2	-0.00	-3.14	0.00
C.101	-C.70	-1.15	-C.E2	0.00	-3.14	-0.00

Table 1 i

TYPE	PUC		NUC		PUC	NUG
	EST	TRUE	EST	TRUE		
C.C31	-1.68	-1.16	-0.19	-0.00	-3.45	0.00
C.C32	-1.39	-1.16	-0.28	-0.00	-3.45	0.00
C.C33	-1.32	-1.16	-0.35	-0.00	-3.45	-0.00
C.C34	-1.43	-1.15	-0.43	0.00	-3.45	-0.00
C.C35	-1.59	-1.15	-0.53	0.00	-3.45	-0.00
C.C36	-1.70	-1.15	-0.60	0.00	-3.46	-0.00
C.C37	-1.75	-1.15	-0.65	0.00	-3.46	-0.00
C.C38	-1.77	-1.15	-0.72	0.00	-3.46	-0.00
C.C39	-1.77	-1.15	-0.78	-0.00	-3.46	0.00
C.C40	-1.75	-1.15	-0.83	-0.00	-3.45	0.00
C.C41	-1.73	-1.15	-0.88	-0.00	-3.45	0.00
C.C42	-1.71	-1.15	-0.91	-0.00	-3.45	0.00
C.C43	-1.69	-1.15	-0.94	-0.00	-3.45	0.00
C.C44	-1.68	-1.15	-0.96	-0.00	-3.45	0.00
C.C45	-1.67	-1.15	-0.97	0.00	-3.45	-0.00
C.C46	-1.66	-1.15	-0.97	0.00	-3.45	-0.00
C.C47	-1.66	-1.15	-0.97	0.00	-3.45	-0.00
C.C48	-1.66	-1.15	-0.96	0.00	-3.45	-0.00
C.C49	-1.66	-1.15	-0.95	0.00	-3.45	-0.00
C.C50	-1.65	-1.15	-0.93	0.00	-3.45	0.00
C.C51	-1.67	-1.15	-0.93	-0.00	-3.45	0.00
C.C52	-1.70	-1.15	-0.91	-0.00	-3.45	0.00
C.C53	-1.72	-1.15	-0.90	-0.00	-3.45	0.00
C.C54	-1.73	-1.15	-0.89	-0.00	-3.45	0.00
C.C55	-1.75	-1.15	-0.89	-0.00	-3.45	0.00
C.C56	-1.77	-1.15	-0.87	0.00	-3.45	-0.00
C.C57	-1.78	-1.15	-0.85	0.00	-3.45	-0.00
C.C58	-1.79	-1.15	-0.84	0.00	-3.45	-0.00
C.C59	-1.80	-1.15	-0.82	0.00	-3.45	-0.00
C.C60	-1.80	-1.15	-0.81	0.00	-3.45	-0.00
C.C61	-1.81	-1.15	-0.80	0.00	-3.45	-0.00
C.C62	-1.83	-1.15	-0.78	-0.00	-3.45	0.00
C.C63	-1.84	-1.15	-0.75	-0.00	-3.45	0.00
C.C64	-1.86	-1.15	-0.73	-0.00	-3.45	0.00
C.C65	-1.89	-1.15	-0.71	-0.00	-3.45	0.00
C.C66	-1.91	-1.15	-0.69	-0.00	-3.45	0.00
C.C67	-1.92	-1.15	-0.68	0.00	-3.45	-0.00
C.C68	-1.92	-1.15	-0.67	0.00	-3.45	-0.00
C.C69	-1.93	-1.15	-0.66	0.00	-3.45	-0.00
C.C70	-1.94	-1.15	-0.65	0.00	-3.45	-0.00
C.C71	-1.95	-1.15	-0.65	0.00	-3.45	-0.00
C.C72	-1.95	-1.15	-0.66	0.00	-3.45	-0.00
C.C73	-1.95	-1.15	-0.66	-0.00	-3.45	0.00
C.C74	-1.96	-1.15	-0.68	-0.00	-3.45	0.00
C.C75	-1.96	-1.15	-0.70	-0.00	-3.45	0.00
C.C76	-1.95	-1.15	-0.69	-0.00	-3.45	0.00

134

Table 1 i - Continued

Page 2

C.C77	-1.93	-1.15	-C.69	-0.00	-3.45	0.00
C.C78	-1.92	-1.15	-C.69	-0.00	-3.45	0.00
C.C79	-1.91	-1.15	-C.69	0.00	-3.45	-0.00
C.C80	-1.91	-1.15	-C.67	0.00	-3.45	-0.00
C.C81	-1.90	-1.15	-C.66	0.00	-3.45	-0.00
C.C82	-1.90	-1.15	-C.66	0.00	-3.45	-0.00
C.C83	-1.89	-1.15	-C.65	0.00	-3.45	-0.00
C.C84	-1.89	-1.15	-C.64	-0.00	-3.45	0.00
C.C85	-1.90	-1.15	-C.63	-0.00	-3.45	0.00
C.C86	-1.90	-1.15	-C.63	-0.00	-3.45	0.00
C.C87	-1.90	-1.15	-C.62	-0.00	-3.45	0.00
C.C88	-1.91	-1.15	-C.61	-0.00	-3.45	0.00
C.C89	-1.91	-1.15	-C.60	-0.00	-3.45	0.00
C.C90	-1.91	-1.15	-C.59	0.00	-3.45	-0.00
C.C91	-1.91	-1.15	-C.58	0.00	-3.45	-0.00
C.C92	-1.90	-1.15	-C.58	0.00	-3.45	-0.00
C.C93	-1.90	-1.15	-C.57	0.00	-3.45	-0.00
C.C94	-1.90	-1.15	-C.56	0.00	-3.45	-0.00
C.C95	-1.89	-1.15	-C.55	0.00	-3.45	-0.00
C.C96	-1.89	-1.15	-C.54	-0.00	-3.45	0.00
C.C97	-1.89	-1.15	-C.53	-0.00	-3.45	0.00
C.C98	-1.88	-1.15	-C.53	-0.00	-3.45	0.00
C.C99	-1.88	-1.15	-C.52	-0.00	-3.45	0.00
C.100	-1.87	-1.15	-C.51	-0.00	-3.45	0.00
C.101	-1.87	-1.15	-C.49	0.00	-3.45	-0.00

Table 1j

TYPE	PUC		AUC		PUC	NUG
	EST	TRUE	EST	TRUE		
C.C31	-1.06	-1.16	C.38	-0.00	-3.77	0.00
C.C32	-0.96	-1.16	C.37	-0.00	-3.77	0.00
C.C33	-0.91	-1.16	C.36	-0.00	-3.77	-0.00
C.C34	-0.94	-1.15	C.35	0.00	-3.77	-0.00
C.C35	-1.02	-1.15	C.34	0.00	-3.77	-0.00
C.C36	-1.10	-1.15	C.34	0.00	-3.77	-0.00
C.C37	-1.16	-1.15	C.34	0.00	-3.77	-0.00
C.C38	-1.24	-1.15	C.34	0.00	-3.77	-0.00
C.C39	-1.32	-1.15	C.34	-0.00	-3.77	0.00
C.C40	-1.39	-1.15	C.34	-0.00	-3.77	0.00
C.C41	-1.46	-1.15	C.34	-0.00	-3.77	0.00
C.C42	-1.52	-1.15	C.34	-0.00	-3.77	0.00
C.C43	-1.57	-1.15	C.34	-0.00	-3.77	0.00
C.C44	-1.62	-1.15	C.33	-0.00	-3.77	0.00
C.C45	-1.65	-1.15	C.32	0.00	-3.77	-0.00
C.C46	-1.67	-1.15	C.32	0.00	-3.77	-0.00
C.C47	-1.68	-1.15	C.30	0.00	-3.77	-0.00
C.C48	-1.68	-1.15	C.29	0.00	-3.77	-0.00
C.C49	-1.67	-1.15	C.28	0.00	-3.77	-0.00
C.C50	-1.65	-1.15	C.27	0.00	-3.77	0.00
C.C51	-1.62	-1.15	C.25	-0.00	-3.77	0.00
C.C52	-1.59	-1.15	C.24	-0.00	-3.77	0.00
C.C53	-1.55	-1.15	C.22	-0.00	-3.77	0.00
C.C54	-1.51	-1.15	C.20	-0.00	-3.77	0.00
C.C55	-1.47	-1.15	C.18	-0.00	-3.77	0.00
C.C56	-1.43	-1.15	C.16	0.00	-3.77	-0.00
C.C57	-1.39	-1.15	C.14	0.00	-3.77	-0.00
C.C58	-1.35	-1.15	C.12	0.00	-3.77	-0.00
C.C59	-1.32	-1.15	C.09	0.00	-3.77	-0.00
C.C60	-1.29	-1.15	C.07	0.00	-3.77	-0.00
C.C61	-1.27	-1.15	C.04	0.00	-3.77	-0.00
C.C62	-1.26	-1.15	C.02	-0.00	-3.77	0.00
C.C63	-1.25	-1.15	-C.01	-0.00	-3.77	0.00
C.C64	-1.24	-1.15	-C.04	-0.00	-3.77	0.00
C.C65	-1.25	-1.15	-C.07	-0.00	-3.77	0.00
C.C66	-1.26	-1.15	-C.10	-0.00	-3.77	0.00
C.C67	-1.28	-1.15	-C.12	0.00	-3.77	-0.00
C.C68	-1.30	-1.15	-C.15	0.00	-3.77	-0.00
C.C69	-1.33	-1.15	-C.17	0.00	-3.77	-0.00
C.C70	-1.36	-1.15	-C.19	0.00	-3.77	-0.00
C.C71	-1.40	-1.15	-C.21	0.00	-3.77	-0.00
C.C72	-1.44	-1.15	-C.22	0.00	-3.77	-0.00
C.C73	-1.47	-1.15	-C.24	-0.00	-3.77	0.00
C.C74	-1.51	-1.15	-C.25	-0.00	-3.77	0.00
C.C75	-1.54	-1.15	-C.25	-0.00	-3.77	0.00
C.C76	-1.58	-1.15	-C.26	-0.00	-3.77	0.00

Table 1j - Continued

Page 2

C.C77	-1.61	-1.15	-0.26	-0.00	-3.77	0.00
C.C78	-1.63	-1.15	-0.25	-0.00	-3.77	0.00
C.C79	-1.65	-1.15	-0.24	0.00	-3.77	-0.00
C.C80	-1.67	-1.15	-0.23	0.00	-3.77	-0.00
C.C81	-1.68	-1.15	-0.21	0.00	-3.77	-0.00
C.C82	-1.69	-1.15	-0.18	0.00	-3.77	-0.00
C.C83	-1.69	-1.15	-0.15	0.00	-3.77	-0.00
C.C84	-1.68	-1.15	-0.12	-0.00	-3.77	0.00
C.C85	-1.67	-1.15	-0.08	-0.00	-3.77	0.00
C.C86	-1.66	-1.15	-0.04	-0.00	-3.77	0.00
C.C87	-1.64	-1.15	0.01	-0.00	-3.77	0.00
C.C88	-1.62	-1.15	0.05	-0.00	-3.77	0.00
C.C89	-1.60	-1.15	0.09	-0.00	-3.77	0.00
C.C90	-1.58	-1.15	0.14	0.00	-3.77	-0.00
C.C91	-1.55	-1.15	0.18	0.00	-3.77	-0.00
C.C92	-1.53	-1.15	0.22	0.00	-3.77	-0.00
C.C93	-1.51	-1.15	0.26	0.00	-3.77	-0.00
C.C94	-1.49	-1.15	0.30	0.00	-3.77	-0.00
C.C95	-1.46	-1.15	0.34	0.00	-3.77	-0.00
C.C96	-1.44	-1.15	0.37	-0.00	-3.77	0.00
C.C97	-1.43	-1.15	0.40	-0.00	-3.77	0.00
C.C98	-1.41	-1.15	0.42	-0.00	-3.77	0.00
C.C99	-1.39	-1.15	0.45	-0.00	-3.77	0.00
C.100	-1.38	-1.15	0.47	-0.00	-3.77	0.00
C.101	-1.36	-1.15	0.49	0.00	-3.77	-0.00

Table 1k

TIME	PUC		RUC		PUC	NUG
	EST	TRUE	EST	TRUE		
C.C31	-1.59	-1.16	-0.20	-0.00	-4.08	0.00
C.C32	-1.68	-1.16	-0.19	-0.00	-4.08	0.00
C.C33	-1.79	-1.16	-0.18	-0.00	-4.08	-0.00
C.C34	-1.72	-1.15	-0.19	0.00	-4.08	-0.00
C.C35	-1.67	-1.15	-0.20	0.00	-4.08	-0.00
C.C36	-1.63	-1.15	-0.19	0.00	-4.08	-0.00
C.C37	-1.60	-1.15	-0.17	0.00	-4.08	-0.00
C.C38	-1.56	-1.15	-0.12	0.00	-4.08	-0.00
C.C39	-1.53	-1.15	-0.05	-0.00	-4.08	0.00
C.C40	-1.49	-1.15	0.04	-0.00	-4.08	0.00
C.C41	-1.45	-1.15	0.12	-0.00	-4.08	0.00
C.C42	-1.41	-1.15	0.20	-0.00	-4.08	0.00
C.C43	-1.37	-1.15	0.28	-0.00	-4.08	0.00
C.C44	-1.33	-1.15	0.34	-0.00	-4.08	0.00
C.C45	-1.30	-1.15	0.37	0.00	-4.08	-0.00
C.C46	-1.27	-1.15	0.39	0.00	-4.08	-0.00
C.C47	-1.25	-1.15	0.40	0.00	-4.08	-0.00
C.C48	-1.23	-1.15	0.39	0.00	-4.08	-0.00
C.C49	-1.22	-1.15	0.37	0.00	-4.08	-0.00
C.C50	-1.21	-1.15	0.34	0.00	-4.08	0.00
C.C51	-1.20	-1.15	0.30	-0.00	-4.08	0.00
C.C52	-1.20	-1.15	0.26	-0.00	-4.08	0.00
C.C53	-1.19	-1.15	0.22	-0.00	-4.08	0.00
C.C54	-1.19	-1.15	0.18	-0.00	-4.08	0.00
C.C55	-1.19	-1.15	0.13	-0.00	-4.08	0.00
C.C56	-1.19	-1.15	0.09	0.00	-4.08	-0.00
C.C57	-1.19	-1.15	0.05	0.00	-4.08	-0.00
C.C58	-1.19	-1.15	0.00	0.00	-4.08	-0.00
C.C59	-1.20	-1.15	-0.03	0.00	-4.08	-0.00
C.C60	-1.20	-1.15	-0.07	0.00	-4.08	-0.00
C.C61	-1.20	-1.15	-0.10	0.00	-4.08	-0.00
C.C62	-1.20	-1.15	-0.14	-0.00	-4.08	0.00
C.C63	-1.21	-1.15	-0.16	-0.00	-4.08	0.00
C.C64	-1.21	-1.15	-0.19	-0.00	-4.08	0.00
C.C65	-1.21	-1.15	-0.21	-0.00	-4.08	0.00
C.C66	-1.21	-1.15	-0.23	-0.00	-4.08	0.00
C.C67	-1.21	-1.15	-0.24	0.00	-4.08	-0.00
C.C68	-1.21	-1.15	-0.25	0.00	-4.08	-0.00
C.C69	-1.21	-1.15	-0.26	0.00	-4.08	-0.00
C.C70	-1.21	-1.15	-0.27	0.00	-4.08	-0.00
C.C71	-1.21	-1.15	-0.27	0.00	-4.08	-0.00
C.C72	-1.21	-1.15	-0.27	0.00	-4.08	-0.00
C.C73	-1.21	-1.15	-0.27	-0.00	-4.08	0.00
C.C74	-1.20	-1.15	-0.27	-0.00	-4.08	0.00

Table 1k - Continued

Page 2

C.C75	-1.20	-1.15	-C.27	-0.00	-4.08	0.00
C.C76	-1.19	-1.15	-C.26	-0.00	-4.08	0.00
C.C77	-1.19	-1.15	-C.26	-0.00	-4.08	0.00
C.C78	-1.18	-1.15	-C.25	-0.00	-4.08	0.00
C.C79	-1.18	-1.15	-C.24	0.00	-4.08	-0.00
C.C80	-1.17	-1.15	-C.24	0.00	-4.08	-0.00
C.C81	-1.16	-1.15	-C.23	0.00	-4.08	-0.00
C.C82	-1.15	-1.15	-C.22	0.00	-4.08	-0.00
C.C83	-1.14	-1.15	-C.22	0.00	-4.08	-0.00
C.C84	-1.13	-1.15	-C.21	-0.00	-4.08	0.00
C.C85	-1.12	-1.15	-C.20	-0.00	-4.08	0.00
C.C86	-1.12	-1.15	-C.20	-0.00	-4.08	0.00
C.C87	-1.11	-1.15	-C.19	-0.00	-4.08	0.00
C.C88	-1.10	-1.15	-C.19	-0.00	-4.08	0.00
C.C89	-1.10	-1.15	-C.19	-0.00	-4.08	0.00
C.C90	-1.09	-1.15	-C.19	0.00	-4.08	-0.00
C.C91	-1.09	-1.15	-C.18	0.00	-4.08	-0.00
C.C92	-1.09	-1.15	-C.17	0.00	-4.08	-0.00
C.C93	-1.09	-1.15	-C.17	0.00	-4.08	-0.00
C.C94	-1.09	-1.15	-C.17	0.00	-4.08	-0.00
C.C95	-1.10	-1.15	-C.17	0.00	-4.08	-0.00
C.C96	-1.11	-1.15	-C.16	-0.00	-4.08	0.00
C.C97	-1.12	-1.15	-C.16	-0.00	-4.08	0.00
C.C98	-1.13	-1.15	-C.16	-0.00	-4.08	0.00
C.C99	-1.14	-1.15	-C.16	-0.00	-4.08	0.00
C.100	-1.15	-1.15	-C.16	-0.00	-4.08	0.00
C.101	-1.16	-1.15	-C.16	0.00	-4.08	-0.00

Table 14

TYPE	PUC		AUC		PUG	NUG
	EST	TRUE	EST	TRUE		
C.C31	-1.40	-1.16	-0.40	-0.00	-4.39	0.00
C.C32	-1.42	-1.16	-0.38	-0.00	-4.39	0.00
C.C33	-1.43	-1.16	-0.37	-0.00	-4.40	-0.00
C.C34	-1.43	-1.15	-0.35	0.00	-4.40	-0.00
C.C35	-1.43	-1.15	-0.33	0.00	-4.40	-0.00
C.C36	-1.42	-1.15	-0.31	0.00	-4.40	-0.00
C.C37	-1.41	-1.15	-0.30	0.00	-4.40	-0.00
C.C38	-1.40	-1.15	-0.28	0.00	-4.40	-0.00
C.C39	-1.38	-1.15	-0.26	-0.00	-4.40	0.00
C.C40	-1.36	-1.15	-0.24	-0.00	-4.40	0.00
C.C41	-1.37	-1.15	-0.22	-0.00	-4.40	0.00
C.C42	-1.39	-1.15	-0.20	-0.00	-4.40	0.00
C.C43	-1.39	-1.15	-0.18	-0.00	-4.40	0.00
C.C44	-1.38	-1.15	-0.16	-0.00	-4.40	0.00
C.C45	-1.34	-1.15	-0.14	0.00	-4.40	-0.00
C.C46	-1.28	-1.15	-0.15	0.00	-4.40	-0.00
C.C47	-1.17	-1.15	-0.18	0.00	-4.40	-0.00
C.C48	-1.12	-1.15	-0.20	0.00	-4.40	-0.00
C.C49	-1.07	-1.15	-0.24	0.00	-4.40	-0.00
C.C50	-0.99	-1.15	-0.27	0.00	-4.40	0.00
C.C51	-0.93	-1.15	-0.31	-0.00	-4.40	0.00
C.C52	-0.88	-1.15	-0.33	-0.00	-4.40	0.00
C.C53	-0.85	-1.15	-0.35	-0.00	-4.40	0.00
C.C54	-0.84	-1.15	-0.37	-0.00	-4.40	0.00
C.C55	-0.85	-1.15	-0.38	-0.00	-4.40	0.00
C.C56	-0.84	-1.15	-0.38	0.00	-4.40	-0.00
C.C57	-0.84	-1.15	-0.38	0.00	-4.40	-0.00
C.C58	-0.84	-1.15	-0.37	0.00	-4.40	-0.00
C.C59	-0.85	-1.15	-0.36	0.00	-4.40	-0.00
C.C60	-0.88	-1.15	-0.35	0.00	-4.40	-0.00
C.C61	-0.89	-1.15	-0.34	0.00	-4.40	-0.00
C.C62	-0.90	-1.15	-0.32	-0.00	-4.40	0.00
C.C63	-0.92	-1.15	-0.30	-0.00	-4.40	0.00
C.C64	-0.97	-1.15	-0.26	-0.00	-4.40	0.00
C.C65	-1.01	-1.15	-0.22	-0.00	-4.40	0.00
C.C66	-1.05	-1.15	-0.19	-0.00	-4.40	0.00
C.C67	-1.08	-1.15	-0.15	0.00	-4.40	-0.00
C.C68	-1.11	-1.15	-0.11	0.00	-4.40	-0.00
C.C69	-1.14	-1.15	-0.08	0.00	-4.40	-0.00
C.C70	-1.16	-1.15	-0.05	0.00	-4.40	-0.00
C.C71	-1.18	-1.15	-0.03	0.00	-4.40	-0.00
C.C72	-1.20	-1.15	0.00	0.00	-4.40	-0.00
C.C73	-1.22	-1.15	0.03	-0.00	-4.40	0.00
C.C74	-1.24	-1.15	0.05	-0.00	-4.40	0.00
C.C75	-1.23	-1.15	0.08	-0.00	-4.40	0.00
C.C76	-1.23	-1.15	0.11	-0.00	-4.40	0.00
C.C77	-1.24	-1.15	0.12	-0.00	-4.40	0.00
C.C78	-1.24	-1.15	0.14	-0.00	-4.40	0.00

Table 14 - Continued

Page 2

C.C75	-1.25	-1.15	C.15	0.00	-4.40	-0.00
C.C90	-1.26	-1.15	C.17	0.00	-4.40	-0.00
C.C81	-1.26	-1.15	C.16	0.00	-4.40	-0.00
C.C82	-1.26	-1.15	C.16	0.00	-4.39	-0.00
C.C83	-1.26	-1.15	C.16	0.00	-4.39	-0.00
C.C84	-1.26	-1.15	C.16	-0.00	-4.39	0.00
C.C95	-1.26	-1.15	C.16	-0.00	-4.39	0.00
C.C86	-1.26	-1.15	C.16	-0.00	-4.39	0.00
C.C87	-1.26	-1.15	C.16	-0.00	-4.39	0.00
C.C88	-1.26	-1.15	C.15	-0.00	-4.39	0.00
C.C89	-1.26	-1.15	C.15	-0.00	-4.39	0.00
C.C90	-1.25	-1.15	C.15	0.00	-4.39	-0.00
C.C91	-1.25	-1.15	C.14	0.00	-4.39	-0.00
C.C92	-1.24	-1.15	C.14	0.00	-4.39	-0.00
C.C93	-1.23	-1.15	C.13	0.00	-4.39	-0.00
C.C94	-1.23	-1.15	C.13	0.00	-4.39	-0.00
C.C95	-1.22	-1.15	C.12	0.00	-4.39	-0.00
C.C96	-1.21	-1.15	C.11	-0.00	-4.39	0.00
C.C97	-1.20	-1.15	C.11	-0.00	-4.39	0.00
C.C98	-1.19	-1.15	C.10	-0.00	-4.39	0.00
C.C99	-1.18	-1.15	C.C9	-0.00	-4.39	0.00
C.100	-1.17	-1.15	C.C8	-0.00	-4.39	0.00
C.101	-1.17	-1.15	C.C8	0.00	-4.39	-0.00

Table 7.2

Closed Loop Boresight Error Control

Laser spot position is estimated from the backscatter statistics. The engagement parameters used for this set of simulation runs is the same as those used in Table 1, except that here for Table 2a, the glint point position is 1.57 detector widths (i.e. $1.57 \times 0.159 \mu\text{rad} \times 1 \times 10^6 = 0.25 \text{ m}$ from the aim-point), while in Tables 2b(1) to 2b(4) the glint point position is 2.20 detector widths (i.e. 0.35 m from the aim-point.) The glint strength in the two cases correspond to 85.0 and 7.91 times the diffuse laser backscatter when the laser spot is near the aim-point. The boresight control process timing can be inferred from the fact that when the μ , ν data values are listed, the backscatter signal is being monitored to determine the current estimated laser spot position as seen on the target. At the end of this period the boresight error control loop is updated and in the next 30 msec period, during which no new μ , ν values are printed, the gimbals slew and settle, before the next backscatter signal measurement period is started. The computer program used to generate this data is listed in Appendix II.

Table 2a

TIME (SEC)	MLD		NUC		PUT	NUT	MUG	NLG	MISS (M)
	EST	TRUE	EST	TRUE					
0.032	2.83	3.05	-0.34	0.00	0.32	0.00	-1.57	0.00	0.43
0.033	2.84	3.04	-0.35	0.00	0.32	-0.00	-1.57	-0.00	0.43
0.034	2.84	3.04	-0.36	-0.00	0.31	-0.00	-1.57	-0.00	0.43
0.035	2.83	3.04	-0.36	-0.00	0.31	-0.00	-1.57	-0.00	0.43
0.036	2.83	3.03	-0.36	-0.00	0.31	-0.00	-1.57	-0.00	0.43
0.037	2.82	3.03	-0.35	-0.00	0.31	-0.00	-1.57	-0.00	0.43
0.038	2.81	3.03	-0.35	-0.00	0.31	-0.00	-1.57	-0.00	0.43
0.039	2.80	3.03	-0.34	0.00	0.31	0.00	-1.57	0.00	0.43
0.040	2.80	3.04	-0.32	0.00	0.31	0.00	-1.57	0.00	0.43
0.041	2.80	3.04	-0.31	0.00	0.31	0.00	-1.57	0.00	0.43
0.042	2.80	3.04	-0.30	0.00	0.31	0.00	-1.57	0.00	0.43
0.043	2.80	3.04	-0.29	0.00	0.31	0.00	-1.57	0.00	0.43
0.044	2.80	3.04	-0.28	0.00	0.31	0.00	-1.57	0.00	0.43
0.045	2.80	3.04	-0.28	-0.00	0.31	-0.00	-1.57	-0.00	0.43
0.046	2.79	3.04	-0.29	-0.00	0.31	-0.00	-1.57	-0.00	0.43
0.047	2.78	3.04	-0.29	-0.00	0.31	-0.00	-1.57	-0.00	0.43
0.048	2.77	3.04	-0.30	-0.00	0.31	-0.00	-1.57	-0.00	0.43
0.049	2.76	3.04	-0.30	-0.00	0.31	-0.00	-1.57	-0.00	0.43
0.050	2.75	3.04	-0.29	0.00	0.31	0.00	-1.57	0.00	0.43
0.051	2.74	3.04	-0.28	0.00	0.31	0.00	-1.57	0.00	0.43
0.052	2.73	3.04	-0.27	0.00	0.31	0.00	-1.57	0.00	0.43
0.053	2.73	3.04	-0.24	0.00	0.31	0.00	-1.57	0.00	0.43
0.054	2.72	3.04	-0.21	0.00	0.31	0.00	-1.57	0.00	0.43
0.055	2.73	3.04	-0.17	0.00	0.31	0.00	-1.57	0.00	0.43
0.056	2.73	3.04	-0.13	-0.00	0.31	-0.00	-1.57	-0.00	0.43
0.057	2.74	3.04	-0.09	-0.00	0.31	-0.00	-1.57	-0.00	0.43
0.058	2.76	3.04	-0.05	-0.00	0.31	-0.00	-1.57	-0.00	0.43
0.059	2.77	3.04	-0.01	-0.00	0.31	-0.00	-1.57	-0.00	0.43
0.060	2.79	3.04	0.03	-0.00	0.31	-0.00	-1.57	-0.00	0.43
0.061	2.80	3.04	0.06	-0.00	0.31	-0.00	-1.57	-0.00	0.43
0.062	2.82	3.04	0.09	0.00	0.31	0.00	-1.57	0.00	0.43
0.063	2.83	3.04	0.11	0.00	0.31	0.00	-1.57	0.00	0.43
0.064	2.85	3.04	0.13	0.00	0.31	0.00	-1.57	0.00	0.43
0.065	2.86	3.04	0.14	0.00	0.31	0.00	-1.57	0.00	0.43
0.066	2.87	3.04	0.16	0.00	0.31	0.00	-1.57	0.00	0.43
0.067									0.43
0.068									0.43
0.069									0.43
0.070									0.43
0.071									0.43
0.072									0.35
0.073									0.11
0.074									0.09
0.075									0.20
0.076									0.21
0.077									0.16
0.078									0.06
0.079									0.03
0.080									0.06

Table 2a - Continued

Page 2

0.081								0.08
0.082								0.08
0.083								0.08
0.084								0.04
0.085								0.03
0.086								0.03
0.087								0.03
0.088								0.03
0.089								0.03
0.090								0.03
0.091								0.03
0.092								0.03
0.093								0.03
0.094								0.03
0.095								0.03
0.096								0.03
0.098	1.66	3.01	0.33	-0.00	2.98	C.16	1.10	0.16
0.099	2.41	3.01	0.36	-0.00	2.98	C.16	1.10	0.16
0.100	2.18	3.02	0.31	-0.00	2.99	C.16	1.10	0.16
0.101	1.89	3.03	0.28	-0.00	2.99	C.16	1.10	0.16
0.102	1.78	3.04	0.26	0.00	2.99	C.16	1.11	0.16
0.103	1.77	3.04	0.25	0.00	2.99	C.16	1.11	0.16
0.104	1.80	3.04	0.25	0.00	2.99	C.16	1.11	0.16
0.105	1.87	3.04	0.24	0.00	2.99	C.16	1.11	0.16
0.106	1.95	3.04	0.24	0.00	2.99	C.16	1.11	0.16
0.107	2.05	3.04	0.23	0.00	2.99	C.16	1.11	0.16
0.108	2.13	3.03	0.22	-0.00	2.99	C.16	1.11	0.16
0.109	2.21	3.03	0.21	-0.00	2.99	C.16	1.11	0.16
0.110	2.28	3.03	0.20	-0.00	2.99	C.16	1.11	0.16
0.111	2.33	3.03	0.19	-0.00	2.99	C.16	1.11	0.16
0.112	2.37	3.03	0.18	-0.00	2.99	C.16	1.11	0.16
0.113	2.40	3.04	0.17	0.00	2.99	C.16	1.11	0.16
0.114	2.43	3.04	0.16	0.00	2.99	C.16	1.11	0.16
0.115	2.45	3.04	0.15	0.00	2.99	C.16	1.11	0.16
0.116	2.47	3.04	0.14	0.00	2.99	C.16	1.11	0.16
0.117	2.49	3.04	0.13	0.00	2.99	C.16	1.11	0.16
0.118	2.50	3.04	0.12	0.00	2.99	C.16	1.11	0.16
0.119	2.52	3.04	0.12	-0.00	2.99	C.16	1.11	0.16
0.120	2.53	3.03	0.11	-0.00	2.99	C.16	1.11	0.16
0.121	2.54	3.03	0.10	-0.00	2.99	C.16	1.11	0.16
0.122	2.55	3.03	0.10	-0.00	2.99	C.16	1.11	0.16
0.123	2.56	3.04	0.09	-0.00	2.99	C.16	1.11	0.16
0.124	2.57	3.04	0.09	-0.00	2.99	C.16	1.11	0.16
0.125	2.57	3.04	0.08	0.00	2.99	C.16	1.11	0.16
0.126	2.58	3.04	0.08	0.00	2.99	C.16	1.11	0.16
0.127	2.59	3.04	0.08	0.00	2.99	C.16	1.11	0.16
0.128	2.60	3.04	0.07	0.00	2.99	C.16	1.11	0.16
0.129	2.61	3.04	0.07	0.00	2.99	C.16	1.11	0.16
0.130	2.62	3.04	0.07	-0.00	2.99	C.16	1.11	0.16
0.131	2.63	3.04	0.07	-0.00	2.99	C.16	1.11	0.16
0.132	2.64	3.03	0.06	-0.00	2.99	C.16	1.11	0.16

0.133									0.03
0.134									0.03
0.135									0.03
0.136									0.03
0.137									0.03
0.138									0.03
0.139									0.05
0.140									0.06
0.141									0.06
0.142									0.10
0.143									0.09
0.144									0.06
0.145									0.07
0.146									0.06
0.147									0.06
0.148									0.06
0.149									0.06
0.150									0.06
0.151									0.07
0.152									0.07
0.153									0.07
0.154									0.07
0.155									0.07
0.156									0.07
0.157									0.07
0.158									0.07
0.159									0.07
0.160									0.07
0.161									0.07
0.162									0.07
0.164	3.66	3.04	-0.07	0.00	2.62	C.C6	0.74	0.06	0.07
0.165	3.62	3.04	-0.06	0.00	2.62	C.C6	0.74	0.06	0.07
0.166	3.57	3.04	-0.06	0.00	2.62	C.C6	0.74	0.06	0.07
0.167	3.53	3.04	-0.06	0.00	2.62	C.C6	0.74	0.06	0.07
0.168	3.50	3.03	-0.06	-0.00	2.62	C.C6	0.74	0.06	0.07
0.169	3.48	3.03	-0.07	-0.00	2.62	C.C6	0.74	0.06	0.07
0.170	3.46	3.03	-0.08	-0.00	2.62	C.C6	0.74	0.06	0.07
0.171	3.45	3.03	-0.10	-0.00	2.62	C.C6	0.74	0.06	0.07
0.172	3.44	3.03	-0.11	-0.00	2.62	C.C6	0.74	0.06	0.07
0.173	3.42	3.03	-0.14	-0.00	2.62	C.C6	0.74	0.06	0.07
0.174	3.39	3.03	-0.16	0.00	2.62	C.C6	0.74	0.06	0.07
0.175	3.36	3.03	-0.19	0.00	2.62	C.C6	0.74	0.06	0.07
0.176	3.32	3.03	-0.21	0.00	2.62	C.C6	0.74	0.06	0.07
0.177	3.27	3.03	-0.24	0.00	2.62	C.C6	0.74	0.06	0.07
0.178	3.22	3.03	-0.27	0.00	2.62	C.C6	0.74	0.06	0.07
0.179	3.16	3.03	-0.30	-0.00	2.62	C.C6	0.74	0.06	0.07
0.180	3.09	3.03	-0.32	-0.00	2.62	C.C6	0.74	0.06	0.07
0.181	3.04	3.03	-0.34	-0.00	2.62	C.C6	0.74	0.06	0.07
0.182	3.00	3.03	-0.34	-0.00	2.62	C.C6	0.74	0.06	0.07
0.183	2.97	3.03	-0.33	-0.00	2.62	C.C6	0.74	0.06	0.07
0.184	2.97	3.03	-0.32	-0.00	2.62	C.C6	0.74	0.06	0.07

Table 2a - Continued

Page 4

0.185	2.99	3.03	-0.30	0.00	2.62	0.06	0.74	0.06	0.07
0.186	3.02	3.03	-0.27	0.00	2.62	0.06	0.74	0.06	0.07
0.187	3.05	3.03	-0.25	0.00	2.62	0.06	0.74	0.06	0.07
0.188	3.08	3.03	-0.24	0.00	2.62	0.06	0.74	0.06	0.07
0.189	3.12	3.03	-0.23	0.00	2.62	0.06	0.74	0.06	0.07
0.190	3.14	3.03	-0.22	0.00	2.62	0.06	0.74	0.06	0.07
0.191	3.17	3.03	-0.22	-0.00	2.62	0.06	0.74	0.06	0.07
0.192	3.19	3.03	-0.22	-0.00	2.62	0.06	0.74	0.06	0.07
0.193	3.20	3.03	-0.22	-0.00	2.62	0.06	0.74	0.06	0.07
0.194	3.21	3.03	-0.22	-0.00	2.62	0.06	0.74	0.06	0.07
0.195	3.22	3.03	-0.22	-0.00	2.62	0.06	0.74	0.06	0.07
0.196	3.22	3.03	-0.22	0.00	2.62	0.06	0.74	0.06	0.07
0.197	3.22	3.03	-0.22	0.00	2.62	0.06	0.74	0.06	0.07
0.198	3.21	3.03	-0.22	0.00	2.62	0.06	0.74	0.06	0.07
0.199									0.07
0.200									0.07
0.201									0.07
0.202									0.07
0.203									0.07
0.204									0.05
0.205									0.03
0.206									0.07
0.207									0.10
0.208									0.10
0.209									0.09
0.210									0.07
0.211									0.05
0.212									0.04
0.213									0.03
0.214									0.03
0.215									0.04
0.216									0.04
0.217									0.05
0.218									0.05
0.219									0.06
0.220									0.05
0.221									0.05
0.222									0.05
0.223									0.05
0.224									0.05
0.225									0.05
0.226									0.05
0.227									0.05
0.228									0.05
0.230	2.44	3.03	-0.93	0.00	3.24	-0.23	1.36	-0.23	0.05
0.231	2.30	3.03	-0.79	0.00	3.24	-0.23	1.36	-0.23	0.05
0.232	2.19	3.03	-0.70	0.00	3.24	-0.23	1.36	-0.23	0.05
0.233	2.15	3.03	-0.64	0.00	3.24	-0.23	1.36	-0.23	0.05
0.234	2.13	3.03	-0.61	-0.00	3.24	-0.23	1.36	-0.23	0.05
0.235	2.13	3.04	-0.60	-0.00	3.24	-0.23	1.36	-0.23	0.05
0.236	2.17	3.04	-0.59	-0.00	3.24	-0.23	1.36	-0.23	0.05

0.237	2.22	3.04	-0.55	-0.00	3.24	-0.23	1.36	-0.23	0.05
0.238	2.27	3.03	-0.55	-0.00	3.24	-0.23	1.36	-0.23	0.05
0.239	2.33	3.03	-0.55	-0.00	3.24	-0.23	1.36	-0.23	0.05
0.240	2.39	3.03	-0.58	0.00	3.24	-0.23	1.36	-0.23	0.05
0.241	2.45	3.03	-0.57	0.00	3.24	-0.23	1.36	-0.23	0.05
0.242	2.51	3.03	-0.56	0.00	3.24	-0.23	1.36	-0.23	0.05
0.243	2.56	3.03	-0.54	0.00	3.24	-0.23	1.36	-0.23	0.05
0.244	2.61	3.03	-0.51	0.00	3.24	-0.23	1.36	-0.23	0.05
0.245	2.67	3.03	-0.48	0.00	3.24	-0.23	1.36	-0.23	0.05
0.246	2.72	3.03	-0.45	-0.00	3.24	-0.23	1.36	-0.23	0.05
0.247	2.76	3.03	-0.41	-0.00	3.24	-0.23	1.36	-0.23	0.05
0.248	2.81	3.03	-0.38	-0.00	3.24	-0.23	1.36	-0.23	0.05
0.249	2.85	3.03	-0.34	-0.00	3.24	-0.23	1.36	-0.23	0.05
0.250	2.89	3.03	-0.30	-0.00	3.24	-0.23	1.36	-0.23	0.05
0.251	2.93	3.03	-0.26	0.00	3.24	-0.23	1.36	-0.23	0.05
0.252	2.97	3.03	-0.22	0.00	3.24	-0.23	1.36	-0.23	0.05
0.253	3.00	3.03	-0.18	0.00	3.24	-0.23	1.36	-0.23	0.05
0.254	3.02	3.03	-0.15	0.00	3.24	-0.23	1.36	-0.23	0.05
0.255	3.05	3.03	-0.11	0.00	3.24	-0.23	1.36	-0.23	0.05
0.256	3.07	3.03	-0.06	0.00	3.24	-0.23	1.36	-0.23	0.05
0.257	3.09	3.03	-0.05	-0.00	3.24	-0.23	1.36	-0.23	0.05
0.258	3.11	3.03	-0.02	-0.00	3.24	-0.23	1.36	-0.23	0.05
0.259	3.12	3.03	0.01	-0.00	3.24	-0.23	1.36	-0.23	0.05
0.260	3.13	3.03	0.03	-0.00	3.24	-0.23	1.36	-0.23	0.05
0.261	3.14	3.03	0.05	-0.00	3.24	-0.23	1.36	-0.23	0.05
0.262	3.15	3.03	0.07	0.00	3.24	-0.23	1.36	-0.23	0.05
0.263	3.16	3.03	0.09	0.00	3.24	-0.23	1.36	-0.23	0.05
0.264	3.17	3.03	0.10	0.00	3.24	-0.23	1.36	-0.23	0.05
0.265									0.05
0.266									0.05
0.267									0.05
0.268									0.05
0.269									0.05
0.270									0.04
0.271									0.02
0.272									0.04
0.273									0.05
0.274									0.05
0.275									0.04
0.276									0.04
0.277									0.03
0.278									0.03
0.279									0.02
0.280									0.02
0.281									0.03
0.282									0.03
0.283									0.03
0.284									0.03
0.285									0.03
0.286									0.03
0.287									0.03

Table 2a - Continued

Page 6

0.288									0.03
0.289									0.03
0.290									0.03
0.291									0.03
0.292									0.03
0.293									0.03
0.294									0.03
0.296	3.22	3.03	0.60	-0.00	3.16	0.12	1.28	0.12	0.03
0.297	3.07	3.03	0.60	-0.00	3.16	0.12	1.28	0.12	0.03
0.298	2.93	3.03	0.60	-0.00	3.16	0.12	1.28	0.12	0.03
0.299	2.87	3.03	0.61	-0.00	3.16	0.12	1.28	0.12	0.03
0.300	2.87	3.03	0.61	0.00	3.16	0.12	1.28	0.12	0.03
0.301	2.89	3.03	0.61	0.00	3.16	0.12	1.28	0.12	0.03
0.302	2.93	3.03	0.61	0.00	3.16	0.12	1.28	0.12	0.03
0.303	2.94	3.03	0.57	0.00	3.16	0.12	1.28	0.12	0.03
0.304	2.89	3.03	0.51	0.00	3.16	0.12	1.28	0.12	0.03
0.305	2.82	3.03	0.46	0.00	3.16	0.12	1.28	0.12	0.03
0.306	2.76	3.03	0.41	-0.00	3.16	0.12	1.28	0.12	0.03
0.307	2.69	3.03	0.37	-0.00	3.16	0.12	1.28	0.12	0.03
0.308	2.64	3.03	0.34	-0.00	3.16	0.12	1.28	0.12	0.03
0.309	2.60	3.03	0.32	-0.00	3.16	0.12	1.28	0.12	0.03
0.310	2.57	3.03	0.30	-0.00	3.16	0.12	1.28	0.12	0.03
0.311	2.55	3.03	0.28	-0.00	3.16	0.12	1.28	0.12	0.03
0.312	2.53	3.03	0.27	0.00	3.16	0.12	1.28	0.12	0.03
0.313	2.51	3.03	0.26	0.00	3.16	0.12	1.28	0.12	0.03
0.314	2.50	3.03	0.25	0.00	3.16	0.12	1.28	0.12	0.03
0.315	2.48	3.03	0.24	0.00	3.16	0.12	1.28	0.12	0.03
0.316	2.47	3.03	0.24	0.00	3.16	0.12	1.28	0.12	0.03
0.317	2.45	3.03	0.23	-0.00	3.16	0.12	1.28	0.12	0.03
0.318	2.43	3.03	0.23	-0.00	3.16	0.12	1.28	0.12	0.03
0.319	2.42	3.03	0.22	-0.00	3.16	0.12	1.28	0.12	0.03
0.320	2.40	3.03	0.22	-0.00	3.16	0.12	1.28	0.12	0.03
0.321	2.38	3.03	0.21	-0.00	3.16	0.12	1.28	0.12	0.03
0.322	2.36	3.03	0.21	-0.00	3.16	0.12	1.28	0.12	0.03
0.323	2.35	3.03	0.20	0.00	3.16	0.12	1.28	0.12	0.03
0.324	2.33	3.03	0.20	0.00	3.16	0.12	1.28	0.12	0.03
0.325	2.31	3.03	0.20	0.00	3.16	0.12	1.28	0.12	0.03
0.326	2.29	3.03	0.19	0.00	3.16	0.12	1.28	0.12	0.03
0.327	2.28	3.03	0.19	0.00	3.16	0.12	1.28	0.12	0.03
0.328	2.27	3.03	0.19	-0.00	3.16	0.12	1.28	0.12	0.03
0.329	2.25	3.03	0.18	-0.00	3.16	0.12	1.28	0.12	0.03
0.330	2.24	3.03	0.18	-0.00	3.16	0.12	1.28	0.12	0.03
0.331									0.03
0.332									0.03
0.333									0.03
0.334									0.03
0.335									0.03
0.336									0.03
0.337									0.10
0.338									0.17
0.339									0.21

0.340									0.21
0.341									0.20
0.342									0.17
0.343									0.14
0.344									0.12
0.345									0.11
0.346									0.11
0.347									0.12
0.348									0.13
0.349									0.14
0.350									0.14
0.351									0.14
0.352									0.14
0.353									0.14
0.354									0.14
0.355									0.13
0.356									0.13
0.357									0.13
0.358									0.13
0.359									0.13
0.360									0.14
0.362	3.28	3.04	-0.26	-0.00	2.20	0.18	0.32	0.18	0.14
0.363	3.34	3.04	-0.25	-0.00	2.20	0.18	0.32	0.18	0.14
0.364	3.37	3.04	-0.23	-0.00	2.20	0.18	0.32	0.18	0.14
0.365	3.38	3.03	-0.22	-0.00	2.20	0.18	0.32	0.18	0.14
0.366	3.39	3.03	-0.21	0.00	2.20	0.18	0.32	0.18	0.14
0.367	3.39	3.03	-0.20	0.00	2.20	0.18	0.32	0.18	0.14
0.368	3.40	3.03	-0.20	0.00	2.20	0.18	0.32	0.18	0.14
0.369	3.40	3.03	-0.19	0.00	2.20	0.18	0.32	0.18	0.14
0.370	3.40	3.03	-0.18	0.00	2.20	0.18	0.32	0.18	0.14
0.371	3.40	3.03	-0.18	0.00	2.20	0.18	0.32	0.18	0.14
0.372	3.40	3.03	-0.17	-0.00	2.20	0.18	0.32	0.18	0.14
0.373	3.39	3.03	-0.17	-0.00	2.20	0.18	0.32	0.18	0.14
0.374	3.39	3.03	-0.16	-0.00	2.20	0.18	0.32	0.18	0.14
0.375	3.39	3.03	-0.16	-0.00	2.20	0.18	0.32	0.18	0.14
0.376	3.39	3.03	-0.16	-0.00	2.20	0.18	0.32	0.18	0.14
0.377	3.38	3.03	-0.16	-0.00	2.20	0.18	0.32	0.18	0.14
0.378	3.38	3.03	-0.16	0.00	2.20	0.18	0.32	0.18	0.14
0.379	3.37	3.03	-0.16	0.00	2.20	0.18	0.32	0.18	0.14
0.380	3.37	3.03	-0.16	0.00	2.20	0.18	0.32	0.18	0.14
0.381	3.36	3.03	-0.16	0.00	2.20	0.18	0.32	0.18	0.14
0.382	3.36	3.03	-0.16	0.00	2.20	0.18	0.32	0.18	0.14
0.383	3.35	3.03	-0.16	-0.00	2.20	0.18	0.32	0.18	0.14
0.384	3.35	3.03	-0.16	-0.00	2.20	0.18	0.32	0.18	0.14
0.385	3.34	3.03	-0.16	-0.00	2.20	0.18	0.32	0.18	0.14
0.386	3.34	3.03	-0.16	-0.00	2.20	0.18	0.32	0.18	0.14
0.387	3.33	3.03	-0.17	-0.00	2.20	0.18	0.32	0.18	0.14
0.388	3.33	3.03	-0.17	-0.00	2.20	0.18	0.32	0.18	0.14
0.389	3.32	3.03	-0.17	0.00	2.20	0.18	0.32	0.18	0.14

Table 2a - Continued

Page 8

0.390	3.32	3.03	-0.17	0.00	2.20	0.18	0.32	0.18	0.14
0.391	3.31	3.03	-0.17	0.00	2.20	0.18	0.32	0.18	0.14
0.392	3.31	3.03	-0.17	0.00	2.20	0.18	0.32	0.18	0.14
0.393	3.30	3.03	-0.17	0.00	2.20	0.18	0.32	0.18	0.14
0.394	3.30	3.03	-0.17	-0.00	2.20	0.18	0.32	0.18	0.14
0.395	3.29	3.03	-0.17	-0.00	2.20	0.18	0.32	0.18	0.14
0.396	3.29	3.03	-0.17	-0.00	2.20	0.18	0.32	0.18	0.14
0.397									0.14
0.398									0.14
0.399									0.14
0.400									0.14
0.401									0.14
0.402									0.10
0.403									0.02
0.404									0.10
0.405									0.15
0.406									0.15
0.407									0.13
0.408									0.10
0.409									0.06
0.410									0.04
0.411									0.03
0.412									0.03
0.413									0.04
0.414									0.05
0.415									0.06
0.416									0.07
0.417									0.07
0.418									0.07
0.419									0.06
0.420									0.06
0.421									0.06
0.422									0.05
0.423									0.05
0.424									0.06
0.425									0.06
0.426									0.06
0.428	2.61	3.02	0.21	0.00	3.34	-0.19	1.46	-0.19	0.06
0.429	3.14	3.02	0.21	0.00	3.34	-0.19	1.46	-0.19	0.06
0.430	3.27	3.02	0.15	0.00	3.34	-0.19	1.46	-0.19	0.06
0.431	3.10	3.03	0.06	0.00	3.34	-0.19	1.46	-0.19	0.06
0.432	2.94	3.03	0.04	-0.00	3.34	-0.19	1.47	-0.19	0.06
0.433	2.87	3.03	0.02	-0.00	3.34	-0.19	1.47	-0.19	0.06
0.434	2.84	3.03	0.02	-0.00	3.34	-0.19	1.47	-0.19	0.06
0.435	2.85	3.03	0.04	-0.00	3.34	-0.19	1.47	-0.19	0.06
0.436	2.88	3.03	0.06	-0.00	3.34	-0.19	1.47	-0.19	0.06
0.437	2.91	3.03	0.09	-0.00	3.34	-0.19	1.47	-0.19	0.06
0.438	2.92	3.03	0.11	0.00	3.34	-0.19	1.47	-0.19	0.06
0.439	2.93	3.03	0.13	0.00	3.34	-0.19	1.46	-0.19	0.06
0.440	2.92	3.03	0.14	0.00	3.34	-0.19	1.46	-0.19	0.06
0.441	2.91	3.03	0.15	0.00	3.34	-0.19	1.47	-0.19	0.06

0.442	2.90	3.03	0.14	0.00	3.34	-0.19	1.47	-0.19	0.06
0.443	2.90	3.03	0.13	0.00	3.34	-0.19	1.47	-0.19	0.06
0.444	2.89	3.03	0.12	-0.00	3.34	-0.19	1.47	-0.19	0.06
0.445	2.90	3.03	0.10	-0.00	3.34	-0.19	1.47	-0.19	0.06
0.446	2.91	3.03	0.07	-0.00	3.34	-0.19	1.47	-0.19	0.06
0.447	2.93	3.03	0.04	-0.00	3.34	-0.19	1.47	-0.19	0.06
0.448	2.95	3.03	0.01	-0.00	3.34	-0.19	1.47	-0.19	0.06
0.449	2.99	3.03	-0.02	0.00	3.34	-0.19	1.47	-0.19	0.06
0.450	3.03	3.03	-0.06	0.00	3.34	-0.19	1.47	-0.19	0.06
0.451	3.07	3.03	-0.09	0.00	3.34	-0.19	1.47	-0.19	0.06
0.452	3.11	3.03	-0.12	0.00	3.34	-0.19	1.47	-0.19	0.06
0.453	3.16	3.03	-0.15	0.00	3.34	-0.19	1.47	-0.19	0.06
0.454	3.21	3.03	-0.18	0.00	3.34	-0.19	1.47	-0.19	0.06
0.455	3.25	3.03	-0.20	-0.00	3.34	-0.19	1.47	-0.19	0.06
0.456	3.29	3.03	-0.22	-0.00	3.34	-0.19	1.47	-0.19	0.06
0.457	3.33	3.03	-0.24	-0.00	3.34	-0.19	1.47	-0.19	0.06
0.458	3.37	3.03	-0.26	-0.00	3.34	-0.19	1.47	-0.19	0.06
0.459	3.41	3.03	-0.27	-0.00	3.34	-0.19	1.47	-0.19	0.06
0.460	3.44	3.03	-0.28	0.00	3.34	-0.19	1.47	-0.19	0.06
0.461	3.48	3.03	-0.29	0.00	3.34	-0.19	1.47	-0.19	0.06
0.462	3.50	3.03	-0.30	0.00	3.34	-0.19	1.47	-0.19	0.06
0.463									0.06
0.464									0.06
0.465									0.06
0.466									0.06
0.467									0.06
0.468									0.06
0.469									0.06
0.470									0.10
0.471									0.11
0.472									0.11
0.473									0.10
0.474									0.10
0.475									0.09
0.476									0.09
0.477									0.09
0.478									0.09
0.479									0.09
0.480									0.09
0.481									0.09
0.482									0.09
0.483									0.09
0.484									0.09
0.485									0.09
0.486									0.09
0.487									0.09
0.488									0.09
0.489									0.09
0.490									0.09
0.491									0.09
0.492									0.09

Table 2a - Continued

Page 10

0.494	2.58	3.03	0.23	0.00	3.51	-0.30	1.64	-0.30	0.09
0.495	2.66	3.03	0.23	0.00	3.51	-0.30	1.64	-0.30	0.09
0.496	2.71	3.03	0.22	0.00	3.51	-0.30	1.64	-0.30	0.09
0.497	2.75	3.03	0.21	0.00	3.51	-0.30	1.64	-0.30	0.09
0.498	2.79	3.03	0.21	-0.00	3.51	-0.30	1.64	-0.30	0.09
0.499	2.81	3.03	0.21	-0.00	3.51	-0.30	1.64	-0.30	0.09
0.500	2.83	3.03	0.22	-0.00	3.51	-0.30	1.64	-0.30	0.09
0.501	2.84	3.03	0.22	-0.00	3.51	-0.30	1.64	-0.30	0.09

15

Table 2b (1)

TIME (SEC)	MLD		NUC		PUT	AUT	MUG	NLG	MISS (P)
	EST	TRUE	EST	TRUE					
0.032	3.13	3.05	0.51	0.00	0.32	0.00	-2.20	0.00	0.43
0.033	3.13	3.04	0.52	0.00	0.32	-0.00	-2.20	-0.00	0.43
0.034	3.13	3.04	0.53	-0.00	0.31	-0.00	-2.20	-0.00	0.43
0.035	3.13	3.04	0.54	-0.00	0.31	-0.00	-2.20	-0.00	0.43
0.036	3.12	3.03	0.55	-0.00	0.31	-0.00	-2.20	-0.00	0.43
0.037	3.13	3.03	0.55	-0.00	0.31	-0.00	-2.20	-0.00	0.43
0.038	3.12	3.03	0.56	-0.00	0.31	-0.00	-2.20	-0.00	0.43
0.039	3.12	3.03	0.56	0.00	0.31	0.00	-2.20	0.00	0.43
0.040	3.12	3.04	0.56	0.00	0.31	0.00	-2.20	0.00	0.43
0.041	3.11	3.04	0.56	0.00	0.31	0.00	-2.20	0.00	0.43
0.042	3.11	3.04	0.56	0.00	0.31	0.00	-2.20	0.00	0.43
0.043	3.10	3.04	0.56	0.00	0.31	0.00	-2.20	0.00	0.43
0.044	3.09	3.04	0.55	0.00	0.31	0.00	-2.20	0.00	0.43
0.045	3.07	3.04	0.55	-0.00	0.31	-0.00	-2.20	-0.00	0.43
0.046	3.06	3.04	0.55	-0.00	0.31	-0.00	-2.20	-0.00	0.43
0.047	3.04	3.04	0.55	-0.00	0.31	-0.00	-2.20	-0.00	0.43
0.048	3.03	3.04	0.55	-0.00	0.31	-0.00	-2.20	-0.00	0.43
0.049	3.01	3.04	0.55	-0.00	0.31	-0.00	-2.20	-0.00	0.43
0.050	3.00	3.04	0.54	0.00	0.31	0.00	-2.20	0.00	0.43
0.051	2.99	3.04	0.54	0.00	0.31	0.00	-2.20	0.00	0.43
0.052	2.98	3.04	0.54	0.00	0.31	0.00	-2.20	0.00	0.43
0.053	2.98	3.04	0.55	0.00	0.31	0.00	-2.20	0.00	0.43
0.054	2.98	3.04	0.55	0.00	0.31	0.00	-2.20	0.00	0.43
0.055	2.99	3.04	0.55	0.00	0.31	0.00	-2.20	0.00	0.43
0.056	3.01	3.04	0.55	-0.00	0.31	-0.00	-2.20	-0.00	0.43
0.057	3.03	3.04	0.55	-0.00	0.31	-0.00	-2.20	-0.00	0.43
0.058	3.05	3.04	0.55	-0.00	0.31	-0.00	-2.20	-0.00	0.43
0.059	3.08	3.04	0.54	-0.00	0.31	-0.00	-2.20	-0.00	0.43
0.060	3.11	3.04	0.54	-0.00	0.31	-0.00	-2.20	-0.00	0.43
0.061	3.13	3.04	0.53	-0.00	0.31	-0.00	-2.20	-0.00	0.43
0.062	3.15	3.04	0.53	0.00	0.31	0.00	-2.20	0.00	0.43
0.063	3.17	3.04	0.52	0.00	0.31	0.00	-2.20	0.00	0.43
0.064	3.18	3.04	0.52	0.00	0.31	0.00	-2.20	0.00	0.43
0.065	3.19	3.04	0.51	0.00	0.31	0.00	-2.20	0.00	0.43
0.066	3.20	3.04	0.50	0.00	0.31	0.00	-2.20	0.00	0.43
0.067									0.43
0.068									0.43
0.069									0.43
0.070									0.43
0.071									0.43
0.072									0.34
0.073									0.09
0.074									0.19
0.075									0.30
0.076									0.32
0.077									0.26
0.078									0.18

Table 2b (1) - Continued

Page 2

0.079									0.10
0.080									0.07
0.081									0.08
0.082									0.08
0.083									0.07
0.084									0.08
0.085									0.10
0.086									0.11
0.087									0.12
0.088									0.11
0.089									0.11
0.090									0.10
0.091									0.09
0.092									0.09
0.093									0.09
0.094									0.09
0.095									0.09
0.096									0.10
0.098	1.17	3.01	0.23	-0.00	3.33	0.53	0.82	0.53	0.10
0.099	1.89	3.01	0.16	-0.00	3.33	0.53	0.82	0.53	0.10
0.100	1.79	3.02	0.49	-0.00	3.33	0.53	0.82	0.53	0.10
0.101	1.48	3.03	0.62	-0.00	3.34	0.53	0.83	0.53	0.10
0.102	1.36	3.04	0.65	0.00	3.34	0.53	0.83	0.53	0.10
0.103	1.34	3.04	0.65	0.00	3.34	0.53	0.83	0.53	0.10
0.104	1.37	3.04	0.65	0.00	3.34	0.53	0.83	0.53	0.10
0.105	1.45	3.04	0.64	0.00	3.34	0.53	0.83	0.53	0.10
0.106	1.55	3.04	0.63	0.00	3.34	0.53	0.83	0.53	0.10
0.107	1.67	3.04	0.61	0.00	3.34	0.53	0.83	0.53	0.10
0.108	1.79	3.03	0.59	-0.00	3.34	0.53	0.83	0.53	0.10
0.109	1.90	3.03	0.57	-0.00	3.34	0.53	0.83	0.53	0.10
0.110	2.00	3.03	0.56	-0.00	3.34	0.53	0.83	0.53	0.10
0.111	2.08	3.03	0.56	-0.00	3.34	0.53	0.83	0.53	0.10
0.112	2.15	3.03	0.57	-0.00	3.34	0.53	0.83	0.53	0.10
0.113	2.21	3.04	0.58	0.00	3.34	0.53	0.83	0.53	0.10
0.114	2.26	3.04	0.58	0.00	3.34	0.53	0.83	0.53	0.10
0.115	2.31	3.04	0.59	0.00	3.34	0.53	0.83	0.53	0.10
0.116	2.34	3.04	0.59	0.00	3.34	0.53	0.83	0.53	0.10
0.117	2.38	3.04	0.59	0.00	3.34	0.53	0.83	0.53	0.10
0.118	2.41	3.04	0.58	0.00	3.34	0.53	0.83	0.53	0.10
0.119	2.43	3.04	0.58	-0.00	3.34	0.53	0.83	0.53	0.10
0.120	2.45	3.03	0.57	-0.00	3.34	0.53	0.83	0.53	0.10
0.121	2.47	3.03	0.56	-0.00	3.34	0.53	0.83	0.53	0.10
0.122	2.49	3.03	0.54	-0.00	3.34	0.53	0.83	0.53	0.10
0.123	2.50	3.03	0.53	-0.00	3.34	0.53	0.83	0.53	0.10
0.124	2.51	3.04	0.52	-0.00	3.34	0.53	0.83	0.53	0.10
0.125	2.52	3.04	0.51	0.00	3.34	0.53	0.83	0.53	0.10
0.126	2.53	3.04	0.49	0.00	3.34	0.53	0.83	0.53	0.10
0.127	2.53	3.04	0.48	0.00	3.34	0.53	0.83	0.53	0.10
0.128	2.54	3.04	0.47	0.00	3.34	0.53	0.83	0.53	0.10
0.129	2.54	3.04	0.46	0.00	3.34	0.53	0.83	0.53	0.10
0.130	2.54	3.04	0.45	-0.00	3.34	0.53	0.83	0.53	0.10

Table 2b (1) - Continued

Page 3

0.131	2.53	3.04	0.44	-0.00	3.34	C.53	0.83	0.53	0.10
0.132	2.53	3.03	0.43	-0.00	3.34	C.53	0.83	0.53	0.10
0.133									0.10
0.134									0.10
0.135									0.10
0.136									0.10
0.137									0.10
0.138									0.08
0.139									0.09
0.140									0.13
0.141									0.16
0.142									0.17
0.143									0.15
0.144									0.13
0.145									0.11
0.146									0.10
0.147									0.10
0.148									0.10
0.149									0.10
0.150									0.11
0.151									0.11
0.152									0.11
0.153									0.12
0.154									0.12
0.155									0.11
0.156									0.11
0.157									0.11
0.158									0.11
0.159									0.11
0.160									0.11
0.161									0.11
0.162									0.11
0.164	2.06	3.04	0.21	0.00	2.49	C.43	-0.02	0.43	0.11
0.165	2.43	3.04	0.51	0.00	2.49	C.43	-0.02	0.43	0.11
0.166	2.63	3.04	0.61	0.00	2.49	C.43	-0.02	0.43	0.11
0.167	2.72	3.04	0.64	0.00	2.49	C.43	-0.02	0.43	0.11
0.168	2.79	3.03	0.66	-0.00	2.49	C.43	-0.02	0.43	0.11
0.169	2.85	3.03	0.66	-0.00	2.49	C.43	-0.02	0.43	0.11
0.170	2.90	3.03	0.69	-0.00	2.49	C.43	-0.02	0.43	0.11
0.171	2.94	3.03	0.70	-0.00	2.49	C.43	-0.02	0.43	0.11
0.172	2.97	3.03	0.71	-0.00	2.49	C.43	-0.02	0.43	0.11
0.173	3.00	3.03	0.71	-0.00	2.49	C.43	-0.02	0.43	0.11
0.174	3.04	3.03	0.71	0.00	2.49	C.43	-0.02	0.43	0.11
0.175	3.06	3.04	0.72	0.00	2.49	C.43	-0.02	0.43	0.11
0.176	3.09	3.04	0.72	0.00	2.49	C.43	-0.02	0.43	0.11
0.177	3.12	3.03	0.72	0.00	2.49	C.43	-0.02	0.43	0.11
0.178	3.15	3.03	0.71	0.00	2.49	C.43	-0.02	0.43	0.11
0.179	3.18	3.03	0.71	-0.00	2.49	C.43	-0.02	0.43	0.11
0.180	3.20	3.03	0.71	-0.00	2.49	C.43	-0.02	0.43	0.11
0.181	3.22	3.03	0.71	-0.00	2.49	C.43	-0.02	0.43	0.11
0.182	3.24	3.03	0.70	-0.00	2.49	C.43	-0.02	0.43	0.11

Table 2b (1) - Continued

Page 4

0.183	3.25	3.03	0.70	-0.00	2.49	0.43	-0.02	0.43	0.11
0.184	3.25	3.03	0.70	-0.00	2.49	0.43	-0.02	0.43	0.11
0.185	3.23	3.03	0.71	0.00	2.49	0.43	-0.02	0.43	0.11
0.186	3.20	3.03	0.71	0.00	2.49	0.43	-0.02	0.43	0.11
0.187	3.17	3.03	0.72	0.00	2.49	0.43	-0.02	0.43	0.11
0.188	3.12	3.03	0.74	0.00	2.49	0.43	-0.02	0.43	0.11
0.189	3.06	3.03	0.76	0.00	2.49	0.43	-0.02	0.43	0.11
0.190	3.01	3.03	0.78	0.00	2.49	0.43	-0.02	0.43	0.11
0.191	2.95	3.03	0.80	-0.00	2.49	0.43	-0.02	0.43	0.11
0.192	2.90	3.03	0.82	-0.00	2.49	0.43	-0.02	0.43	0.11
0.193	2.86	3.03	0.84	-0.00	2.49	0.43	-0.02	0.43	0.11
0.194	2.82	3.03	0.86	-0.00	2.49	0.43	-0.02	0.43	0.11
0.195	2.79	3.03	0.87	-0.00	2.49	0.43	-0.02	0.43	0.11
0.196	2.76	3.03	0.88	0.00	2.49	0.43	-0.02	0.43	0.11
0.197	2.74	3.03	0.89	0.00	2.49	0.43	-0.02	0.43	0.11
0.198	2.72	3.03	0.90	0.00	2.49	0.43	-0.02	0.43	0.11
0.199									0.11
0.200									0.11
0.201									0.11
0.202									0.11
0.203									0.11
0.204									0.11
0.205									0.14
0.206									0.17
0.207									0.19
0.208									0.19
0.209									0.19
0.210									0.17
0.211									0.16
0.212									0.15
0.213									0.14
0.214									0.14
0.215									0.15
0.216									0.15
0.217									0.16
0.218									0.16
0.219									0.16
0.220									0.16
0.221									0.16
0.222									0.16
0.223									0.15
0.224									0.15
0.225									0.15
0.226									0.15
0.227									0.15
0.228									0.15
0.230	2.58	3.03	0.21	-0.00	2.73	0.92	0.22	0.92	0.15
0.231	2.57	3.03	0.19	-0.00	2.73	0.92	0.22	0.92	0.15
0.232	2.58	3.03	0.15	-0.00	2.73	0.92	0.22	0.92	0.15
0.233	2.60	3.03	0.09	-0.00	2.73	0.92	0.22	0.92	0.15
0.234	2.60	3.03	0.05	0.00	2.73	0.92	0.22	0.92	0.15

0.235	2.60	3.03	0.01	0.00	2.73	0.92	0.22	0.92	0.15
0.236	2.61	3.03	-0.03	0.00	2.73	0.92	0.22	0.92	0.15
0.237	2.61	3.03	-0.08	0.00	2.73	0.92	0.22	0.92	0.15
0.238	2.61	3.03	-0.12	0.00	2.73	0.92	0.22	0.92	0.15
0.239	2.61	3.03	-0.16	0.00	2.73	0.92	0.22	0.92	0.15
0.240	2.60	3.03	-0.20	-0.00	2.73	0.92	0.22	0.92	0.15
0.241	2.61	3.03	-0.23	-0.00	2.73	0.92	0.22	0.92	0.15
0.242	2.61	3.03	-0.24	-0.00	2.73	0.92	0.22	0.92	0.15
0.243	2.63	3.03	-0.22	-0.00	2.73	0.92	0.22	0.92	0.15
0.244	2.66	3.03	-0.16	-0.00	2.73	0.92	0.22	0.92	0.15
0.245	2.70	3.03	-0.10	-0.00	2.73	0.92	0.22	0.92	0.15
0.246	2.76	3.03	-0.01	0.00	2.73	0.92	0.22	0.92	0.15
0.247	2.82	3.03	0.09	0.00	2.73	0.92	0.22	0.92	0.15
0.248	2.88	3.03	0.17	0.00	2.73	0.92	0.22	0.92	0.15
0.249	2.94	3.03	0.23	0.00	2.73	0.92	0.22	0.92	0.15
0.250	2.98	3.03	0.27	0.00	2.73	0.92	0.22	0.92	0.15
0.251	3.01	3.03	0.29	-0.00	2.73	0.92	0.22	0.92	0.15
0.252	3.04	3.03	0.30	-0.00	2.73	0.92	0.22	0.92	0.15
0.253	3.06	3.03	0.30	-0.00	2.73	0.92	0.22	0.92	0.15
0.254	3.07	3.03	0.29	-0.00	2.73	0.92	0.22	0.92	0.15
0.255	3.08	3.03	0.28	-0.00	2.73	0.92	0.22	0.92	0.15
0.256	3.09	3.03	0.26	-0.00	2.73	0.92	0.22	0.92	0.15
0.257	3.10	3.03	0.25	0.00	2.73	0.92	0.22	0.92	0.15
0.258	3.11	3.03	0.24	0.00	2.73	0.92	0.22	0.92	0.15
0.259	3.11	3.03	0.22	0.00	2.73	0.92	0.22	0.92	0.15
0.260	3.12	3.03	0.21	0.00	2.73	0.92	0.22	0.92	0.15
0.261	3.13	3.03	0.20	0.00	2.73	0.92	0.22	0.92	0.15
0.262	3.13	3.03	0.18	-0.00	2.73	0.92	0.22	0.92	0.15
0.263	3.14	3.03	0.17	-0.00	2.73	0.92	0.22	0.92	0.15
0.264	3.14	3.03	0.16	-0.00	2.73	0.92	0.22	0.92	0.15
0.265									0.15
0.266									0.15
0.267									0.15
0.268									0.15
0.269									0.15
0.270									0.13
0.271									0.09
0.272									0.04
0.273									0.07
0.274									0.07
0.275									0.06
0.276									0.04
0.277									0.03
0.278									0.04
0.279									0.04
0.280									0.04
0.281									0.04
0.282									0.03
0.283									0.03
0.284									0.03
0.285									0.03

Table 2b (1) - Continued

Page 6

0.286									0.03
0.287									0.03
0.288									0.03
0.289									0.03
0.290									0.03
0.291									0.03
0.292									0.03
0.293									0.03
0.294									0.03
0.296	3.78	3.03	-0.14	0.01	3.16	0.13	0.65	0.13	0.03
0.297	3.80	3.03	-0.12	0.01	3.16	0.13	0.65	0.13	0.03
0.298	3.81	3.03	-0.10	0.00	3.16	0.13	0.65	0.13	0.03
0.299	3.81	3.03	-0.09	0.00	3.16	0.13	0.65	0.13	0.03
0.300	3.82	3.03	-0.08	-0.00	3.16	0.12	0.66	0.12	0.03
0.301	3.83	3.03	-0.07	-0.00	3.16	0.12	0.66	0.12	0.03
0.302	3.83	3.03	-0.06	-0.00	3.16	0.12	0.66	0.12	0.03
0.303	3.83	3.03	-0.05	-0.00	3.16	0.12	0.66	0.12	0.03
0.304	3.83	3.03	-0.04	-0.00	3.16	0.12	0.66	0.12	0.03
0.305	3.83	3.03	-0.03	-0.00	3.16	0.12	0.66	0.12	0.03
0.306	3.83	3.03	-0.02	0.00	3.16	0.13	0.66	0.13	0.03
0.307	3.82	3.03	-0.01	0.00	3.16	0.13	0.66	0.13	0.03
0.308	3.81	3.03	0.00	0.00	3.16	0.13	0.66	0.13	0.03
0.309	3.80	3.03	0.01	0.00	3.16	0.13	0.66	0.13	0.03
0.310	3.79	3.03	0.02	0.00	3.16	0.13	0.66	0.13	0.03
0.311	3.78	3.03	0.03	0.00	3.16	0.13	0.66	0.13	0.03
0.312	3.77	3.03	0.04	-0.00	3.16	0.12	0.66	0.12	0.03
0.313	3.75	3.03	0.05	-0.00	3.16	0.12	0.66	0.12	0.03
0.314	3.74	3.03	0.06	-0.00	3.16	0.12	0.66	0.12	0.03
0.315	3.72	3.03	0.07	-0.00	3.16	0.12	0.66	0.12	0.03
0.316	3.71	3.03	0.07	-0.00	3.16	0.12	0.66	0.12	0.03
0.317	3.69	3.03	0.08	0.00	3.16	0.13	0.66	0.13	0.03
0.318	3.67	3.03	0.08	0.00	3.16	0.13	0.66	0.13	0.03
0.319	3.65	3.03	0.09	0.00	3.16	0.13	0.66	0.13	0.03
0.320	3.63	3.03	0.09	0.00	3.16	0.13	0.66	0.13	0.03
0.321	3.61	3.03	0.09	0.00	3.16	0.13	0.66	0.13	0.03
0.322	3.59	3.03	0.09	0.00	3.16	0.13	0.66	0.13	0.03
0.323	3.57	3.03	0.09	-0.00	3.16	0.13	0.66	0.13	0.03
0.324	3.54	3.03	0.09	-0.00	3.16	0.13	0.66	0.13	0.03
0.325	3.51	3.03	0.09	-0.00	3.16	0.13	0.66	0.13	0.03
0.326	3.47	3.03	0.09	-0.00	3.16	0.13	0.66	0.13	0.03
0.327	3.43	3.03	0.10	-0.00	3.16	0.13	0.66	0.13	0.03
0.328	3.39	3.03	0.10	0.00	3.16	0.13	0.66	0.13	0.03
0.329	3.33	3.03	0.10	0.00	3.16	0.13	0.66	0.13	0.03
0.330	3.27	3.03	0.10	0.00	3.16	0.13	0.66	0.13	0.03
0.331									0.03
0.332									0.03
0.333									0.03
0.334									0.03
0.335									0.03
0.336									0.03
0.337									0.04

0.318									0.05
0.319									0.05
0.340									0.05
0.341									0.05
0.342									0.05
0.343									0.04
0.344									0.04
0.345									0.04
0.346									0.04
0.347									0.04
0.348									0.04
0.349									0.04
0.350									0.04
0.351									0.04
0.352									0.04
0.353									0.04
0.354									0.04
0.355									0.04
0.356									0.04
0.357									0.04
0.358									0.04
0.359									0.04
0.360									0.04
0.362	2.08	3.03	0.43	0.00	3.28	0.10	0.77	0.10	0.04
0.363	2.02	3.03	0.40	0.00	3.28	0.10	0.77	0.10	0.04
0.364	1.99	3.03	0.37	0.00	3.28	0.10	0.77	0.10	0.04
0.365	1.97	3.03	0.36	0.00	3.28	0.10	0.77	0.10	0.04
0.366	1.96	3.03	0.35	-0.00	3.28	0.10	0.77	0.10	0.04
0.367	1.97	3.03	0.34	-0.00	3.28	0.10	0.77	0.10	0.04
0.368	1.97	3.03	0.33	-0.00	3.28	0.10	0.77	0.10	0.04
0.369	1.98	3.03	0.32	-0.00	3.28	0.10	0.77	0.10	0.04
0.370	1.99	3.03	0.31	-0.00	3.28	0.10	0.77	0.10	0.04
0.371	2.01	3.03	0.30	-0.00	3.28	0.10	0.77	0.10	0.04
0.372	2.02	3.03	0.29	0.00	3.28	0.10	0.77	0.10	0.04
0.373	2.04	3.03	0.28	0.00	3.28	0.10	0.77	0.10	0.04
0.374	2.06	3.03	0.26	0.00	3.28	0.10	0.77	0.10	0.04
0.375	2.07	3.03	0.25	0.00	3.28	0.10	0.77	0.10	0.04
0.376	2.09	3.03	0.24	0.00	3.28	0.10	0.77	0.10	0.04
0.377	2.11	3.03	0.22	0.00	3.28	0.10	0.77	0.10	0.04
0.378	2.14	3.03	0.21	-0.00	3.28	0.10	0.77	0.10	0.04
0.379	2.16	3.03	0.20	-0.00	3.28	0.10	0.77	0.10	0.04
0.380	2.19	3.03	0.18	-0.00	3.28	0.10	0.77	0.10	0.04
0.381	2.22	3.03	0.17	-0.00	3.28	0.10	0.77	0.10	0.04
0.382	2.25	3.03	0.15	-0.00	3.28	0.10	0.77	0.10	0.04
0.383	2.28	3.03	0.14	0.00	3.28	0.10	0.77	0.10	0.04
0.384	2.32	3.03	0.12	0.00	3.28	0.10	0.77	0.10	0.04
0.385	2.35	3.03	0.11	0.00	3.28	0.10	0.77	0.10	0.04
0.386	2.39	3.03	0.09	0.00	3.28	0.10	0.77	0.10	0.04
0.387	2.42	3.03	0.07	0.00	3.28	0.10	0.77	0.10	0.04
0.388	2.46	3.03	0.06	0.00	3.28	0.10	0.77	0.10	0.04
0.389	2.49	3.03	0.04	-0.00	3.28	0.10	0.77	0.10	0.04

Table 2b (1) - Continued

Page 8

0.350	2.53	3.03	0.03	-0.00	3.28	0.10	0.77	0.10	0.04
0.351	2.56	3.03	0.02	-0.00	3.28	0.10	0.77	0.10	0.04
0.352	2.59	3.03	0.00	-0.00	3.28	0.10	0.77	0.10	0.04
0.353	2.62	3.03	-0.01	-0.00	3.28	0.10	0.77	0.10	0.04
0.354	2.65	3.03	-0.03	0.00	3.28	0.10	0.77	0.10	0.04
0.355	2.68	3.03	-0.04	0.00	3.28	0.10	0.77	0.10	0.04
0.356	2.71	3.03	-0.06	0.00	3.28	0.10	0.77	0.10	0.04
0.357									0.04
0.358									0.04
0.359									0.04
0.400									0.04
0.401									0.04
0.402									0.02
0.403									0.03
0.404									0.06
0.405									0.10
0.406									0.11
0.407									0.10
0.408									0.09
0.409									0.06
0.410									0.05
0.411									0.04
0.412									0.04
0.413									0.05
0.414									0.09
0.415									0.06
0.416									0.06
0.417									0.06
0.418									0.06
0.419									0.06
0.420									0.06
0.421									0.06
0.422									0.06
0.423									0.06
0.424									0.06
0.425									0.06
0.426									0.06
0.428	3.02	3.04	-0.42	0.00	2.68	-0.07	0.18	-0.07	0.06
0.429	3.02	3.04	-0.42	0.00	2.68	-0.07	0.18	-0.07	0.06
0.430	3.02	3.03	-0.42	0.00	2.68	-0.07	0.18	-0.07	0.06
0.431	3.04	3.03	-0.42	0.00	2.68	-0.07	0.18	-0.07	0.06
0.432	3.04	3.03	-0.42	-0.00	2.68	-0.07	0.18	-0.07	0.06
0.433	3.05	3.03	-0.42	-0.00	2.68	-0.07	0.18	-0.07	0.06
0.434	3.06	3.03	-0.41	-0.00	2.68	-0.07	0.18	-0.07	0.06
0.435	3.07	3.03	-0.41	-0.00	2.68	-0.07	0.18	-0.07	0.06
0.436	3.08	3.03	-0.40	-0.00	2.68	-0.07	0.18	-0.07	0.06
0.437	3.09	3.03	-0.40	-0.00	2.68	-0.07	0.18	-0.07	0.06
0.438	3.11	3.03	-0.39	0.00	2.68	-0.07	0.18	-0.07	0.06
0.439	3.12	3.03	-0.38	0.00	2.68	-0.07	0.18	-0.07	0.06

160

Table 2b (1) - Continued

Page 9

0.440	3.14	3.03	-0.37	0.00	2.68	-0.07	0.18	-0.07	0.06
0.441	3.15	3.03	-0.36	0.00	2.68	-0.07	0.18	-0.07	0.06
0.442	3.17	3.03	-0.35	0.00	2.68	-0.07	0.18	-0.07	0.06
0.443	3.19	3.03	-0.35	0.00	2.68	-0.07	0.18	-0.07	0.06
0.444	3.20	3.03	-0.34	-0.00	2.68	-0.07	0.18	-0.07	0.06
0.445	3.21	3.03	-0.33	-0.00	2.68	-0.07	0.18	-0.07	0.06
0.446	3.22	3.03	-0.33	-0.00	2.68	-0.07	0.18	-0.07	0.06
0.447	3.23	3.03	-0.34	-0.00	2.68	-0.07	0.18	-0.07	0.06
0.448	3.23	3.03	-0.35	-0.00	2.68	-0.07	0.18	-0.07	0.06
0.449	3.23	3.03	-0.36	0.00	2.68	-0.07	0.18	-0.07	0.06
0.450	3.23	3.03	-0.36	0.00	2.68	-0.07	0.18	-0.07	0.06
0.451	3.23	3.03	-0.41	0.00	2.68	-0.07	0.18	-0.07	0.06
0.452	3.23	3.03	-0.43	0.00	2.68	-0.07	0.18	-0.07	0.06
0.453	3.22	3.03	-0.46	0.00	2.68	-0.07	0.18	-0.07	0.06
0.454	3.22	3.03	-0.46	0.00	2.68	-0.07	0.18	-0.07	0.06
0.455	3.22	3.03	-0.51	-0.00	2.68	-0.07	0.18	-0.07	0.06
0.456	3.21	3.03	-0.53	-0.00	2.68	-0.07	0.18	-0.07	0.06
0.457	3.21	3.03	-0.55	-0.00	2.68	-0.07	0.18	-0.07	0.06
0.458	3.21	3.03	-0.56	-0.00	2.68	-0.07	0.18	-0.07	0.06
0.459	3.21	3.03	-0.57	-0.00	2.68	-0.07	0.18	-0.07	0.06
0.460	3.21	3.03	-0.58	0.00	2.68	-0.07	0.18	-0.07	0.06
0.461	3.21	3.03	-0.59	0.00	2.68	-0.07	0.18	-0.07	0.06
0.462	3.20	3.03	-0.59	0.00	2.68	-0.07	0.18	-0.07	0.06
0.463									0.06
0.464									0.06
0.465									0.06
0.466									0.06
0.467									0.06
0.468									0.05
0.469									0.06
0.470									0.13
0.471									0.16
0.472									0.16
0.473									0.15
0.474									0.13
0.475									0.11
0.476									0.09
0.477									0.09
0.478									0.09
0.479									0.09
0.480									0.10
0.481									0.10
0.482									0.11
0.483									0.11
0.484									0.11
0.485									0.11
0.486									0.10
0.487									0.10
0.488									0.10
0.489									0.10
0.490									0.10

Table 2b (1) - Continued

Page 10

0.451									0.10
0.452									0.10
0.454	2.41	3.02	0.07	0.00	3.23	-0.61	0.73	-0.61	0.10
0.455	2.63	3.03	0.08	0.00	3.23	-0.61	0.73	-0.61	0.10
0.456	2.79	3.03	0.07	0.00	3.23	-0.61	0.73	-0.61	0.10
0.457	2.90	3.03	0.07	0.00	3.23	-0.61	0.73	-0.61	0.10
0.458	2.97	3.03	0.09	-0.00	3.23	-0.62	0.73	-0.62	0.10
0.459	3.02	3.03	0.12	-0.00	3.23	-0.62	0.73	-0.62	0.10
0.500	3.06	3.03	0.15	-0.00	3.23	-0.62	0.73	-0.62	0.10
0.501	3.08	3.03	0.18	-0.00	3.23	-0.62	0.73	-0.62	0.10

Table 2b (2)

TIME	MLD		NUC		MUT	MUT	MUG	NLG	MISSE
(SEC)	EST	TRUE	EST	TRUE					(M)
0.032	2.73	3.05	-0.30	0.00	0.32	0.00	-2.20	0.00	0.43
0.033	2.78	3.04	-0.32	0.00	0.32	-0.00	-2.20	-0.00	0.43
0.034	2.81	3.04	-0.35	-0.00	0.31	-0.00	-2.20	-0.00	0.43
0.035	2.84	3.04	-0.40	-0.00	0.31	-0.00	-2.20	-0.00	0.43
0.036	2.86	3.03	-0.44	-0.00	0.31	-0.00	-2.20	-0.00	0.43
0.037	2.89	3.03	-0.48	-0.00	0.31	-0.00	-2.20	-0.00	0.43
0.038	2.91	3.03	-0.50	-0.00	0.31	-0.00	-2.20	-0.00	0.43
0.039	2.92	3.03	-0.50	0.00	0.31	0.00	-2.20	0.00	0.43
0.040	2.93	3.04	-0.51	0.00	0.31	0.00	-2.20	0.00	0.43
0.041	2.94	3.04	-0.50	0.00	0.31	0.00	-2.20	0.00	0.43
0.042	2.93	3.04	-0.49	0.00	0.31	0.00	-2.20	0.00	0.43
0.043	2.92	3.04	-0.48	0.00	0.31	0.00	-2.20	0.00	0.43
0.044	2.91	3.04	-0.46	0.00	0.31	0.00	-2.20	0.00	0.43
0.045	2.89	3.04	-0.44	-0.00	0.31	-0.00	-2.20	-0.00	0.43
0.046	2.87	3.04	-0.41	-0.00	0.31	-0.00	-2.20	-0.00	0.43
0.047	2.85	3.04	-0.38	-0.00	0.31	-0.00	-2.20	-0.00	0.43
0.048	2.82	3.04	-0.35	-0.00	0.31	-0.00	-2.20	-0.00	0.43
0.049	2.79	3.04	-0.32	-0.00	0.31	-0.00	-2.20	-0.00	0.43
0.050	2.77	3.04	-0.28	0.00	0.31	0.00	-2.20	0.00	0.43
0.051	2.74	3.04	-0.25	0.00	0.31	0.00	-2.20	0.00	0.43
0.052	2.72	3.04	-0.22	0.00	0.31	0.00	-2.20	0.00	0.43
0.053	2.70	3.04	-0.19	0.00	0.31	0.00	-2.20	0.00	0.43
0.054	2.68	3.04	-0.16	0.00	0.31	0.00	-2.20	0.00	0.43
0.055	2.67	3.04	-0.13	0.00	0.31	0.00	-2.20	0.00	0.43
0.056	2.66	3.04	-0.10	-0.00	0.31	-0.00	-2.20	-0.00	0.43
0.057	2.66	3.04	-0.09	-0.00	0.31	-0.00	-2.20	-0.00	0.43
0.058	2.65	3.04	-0.06	-0.00	0.31	-0.00	-2.20	-0.00	0.43
0.059	2.65	3.04	-0.04	-0.00	0.31	-0.00	-2.20	-0.00	0.43
0.060	2.65	3.04	-0.03	-0.00	0.31	-0.00	-2.20	-0.00	0.43
0.061	2.65	3.04	-0.02	-0.00	0.31	-0.00	-2.20	-0.00	0.43
0.062	2.64	3.04	-0.01	0.00	0.31	0.00	-2.20	0.00	0.43
0.063	2.63	3.04	-0.01	0.00	0.31	0.00	-2.20	0.00	0.43
0.064	2.62	3.04	-0.02	0.00	0.31	0.00	-2.20	0.00	0.43
0.065	2.60	3.04	-0.03	0.00	0.31	0.00	-2.20	0.00	0.43
0.066	2.57	3.04	-0.06	0.00	0.31	0.00	-2.20	0.00	0.43
0.067									0.43
0.068									0.43
0.069									0.43
0.070									0.43
0.071									0.43
0.072									0.36
0.073									0.14
0.074									0.03
0.075									0.12
0.076									0.14
0.077									0.09
0.078									0.02
0.079									0.09
0.080									0.10

Table 2b (2) - Continued

Page 2

0.081									0.12
0.082									0.12
0.083									0.10
0.084									0.07
0.085									0.05
0.086									0.04
0.087									0.04
0.088									0.04
0.089									0.05
0.090									0.05
0.091									0.06
0.092									0.06
0.093									0.06
0.094									0.06
0.095									0.06
0.096									0.06
0.098	2.75	3.01	-0.54	0.00	2.67	-0.06	0.16	-0.06	0.06
0.099	2.71	3.02	-0.54	0.00	2.67	-0.06	0.16	-0.06	0.06
0.100	2.63	3.02	-0.52	0.00	2.68	-0.06	0.17	-0.06	0.06
0.101	2.58	3.03	-0.49	0.00	2.68	-0.06	0.17	-0.06	0.06
0.102	2.58	3.04	-0.47	-0.00	2.68	-0.06	0.17	-0.06	0.06
0.103	2.60	3.04	-0.44	-0.00	2.68	-0.06	0.17	-0.06	0.06
0.104	2.65	3.04	-0.42	-0.00	2.68	-0.06	0.17	-0.06	0.06
0.105	2.69	3.04	-0.39	-0.00	2.68	-0.06	0.17	-0.06	0.06
0.106	2.73	3.04	-0.34	-0.00	2.68	-0.06	0.17	-0.06	0.06
0.107	2.75	3.04	-0.29	-0.00	2.68	-0.06	0.17	-0.06	0.06
0.108	2.77	3.03	-0.23	0.00	2.68	-0.06	0.17	-0.06	0.06
0.109	2.76	3.03	-0.15	0.00	2.68	-0.06	0.17	-0.06	0.06
0.110	2.73	3.03	-0.07	0.00	2.68	-0.06	0.17	-0.06	0.06
0.111	2.69	3.03	0.01	0.00	2.68	-0.06	0.17	-0.06	0.06
0.112	2.64	3.03	0.08	0.00	2.68	-0.06	0.17	-0.06	0.06
0.113	2.59	3.04	0.15	-0.00	2.68	-0.06	0.17	-0.06	0.06
0.114	2.54	3.04	0.21	-0.00	2.68	-0.06	0.17	-0.06	0.06
0.115	2.49	3.04	0.26	-0.00	2.68	-0.06	0.17	-0.06	0.06
0.116	2.46	3.04	0.29	-0.00	2.68	-0.06	0.17	-0.06	0.06
0.117	2.43	3.04	0.32	-0.00	2.68	-0.06	0.17	-0.06	0.06
0.118	2.41	3.04	0.33	-0.00	2.68	-0.06	0.17	-0.06	0.06
0.119	2.39	3.04	0.34	0.00	2.68	-0.06	0.17	-0.06	0.06
0.120	2.38	3.03	0.35	0.00	2.68	-0.06	0.17	-0.06	0.06
0.121	2.38	3.03	0.35	0.00	2.68	-0.06	0.17	-0.06	0.06
0.122	2.38	3.03	0.35	0.00	2.68	-0.06	0.17	-0.06	0.06
0.123	2.38	3.04	0.35	0.00	2.68	-0.06	0.17	-0.06	0.06
0.124	2.38	3.04	0.34	0.00	2.68	-0.06	0.17	-0.06	0.06
0.125	2.38	3.04	0.34	-0.00	2.68	-0.06	0.17	-0.06	0.06
0.126	2.38	3.04	0.33	-0.00	2.68	-0.06	0.17	-0.06	0.06
0.127	2.38	3.04	0.33	-0.00	2.68	-0.06	0.17	-0.06	0.06
0.128	2.37	3.04	0.32	-0.00	2.68	-0.06	0.17	-0.06	0.06
0.129	2.37	3.04	0.32	-0.00	2.68	-0.06	0.17	-0.06	0.06
0.130	2.37	3.04	0.31	0.00	2.68	-0.06	0.17	-0.06	0.06
0.131	2.36	3.04	0.30	0.00	2.68	-0.06	0.17	-0.06	0.06
0.132	2.36	3.03	0.30	0.00	2.68	-0.06	0.17	-0.06	0.06

0.133									0.06
0.134									0.06
0.135									0.06
0.136									0.06
0.137									0.06
0.138									0.07
0.139									0.10
0.140									0.14
0.141									0.16
0.142									0.16
0.143									0.15
0.144									0.14
0.145									0.12
0.146									0.11
0.147									0.11
0.148									0.11
0.149									0.11
0.150									0.12
0.151									0.12
0.152									0.12
0.153									0.12
0.154									0.12
0.155									0.12
0.156									0.12
0.157									0.12
0.158									0.12
0.159									0.12
0.160									0.12
0.161									0.12
0.162									0.12
0.164	3.02	3.04	0.34	-0.00	2.34	0.31	-0.17	0.31	0.12
0.165	3.06	3.04	0.36	-0.00	2.34	0.31	-0.17	0.31	0.12
0.166	3.12	3.04	0.37	-0.00	2.34	0.31	-0.17	0.31	0.12
0.167	3.17	3.04	0.37	-0.00	2.34	0.31	-0.17	0.31	0.12
0.168	3.23	3.03	0.35	0.00	2.34	0.31	-0.17	0.31	0.12
0.169	3.28	3.03	0.34	0.00	2.34	0.31	-0.17	0.31	0.12
0.170	3.32	3.03	0.32	0.00	2.34	0.31	-0.17	0.31	0.12
0.171	3.36	3.03	0.30	0.00	2.34	0.31	-0.17	0.31	0.12
0.172	3.39	3.03	0.28	0.00	2.34	0.31	-0.17	0.31	0.12
0.173	3.41	3.03	0.25	0.00	2.34	0.31	-0.17	0.31	0.12
0.174	3.44	3.03	0.23	-0.00	2.34	0.31	-0.17	0.31	0.12
0.175	3.45	3.03	0.20	-0.00	2.34	0.31	-0.17	0.31	0.12
0.176	3.46	3.03	0.16	-0.00	2.34	0.31	-0.17	0.31	0.12
0.177	3.46	3.03	0.13	-0.00	2.34	0.31	-0.17	0.31	0.12
0.178	3.46	3.03	0.09	-0.00	2.34	0.31	-0.17	0.31	0.12
0.179	3.45	3.03	0.04	0.00	2.34	0.31	-0.17	0.31	0.12
0.180	3.43	3.03	-0.00	0.00	2.34	0.31	-0.17	0.31	0.12
0.181	3.41	3.03	-0.06	0.00	2.34	0.31	-0.17	0.31	0.12
0.182	3.39	3.03	-0.11	0.00	2.34	0.31	-0.17	0.31	0.12
0.183	3.36	3.03	-0.16	0.00	2.34	0.31	-0.17	0.31	0.12
0.184	3.33	3.03	-0.22	0.00	2.34	0.31	-0.17	0.31	0.12

Table 2b (2) - Continued

Page 4

0.185	3.30	3.03	-0.27	-0.00	2.34	0.31	-0.17	0.31	0.12
0.186	3.26	3.03	-0.33	-0.00	2.34	0.31	-0.17	0.31	0.12
0.187	3.23	3.03	-0.38	-0.00	2.34	0.31	-0.17	0.31	0.12
0.188	3.20	3.03	-0.43	-0.00	2.34	0.31	-0.17	0.31	0.12
0.189	3.17	3.03	-0.48	-0.00	2.34	0.31	-0.17	0.31	0.12
0.190	3.15	3.03	-0.52	-0.00	2.34	0.31	-0.17	0.31	0.12
0.191	3.12	3.03	-0.56	0.00	2.34	0.31	-0.17	0.31	0.12
0.192	3.10	3.03	-0.59	0.00	2.34	0.31	-0.17	0.31	0.12
0.193	3.08	3.03	-0.62	0.00	2.34	0.31	-0.17	0.31	0.12
0.194	3.06	3.03	-0.64	0.00	2.34	0.31	-0.17	0.31	0.12
0.195	3.05	3.03	-0.66	0.00	2.34	0.31	-0.17	0.31	0.12
0.196	3.04	3.03	-0.68	-0.00	2.34	0.31	-0.17	0.31	0.12
0.197	3.03	3.03	-0.69	-0.00	2.34	0.31	-0.17	0.31	0.12
0.198	3.02	3.03	-0.69	-0.00	2.34	0.31	-0.17	0.31	0.12
0.199									0.12
0.200									0.12
0.201									0.12
0.202									0.12
0.203									0.12
0.204									0.09
0.205									0.08
0.206									0.16
0.207									0.20
0.208									0.21
0.209									0.19
0.210									0.15
0.211									0.12
0.212									0.10
0.213									0.09
0.214									0.09
0.215									0.10
0.216									0.11
0.217									0.12
0.218									0.13
0.219									0.13
0.220									0.13
0.221									0.12
0.222									0.12
0.223									0.12
0.224									0.12
0.225									0.12
0.226									0.12
0.227									0.12
0.228									0.12
0.229	3.19	3.03	-0.22	0.01	3.05	-0.74	0.54	-0.74	0.12
0.231	3.01	3.03	-0.26	0.01	3.05	-0.74	0.54	-0.74	0.12
0.232	2.85	3.03	-0.29	0.01	3.05	-0.74	0.54	-0.74	0.12
0.233	2.74	3.03	-0.31	0.00	3.05	-0.74	0.54	-0.74	0.12
0.234	2.66	3.03	-0.35	-0.00	3.05	-0.74	0.54	-0.74	0.12
0.235	2.62	3.04	-0.40	-0.00	3.05	-0.74	0.54	-0.74	0.12
0.236	2.63	3.04	-0.44	-0.00	3.05	-0.74	0.54	-0.74	0.12

0.237	2.66	3.04	-0.47	-0.00	3.05	-0.74	0.54	-0.74	0.12
0.238	2.71	3.03	-0.51	-0.00	3.05	-0.74	0.54	-0.74	0.12
0.239	2.76	3.03	-0.54	-0.00	3.05	-0.74	0.54	-0.74	0.12
0.240	2.80	3.03	-0.56	0.00	3.05	-0.74	0.54	-0.74	0.12
0.241	2.84	3.03	-0.57	0.00	3.05	-0.74	0.54	-0.74	0.12
0.242	2.88	3.03	-0.58	0.00	3.05	-0.74	0.54	-0.74	0.12
0.243	2.91	3.03	-0.59	0.00	3.05	-0.74	0.54	-0.74	0.12
0.244	2.94	3.03	-0.59	0.00	3.05	-0.74	0.54	-0.74	0.12
0.245	2.96	3.03	-0.59	0.00	3.05	-0.74	0.54	-0.74	0.12
0.246	2.98	3.03	-0.59	-0.00	3.05	-0.74	0.54	-0.74	0.12
0.247	3.00	3.03	-0.58	-0.00	3.05	-0.74	0.54	-0.74	0.12
0.248	3.01	3.03	-0.58	-0.00	3.05	-0.74	0.54	-0.74	0.12
0.249	3.02	3.03	-0.58	-0.00	3.05	-0.74	0.54	-0.74	0.12
0.250	3.03	3.03	-0.57	-0.00	3.05	-0.74	0.54	-0.74	0.12
0.251	3.03	3.03	-0.57	0.00	3.05	-0.74	0.54	-0.74	0.12
0.252	3.04	3.03	-0.57	0.00	3.05	-0.74	0.54	-0.74	0.12
0.253	3.04	3.03	-0.57	0.00	3.05	-0.74	0.54	-0.74	0.12
0.254	3.04	3.03	-0.57	0.00	3.05	-0.74	0.54	-0.74	0.12
0.255	3.04	3.03	-0.57	0.00	3.05	-0.74	0.54	-0.74	0.12
0.256	3.04	3.03	-0.57	0.00	3.05	-0.74	0.54	-0.74	0.12
0.257	3.04	3.03	-0.58	-0.00	3.05	-0.74	0.54	-0.74	0.12
0.258	3.03	3.03	-0.58	-0.00	3.05	-0.74	0.54	-0.74	0.12
0.259	3.03	3.03	-0.59	-0.00	3.05	-0.74	0.54	-0.74	0.12
0.260	3.03	3.03	-0.59	-0.00	3.05	-0.74	0.54	-0.74	0.12
0.261	3.02	3.03	-0.60	-0.00	3.05	-0.74	0.54	-0.74	0.12
0.262	3.02	3.03	-0.60	0.00	3.05	-0.74	0.54	-0.74	0.12
0.263	3.01	3.03	-0.61	0.00	3.05	-0.74	0.54	-0.74	0.12
0.264	3.00	3.03	-0.61	0.00	3.05	-0.74	0.54	-0.74	0.12
0.265									0.12
0.266									0.12
0.267									0.12
0.268									0.12
0.269									0.12
0.270									0.11
0.271									0.10
0.272									0.09
0.273									0.09
0.274									0.09
0.275									0.09
0.276									0.09
0.277									0.10
0.278									0.10
0.279									0.10
0.280									0.10
0.281									0.10
0.282									0.10
0.283									0.10
0.284									0.10
0.285									0.10
0.286									0.10
0.287									0.10

Table 2b (2) - Continued

Page 6

0.285									0.10
0.289									0.10
0.290									0.10
0.291									0.10
0.292									0.10
0.293									0.10
0.294									0.10
0.296	3.13	3.03	-0.54	-0.00	3.00	-0.61	0.50	-0.61	0.10
0.297	3.13	3.03	-0.53	-0.00	3.00	-0.60	0.50	-0.60	0.10
0.298	3.13	3.03	-0.51	-0.00	3.00	-0.60	0.50	-0.60	0.10
0.299	3.13	3.03	-0.49	-0.00	3.00	-0.60	0.50	-0.60	0.10
0.300	3.12	3.03	-0.47	0.00	3.00	-0.60	0.50	-0.60	0.10
0.301	3.11	3.03	-0.46	0.00	3.00	-0.60	0.50	-0.60	0.10
0.302	3.09	3.03	-0.44	0.00	3.00	-0.60	0.50	-0.60	0.10
0.303	3.07	3.03	-0.42	0.00	3.00	-0.60	0.50	-0.60	0.10
0.304	3.05	3.03	-0.40	0.00	3.00	-0.60	0.50	-0.60	0.10
0.305	3.03	3.03	-0.38	0.00	3.00	-0.60	0.50	-0.60	0.10
0.306	3.00	3.03	-0.36	-0.00	3.00	-0.60	0.50	-0.60	0.10
0.307	2.98	3.03	-0.34	-0.00	3.00	-0.60	0.50	-0.60	0.10
0.308	2.95	3.03	-0.32	-0.00	3.00	-0.60	0.50	-0.60	0.10
0.309	2.93	3.03	-0.30	-0.00	3.00	-0.60	0.50	-0.60	0.10
0.310	2.90	3.03	-0.28	-0.00	3.00	-0.60	0.50	-0.60	0.10
0.311	2.88	3.03	-0.25	-0.00	3.00	-0.60	0.50	-0.60	0.10
0.312	2.85	3.03	-0.23	0.00	3.00	-0.60	0.50	-0.60	0.10
0.313	2.83	3.03	-0.21	0.00	3.00	-0.60	0.50	-0.60	0.10
0.314	2.81	3.03	-0.18	0.00	3.00	-0.60	0.50	-0.60	0.10
0.315	2.79	3.03	-0.16	0.00	3.00	-0.60	0.50	-0.60	0.10
0.316	2.77	3.03	-0.14	0.00	3.00	-0.60	0.50	-0.60	0.10
0.317	2.75	3.03	-0.11	-0.00	3.00	-0.60	0.50	-0.60	0.10
0.318	2.73	3.03	-0.09	-0.00	3.00	-0.60	0.50	-0.60	0.10
0.319	2.72	3.03	-0.07	-0.00	3.00	-0.60	0.50	-0.60	0.10
0.320	2.70	3.03	-0.05	-0.00	3.00	-0.60	0.50	-0.60	0.10
0.321	2.69	3.03	-0.03	-0.00	3.00	-0.60	0.50	-0.60	0.10
0.322	2.68	3.03	-0.02	-0.00	3.00	-0.60	0.50	-0.60	0.10
0.323	2.67	3.03	-0.00	0.00	3.00	-0.60	0.50	-0.60	0.10
0.324	2.66	3.03	0.00	0.00	3.00	-0.60	0.50	-0.60	0.10
0.325	2.65	3.03	0.01	0.00	3.00	-0.60	0.50	-0.60	0.10
0.326	2.65	3.03	0.01	0.00	3.00	-0.60	0.50	-0.60	0.10
0.327	2.65	3.03	0.01	0.00	3.00	-0.60	0.50	-0.60	0.10
0.328	2.65	3.03	0.01	-0.00	3.00	-0.60	0.50	-0.60	0.10
0.329	2.65	3.03	0.00	-0.00	3.00	-0.60	0.50	-0.60	0.10
0.330	2.66	3.03	-0.00	-0.00	3.00	-0.60	0.50	-0.60	0.10
0.331									0.10
0.332									0.10
0.333									0.10
0.334									0.10
0.335									0.10
0.336									0.08
0.337									0.08
0.338									0.08
0.339									0.10

0.340									0.11
0.341									0.10
0.342									0.08
0.343									0.06
0.344									0.06
0.345									0.05
0.346									0.05
0.347									0.06
0.348									0.06
0.349									0.06
0.350									0.07
0.351									0.07
0.352									0.07
0.353									0.06
0.354									0.06
0.355									0.06
0.356									0.06
0.357									0.06
0.358									0.06
0.359									0.06
0.360									0.06
0.362	3.04	3.03	0.35	-0.01	2.64	C.C2	0.14	0.02	0.06
0.363	3.06	3.03	0.28	-0.01	2.64	C.C2	0.14	0.02	0.06
0.364	3.07	3.03	0.21	-0.00	2.64	C.C2	0.14	0.02	0.06
0.365	3.09	3.03	0.13	-0.00	2.64	C.C2	0.14	0.02	0.06
0.366	3.12	3.03	0.06	0.00	2.64	C.C3	0.13	0.03	0.06
0.367	3.18	3.03	-0.00	0.00	2.64	C.C3	0.13	0.03	0.06
0.368	3.24	3.03	-0.06	0.00	2.64	C.C3	0.13	0.03	0.06
0.369	3.30	3.03	-0.11	0.00	2.64	C.C3	0.13	0.03	0.06
0.370	3.37	3.03	-0.15	0.00	2.64	C.C3	0.13	0.03	0.06
0.371	3.44	3.03	-0.18	0.00	2.64	C.C2	0.13	0.02	0.06
0.372	3.50	3.03	-0.20	-0.00	2.64	C.C2	0.14	0.02	0.06
0.373	3.57	3.03	-0.21	-0.00	2.64	C.C2	0.14	0.02	0.06
0.374	3.62	3.03	-0.22	-0.00	2.64	C.C2	0.14	0.02	0.06
0.375	3.68	3.03	-0.22	-0.00	2.64	C.C2	0.14	0.02	0.06
0.376	3.72	3.03	-0.22	-0.00	2.64	C.C2	0.14	0.02	0.06
0.377	3.77	3.03	-0.22	-0.00	2.64	C.C2	0.14	0.02	0.06
0.378	3.80	3.03	-0.21	0.00	2.64	C.C2	0.14	0.02	0.06
0.379	3.84	3.03	-0.21	0.00	2.64	C.C2	0.14	0.02	0.06
0.380	3.87	3.03	-0.20	0.00	2.64	C.C2	0.14	0.02	0.06
0.381	3.89	3.03	-0.19	0.00	2.64	C.C2	0.14	0.02	0.06
0.382	3.91	3.03	-0.19	0.00	2.64	C.C2	0.14	0.02	0.06
0.383	3.93	3.03	-0.18	-0.00	2.64	C.C2	0.14	0.02	0.06
0.384	3.94	3.03	-0.18	-0.00	2.64	C.C2	0.14	0.02	0.06
0.385	3.96	3.03	-0.18	-0.00	2.64	C.C2	0.14	0.02	0.06
0.386	3.96	3.03	-0.17	-0.00	2.64	C.C2	0.14	0.02	0.06
0.387	3.97	3.03	-0.17	-0.00	2.64	C.C2	0.14	0.02	0.06
0.388	3.97	3.03	-0.17	-0.00	2.64	C.C2	0.14	0.02	0.06
0.389	3.96	3.03	-0.17	0.00	2.64	C.C2	0.14	0.02	0.06
0.390	3.96	3.03	-0.17	0.00	2.64	C.C2	0.14	0.02	0.06
0.391	3.94	3.03	-0.17	0.00	2.64	C.C2	0.14	0.02	0.06

Table 2b (2) - Continued

Page 8

0.392	1.93	1.03	-0.17	0.00	2.64	0.02	0.14	0.02	0.06
0.393	1.91	1.03	-0.17	0.00	2.64	0.02	0.14	0.02	0.06
0.394	1.89	1.03	-0.17	-0.00	2.64	0.02	0.14	0.02	0.06
0.395	1.87	1.03	-0.17	-0.00	2.64	0.02	0.14	0.02	0.06
0.396	1.84	1.03	-0.17	-0.00	2.64	0.02	0.14	0.02	0.06
0.397									0.06
0.398									0.06
0.399									0.06
0.400									0.06
0.401									0.06
0.402									0.06
0.403									0.06
0.404									0.19
0.405									0.24
0.406									0.25
0.407									0.22
0.408									0.18
0.409									0.15
0.410									0.12
0.411									0.11
0.412									0.11
0.413									0.12
0.414									0.13
0.415									0.14
0.416									0.15
0.417									0.15
0.418									0.15
0.419									0.15
0.420									0.14
0.421									0.14
0.422									0.14
0.423									0.14
0.424									0.14
0.425									0.14
0.426									0.14
0.428	1.41	1.02	-0.41	0.00	1.90	-0.18	1.40	-0.18	0.14
0.429	1.76	1.02	0.04	0.00	1.90	-0.18	1.40	-0.18	0.14
0.430	1.54	1.02	0.29	0.00	1.90	-0.18	1.40	-0.18	0.14
0.431	1.36	1.03	0.25	0.00	1.90	-0.18	1.40	-0.18	0.14
0.432	1.29	1.03	0.22	-0.00	1.90	-0.18	1.40	-0.18	0.14
0.433	1.27	1.03	0.22	-0.00	1.90	-0.18	1.40	-0.18	0.14
0.434	1.28	1.03	0.24	-0.00	1.90	-0.18	1.40	-0.18	0.14
0.435	1.33	1.03	0.25	-0.00	1.90	-0.18	1.40	-0.18	0.14
0.436	1.44	1.03	0.23	-0.00	1.90	-0.18	1.40	-0.18	0.14
0.437	1.58	1.03	0.17	-0.00	1.90	-0.18	1.40	-0.18	0.14
0.438	1.74	1.03	0.08	0.00	1.90	-0.18	1.40	-0.18	0.14
0.439	1.87	1.03	-0.02	0.00	1.90	-0.18	1.40	-0.18	0.14
0.440	1.99	1.03	-0.10	0.00	1.90	-0.18	1.40	-0.18	0.14
0.441	2.05	1.03	-0.17	0.00	1.90	-0.18	1.40	-0.18	0.14
0.442	2.11	1.03	-0.22	0.00	1.90	-0.18	1.40	-0.18	0.14
0.443	2.15	1.03	-0.26	0.00	1.90	-0.18	1.40	-0.18	0.14

0.444	2.18	3.03	-0.29	-0.00	3.90	-0.18	1.40	-0.18	0.14
0.445	2.20	3.03	-0.32	-0.00	3.90	-0.18	1.40	-0.18	0.14
0.446	2.21	3.03	-0.34	-0.00	3.90	-0.18	1.40	-0.18	0.14
0.447	2.22	3.03	-0.35	-0.00	3.90	-0.18	1.40	-0.18	0.14
0.448	2.22	3.03	-0.36	-0.00	3.90	-0.18	1.40	-0.18	0.14
0.449	2.22	3.03	-0.37	0.00	3.90	-0.18	1.40	-0.18	0.14
0.450	2.22	3.03	-0.38	0.00	3.90	-0.18	1.40	-0.18	0.14
0.451	2.22	3.03	-0.39	0.00	3.90	-0.18	1.40	-0.18	0.14
0.452	2.23	3.03	-0.39	0.00	3.90	-0.18	1.40	-0.18	0.14
0.453	2.23	3.03	-0.40	0.00	3.90	-0.18	1.40	-0.18	0.14
0.454	2.23	3.03	-0.40	0.00	3.90	-0.18	1.40	-0.18	0.14
0.455	2.23	3.03	-0.41	-0.00	3.90	-0.18	1.40	-0.18	0.14
0.456	2.24	3.03	-0.41	-0.00	3.90	-0.18	1.40	-0.18	0.14
0.457	2.24	3.03	-0.41	-0.00	3.90	-0.18	1.40	-0.18	0.14
0.458	2.25	3.03	-0.42	-0.00	3.90	-0.18	1.40	-0.18	0.14
0.459	2.25	3.03	-0.42	-0.00	3.90	-0.19	1.40	-0.18	0.14
0.460	2.26	3.03	-0.43	0.00	3.90	-0.18	1.40	-0.18	0.14
0.461	2.27	3.03	-0.43	0.00	3.90	-0.18	1.40	-0.18	0.14
0.462	2.28	3.03	-0.44	0.00	3.90	-0.18	1.40	-0.18	0.14
0.463									0.14
0.464									0.14
0.465									0.14
0.466									0.14
0.467									0.14
0.468									0.10
0.469									0.09
0.470									0.21
0.471									0.27
0.472									0.29
0.473									0.26
0.474									0.20
0.475									0.16
0.476									0.12
0.477									0.11
0.478									0.11
0.479									0.12
0.480									0.14
0.481									0.15
0.482									0.16
0.483									0.17
0.484									0.16
0.485									0.16
0.486									0.15
0.487									0.15
0.488									0.15
0.489									0.15
0.490									0.15
0.491									0.15
0.492									0.15
0.494	3.16	3.04	0.58	0.00	2.21	-0.45	-0.29	-0.45	0.15
0.495	3.24	3.04	0.48	0.00	2.21	-0.45	-0.29	-0.45	0.15

Table 2b (2) - Continued

Page 10

0.496	3.31	3.04	0.40	0.00	2.21	-0.45	-0.29	-0.45	0.15
0.497	3.37	3.03	0.30	0.00	2.21	-0.45	-0.30	-0.45	0.15
0.498	3.41	3.03	0.16	-0.00	2.20	-0.45	-0.30	-0.45	0.15
0.499	3.44	3.03	0.04	-0.00	2.20	-0.45	-0.30	-0.45	0.15
0.500	3.45	3.02	-0.05	-0.00	2.20	-0.45	-0.30	-0.45	0.15
0.501	3.45	3.03	-0.14	-0.00	2.20	-0.45	-0.30	-0.45	0.15

Table 2b (3)

TIME (SEC)	MLD		NUD		MUT	MUT	MUG	MLG	MISS (P)
	EST	TRUE	EST	TRUE					
0.032	3.39	3.05	-0.42	0.00	0.32	0.00	-2.20	0.00	0.43
0.033	3.36	3.04	-0.43	0.00	0.32	-0.00	-2.20	-0.00	0.43
0.034	3.33	3.04	-0.44	-0.00	0.31	-0.00	-2.20	-0.00	0.43
0.035	3.29	3.04	-0.42	-0.00	0.31	-0.00	-2.20	-0.00	0.43
0.036	3.27	3.03	-0.40	-0.00	0.31	-0.00	-2.20	-0.00	0.43
0.037	3.25	3.03	-0.37	-0.00	0.31	-0.00	-2.20	-0.00	0.43
0.038	3.24	3.03	-0.31	-0.00	0.31	-0.00	-2.20	-0.00	0.43
0.039	3.24	3.03	-0.25	0.00	0.31	0.00	-2.20	0.00	0.43
0.040	3.24	3.04	-0.18	0.00	0.31	0.00	-2.20	0.00	0.43
0.041	3.25	3.04	-0.11	0.00	0.31	0.00	-2.20	0.00	0.43
0.042	3.25	3.04	-0.04	0.00	0.31	0.00	-2.20	0.00	0.43
0.043	3.27	3.04	0.02	0.00	0.31	0.00	-2.20	0.00	0.43
0.044	3.28	3.04	0.08	0.00	0.31	0.00	-2.20	0.00	0.43
0.045	3.29	3.04	0.13	-0.00	0.31	-0.00	-2.20	-0.00	0.43
0.046	3.31	3.04	0.17	-0.00	0.31	-0.00	-2.20	-0.00	0.43
0.047	3.32	3.04	0.20	-0.00	0.31	-0.00	-2.20	-0.00	0.43
0.048	3.34	3.04	0.23	-0.00	0.31	-0.00	-2.20	-0.00	0.43
0.049	3.35	3.04	0.25	-0.00	0.31	-0.00	-2.20	-0.00	0.43
0.050	3.37	3.04	0.26	0.00	0.31	0.00	-2.20	0.00	0.43
0.051	3.38	3.04	0.27	0.00	0.31	0.00	-2.20	0.00	0.43
0.052	3.39	3.04	0.27	0.00	0.31	0.00	-2.20	0.00	0.43
0.053	3.41	3.04	0.27	0.00	0.31	0.00	-2.20	0.00	0.43
0.054	3.42	3.04	0.27	0.00	0.31	0.00	-2.20	0.00	0.43
0.055	3.43	3.04	0.27	0.00	0.31	0.00	-2.20	0.00	0.43
0.056	3.44	3.04	0.27	-0.00	0.31	-0.00	-2.20	-0.00	0.43
0.057	3.45	3.04	0.27	-0.00	0.31	-0.00	-2.20	-0.00	0.43
0.058	3.46	3.04	0.27	-0.00	0.31	-0.00	-2.20	-0.00	0.43
0.059	3.47	3.04	0.28	-0.00	0.31	-0.00	-2.20	-0.00	0.43
0.060	3.48	3.04	0.28	-0.00	0.31	-0.00	-2.20	-0.00	0.43
0.061	3.50	3.04	0.29	-0.00	0.31	-0.00	-2.20	-0.00	0.43
0.062	3.51	3.04	0.29	0.00	0.31	0.00	-2.20	0.00	0.43
0.063	3.52	3.04	0.30	0.00	0.31	0.00	-2.20	0.00	0.43
0.064	3.54	3.04	0.30	0.00	0.31	0.00	-2.20	0.00	0.43
0.065	3.55	3.04	0.30	0.00	0.31	0.00	-2.20	0.00	0.43
0.066	3.56	3.04	0.30	0.00	0.31	0.00	-2.20	0.00	0.43
0.067									0.43
0.068									0.43
0.069									0.43
0.070									0.43
0.071									0.43
0.072									0.33
0.073									0.04
0.074									0.24
0.075									0.37
0.076									0.39
0.077									0.33
0.078									0.23
0.079									0.13
0.080									0.06

Table 2b (3) - Continued

Page 2

0.081									0.04
0.082									0.05
0.083									0.07
0.084									0.10
0.085									0.13
0.086									0.14
0.087									0.15
0.088									0.14
0.089									0.13
0.090									0.12
0.091									0.11
0.092									0.11
0.093									0.11
0.094									0.11
0.095									0.12
0.096									0.12
0.098	1.04	3.04	0.42	-0.00	3.71	0.32	1.19	0.32	0.12
0.099	1.38	3.01	0.24	-0.00	3.71	0.32	1.20	0.32	0.12
0.100	1.64	3.02	-0.04	-0.00	3.71	0.32	1.20	0.32	0.12
0.101	1.52	3.03	-0.03	-0.00	3.71	0.32	1.20	0.32	0.12
0.102	1.46	3.04	-0.00	0.00	3.71	0.32	1.20	0.32	0.12
0.103	1.46	3.04	-0.00	0.00	3.72	0.32	1.21	0.32	0.12
0.104	1.49	3.05	-0.03	0.00	3.72	0.32	1.21	0.32	0.12
0.105	1.54	3.04	-0.06	0.00	3.72	0.32	1.21	0.32	0.12
0.106	1.62	3.04	-0.11	0.00	3.71	0.32	1.20	0.32	0.12
0.107	1.70	3.04	-0.15	0.00	3.71	0.32	1.20	0.32	0.12
0.108	1.79	3.03	-0.16	-0.00	3.71	0.32	1.20	0.32	0.12
0.109	1.87	3.03	-0.21	-0.00	3.71	0.32	1.20	0.32	0.12
0.110	1.96	3.03	-0.22	-0.00	3.71	0.32	1.20	0.32	0.12
0.111	2.06	3.03	-0.24	-0.00	3.71	0.32	1.20	0.32	0.12
0.112	2.15	3.03	-0.25	-0.00	3.71	0.32	1.20	0.32	0.12
0.113	2.25	3.04	-0.25	0.00	3.71	0.32	1.20	0.32	0.12
0.114	2.34	3.04	-0.25	0.00	3.71	0.32	1.20	0.32	0.12
0.115	2.42	3.04	-0.25	0.00	3.71	0.32	1.20	0.32	0.12
0.116	2.50	3.04	-0.24	0.00	3.71	0.32	1.20	0.32	0.12
0.117	2.55	3.04	-0.23	0.00	3.71	0.32	1.20	0.32	0.12
0.118	2.60	3.04	-0.22	0.00	3.71	0.32	1.20	0.32	0.12
0.119	2.64	3.04	-0.21	-0.00	3.71	0.32	1.20	0.32	0.12
0.120	2.65	3.03	-0.20	-0.00	3.71	0.32	1.20	0.32	0.12
0.121	2.66	3.03	-0.19	-0.00	3.71	0.32	1.20	0.32	0.12
0.122	2.67	3.03	-0.19	-0.00	3.71	0.32	1.20	0.32	0.12
0.123	2.66	3.03	-0.18	-0.00	3.71	0.32	1.20	0.32	0.12
0.124	2.65	3.04	-0.17	-0.00	3.71	0.32	1.20	0.32	0.12
0.125	2.63	3.04	-0.17	0.00	3.71	0.32	1.20	0.32	0.12
0.126	2.60	3.04	-0.16	0.00	3.71	0.32	1.20	0.32	0.12
0.127	2.57	3.04	-0.16	0.00	3.71	0.32	1.20	0.32	0.12
0.128	2.54	3.04	-0.15	0.00	3.71	0.32	1.20	0.32	0.12
0.129	2.51	3.04	-0.15	0.00	3.71	0.32	1.20	0.32	0.12
0.130	2.47	3.04	-0.15	-0.00	3.71	0.32	1.20	0.32	0.12
0.131	2.44	3.04	-0.14	-0.00	3.71	0.32	1.20	0.32	0.12
0.132	2.40	3.03	-0.14	-0.00	3.71	0.32	1.20	0.32	0.12

0.133									0.12
0.134									0.12
0.135									0.12
0.136									0.12
0.137									0.12
0.138									0.07
0.139									0.06
0.140									0.16
0.141									0.22
0.142									0.23
0.143									0.20
0.144									0.16
0.145									0.12
0.146									0.09
0.147									0.07
0.148									0.06
0.149									0.09
0.150									0.10
0.151									0.12
0.152									0.12
0.153									0.13
0.154									0.13
0.155									0.12
0.156									0.12
0.157									0.11
0.158									0.11
0.159									0.11
0.160									0.11
0.161									0.11
0.162									0.11
0.164	3.47	3.05	0.20	0.00	2.34	-0.16	-0.17	-0.16	0.12
0.165	3.49	3.05	0.18	0.00	2.34	-0.16	-0.17	-0.16	0.12
0.166	3.50	3.04	0.16	0.00	2.34	-0.16	-0.17	-0.16	0.11
0.167	3.51	3.04	0.14	0.00	2.34	-0.16	-0.17	-0.16	0.11
0.168	3.52	3.03	0.13	-0.00	2.34	-0.16	-0.17	-0.16	0.11
0.169	3.54	3.03	0.11	-0.00	2.34	-0.16	-0.17	-0.16	0.11
0.170	3.56	3.03	0.10	-0.00	2.34	-0.16	-0.17	-0.16	0.11
0.171	3.57	3.03	0.09	-0.00	2.34	-0.16	-0.17	-0.16	0.11
0.172	3.57	3.03	0.08	-0.00	2.34	-0.16	-0.17	-0.16	0.11
0.173	3.53	3.03	0.08	-0.00	2.34	-0.16	-0.17	-0.16	0.11
0.174	3.43	3.04	0.10	0.00	2.34	-0.16	-0.17	-0.16	0.11
0.175	3.31	3.04	0.13	0.00	2.34	-0.16	-0.17	-0.16	0.11
0.176	3.18	3.04	0.16	0.00	2.34	-0.16	-0.17	-0.16	0.11
0.177	3.10	3.04	0.18	0.00	2.34	-0.16	-0.17	-0.16	0.11
0.178	3.06	3.03	0.19	0.00	2.34	-0.16	-0.17	-0.16	0.11
0.179	3.06	3.03	0.19	-0.00	2.34	-0.16	-0.17	-0.16	0.11
0.180	3.07	3.03	0.19	-0.00	2.34	-0.16	-0.17	-0.16	0.11
0.181	3.08	3.03	0.18	-0.00	2.34	-0.16	-0.17	-0.16	0.11
0.182	3.10	3.03	0.17	-0.00	2.34	-0.16	-0.17	-0.16	0.11
0.183	3.12	3.03	0.17	-0.00	2.34	-0.16	-0.17	-0.16	0.11
0.184	3.14	3.03	0.16	-0.00	2.34	-0.16	-0.17	-0.16	0.11

Table 2b (3) - Continued

Page 4

0.185	3.15	3.03	0.15	0.00	2.34	-0.16	-0.17	-0.16	0.11
0.186	3.17	3.03	0.15	0.00	2.34	-0.16	-0.17	-0.16	0.11
0.187	3.18	3.03	0.14	0.00	2.34	-0.16	-0.17	-0.16	0.11
0.188	3.20	3.03	0.14	0.00	2.34	-0.16	-0.17	-0.16	0.11
0.189	3.21	3.03	0.14	0.00	2.34	-0.16	-0.17	-0.16	0.11
0.190	3.22	3.03	0.14	0.00	2.34	-0.16	-0.17	-0.16	0.11
0.191	3.23	3.03	0.13	-0.00	2.34	-0.16	-0.17	-0.16	0.11
0.192	3.24	3.03	0.13	-0.00	2.34	-0.16	-0.17	-0.16	0.11
0.193	3.25	3.03	0.13	-0.00	2.34	-0.16	-0.17	-0.16	0.11
0.194	3.26	3.03	0.13	-0.00	2.34	-0.16	-0.17	-0.16	0.11
0.195	3.26	3.03	0.13	-0.00	2.34	-0.16	-0.17	-0.16	0.11
0.196	3.25	3.03	0.13	0.00	2.34	-0.16	-0.17	-0.16	0.11
0.197	3.24	3.03	0.12	0.00	2.34	-0.16	-0.17	-0.16	0.11
0.198	3.23	3.03	0.12	0.00	2.34	-0.16	-0.17	-0.16	0.11
0.199									0.11
0.200									0.11
0.201									0.11
0.202									0.11
0.203									0.11
0.204									0.36
0.205									0.01
0.206									0.06
0.207									0.12
0.208									0.12
0.209									0.10
0.210									0.06
0.211									0.35
0.212									0.35
0.213									0.32
0.214									0.32
0.215									0.03
0.216									0.34
0.217									0.05
0.218									0.35
0.219									0.05
0.220									0.35
0.221									0.35
0.222									0.34
0.223									0.34
0.224									0.34
0.225									0.34
0.226									0.34
0.227									0.34
0.228									0.34
0.230	2.73	3.03	0.43	-0.00	3.27	0.13	0.76	0.13	0.04
0.231	2.65	3.03	0.43	-0.00	3.27	0.13	0.76	0.13	0.34
0.232	2.54	3.03	0.44	-0.00	3.27	0.13	0.76	0.13	0.04
0.233	2.44	3.03	0.46	-0.00	3.27	0.13	0.76	0.13	0.04
0.234	2.38	3.03	0.47	0.00	3.27	0.13	0.77	0.13	0.04
0.235	2.33	3.04	0.48	0.00	3.27	0.13	0.77	0.13	0.04
0.236	2.30	3.04	0.50	0.00	3.27	0.13	0.77	0.13	0.04

0.237	2.29	3.04	0.52	0.00	3.27	0.13	0.77	0.13	0.04
0.238	2.27	3.03	0.53	0.00	3.27	0.13	0.77	0.13	0.04
0.239	2.26	3.03	0.54	0.00	3.27	0.13	0.77	0.13	0.04
0.240	2.25	3.03	0.56	-0.00	3.27	0.13	0.77	0.13	0.04
0.241	2.24	3.03	0.57	-0.00	3.27	0.13	0.77	0.13	0.04
0.242	2.22	3.03	0.57	-0.00	3.27	0.13	0.77	0.13	0.04
0.243	2.21	3.03	0.57	-0.00	3.27	0.13	0.77	0.13	0.04
0.244	2.19	3.03	0.57	-0.00	3.27	0.13	0.77	0.13	0.04
0.245	2.18	3.03	0.56	-0.00	3.27	0.13	0.77	0.13	0.04
0.246	2.17	3.03	0.54	0.00	3.27	0.13	0.77	0.13	0.04
0.247	2.16	3.03	0.51	0.00	3.27	0.13	0.77	0.13	0.04
0.248	2.16	3.03	0.47	0.00	3.27	0.13	0.77	0.13	0.04
0.249	2.17	3.03	0.43	0.00	3.27	0.13	0.77	0.13	0.04
0.250	2.19	3.03	0.37	0.00	3.27	0.13	0.77	0.13	0.04
0.251	2.22	3.03	0.31	-0.00	3.27	0.13	0.77	0.13	0.04
0.252	2.26	3.03	0.23	-0.00	3.27	0.13	0.77	0.13	0.04
0.253	2.31	3.03	0.16	-0.00	3.27	0.13	0.77	0.13	0.04
0.254	2.36	3.03	0.09	-0.00	3.27	0.13	0.77	0.13	0.04
0.255	2.43	3.03	0.02	-0.00	3.27	0.13	0.77	0.13	0.04
0.256	2.49	3.03	-0.04	-0.00	3.27	0.13	0.77	0.13	0.04
0.257	2.56	3.03	-0.09	0.00	3.27	0.13	0.77	0.13	0.04
0.258	2.62	3.03	-0.13	0.00	3.27	0.13	0.77	0.13	0.04
0.259	2.68	3.03	-0.16	0.00	3.27	0.13	0.77	0.13	0.04
0.260	2.74	3.03	-0.19	0.00	3.27	0.13	0.77	0.13	0.04
0.261	2.79	3.03	-0.20	0.00	3.27	0.13	0.77	0.13	0.04
0.262	2.83	3.03	-0.20	-0.00	3.27	0.13	0.77	0.13	0.04
0.263	2.88	3.03	-0.20	-0.00	3.27	0.13	0.77	0.13	0.04
0.264	2.91	3.03	-0.19	-0.00	3.27	0.13	0.77	0.13	0.04
0.265									0.04
0.266									0.04
0.267									0.04
0.268									0.04
0.269									0.04
0.270									0.03
0.271									0.02
0.272									0.06
0.273									0.06
0.274									0.06
0.275									0.07
0.276									0.06
0.277									0.04
0.278									0.03
0.279									0.03
0.280									0.03
0.281									0.03
0.282									0.04
0.283									0.04
0.284									0.04
0.285									0.04
0.286									0.04
0.287									0.04

Table 2b (3) - Continued

Page 6

0.248								0.04	
0.249								0.04	
0.250								0.04	
0.251								0.04	
0.252								0.04	
0.253								0.04	
0.254								0.04	
0.256	2.24	3.04	0.12	0.00	2.50	-0.20	0.39	-0.20	0.04
0.257	2.25	3.04	0.14	0.00	2.50	-0.20	0.39	-0.20	0.04
0.258	2.24	3.03	0.15	0.00	2.50	-0.20	0.39	-0.20	0.04
0.259	2.25	3.03	0.16	0.00	2.50	-0.20	0.39	-0.20	0.04
0.300	2.26	3.03	0.17	-0.00	2.50	-0.20	0.39	-0.20	0.04
0.301	2.27	3.03	0.17	-0.00	2.50	-0.20	0.39	-0.20	0.04
0.302	2.28	3.03	0.17	-0.00	2.50	-0.20	0.39	-0.20	0.04
0.303	2.29	3.03	0.16	-0.00	2.50	-0.20	0.39	-0.20	0.04
0.304	2.31	3.03	0.14	-0.00	2.50	-0.20	0.39	-0.20	0.04
0.305	2.32	3.03	0.11	-0.00	2.50	-0.20	0.39	-0.20	0.04
0.306	2.34	3.03	0.07	0.00	2.50	-0.20	0.39	-0.20	0.04
0.307	2.34	3.03	0.02	0.00	2.50	-0.20	0.39	-0.20	0.04
0.308	2.33	3.03	-0.03	0.00	2.50	-0.20	0.39	-0.20	0.04
0.309	2.31	3.03	-0.06	0.00	2.50	-0.20	0.39	-0.20	0.04
0.310	2.28	3.03	-0.13	0.00	2.50	-0.20	0.39	-0.20	0.04
0.311	2.23	3.03	-0.16	0.00	2.50	-0.20	0.39	-0.20	0.04
0.312	2.17	3.03	-0.23	-0.00	2.50	-0.20	0.39	-0.20	0.04
0.313	2.10	3.03	-0.28	-0.00	2.50	-0.20	0.39	-0.20	0.04
0.314	2.01	3.03	-0.32	-0.00	2.50	-0.20	0.39	-0.20	0.04
0.315	2.53	3.03	-0.35	-0.00	2.50	-0.20	0.39	-0.20	0.04
0.316	2.64	3.03	-0.39	-0.00	2.50	-0.20	0.39	-0.20	0.04
0.317	2.76	3.03	-0.41	0.00	2.50	-0.20	0.39	-0.20	0.04
0.318	2.68	3.03	-0.43	0.00	2.50	-0.20	0.39	-0.20	0.04
0.319	2.61	3.03	-0.45	0.00	2.50	-0.20	0.39	-0.20	0.04
0.320	2.55	3.03	-0.47	0.00	2.50	-0.20	0.39	-0.20	0.04
0.321	2.49	3.03	-0.48	0.00	2.50	-0.20	0.39	-0.20	0.04
0.322	2.45	3.03	-0.49	0.00	2.50	-0.20	0.39	-0.20	0.04
0.323	2.41	3.03	-0.50	-0.00	2.50	-0.20	0.39	-0.20	0.04
0.324	2.38	3.03	-0.51	-0.00	2.50	-0.20	0.39	-0.20	0.04
0.325	2.36	3.03	-0.51	-0.00	2.50	-0.20	0.39	-0.20	0.04
0.326	2.34	3.03	-0.52	-0.00	2.50	-0.20	0.39	-0.20	0.04
0.327	2.32	3.03	-0.53	-0.00	2.50	-0.20	0.39	-0.20	0.04
0.328	2.31	3.03	-0.53	0.00	2.50	-0.20	0.39	-0.20	0.04
0.329	2.31	3.03	-0.54	0.00	2.50	-0.20	0.39	-0.20	0.04
0.330	2.30	3.03	-0.54	0.00	2.50	-0.20	0.39	-0.20	0.04
0.331									0.04
0.332									0.04
0.333									0.04
0.334									0.04
0.335									0.04
0.336									0.06
0.337									0.12
0.338									0.17
0.339									0.20

0.340									0.21
0.341									0.19
0.342									0.17
0.343									0.15
0.344									0.14
0.345									0.13
0.346									0.13
0.347									0.14
0.348									0.14
0.349									0.15
0.350									0.16
0.351									0.16
0.352									0.16
0.353									0.15
0.354									0.15
0.355									0.15
0.356									0.15
0.357									0.15
0.358									0.15
0.359									0.15
0.360									0.15
0.362	3.44	3.04	0.22	0.00	2.28	-0.56	-0.23	-0.56	0.15
0.363	3.35	3.04	0.18	0.00	2.28	-0.56	-0.23	-0.56	0.15
0.364	3.28	3.04	0.15	0.00	2.28	-0.56	-0.23	-0.56	0.15
0.365	3.22	3.03	0.14	0.00	2.27	-0.56	-0.23	-0.56	0.15
0.366	3.17	3.03	0.14	-0.00	2.27	-0.56	-0.23	-0.56	0.15
0.367	3.14	3.03	0.15	-0.00	2.27	-0.56	-0.23	-0.56	0.15
0.368	3.11	3.03	0.15	-0.00	2.27	-0.56	-0.23	-0.56	0.15
0.369	3.08	3.03	0.17	-0.00	2.27	-0.56	-0.23	-0.56	0.15
0.370	3.06	3.03	0.18	-0.00	2.27	-0.56	-0.23	-0.56	0.15
0.371	3.04	3.03	0.20	-0.00	2.27	-0.56	-0.23	-0.56	0.15
0.372	3.03	3.03	0.21	0.00	2.27	-0.56	-0.23	-0.56	0.15
0.373	3.01	3.03	0.22	0.00	2.27	-0.56	-0.23	-0.56	0.15
0.374	3.00	3.03	0.24	0.00	2.27	-0.56	-0.23	-0.56	0.15
0.375	2.98	3.03	0.25	0.00	2.27	-0.56	-0.23	-0.56	0.15
0.376	2.97	3.03	0.27	0.00	2.27	-0.56	-0.23	-0.56	0.15
0.377	2.96	3.03	0.28	0.00	2.27	-0.56	-0.23	-0.56	0.15
0.378	2.96	3.03	0.29	-0.00	2.27	-0.56	-0.23	-0.56	0.15
0.379	2.95	3.03	0.31	-0.00	2.27	-0.56	-0.23	-0.56	0.15
0.380	2.94	3.03	0.32	-0.00	2.27	-0.56	-0.23	-0.56	0.15
0.381	2.94	3.03	0.33	-0.00	2.27	-0.56	-0.23	-0.56	0.15
0.382	2.93	3.03	0.35	-0.00	2.27	-0.56	-0.23	-0.56	0.15
0.383	2.93	3.03	0.36	0.00	2.27	-0.56	-0.23	-0.56	0.15
0.384	2.93	3.03	0.36	0.00	2.27	-0.56	-0.23	-0.56	0.15
0.385	2.92	3.03	0.37	0.00	2.27	-0.56	-0.23	-0.56	0.15
0.386	2.91	3.03	0.37	0.00	2.27	-0.56	-0.23	-0.56	0.15
0.387	2.91	3.03	0.36	0.00	2.27	-0.56	-0.23	-0.56	0.15
0.388	2.90	3.03	0.35	0.00	2.27	-0.56	-0.23	-0.56	0.15
0.389	2.88	3.03	0.34	-0.00	2.27	-0.56	-0.23	-0.56	0.15
0.390	2.87	3.03	0.31	-0.00	2.27	-0.56	-0.23	-0.56	0.15
0.391	2.85	3.03	0.28	-0.00	2.27	-0.56	-0.23	-0.56	0.15

Table 2b (3) - Continued

Page 8

0.352	2.83	3.03	0.25	-0.00	2.27	-0.56	-0.23	-0.56	0.15
0.353	2.81	3.03	0.20	-0.00	2.27	-0.56	-0.23	-0.56	0.15
0.354	2.78	3.03	0.16	0.00	2.27	-0.56	-0.23	-0.56	0.15
0.355	2.76	3.03	0.11	0.00	2.27	-0.56	-0.23	-0.56	0.15
0.356	2.74	3.03	0.06	0.00	2.27	-0.56	-0.23	-0.56	0.15
0.357									0.15
0.358									0.15
0.359									0.15
0.400									0.15
0.401									0.15
0.402									0.15
0.403									0.06
0.404									0.04
0.405									0.06
0.406									0.07
0.407									0.06
0.408									0.04
0.409									0.04
0.410									0.05
0.411									0.06
0.412									0.06
0.413									0.05
0.414									0.05
0.415									0.05
0.416									0.04
0.417									0.04
0.418									0.04
0.419									0.04
0.420									0.05
0.421									0.05
0.422									0.05
0.423									0.05
0.424									0.05
0.425									0.05
0.426									0.05
0.428	2.58	3.03	0.15	-0.01	2.76	0.08	0.25	0.02	0.05
0.429	2.54	3.03	0.15	-0.01	2.76	0.08	0.25	0.02	0.05
0.430	2.76	3.03	0.00	-0.00	2.76	0.08	0.26	0.02	0.05
0.431	2.56	3.03	-0.26	-0.00	2.76	0.08	0.26	0.02	0.05
0.432	2.45	3.03	-0.43	0.00	2.76	0.08	0.26	0.02	0.05
0.433	2.40	3.03	-0.52	0.00	2.76	0.08	0.26	0.02	0.05
0.434	2.38	3.03	-0.60	0.00	2.76	0.08	0.26	0.02	0.05
0.435	2.40	3.03	-0.64	0.00	2.76	0.08	0.26	0.02	0.05
0.436	2.42	3.03	-0.65	0.00	2.76	0.08	0.26	0.02	0.05
0.437	2.45	3.03	-0.64	0.00	2.76	0.08	0.26	0.02	0.05
0.438	2.48	3.03	-0.62	-0.00	2.76	0.08	0.26	0.02	0.05
0.439	2.50	3.03	-0.55	-0.00	2.76	0.08	0.26	0.02	0.05
0.440	2.52	3.03	-0.56	-0.00	2.76	0.08	0.26	0.02	0.05
0.441	2.54	3.03	-0.53	-0.00	2.76	0.08	0.26	0.02	0.05
0.442	2.56	3.03	-0.49	-0.00	2.76	0.08	0.26	0.02	0.05
0.443	2.57	3.03	-0.46	-0.00	2.76	0.08	0.26	0.02	0.05

Table 2b (3) - Continued

Page 9

0.444	2.58	3.03	-0.44	0.00	2.76	0.08	0.26	0.08	0.05
0.445	2.59	3.03	-0.41	0.00	2.76	0.08	0.26	0.08	0.05
0.446	2.60	3.03	-0.38	0.00	2.76	0.08	0.26	0.08	0.05
0.447	2.60	3.03	-0.36	0.00	2.76	0.08	0.26	0.08	0.05
0.448	2.61	3.03	-0.34	0.00	2.76	0.08	0.26	0.08	0.05
0.449	2.61	3.03	-0.32	0.00	2.76	0.08	0.26	0.08	0.05
0.450	2.61	3.03	-0.30	0.00	2.76	0.08	0.26	0.08	0.05
0.451	2.62	3.03	-0.29	0.00	2.76	0.08	0.26	0.08	0.05
0.452	2.62	3.03	-0.28	0.00	2.76	0.08	0.26	0.08	0.05
0.453	2.62	3.03	-0.26	0.00	2.76	0.08	0.26	0.08	0.05
0.454	2.62	3.03	-0.25	0.00	2.76	0.08	0.26	0.08	0.05
0.455	2.62	3.03	-0.24	0.00	2.76	0.08	0.26	0.08	0.05
0.456	2.62	3.03	-0.24	0.00	2.76	0.08	0.26	0.08	0.05
0.457	2.62	3.03	-0.23	0.00	2.76	0.08	0.26	0.08	0.05
0.458	2.62	3.03	-0.22	0.00	2.76	0.08	0.26	0.08	0.05
0.459	2.62	3.03	-0.22	0.00	2.76	0.08	0.26	0.08	0.05
0.460	2.62	3.03	-0.22	0.00	2.76	0.08	0.26	0.08	0.05
0.461	2.62	3.03	-0.21	0.00	2.76	0.08	0.26	0.08	0.05
0.462	2.62	3.03	-0.21	0.00	2.76	0.08	0.26	0.08	0.05
0.463									0.05
0.464									0.05
0.465									0.05
0.466									0.05
0.467									0.05
0.468									0.05
0.469									0.07
0.470									0.08
0.471									0.10
0.472									0.10
0.473									0.09
0.474									0.08
0.475									0.08
0.476									0.07
0.477									0.07
0.478									0.07
0.479									0.07
0.480									0.07
0.481									0.05
0.482									0.08
0.483									0.08
0.484									0.08
0.485									0.08
0.486									0.08
0.487									0.07
0.488									0.07
0.489									0.07
0.490									0.07
0.491									0.07
0.492									0.08
0.494	2.69	3.03	0.19	0.00	2.62	-0.22	0.12	-0.22	0.08
0.495	2.73	3.03	0.19	0.00	2.62	-0.22	0.12	-0.22	0.08

Table 2b (3) - Continued

Page 10

0.456	2.79	3.03	0.16	0.00	2.62	-0.22	0.12	-0.22	0.06
0.457	2.84	3.03	0.15	0.00	2.62	-0.22	0.12	-0.22	0.06
0.458	2.89	3.03	0.14	-0.00	2.62	-0.22	0.12	-0.22	0.06
0.459	2.95	3.03	0.12	-0.00	2.62	-0.22	0.12	-0.22	0.06
0.500	3.01	3.03	0.10	-0.00	2.62	-0.22	0.12	-0.22	0.06
0.501	3.08	3.03	0.07	-0.00	2.62	-0.22	0.12	-0.22	0.06

Table 2b (4)

TIME (SEC)	MLD		NUC		MUT	MUT	MUG	MUG	MISS (M)
	EST	TRLE	EST	TRUE					
0.032	3.19	3.05	0.22	0.00	0.32	0.00	-2.20	0.00	0.43
0.033	3.21	3.04	0.23	0.00	0.32	-0.00	-2.20	-0.00	0.43
0.034	3.20	3.04	0.22	-0.00	0.31	-0.00	-2.20	-0.00	0.43
0.035	3.17	3.04	0.20	-0.00	0.31	-0.00	-2.20	-0.00	0.43
0.036	3.15	3.03	0.19	-0.00	0.31	-0.00	-2.20	-0.00	0.43
0.037	3.13	3.03	0.18	-0.00	0.31	-0.00	-2.20	-0.00	0.43
0.038	3.11	3.03	0.17	-0.00	0.31	-0.00	-2.20	-0.00	0.43
0.039	3.09	3.03	0.15	0.00	0.31	0.00	-2.20	0.00	0.43
0.040	3.08	3.04	0.13	0.00	0.31	0.00	-2.20	0.00	0.43
0.041	3.06	3.04	0.11	0.00	0.31	0.00	-2.20	0.00	0.43
0.042	3.05	3.04	0.09	0.00	0.31	0.00	-2.20	0.00	0.43
0.043	3.04	3.04	0.07	0.00	0.31	0.00	-2.20	0.00	0.43
0.044	3.04	3.04	0.06	0.00	0.31	0.00	-2.20	0.00	0.43
0.045	3.04	3.04	0.04	-0.00	0.31	-0.00	-2.20	-0.00	0.43
0.046	3.03	3.04	0.02	-0.00	0.31	-0.00	-2.20	-0.00	0.43
0.047	3.04	3.04	0.01	-0.00	0.31	-0.00	-2.20	-0.00	0.43
0.048	3.04	3.04	-0.01	-0.00	0.31	-0.00	-2.20	-0.00	0.43
0.049	3.04	3.04	-0.02	-0.00	0.31	-0.00	-2.20	-0.00	0.43
0.050	3.04	3.04	-0.02	0.00	0.31	0.00	-2.20	0.00	0.43
0.051	3.04	3.04	-0.03	0.00	0.31	0.00	-2.20	0.00	0.43
0.052	3.04	3.04	-0.03	0.00	0.31	0.00	-2.20	0.00	0.43
0.053	3.03	3.04	-0.03	0.00	0.31	0.00	-2.20	0.00	0.43
0.054	3.03	3.04	-0.03	0.00	0.31	0.00	-2.20	0.00	0.43
0.055	3.02	3.04	-0.02	0.00	0.31	0.00	-2.20	0.00	0.43
0.056	3.00	3.04	-0.02	-0.00	0.31	-0.00	-2.20	-0.00	0.43
0.057	2.99	3.04	-0.02	-0.00	0.31	-0.00	-2.20	-0.00	0.43
0.058	2.97	3.04	-0.01	-0.00	0.31	-0.00	-2.20	-0.00	0.43
0.059	2.96	3.04	-0.01	-0.00	0.31	-0.00	-2.20	-0.00	0.43
0.060	2.94	3.04	-0.01	-0.00	0.31	-0.00	-2.20	-0.00	0.43
0.061	2.92	3.04	-0.00	-0.00	0.31	-0.00	-2.20	-0.00	0.43
0.062	2.90	3.04	0.00	0.00	0.31	0.00	-2.20	0.00	0.43
0.063	2.89	3.04	0.00	0.00	0.31	0.00	-2.20	0.00	0.43
0.064	2.88	3.04	0.01	0.00	0.31	0.00	-2.20	0.00	0.43
0.065	2.87	3.04	0.01	0.00	0.31	0.00	-2.20	0.00	0.43
0.066	2.87	3.04	0.01	0.00	0.31	0.00	-2.20	0.00	0.43
0.067									0.43
0.068									0.43
0.069									0.43
0.070									0.43
0.071									0.43
0.072									0.35
0.073									0.11
0.074									0.09
0.075									0.19
0.076									0.21
0.077									0.16
0.078									0.08
0.079									0.00
0.080									0.06

Table 2b (4) - Continued

Page 2

0.081									0.08
0.082									0.08
0.083									0.08
0.084									0.08
0.085									0.08
0.086									0.08
0.087									0.08
0.088									0.08
0.089									0.08
0.090									0.08
0.091									0.08
0.092									0.08
0.093									0.08
0.094									0.08
0.095									0.08
0.096									0.08
0.098	2.54	3.01	-0.33	-0.00	2.58	C.C1	0.47	0.01	0.01
0.099	2.50	3.01	-0.40	-0.00	2.58	C.C1	0.47	0.01	0.01
0.100	2.52	3.02	-0.41	-0.00	2.58	C.C1	0.47	0.01	0.01
0.101	2.77	3.03	-0.41	-0.00	2.59	C.C1	0.48	0.01	0.01
0.102	2.74	3.04	-0.43	0.00	2.59	C.C1	0.48	0.01	0.01
0.103	2.76	3.04	-0.45	0.00	2.59	C.C1	0.48	0.01	0.01
0.104	2.80	3.04	-0.45	0.00	2.59	C.C1	0.48	0.01	0.01
0.105	2.85	3.04	-0.45	0.00	2.59	C.C1	0.48	0.01	0.01
0.106	2.90	3.04	-0.45	0.00	2.59	C.C1	0.48	0.01	0.01
0.107	2.94	3.04	-0.44	0.00	2.59	C.C1	0.48	0.01	0.01
0.108	2.98	3.03	-0.42	-0.00	2.59	C.C1	0.48	0.01	0.01
0.109	3.00	3.03	-0.40	-0.00	2.59	C.C1	0.48	0.01	0.01
0.110	3.02	3.03	-0.37	-0.00	2.59	C.C1	0.48	0.01	0.01
0.111	3.03	3.03	-0.35	-0.00	2.59	C.C1	0.48	0.01	0.01
0.112	3.04	3.03	-0.32	-0.00	2.59	C.C1	0.48	0.01	0.01
0.113	3.04	3.04	-0.28	0.00	2.59	C.C1	0.48	0.01	0.01
0.114	3.05	3.04	-0.25	0.00	2.59	C.C1	0.48	0.01	0.01
0.115	3.05	3.04	-0.22	0.00	2.59	C.C1	0.48	0.01	0.01
0.116	3.05	3.04	-0.18	0.00	2.59	C.C1	0.48	0.01	0.01
0.117	3.05	3.04	-0.15	0.00	2.59	C.C1	0.48	0.01	0.01
0.118	3.05	3.04	-0.12	0.00	2.59	C.C1	0.48	0.01	0.01
0.119	3.05	3.04	-0.08	-0.00	2.59	C.C1	0.48	0.01	0.01
0.120	3.04	3.03	-0.06	-0.00	2.59	C.C1	0.48	0.01	0.01
0.121	3.04	3.03	-0.03	-0.00	2.59	C.C1	0.48	0.01	0.01
0.122	3.04	3.03	-0.01	-0.00	2.59	C.C1	0.48	0.01	0.01
0.123	3.04	3.04	0.01	-0.00	2.59	C.C1	0.48	0.01	0.01
0.124	3.04	3.04	0.03	-0.00	2.59	C.C1	0.48	0.01	0.01
0.125	3.04	3.04	0.04	0.00	2.59	C.C1	0.48	0.01	0.01
0.126	3.04	3.04	0.05	0.00	2.59	C.C1	0.48	0.01	0.01
0.127	3.04	3.04	0.05	0.00	2.59	C.C1	0.48	0.01	0.01
0.128	3.04	3.04	0.06	0.00	2.59	C.C1	0.48	0.01	0.01
0.129	3.04	3.04	0.06	0.00	2.59	C.C1	0.48	0.01	0.01
0.130	3.04	3.04	0.06	-0.00	2.59	C.C1	0.48	0.01	0.01
0.131	3.05	3.04	0.05	-0.00	2.59	C.C1	0.48	0.01	0.01
0.132	3.05	3.03	0.05	-0.00	2.59	C.C1	0.48	0.01	0.01

0.133									0.01
0.134									0.01
0.135									0.01
0.136									0.01
0.137									0.01
0.138									0.01
0.139									0.01
0.140									0.01
0.141									0.01
0.142									0.01
0.143									0.01
0.144									0.01
0.145									0.01
0.146									0.01
0.147									0.01
0.148									0.01
0.149									0.01
0.150									0.01
0.151									0.01
0.152									0.01
0.153									0.01
0.154									0.01
0.155									0.01
0.156									0.01
0.157									0.01
0.158									0.01
0.159									0.01
0.160									0.01
0.161									0.01
0.162									0.01
0.164	2.59	3.03	-0.06	-0.00	3.05	0.06	0.54	0.06	0.01
0.165	2.49	3.03	-0.10	-0.00	3.05	0.06	0.54	0.06	0.01
0.166	2.42	3.03	-0.14	-0.00	3.05	0.06	0.54	0.06	0.01
0.167	2.40	3.03	-0.18	-0.00	3.05	0.06	0.54	0.06	0.01
0.168	2.42	3.03	-0.22	0.00	3.05	0.06	0.54	0.06	0.01
0.169	2.41	3.03	-0.25	0.00	3.05	0.06	0.54	0.06	0.01
0.170	2.42	3.03	-0.26	0.00	3.05	0.06	0.54	0.06	0.01
0.171	2.45	3.03	-0.32	0.00	3.05	0.06	0.54	0.06	0.01
0.172	2.48	3.03	-0.35	0.00	3.05	0.06	0.54	0.06	0.01
0.173	2.51	3.03	-0.38	0.00	3.05	0.06	0.54	0.06	0.01
0.174	2.55	3.03	-0.40	-0.00	3.05	0.06	0.54	0.06	0.01
0.175	2.59	3.03	-0.44	-0.00	3.05	0.06	0.54	0.06	0.01
0.176	2.62	3.03	-0.46	-0.00	3.05	0.06	0.54	0.06	0.01
0.177	2.66	3.03	-0.48	-0.00	3.05	0.06	0.54	0.06	0.01
0.178	2.69	3.03	-0.50	-0.00	3.05	0.06	0.54	0.06	0.01
0.179	2.72	3.03	-0.51	0.00	3.05	0.06	0.54	0.06	0.01
0.180	2.74	3.03	-0.53	0.00	3.05	0.06	0.54	0.06	0.01
0.181	2.76	3.03	-0.53	0.00	3.05	0.06	0.54	0.06	0.01
0.182	2.78	3.03	-0.54	0.00	3.05	0.06	0.54	0.06	0.01
0.183	2.79	3.03	-0.55	0.00	3.05	0.06	0.54	0.06	0.01
0.184	2.80	3.03	-0.55	0.00	3.05	0.06	0.54	0.06	0.01

Table 2b (4) - Continued

Page 4

0.185	2.81	3.03	-0.55	-0.00	3.05	0.06	0.54	0.06	0.01
0.186	2.81	3.03	-0.54	-0.00	3.05	0.06	0.54	0.06	0.01
0.187	2.81	3.03	-0.53	-0.00	3.05	0.06	0.54	0.06	0.01
0.188	2.80	3.03	-0.52	-0.00	3.05	0.06	0.54	0.06	0.01
0.189	2.79	3.03	-0.51	-0.00	3.05	0.06	0.54	0.06	0.01
0.190	2.77	3.03	-0.49	-0.00	3.05	0.06	0.54	0.06	0.01
0.191	2.75	3.03	-0.47	0.00	3.05	0.06	0.54	0.06	0.01
0.192	2.72	3.03	-0.45	0.00	3.05	0.06	0.54	0.06	0.01
0.193	2.70	3.03	-0.43	0.00	3.05	0.06	0.54	0.06	0.01
0.194	2.66	3.03	-0.40	0.00	3.05	0.06	0.54	0.06	0.01
0.195	2.63	3.03	-0.38	0.00	3.05	0.06	0.54	0.06	0.01
0.196	2.59	3.03	-0.35	-0.00	3.05	0.06	0.54	0.06	0.01
0.197	2.55	3.03	-0.33	-0.00	3.05	0.06	0.54	0.06	0.01
0.198	2.52	3.03	-0.31	-0.00	3.05	0.06	0.54	0.06	0.01
0.199									0.01
0.200									0.01
0.201									0.01
0.202									0.01
0.203									0.01
0.204									0.01
0.205									0.01
0.206									0.12
0.207									0.12
0.208									0.12
0.209									0.14
0.210									0.12
0.211									0.10
0.212									0.09
0.213									0.08
0.214									0.06
0.215									0.09
0.216									0.10
0.217									0.10
0.218									0.11
0.219									0.11
0.220									0.11
0.221									0.10
0.222									0.10
0.223									0.10
0.224									0.10
0.225									0.10
0.226									0.10
0.227									0.10
0.228									0.10
0.230	3.32	3.04	-0.25	0.00	2.49	-0.32	-0.02	-0.32	0.10
0.231	3.30	3.04	-0.27	0.00	2.49	-0.32	-0.02	-0.32	0.10
0.232	3.27	3.04	-0.28	0.00	2.49	-0.32	-0.02	-0.32	0.10
0.233	3.22	3.03	-0.28	0.00	2.49	-0.32	-0.02	-0.32	0.10
0.234	3.19	3.03	-0.29	-0.00	2.49	-0.32	-0.02	-0.32	0.10
0.235	3.17	3.03	-0.28	-0.00	2.49	-0.32	-0.02	-0.32	0.10
0.236	3.14	3.03	-0.28	-0.00	2.49	-0.32	-0.02	-0.32	0.10

0.237	3.10	3.03	-0.26	-0.00	2.49	-0.32	-0.02	-0.32	0.10
0.238	3.07	3.03	-0.25	-0.00	2.49	-0.32	-0.02	-0.32	0.10
0.239	3.04	3.03	-0.24	-0.00	2.49	-0.32	-0.02	-0.32	0.10
0.240	3.00	3.03	-0.22	0.00	2.49	-0.32	-0.02	-0.32	0.10
0.241	2.96	3.03	-0.21	0.00	2.49	-0.32	-0.02	-0.32	0.10
0.242	2.92	3.03	-0.19	0.00	2.49	-0.32	-0.02	-0.32	0.10
0.243	2.87	3.03	-0.17	0.00	2.49	-0.32	-0.02	-0.32	0.10
0.244	2.83	3.03	-0.16	0.00	2.49	-0.32	-0.02	-0.32	0.10
0.245	2.78	3.03	-0.14	0.00	2.49	-0.32	-0.02	-0.32	0.10
0.246	2.73	3.03	-0.12	-0.00	2.49	-0.32	-0.02	-0.32	0.10
0.247	2.70	3.03	-0.09	-0.00	2.49	-0.32	-0.02	-0.32	0.10
0.248	2.66	3.03	-0.08	-0.00	2.49	-0.32	-0.02	-0.32	0.10
0.249	2.63	3.03	-0.06	-0.00	2.49	-0.32	-0.02	-0.32	0.10
0.250	2.61	3.03	-0.04	-0.00	2.49	-0.32	-0.02	-0.32	0.10
0.251	2.60	3.03	-0.02	0.00	2.49	-0.32	-0.02	-0.32	0.10
0.252	2.60	3.03	-0.01	0.00	2.49	-0.32	-0.02	-0.32	0.10
0.253	2.61	3.03	0.00	0.00	2.49	-0.32	-0.02	-0.32	0.10
0.254	2.63	3.03	0.00	0.00	2.49	-0.32	-0.02	-0.32	0.10
0.255	2.65	3.03	0.00	0.00	2.49	-0.32	-0.02	-0.32	0.10
0.256	2.68	3.03	0.00	0.00	2.49	-0.32	-0.02	-0.32	0.10
0.257	2.71	3.03	0.00	-0.00	2.49	-0.32	-0.02	-0.32	0.10
0.258	2.74	3.03	-0.01	-0.00	2.49	-0.32	-0.02	-0.32	0.10
0.259	2.78	3.03	-0.01	-0.00	2.49	-0.32	-0.02	-0.32	0.10
0.260	2.81	3.03	-0.03	-0.00	2.49	-0.32	-0.02	-0.32	0.10
0.261	2.85	3.03	-0.04	-0.00	2.49	-0.32	-0.02	-0.32	0.10
0.262	2.88	3.03	-0.06	0.00	2.49	-0.32	-0.02	-0.32	0.10
0.263	2.90	3.03	-0.08	0.00	2.49	-0.32	-0.02	-0.32	0.10
0.264	2.92	3.03	-0.10	0.00	2.49	-0.32	-0.02	-0.32	0.10
0.265									0.10
0.266									0.10
0.267									0.10
0.268									0.10
0.269									0.10
0.270									0.09
0.271									0.04
0.272									0.01
0.273									0.02
0.274									0.02
0.275									0.01
0.276									0.01
0.277									0.02
0.278									0.03
0.279									0.03
0.280									0.03
0.281									0.03
0.282									0.02
0.283									0.02
0.284									0.02
0.285									0.02
0.286									0.02
0.287									0.02

Table 2b (4) - Continued

Page 6

0.288								0.02	
0.289								0.02	
0.290								0.02	
0.291								0.02	
0.292								0.02	
0.293								0.02	
0.294								0.02	
0.296	3.16	3.03	0.32	-0.00	2.94	-0.09	0.43	-0.09	0.02
0.297	3.17	3.03	0.35	-0.00	2.94	-0.09	0.43	-0.09	0.02
0.298	3.17	3.03	0.38	-0.00	2.94	-0.09	0.43	-0.09	0.02
0.299	3.16	3.03	0.39	-0.00	2.94	-0.09	0.43	-0.09	0.02
0.300	3.13	3.03	0.40	0.00	2.94	-0.09	0.43	-0.09	0.02
0.301	3.11	3.03	0.40	0.00	2.94	-0.09	0.43	-0.09	0.02
0.302	3.09	3.03	0.40	0.00	2.94	-0.09	0.43	-0.09	0.02
0.303	3.07	3.03	0.39	0.00	2.94	-0.09	0.43	-0.09	0.02
0.304	3.05	3.03	0.38	0.00	2.94	-0.09	0.43	-0.09	0.02
0.305	3.03	3.03	0.37	0.00	2.94	-0.09	0.43	-0.09	0.02
0.306	3.01	3.03	0.36	-0.00	2.94	-0.09	0.43	-0.09	0.02
0.307	2.99	3.03	0.34	-0.00	2.94	-0.09	0.43	-0.09	0.02
0.308	2.98	3.03	0.32	-0.00	2.94	-0.09	0.43	-0.09	0.02
0.309	2.96	3.03	0.31	-0.00	2.94	-0.09	0.43	-0.09	0.02
0.310	2.95	3.03	0.29	-0.00	2.94	-0.09	0.43	-0.09	0.02
0.311	2.94	3.03	0.27	-0.00	2.94	-0.09	0.43	-0.09	0.02
0.312	2.93	3.03	0.26	0.00	2.94	-0.09	0.43	-0.09	0.02
0.313	2.93	3.03	0.24	0.00	2.94	-0.09	0.43	-0.09	0.02
0.314	2.92	3.03	0.23	0.00	2.94	-0.09	0.43	-0.09	0.02
0.315	2.92	3.03	0.21	0.00	2.94	-0.09	0.43	-0.09	0.02
0.316	2.91	3.03	0.20	0.00	2.94	-0.09	0.43	-0.09	0.02
0.317	2.91	3.03	0.19	-0.00	2.94	-0.09	0.43	-0.09	0.02
0.318	2.91	3.03	0.18	-0.00	2.94	-0.09	0.43	-0.09	0.02
0.319	2.91	3.03	0.17	-0.00	2.94	-0.09	0.43	-0.09	0.02
0.320	2.91	3.03	0.16	-0.00	2.94	-0.09	0.43	-0.09	0.02
0.321	2.91	3.03	0.16	-0.00	2.94	-0.09	0.43	-0.09	0.02
0.322	2.91	3.03	0.15	-0.00	2.94	-0.09	0.43	-0.09	0.02
0.323	2.91	3.03	0.15	0.00	2.94	-0.09	0.43	-0.09	0.02
0.324	2.91	3.03	0.15	0.00	2.94	-0.09	0.43	-0.09	0.02
0.325	2.90	3.03	0.15	0.00	2.94	-0.09	0.43	-0.09	0.02
0.326	2.89	3.03	0.15	0.00	2.94	-0.09	0.43	-0.09	0.02
0.327	2.87	3.03	0.15	0.00	2.94	-0.09	0.43	-0.09	0.02
0.328	2.85	3.03	0.15	-0.00	2.94	-0.09	0.43	-0.09	0.02
0.329	2.83	3.03	0.15	-0.00	2.94	-0.09	0.43	-0.09	0.02
0.330	2.80	3.03	0.16	-0.00	2.94	-0.09	0.43	-0.09	0.02
0.331									0.02
0.332									0.02
0.333									0.02
0.334									0.02
0.335									0.02
0.336									0.02
0.337									0.04
0.338									0.06
0.339									0.07

0.340									0.07
0.341									0.06
0.342									0.06
0.343									0.05
0.344									0.04
0.345									0.04
0.346									0.04
0.347									0.04
0.348									0.04
0.349									0.05
0.350									0.05
0.351									0.05
0.352									0.05
0.353									0.05
0.354									0.05
0.355									0.05
0.356									0.05
0.357									0.05
0.358									0.05
0.359									0.05
0.360									0.05

0.362	2.45	3.03	0.30	-0.00	2.79	0.17	0.29	0.17	0.05
0.363	2.75	3.03	0.40	-0.00	2.79	0.17	0.29	0.17	0.05
0.364	2.92	3.03	0.46	-0.00	2.79	0.17	0.29	0.17	0.05
0.365	3.01	3.03	0.56	-0.00	2.79	0.17	0.29	0.17	0.05
0.366	3.06	3.03	0.52	0.00	2.79	0.17	0.29	0.17	0.05
0.367	3.13	3.03	0.55	0.00	2.79	0.17	0.29	0.17	0.05
0.368	3.19	3.03	0.58	0.00	2.79	0.17	0.29	0.17	0.05
0.369	3.24	3.03	0.60	0.00	2.79	0.17	0.29	0.17	0.05
0.370	3.28	3.03	0.62	0.00	2.79	0.17	0.29	0.17	0.05
0.371	3.31	3.03	0.64	0.00	2.79	0.17	0.29	0.17	0.05
0.372	3.33	3.03	0.66	-0.00	2.79	0.17	0.29	0.17	0.05
0.373	3.33	3.03	0.67	-0.00	2.79	0.17	0.29	0.17	0.05
0.374	3.31	3.03	0.68	-0.00	2.79	0.17	0.29	0.17	0.05
0.375	3.27	3.03	0.69	-0.00	2.79	0.17	0.29	0.17	0.05
0.376	3.20	3.03	0.69	-0.00	2.79	0.17	0.29	0.17	0.05
0.377	3.11	3.03	0.69	-0.00	2.79	0.17	0.29	0.17	0.05
0.378	3.00	3.03	0.69	0.00	2.79	0.17	0.29	0.17	0.05
0.379	2.89	3.03	0.68	0.00	2.79	0.17	0.29	0.17	0.05
0.380	2.78	3.03	0.67	0.00	2.79	0.17	0.29	0.17	0.05
0.381	2.68	3.03	0.66	0.00	2.79	0.17	0.29	0.17	0.05
0.382	2.60	3.03	0.65	0.00	2.79	0.17	0.29	0.17	0.05
0.383	2.53	3.03	0.64	-0.00	2.79	0.17	0.29	0.17	0.05
0.384	2.48	3.03	0.62	-0.00	2.79	0.17	0.29	0.17	0.05
0.385	2.45	3.03	0.61	-0.00	2.79	0.17	0.29	0.17	0.05
0.386	2.42	3.03	0.60	-0.00	2.79	0.17	0.29	0.17	0.05
0.387	2.40	3.03	0.59	-0.00	2.79	0.17	0.29	0.17	0.05
0.388	2.39	3.03	0.59	-0.00	2.79	0.17	0.29	0.17	0.05
0.389	2.38	3.03	0.58	0.00	2.79	0.17	0.29	0.17	0.05

Table 2b (4) - Continued

Page 8

0.390	2.37	1.03	0.57	0.00	2.79	0.17	0.29	0.17	0.09
0.391	2.37	1.03	0.56	0.00	2.79	0.17	0.29	0.17	0.09
0.392	2.37	1.03	0.55	0.00	2.79	0.17	0.29	0.17	0.09
0.393	2.38	1.03	0.54	0.00	2.79	0.17	0.29	0.17	0.09
0.394	2.38	1.03	0.54	-0.00	2.79	0.17	0.29	0.17	0.09
0.395	2.39	1.03	0.53	-0.00	2.79	0.17	0.29	0.17	0.09
0.396	2.39	1.03	0.52	+0.00	2.79	0.17	0.29	0.17	0.09
0.397									0.09
0.398									0.09
0.399									0.09
0.400									0.09
0.401									0.09
0.402									0.09
0.403									0.11
0.404									0.11
0.405									0.11
0.406									0.11
0.407									0.17
0.408									0.11
0.409									0.11
0.410									0.11
0.411									0.11
0.412									0.11
0.413									0.11
0.414									0.11
0.415									0.11
0.416									0.11
0.417									0.11
0.418									0.11
0.419									0.11
0.420									0.11
0.421									0.11
0.422									0.11
0.423									0.11
0.424									0.11
0.425									0.11
0.426									0.11
0.428	2.40	1.03	-0.27	-0.00	2.37	0.54	-0.13	0.54	0.14
0.429	2.79	1.03	-0.41	-0.00	2.37	0.54	-0.13	0.54	0.14
0.430	2.40	1.03	-0.46	-0.00	2.37	0.54	-0.13	0.54	0.14
0.431	2.40	1.03	-0.52	-0.00	2.37	0.54	-0.13	0.54	0.14
0.432	2.40	1.03	-0.58	0.00	2.37	0.54	-0.13	0.54	0.14
0.433	2.40	1.03	-0.60	0.00	2.37	0.54	-0.13	0.54	0.14
0.434	2.40	1.03	-0.60	0.00	2.37	0.54	-0.13	0.54	0.14
0.435	2.40	1.03	-0.60	0.00	2.37	0.54	-0.13	0.54	0.14
0.436	2.40	1.03	-0.59	0.00	2.37	0.54	-0.13	0.54	0.14
0.437	2.40	1.03	-0.57	0.00	2.37	0.54	-0.13	0.54	0.14
0.438	2.79	1.03	-0.54	-0.00	2.37	0.54	-0.13	0.54	0.14
0.439	2.79	1.03	-0.51	-0.00	2.37	0.54	-0.13	0.54	0.14
0.440	2.79	1.03	-0.47	-0.00	2.37	0.54	-0.13	0.54	0.14
0.441	2.78	1.03	-0.42	-0.00	2.37	0.54	-0.13	0.54	0.14

0.442	2.77	3.03	-0.38	-0.00	2.37	0.54	-0.13	0.54	0.14
0.443	2.76	3.03	-0.34	-0.00	2.37	0.54	-0.13	0.54	0.14
0.444	2.74	3.03	-0.30	0.00	2.37	0.54	-0.13	0.54	0.14
0.445	2.73	3.03	-0.26	0.00	2.37	0.54	-0.13	0.54	0.14
0.446	2.70	3.03	-0.23	0.00	2.37	0.54	-0.13	0.54	0.14
0.447	2.68	3.03	-0.21	0.00	2.37	0.54	-0.13	0.54	0.14
0.448	2.66	3.03	-0.19	0.00	2.37	0.54	-0.13	0.54	0.14
0.449	2.63	3.03	-0.18	-0.00	2.37	0.54	-0.13	0.54	0.14
0.450	2.60	3.03	-0.16	-0.00	2.37	0.54	-0.13	0.54	0.14
0.451	2.57	3.03	-0.15	-0.00	2.37	0.54	-0.13	0.54	0.14
0.452	2.54	3.03	-0.14	-0.00	2.37	0.54	-0.13	0.54	0.14
0.453	2.51	3.03	-0.13	-0.00	2.37	0.54	-0.13	0.54	0.14
0.454	2.48	3.03	-0.12	-0.00	2.37	0.54	-0.13	0.54	0.14
0.455	2.45	3.03	-0.11	0.00	2.37	0.54	-0.13	0.54	0.14
0.456	2.42	3.03	-0.10	0.00	2.37	0.54	-0.13	0.54	0.14
0.457	2.39	3.03	-0.09	0.00	2.37	0.54	-0.13	0.54	0.14
0.458	2.36	3.03	-0.08	0.00	2.37	0.54	-0.13	0.54	0.14
0.459	2.34	3.03	-0.07	0.00	2.37	0.54	-0.13	0.54	0.14
0.460	2.32	3.03	-0.07	-0.00	2.37	0.54	-0.13	0.54	0.14
0.461	2.32	3.03	-0.07	-0.00	2.37	0.54	-0.13	0.54	0.14
0.462	2.32	3.03	-0.07	-0.00	2.37	0.54	-0.13	0.54	0.14
0.463									0.14
0.464									0.14
0.465									0.14
0.466									0.14
0.467									0.14
0.468									0.13
0.469									0.11
0.470									0.12
0.471									0.14
0.472									0.14
0.473									0.13
0.474									0.12
0.475									0.12
0.476									0.11
0.477									0.11
0.478									0.11
0.479									0.11
0.480									0.11
0.481									0.12
0.482									0.12
0.483									0.12
0.484									0.12
0.485									0.12
0.486									0.12
0.487									0.12
0.488									0.12
0.489									0.12
0.490									0.12
0.491									0.12
0.492									0.12

Table 2b (4) - Continued

Page 10

0.454	3.52	3.03	-0.21	0.01	2.31	-0.10	-0.15	-0.10	0.12
0.455	3.49	3.03	-0.15	0.01	2.31	-0.10	-0.15	-0.10	0.12
0.456	3.45	3.03	-0.07	0.00	2.31	-0.10	-0.15	-0.10	0.12
0.457	3.41	3.03	0.00	0.00	2.31	-0.10	-0.15	-0.10	0.12
0.458	3.37	3.03	0.05	-0.00	2.31	-0.10	-0.15	-0.10	0.12
0.459	3.32	3.03	0.11	-0.00	2.31	-0.10	-0.15	-0.10	0.12
0.500	3.48	3.03	0.16	-0.00	2.31	-0.10	-0.15	-0.10	0.12
0.501	3.44	3.03	0.23	-0.00	2.31	-0.10	-0.15	-0.10	0.12

Computer Program For Simulation/Evaluation
of The Estimation of Laser Spot Position
From The Fluctuating Backscatter Signal


```

REAL IC,IG,MLD,NLD,MLG,NLG,IGZ,IG1,MLED,AUED
DIMENSION RSZ(3),VS(3),RTZ(3),VT(3),AT2(20,20),S(20,20),X
CR(3),CV(3),LDV(3),C(3),CVSF(3),UT(3),LG(3),ERR(3),X
Z(3),XI(3),ETA(3),CB(3),LL(3),RTS(3),OLM(3),LDR(3),X
FTCLC(3),RSOLD(3),LLCLC(3),EE(2),GC(3),AT1(20,20),X
EDR(20,20),SS(20,20),SSS(20,20)

```

```

DCUELE PRECISION RSZ,VS,RTZ,VT,CR,CV,LDV,C,CVSF,UT,LG,ERR,Z,XI,X
ETA,DE,LL,RTS,OLM,UDP,RSOLD,RSOLD,ULOLD,EE,CO
DCUELE PRECISION THETA, PLI,PHINT1,PHINT2,THINT2,DTTH,C2TH,X
OIPF,C2FH,DTL,SF,F,TI,PI,SOT,ERRCL,CTER,EDFAZ,CPRER,XI,F,CPR,CM,X
DLRA,CVF

```

```

DC SOC REF = .2,.75,.05
NPRINT = 1
PI = 3.141592654
Z(1) = C.
Z(2) = C.
Z(3) = 1.
T = 0.
DI = 1.E-3
N = 0.

```

```

C-----
C-
C-      SET OPTICAL SYSTEM PARAMETERS.
C-
C-----

```

```

IGZ = 1000.
IC = 1.
SIGMA = 1.
WL = 1.E-6
DETH = 1./((2*PI/WL)*SIGMA)

```

```

C*****
C*
C*      SPECIFY ENGAGEMENT PARAMETERS.
C*
C*****

```

```

RSZ(1) = C.
RSZ(2) = C.
RSZ(3) = C.
VS(1) = 0.
VS(2) = 0.
VS(3) = 0.

```

```

RTZ(1) = C.
RTZ(2) = 1.E6
RTZ(3) = C.
VT(1) = 50.C
VT(2) = 1.E4
VT(3) = 0.
DE(1)=0.
DE(2)=0.
EE(1)=0.
EE(2)=0.
GE(1)=REP
GE(2)=0.
GE(3)=0.

```

```

C*****
C*
C*      CONVERT TO DIFFERENCE COORDINATES.
C*
C*****

```

```

CALL CSLM (RTZ,RSZ,DR,-1)
CALL CSUM (VT,VS,CV,-1)
CALL CUVECT (DR, LDR, DRM, IE)
CALL CUVECT (CV, LDV, DVM, IE)

```

```

C*****
C*
C*      CALCULATE DISTANCE AT CLOSEST APPROACH.
C*
C*****

```

```

CALL EDCT (LDR, UDV, CURV)
SF = CURV*DRM
CALL DSCMLT (SF, UDV, DVSE)
CALL CSLM (DR, DVSE, D, -1)
CALL CUVECT (D, D, DM, IE)
PRINT 10, DR, UDV, RSZ, VS, RTZ, VT, DR, IGZ, ID, GE(1), GE(2), GE(3)
10 FORMAT ("1", "CLOSEST APPROACH=", E10.3, "/" " DOT PRODUCT = " X
, E10.3, "/" " RSZ VECTOR = " .3E10.3, "/" " VS VECTOR = " .3E10.3, "/" X
, " RTZ VECTOR = " .3E10.3, "/" " VT VECTOR = " .3E10.3, "/" " DE VECTOR = " X
, .3E10.3, "/" " IGZ = " .E10.3, "/" " ID = " .E10.3, "/" " GD = " .3E10.3)
PRINT 11
PRINT 12
11 FORMAT ("1", 1X, "TIME", 12X, "PUD", 13X, "NUC", 9), "MUG", 4X, "NUG")
12 FORMAT (14X, "EST", 4X, "TRUE", 5X, "EST", 4X, "TLE", /)

```

```

C*****
C*
C*      INITIALIZE SERVO/CIPBAL AND SET SERVO PARAMETERS.
C*

```

C*****

```

SCT=SQRT(LDF(1)*UCR(1)+LDF(2)*UCR(2))
THETAZ=ATAN2(SCT,UCR(3))
PHI2 = ATAN2(UCR(2), UCR(1))
SFREQ = 100.
GAIN = 27.9155*SFREQ*SFREQ
CLEAD=EXP(-(T+2*PI*SFREQ))
PHINT1 = C.
PHINT2 = PHI2
THINT1 = C.
THINT2 = THETAZ
OTHER = 0.
OFMER = Q.
THETA = THINT2
PHI = PHINT2
CALL CSEHREC (THETA, PHI, 1.00, UC)
TTF = DCM/(1.E8*DT)
TDELAY = 3.*TTF+2./(SFREQ*DT)

```

C-----
C-
C- SET UP RANDOM ARRAY CONTROL/GENERATION PARAMETERS
C- AND OBTAIN INITIAL VALUES OF A-TILDE'S.
C-
C-----

```

F = 1
ALPHA = DCM*DSORT(1.00-CURV*CURV)/DCM
T4 = C.707107*SIGMA/(4.*DCM*ALPHA)
TS = TDELAY*DT
CALL RINT(F,TS,T4,ATS,AT2)

```

C=====

C- SET UP BIAS ESTIMATION PARAMETERS.

C-
C=====

```

TLP=0.
TRT=2.*CRF/1.E8
NEST=10
THFS=1.5/SFREQ
TEST=NEST*T4
NS=C
DO 20 I=1,20
DO 21 J=1,20
SS(I,J)=0.
21 SS(I,J)=C.
20 CONTINUE

```

C*****


```

C*
C*      INCREMENT CLOCK.
C*
C*****

100 N = N + 1
    T = T + DT

C*****
C*
C*      INCREMENT TARGET POSITION AND STORE,
C*      OBTAIN DELAYED TARGET POSITION.
C*
C*****

    CALL CWSUM (1,DC,DELE(DT),DR,DV,DR)
    CALL CSTACIN (1,CR)
    CALL CUVECT(DR,UGO,DRM,IE)
    TTF = DRM/(3.ES*DT)
    IF (N<LT,TTF) GO TO 100
    CALL CSTACOT (1,TTF,RTOLD)

C*****
C*
C*      COMPUTE TARGET TRACKING ERROR AS SEEN BY
C*      SENSOR ON THE GIMBALS (USING THE DELAYED
C*      TARGET POSITION).
C*
C*****

    CALL CUVECT (RTOLD,UT,R,IE)
    CALL CSUM (LT,UG,ERR,-1)
    CALL DCROSS (2,UG,XI)
    CALL CUVECT (XI,XI,XIP,IE)
    CALL DCROSS (UG,XI,ETA)
    CALL CDOCT (ERR,ETA,ERREL)
    ERREL = -ERREL + ER(1)
    CALL CDOCT (ERR,XI,ERRAZ)
    ERRAZ = ERRAZ + ER(2)

C*****
C*
C*      IMPLEMENT GIMBAL SERVO POINTING UPDATE.
C*
C*****

    ERRAZ = ERRAZ/DSIN (THETA)
    O1TH = (ERREL - CLEAD + OTHER)/(1. - CLEAD)
    O1PT = (ERRAZ - CLEAD + OTHER)/(1. - CLEAD)
    OTHER = ERREL
    OTHER = ERRAZ

```

```

Q2TH = Q1TH * GAIN
Q2PH = Q1PH * GAIN
THINT1 = THINT1 + DT * Q2TH
PHINT1 = PHINT1 + DT * Q2PH
THINT2 = THINT2 + DT * THINT1
PHINT2 = PHINT2 + DT * PHINT1
THETA = THINT2
PHI = PHINT2
CALL CSWFEC (THETA, PHI, 1.00, UG)

```

```

C-----
C-
C-      CALCULATE GLINT POSITION ON SENSOR FOCAL PLANE.
C-
C-----

```

```

      CALL CMNL(LG,RTOLD,GC,CTH,XI,STA,MUG,AUG)

```

```

C*****
C*
C*      INTRODUCE LASER NORESIGHT ERROR.
C*
C*****

```

```

T1= THETA+DE(1)
P1=PHI+CB(2)
CALL CSWFEC(T1,P1,1.00,UL)

```

```

C*****
C*
C*      CALCULATE LASER TARGET MISS DISTANCE.
C*
C*****

```

```

CALL ESTACIN (2,UL)
IF (N.LT.TDELAY) GO TO 100
TTF2=2+TTF
CALL ESTACOT (2, TTF2, ULCLD)
CALL EOCT (LT, LLCLD, DTL)
SF = -DTL/R
CALL CWSUP (1.00, SF, RTOLD, LLCLD, DLM)

```

```

C-----
C-
C-      CALCULATE LASER POSITION ON TARGET AS SEEN
C-      ON SENSOR FOCAL PLANE, AND GLINT INTENSITY.
C-      CALCULATE THE ARRAY OF FOCAL PLANE SIGNAL
C-      INTENSITIES.
C-
C-----

```

```

      CALL CMNL(LG,RTOLD,DLM,DETH,XI,STA,MUD,NLD)

```

```

X = MUG-MLD
Y = NUG-NLD
IG = C
IG1 = X*X+Y*Y
IF (IG1.LT.76) IG=IG2*EXP(-IG1)
CALL SIG(F,PUD,AUD,MUG,NUG,IO,IG,T,T4,S)
IF ((N/APRINT)*APRINT.NE.N) GO TO 1C0

```

```

C=====
C=
C= INDEPENDENT GLINT/DIFFUSE SIGNAL ESTIMATOR
C=
C=====

```

```

DC 230 I=1.20
DC 231 J=1.20
SX=SS(I,J)
IF (ABS(SX).LT.1E-16) SX=0
SS(I,J)=SS(I,J)+SX
231 SSS(I,J)=SSS(I,J)+SX*SX
230 CONTINUE
NS=NS+1

```

```

C=====
C=
C= CORRELATE DIFFUSE SIGNAL ESTIMATE.
C=
C=====

```

```

TLP=T
IF (NS.EQ.1) GO TO 240
DC 250 I=1.20
DC 251 J=1.20
SEX=SS(I,J)/NS
SSX=SSS(I,J)/NS
SSSX = SSEX-SEX*SSX
IF (SSSX.LT.0) SSSX=C.
SSORT = SEX*SEX-SSSX
IF (SSORT.LT.0) SSGRT=C
ECR(I,J) = SSX-SORT(SSORT)
251 CONTINUE
250 CONTINUE

```

```

C=====
C=
C= ESTIMATE DIFFUSE RETURN'S POSITION.
C=
C=====

```

```

SEDF=C
MLEC=C.

```



```
NLEC=C.  
DC 260 I=1,20  
DC 261 J=1,20  
SEDF=SECR+E(R(I,J))  
MLEC=MUED+I*E(R(I,J))  
261 NLEC=MUED+J*E(R(I,J))  
260 CONTINUE  
MLEC=MUED/SEDF-10.5  
NLEC=MUED/SEDF-10.5  
PRINT 270,T,MLEC,MUD,MUD,MUG,NLG  
270 FORMAT (1X,F6,3.5X,F6.2,1X,F6.2,3X,F6.2,1X,F6.2,3X,F6.2,1X,F6,2)  
240 CONTINUE  
IF (N.LE.100) GO TO 100  
  
900 CONTINUE  
END
```

304-100-000

```

REAL IC,IS,MLO,NLO,MLG,NLG,IGZ,IG1,MLEC,AUED,MLT,MLT
DIMENSION RSZ(3),VS(3),RTZ(3),VT(3),ATZ(20,20),S(20,20),X
  ER(3),CV(3),LDV(3),DE(3),CVSF(3),LT(3),LG(3),EPF(3),X
  Z(3),XI(3),ETA(3),DB(3),LL(3),PTS(3),OLM(3),LDR(3),X
  RTCLC(3),RSOLD(3),LLCLC(3),EE(2),GC(3),AT1(20,20),X
  EDR(20,20),SS(20,20),SSS(20,20),EXP(3),UDLP(3)

```

```

DCUELE PRECISION RSZ,VS,RTZ,VT,DR,DV,LQV,C,CVSF,UT,LG,EPF,Z,XI,X
ETA,DE,LL,PTS,OLM,UDLP,PTOLD,RSOLD,ULOLD,EE,GC,UDLP
DCUELE PRECISION THETA, PHI,PHINT1,THINT1,PHINT2,THINT2,DTTH,C2TH,X
O1PH,C2PH,DTL,SE,F,TI,PI,SOT,FRSEL,CTHES,BRRAZ,COPER,XIP,CPH,CM,X
DLR,CVP,EXP

```

```

NPRINT = 1
PI = 3.141592654
Z(1) = 0.
Z(2) = 0.
Z(3) = 1.
T = 0.
DT = 1.E-3
N = 0.

```

```

C-----
C-
C-      SET OPTICAL SYSTEM PARAMETERS.
C-
C-----

```

```

ICZ = 1000.
IC = 1.
SIGMA = 1.
WL = 1.E-6
DETH = 1./((2*PI/WL)*SIGMA)

```

```

C*****
C*
C*      SPECIFY ENGAGEMENT PARAMETERS.
C*
C*****

```

```

RSZ(1) = 0.
RSZ(2) = 0.
RSZ(3) = 0.
VS(1) = 0.
VS(2) = 0.
VS(3) = 0.
RTZ(1) = 0.

```



```

R1Z(2) = 1.E6
R1Z(3) = 0.
V1(1) = 50.0
V1(2) = 1.E4
V1(3) = 0.
DE(1)=0.
DE(2)=0.
EE(1)=0.
EE(2)=0.
GE(1)=.25
GE(2)=0.
GE(3)=0.
D>M(1) = 0.
D>M(2) = 0.
D>M(3) = 0.

```

```

C=====
C=
C= SPECIFY/INITIALIZE PIAS SERVO PARAMETERS.
C=
C=====

```

```

PARM = 6.
NE = 30
FACT = 2.0*PI/PIARM

```

```

C*****
C*
C* CONVERT TO DIFFERENCE COORDINATES.
C*
C*****

```

```

CALL DSUM (RTZ,RSZ,DP,-1)
CALL DSUM (VT,VS,DV,-1)
CALL DUVECT (DP, LDF, DDM, IE)
CALL DUVECT (DV, LDM, DVM, IE)

```

```

C*****
C*
C* CALCULATE DISTANCE AT CLOSEST APPROACH.
C*
C*****

```

```

CALL DDOT (LDF, DEV, DURV)
SF = DU-V*DDM
CALL DSCMULT (SF, UDV, DVER)
CALL DSUM (DP, DVER, D, -1)
CALL DUVECT (D, D, DM, IE)
PRINT 10, DP,DURV,RSZ,VS,RTZ,VT,DP,IGZ,IO,GE(1),GE(2),GE(3)
10 FORMAT ("1","CLOSEST APPROACH=",E10.3,"/" DOT PRODUCT ="%)

```

```

E1C.3// " RSZ VECTOR = ".3E1C.3// " VS VECTOR = ".3E1C.3//X
" RTZ VECTOR = ".3E1D.3// " VT VECTOR = ".3E1C.3// " DE VECTOR = "X
.3E1C.3// " IGZ = ".F1C.3// " IC = ".E1D.3// " GD = ".3E1C.3)
PRINT 11
PRINT 12
11 FC PAT ("1".4X."TIME".3X."MJD".10X."NLD".7X."PUT".3X."NLT".X
      4X."PUC".7X."NUG".5X."MISS")
12 FC PAT (5X."(SEC)".4X."EST".3X."TRUE".3X."EST".3X.X
      "TRLE".30X."(M)")

C*****
C*
C*      INITIALIZE SERVO/CIMBAL AND SET SERVO PARAMETERS.
C*
C*****

SCT=SGRT(LDR(1)*UCR(1)+LDR(2)*UCR(2))
THETAZ=ATAN2(SCT,UCR(3))
PHIZ = ATAN2(UCR(2), UCR(1))
SFREQ = 100.
GAIN = 27.9155*SFREQ*SFREQ
CLEAD=EXP(-CT*2*PI*SFREQ)
PHINT1 = 0.
PHINT2 = PHIZ
THINT1 = 0.
THINT2 = THETAZ
OTHER = 0.
OTHER = 0.
THETA = THINT2
PHI = PHINT2
CALL DSPHFEC (THETA, PHI, 1.00, UC)
TIF = DEM/(2.53*DT)
TEDELAY = 3.*TIF+2./(SFREQ*DT)
TSTAB = TDELAY*CT

C-----
C-
C-      SET UP RANDOM ARRAY CONTROL/GENERATION PARAMETERS
C-      AND OBTAIN INITIAL VALUES OF A-TILDE'S.
C-
C-----

F = 1
ALPHA = DIM*DSQRT(1.00-CURV*CURV)/DEM
T4 = 0.7071(7*SIGMA/(4.*DEM*ALPHA)
TS = TDELAY*DT
CALL RINT(F,TS,T4,ATS,AT2)

C=====
C-
C-      SET UP BIAS ESTIMATION PARAMETERS.

```

C=
C=====

TLP=0.
T=T+2.*COP/3.E8
NEST=10
THFS=1.5/SFREC
TEST=NEST*T
NS=C
DO 20 I=1,20
DO 21 J=1,20
S(1,J)=0.
21 SSS(I,J)=0.
20 CONTINUE

C*****
C*
C* INCREMENT CLOCK.
C*
C*****

100 N = N + 1
T = T + DT

C*****
C*
C* INCREMENT TARGET POSITION AND STORE.
C* OBTAIN DELAYED TARGET POSITION.
C*
C*****

CALL DASUM (1,DC, DELE(DT), DF, DV, DF)
CALL DSTACIN (1, DT)
CALL DUVECT(DP, UCP, DRM, IE)
TTF = DRM/(3.E8*DT)
IF (N.LT. TTF) GO TO 100
CALL DSTACDT (1, TTF, RTOLD)

C*****
C*
C* COMPUTE TARGET TRACKING ERROR AS SEEN BY
C* SENSOR ON THE GIMFALS (USING THE DELAYED
C* TARGET POSITION).
C*
C*****

CALL DUVECT (FTCLC, U1, P, IE)
CALL DSUM (LT, UC, FEP, -1)
CALL DCDROSS (2, UC, XI)
CALL DUVECT (XI, XI, XI, IE)
CALL DCDROSS (LG, XI, ETA)


```

CALL CDCT (ERF, ETA, ERREL)
ERREL = -ERREL + EE(1)
CALL CDCT (ERF, XI, EFRAZ)
EFRAZ = EFRAZ + EE(2)

```

```

C*****
C*
C*      IMPLEMENT GIMBAL SERVO POINTING UPDATE.
C*
C*****

```

```

EFRAZ = EFRAZ/DSIN (THETA)
Q1TH = (ERREL - CLEAD * OTHER)/(1. - CLEAD)
Q1PH = (EFRAZ - CLEAD * OTHER)/(1. - CLEAD)
OTHER = ERREL
OTHER = EFRAZ
Q2TH = Q1TH * GAIN
Q2PH = Q1PH * GAIN
THINT1 = THINT1 + DT*Q2TH
PHINT1 = PHINT1 + DT * Q2PH
THINT2 = THINT2 + DT * THINT1
PHINT2 = PHINT2 + DT * PHINT1
THETA = THINT2
PHI = PHINT2
CALL DSPHFEC (THETA, PHI, 1.00, UG)

```

```

C-----
C-
C-      CALCULATE GLINT POSITION ON SENSOR FOCAL PLANE.
C-
C-----

```

```

CALL CMUNL(LG,RTOL,OC,CETW,XI,ETA,PUC,NUC)

```

```

C*****
C*
C*      INTRODUCE LASER BORESIGHT ERROR.
C*
C*****

```

```

T1 = THETA+EB(1)
P1 = PHI+EB(2)
CALL DSPHFEC(T1,P1,1.00,UL)

```

```

C*****
C*
C*      CALCULATE LASER TARGET MISS DISTANCE.
C*
C*****

```

```

CALL CSTACIN (2,UL)

```

```

IF (T.LT.*STAE) GO TO 100
TTF2=2*TTF
CALL ESTAC01 (2, TTF2, LLCLE)
CALL EOCT (LT, LLCLE, DTL)
SF = -DTL*R
CALL EWSUP (1,DC, SF, RTOLD, LLCLE, DLM)
CALL EUECT(DLM,UCLM,CLPM,IE)
IF (T.LT.*UF+1STAE) PRINT 320, T,CLPM
320 FORMAT (5),F5.3,SX,F6.2)
IF (T.LT.*UF+1STAE) GO TO 100

```

```

C-----
C-
C-      CALCULATE LASER POSITION ON TARGET AS SEEN
C-      ON SENSOR FOCAL PLANE, AND CLINT INTENSITY.
C-      CALCULATE THE ARRAY OF FOCAL PLANE SIGNAL
C-      INTENSITIES.
C-----

```

```

CAL ESMULT (-1.00,DLM,DLM)
CAL EMLNL(LG,RTOLD,DLM,DETH,XI,STA,MLO,NLO)
CAL ESMULT (-1.00,DLM,DLM)
X = MLG-MLO
Y = NLG-NLO
IC = 0
IC1 = X*X+Y*Y
IF (IC1,LT,.76) IC=1G2*EXP(-IC1)
CALL SIG(F,PUE,NUE,PUC,NUG,ID,IC,T,14,S)

```

```

C=====
C-
C-      INCREMENT GLINT/DIFFUSE SIGNAL ESTIPATOR
C-
C=====

```

```

230 I=1,20
231 J=1,20
SX=(1,J)
IF (.BS(SX),LT,1E-16) SX=0
SS(1,J)=SS(1,J)+SX
231 SS(I,J)=SS(I,J)+SX*SX
230 CONTINUE
NS=NS+1

```

```

C=====
C-
C-      FORM NEW DIFFUSE SIGNAL ESTIMATE.
C-
C=====

```

```

IF (NS.EQ.1) GO TO 240

```

```

D' 250 I=1.20
D' 251 J=1.20
SSX=SS(I,J)/NS
SSS=SSS(I,J)/NS
SSS = SSSX-SSX*SSX
IF (SSS).LT.0) SSS=C.
SSORT = SSX*SSX-SSS
IF (SSORT.LT.0) SSORT=C
EER(I,J) = SS-SORT(SSORT)
251 CONTINUE
250 CONTINUE

```

```

C=====
C=
C= ESTIMATE DIFFUSE RETURN'S POSITION.
C=
C=====

```

```

SEDF=C
MLEC=C.
NLEC=C.
D' 260 I=1.20
D' 261 J=1.20
SEDF=SECR+EER(I,J)
MLEC=MUED+I+EER(I,J)
261 MLEC=MUED+J+EER(I,J)
260 CONTINUE
MLEC=MUED/SEDF-10.5
NLEC=MUED/SEDF-10.5

```

```

C=====
C=
C= CALCULATE TARGET POSITION ON FOCAL PLANE.
C=
C=====

```

CALL CMLNL (UG,RTCLE,CXP,DETW,XI,ETA,MUT,AUT)

```

C=====
C=
C= CALCULATE ESTIMATED EPRCP SIGNAL
C= AND CLOSE LOOP.
C=
C=====

```

```

IF (T.LT.TUP+1STAE+TEST) GO TO 200
EE1 = -(NLT-NLEC)*DETH
EE2 = (MUT-MUED)*DETW
EE(1) = EE(1)+FACT*EE1
EE(2) = EE(2)+FACT*EE2
TLP = T

```



```
NS = 0
DC 310 I = 1.20
DC 311 J = 1.20
SE(I,J) = 0.
311 SES(I,J) = 0.
310 C TIAUE
300 CONTINUE
PRINT 270,T,MLED,MUC,MUED,NLD,MLT,NLT,MLG,NLG,DLMP
270 FORMAT (5),F5.3,2X,F6.2,F6.2,1X,F6.2,F6.2,1X,F6.2,X
      F6.2,1X,F6.2,F6.2,2X,F6.2)
240 CONTINUE
IF (N.LE.500) GO TO 100
END
```

ADDENDUM

ON

Adaptive Estimation

For

ACT Signal Processing

Robert B. Asher*

November 1977

* Department of Electrical Engineering
Texas Tech University
Lubbock, Texas 79423

ABSTRACT

This report contains the development of an adaptive estimator for glint and diffuse signal separation in adaptive optics. The back-scatter signal from a laser spot is focused onto a square detector array of 4×4 elements. The target rotation rate, the glint position and strength, and the laser spot position and strength are states to be estimated. The estimator is adaptive in the sense that the models used are functions of uncertain parameters, as previously derived, which are estimated by the estimation structure. The complete model realization and estimation structure are contained in this report.

A.1 Introduction

In order to develop an estimation structure for a given problem, it is necessary to obtain the physical models containing all the deterministic and statistical knowledge of the process. This knowledge must be obtained in a form that readily allows for either development of a new theory for estimation or use of an existing theory of estimation. Therefore, once the models are established in a physical form, these models still may be in a form not readily adaptable to an existing theory of estimation. This report considers taking the models as developed in the Optical Sciences Company reports entitled, "Diffuse Backscatter Focal Plane Statistics for a Laser Transmitter/Receiver," [Chapter 4 of this volume (TR-270)], and "Laser Transmitter/Receiver Sensor Definition and Signal Simulation," [Chapter 5 of this volume, (TR-272)], and using existing realization theory (theory of obtaining models in state space form from other statistical forms) in control theory from which the adaptive estimation structure may then be readily obtained. The adaptive estimation structure is given in a form for immediate programming.

In estimation problems, there are two forms that the information about the process to be estimated usually take. The first form is that of a differential (or discrete) equation format. The second form is that of a covariance function format. Estimation theory developments using the covariance function format run into the problem that, in order to synthesize an estimator structure optimal in the minimum mean square error sense, it is necessary to spectrally factor a complicated expression.^{1,2} However, in order to spectrally factor an expression to obtain an estimator realization using the covariance function (actually, the power spectral density), it is necessary to have a rational expression. Recent theories^{3,4} have advanced the state of the art in estimation theory by use of spectral factorization, but these theories are incomplete for several reasons. First,

it is necessary to start with a rational expression from the power spectral density (PSD). Secondly, the theories available, such as for example the Wiener filter, using this approach do not take into account the transient response of the estimator. It is assumed that the steady state response exists (that an infinite data stream is available). The theories available do not take into account any adaptiveness necessary for adaptation upon uncertain parameters or uncertain statistical information.

In using the differential (or discrete) equation form, it is necessary to realize a state space model for the process from the deterministic and/or statistical information about the process. However, in accomplishing this, if a covariance function for a process is the only statistical information available, it is necessary to use existing theories of realization. Since the theories are based upon certain forms for the covariance function, it is necessary to place the function into the form which will lead to an immediate application of the realization theory. Once the state space model is obtained, the existing adaptive estimation theories may be utilized or new theories developed in order to obtain the proper estimation structure.

This report considers the use of an existing theory of realization of state space models from covariance functions in order to develop the proper state space models from which the adaptive estimator may be obtained. It also gives the development of the adaptive estimator, including all assumptions utilized in the development. Furthermore, a computer program flow chart is outlined in order to obtain the required computer program.

The report is divided into sections. The next section considers the problem statement for the estimation problem. The third section yields the measurement models for the problem. The fourth section contains the model realization problem. The fifth section contains the adaptive estimator development as well as the flow chart. The last section contains the conclusions for the theoretical development as well as suggestions for future development.

A.2. Problem Statement

The backscattered signal from the target is focused upon a square detector array of 4×4 elements. As defined in Report No. TR-272 as previously referenced, the elements are of angular size $1/k\sigma \times 1/k\sigma$ where σ^2 is the variance parameter of the transmitter/receiver aperture with gaussian taper, and k is the wavenumber. The coordinates of the centers of the ij^{th} detector are given in Eq. (5) of the previously mentioned report as

$$\theta_{x_{ij}} = \frac{(i-2.5)}{k\sigma} \quad , \quad (1)$$

and

$$\theta_{y_{ij}} = \frac{(j-2.5)}{k\sigma} \quad . \quad (2)$$

Each detector yields an output which is a function of both the diffuse laser spot location and strength and the glint spot location and strength. Furthermore, outputs will be a function of the rotation rate of the target.

The diffuse laser spot is centered at angular location $\{\theta_{x,D}, \theta_{y,D}\}^T$ or $\{(\mu_D/k\sigma), (\nu_D/k\sigma)\}^T$. The cross covariance function for the diffuse signal at the ij^{th} detector with the $i'j'^{\text{th}}$ detector, from Report No. TR-272, is

$$C_D(i, j; i'j'; \tau) = \bar{S}_D(i, j) \bar{S}_D(i', j') \exp \left\{ -\frac{1}{4} [(i-i')^2 + (j-j')^2] \right\} \\ \times \exp \left\{ -\frac{1}{2} (\tau/T)^2 \right\} \quad , \quad (3)$$

where

$$T = \frac{\sigma}{\sqrt{2} R \alpha} \quad , \quad (4)$$

with R the range to the target and α the target rotation rate, and

$$\bar{S}_D(i, j) = I_D \exp \left\{ -\frac{1}{2} \{ [\mu_D - (i-2.5)]^2 + [\nu_D - (j-2.5)]^2 \} \right\} \quad , \quad (5)$$

where I_0 is a constant I_0' times a scale factor. Outputs will be a function of the rotation rate of the target.

A.3. Measurement Models

The measurement equation for the ij^{th} detector is

$$y_{ij}(t) = \frac{1}{2} \{ A_{\parallel}(i, j, t) + A_g(i, j, t) \}^2 + \frac{1}{2} \{ A_{\perp}(i, j, t) \}^2 + n_{ij}(t) ,$$

$$\begin{aligned} i &= 1, 2, 3, 4 \\ j &= 1, 2, 3, 4 \end{aligned} \quad (6)$$

where A_{\parallel} and A_{\perp} are the amplitudes associated with the diffuse signal part of the return, A_g is the glint signal, and $n(t)$ is zero mean white noise with covariance

$$E \{ n_{ij}(t) n_{ij}(t') \} = \sigma_{ij}^2 \delta(t-t') \quad (6a)$$

and

$$E \{ n_{ij}(t) n_{kl}(t) \} = 0 \quad (6b)$$

for $ij \neq kl$. Here and throughout this paper, notation of the form of $\delta(t-t')$ denotes a Kronecker delta (as distinct from a Dirac delta) function.

The amplitude components may be written as

$$A_{\parallel}(i, j, t) = \left(\frac{I_0}{8\pi^{3/2}} \right)^{1/2} \exp \left\{ -\frac{1}{4} \{ [\mu_0 - (i-2.5)]^2 + [\nu_0 - (j-2.5)]^2 \} \right\} \tilde{A}_{\parallel}(i, j, t), \quad (7)$$

$$A_{\perp}(i, j, t) = \left(\frac{I_0}{8\pi^{3/2}} \right)^{1/2} \exp \left\{ -\frac{1}{4} \{ [\mu_0 - (i-2.5)]^2 + [\nu_0 - (j-2.5)]^2 \} \right\} \tilde{A}_{\perp}(i, j, t), \quad (8)$$

and

$$A_g(i, j) = (2I_0)^{1/2} \exp \left\{ -\frac{1}{2} \{ [\mu_g - (i-2.5)]^2 + [\nu_g - (j-2.5)]^2 \} \right\} ,$$

$$i, j = 1, 2, 3, 4 . \quad (9)$$

where μ_0 and ν_0 are the angles associated with the laser spot, μ_g and ν_g are the angles associated with the glint point, i, j are the integers associated with the ij^{th} element, I_0 is the scaling amplitude for the diffuse power, I_g is the scaling amplitude for the glint power, and \tilde{A}_{\parallel} and \tilde{A}_{\perp} are random temporally-varying factors which determine the random temporal variation of the amplitudes. It is assumed that I_0 , I_g , μ_0 , ν_0 , μ_g , and ν_g are unknowns in the measurement model, but that they are constants for the time intervals of estimation.

Therefore, the estimation problem becomes that of estimating the temporally-varying signal components \tilde{A}_{\parallel} and \tilde{A}_{\perp} , while simultaneously estimating the uncertain parameters in the measurement model, I_0 , I_g , μ_0 , ν_0 , μ_g , and ν_g , and the uncertain rotation rate, α , contained in the dynamic model for the random temporally-varying signal factors \tilde{A}_{\parallel} and \tilde{A}_{\perp} .

In order to obtain an estimator, it is necessary to develop a performance measure for the estimator. This performance measure will be the minimum mean square error. As the measurement is nonlinear, an extended estimator^{5,6} algorithm will be used for the adaptive estimator. This structure is based upon a moment expansion approximation which will be explained later.

The measurement equation may then be written as

$$y_{ij}(t) = \frac{1}{2} \left(\frac{I_0}{8\pi^{3/2}} \right) \exp \left\{ -\frac{1}{2} \{ [\mu_0 - (i-2.5)]^2 + [\nu_0 - (j-2.5)]^2 \} \right\} \\ \times \tilde{A}_{\parallel}^2(i, j, t) + \left(\frac{I_0}{8\pi^{3/2}} \right)^{1/2} (2I_g)^{1/2} \exp \left\{ -\frac{1}{2} \{ [\mu_0 - (i-2.5)]^2 \right. \\ \left. + [\nu_0 - (j-2.5)]^2 \} - \frac{1}{2} \{ [\mu_g - (i-2.5)]^2 + [\nu_g - (j-2.5)]^2 \} \right\} \\ \times \tilde{A}_{\perp}(i, j, t) + I_g \exp \left\{ -\{ [\mu_g - (i-2.5)]^2 + [\nu_g - (j-2.5)]^2 \} \right\}$$

$$\begin{aligned}
& + \frac{1}{2} \left(\frac{I_0}{8\pi^{3/2}} \right) \exp \left\{ -\frac{1}{2} \{ [\mu_0 - (i-2.5)]^2 + [\nu_0 - (j-2.5)]^2 \} \right\} \\
& \times \tilde{A}_\perp^2(i, j, t) + n_{ij}(t) \quad , \quad i, j = 1, 2, 3, 4 \quad . \quad (10)
\end{aligned}$$

This equation may be written in a simpler form as

$$\begin{aligned}
y_{ij}(t) = D_1^{ij}(\theta) [\tilde{A}_\parallel^2(i, j, t) + \tilde{A}_\perp^2(i, j, t)] + D_2^{ij}(\theta) \tilde{A}_\parallel(i, j, t) + D_3^{ij}(\theta) \\
+ n_{ij}(t) \quad , \quad (11)
\end{aligned}$$

where the parameter vector $\theta = \{I_0, I_g, \mu_0, \nu_0, \mu_g, \nu_g\}^T$ contains the uncertain parameters to be estimated, and the D_i 's are given as follows:

$$D_1^{ij}(\theta) = \frac{1}{2} \left(\frac{I_0}{8\pi^{3/2}} \right) \exp \left\{ -\frac{1}{2} \{ [\mu_0 - (i-2.5)]^2 + [\nu_0 - (j-2.5)]^2 \} \right\} \quad , \quad (12)$$

$$\begin{aligned}
D_2^{ij}(\theta) = \left(\frac{I_0}{8\pi^{3/2}} \right)^{1/2} (2 I_g)^{1/2} \exp \left\{ -\frac{1}{4} \{ [\mu_0 - (i-2.5)]^2 + [\nu_0 - (j-2.5)]^2 \} \right. \\
\left. - \frac{1}{2} \{ [\mu_g - (i-2.5)]^2 + [\nu_g - (j-2.5)]^2 \} \right\} \quad , \quad (13)
\end{aligned}$$

and

$$D_3^{ij}(\theta) = I_g \exp \left\{ -\{ [\mu_g - (i-2.5)]^2 + [\nu_g - (j-2.5)]^2 \} \right\} \quad . \quad (14)$$

The equation for the y_{ij} 's may be modified to take into account a known time dependence for μ_0 and ν_0 . The known form for the time dependence may contain certain scale factors and/or other parameters reflecting the uncertainty of the μ_0 and ν_0 parameters.

A.4. State Space Realization

The basic problem is to estimate both the parameters I_0 , I_0 , ω_0 , and ν_0 . However, in order to properly estimate these parameters, along with the uncertain rotation rate, it is necessary to also estimate the random temporally-varying terms, \tilde{A}_{\parallel} and \tilde{A}_{\perp} .

Fried has developed the correlation functions for these terms. They are given as

$$R_{\tilde{A}_\ell}(i, j, n) = 8\pi^{3/2} \exp \left\{ -\frac{1}{8} (i^2 + j^2 + \frac{1}{8} n^2) \right\}, \quad \ell = \parallel, \perp, \quad (15)$$

where $n = \tau/T$. The dependency on i and j denotes not the ij^{th} detector, but the separation between the detectors. It may be noted that this correlation function is separable. That is, it may be written as

$$R_{\tilde{A}_\ell}(i, j, n) = 8\pi^{3/2} \exp \left\{ -\frac{1}{8} i^2 \right\} \exp \left\{ -\frac{1}{8} j^2 \right\} \exp \left\{ -\frac{1}{64} n^2 \right\}, \quad \ell = \parallel, \perp. \quad (16)$$

In order to synthesize an estimation structure that will yield a reasonable level of computations, it will be assumed that for the estimator development, the spatial correlation does not influence the problem in a large manner. With this assumption, it is necessary to develop a differential equation model for each ij randomly-varying component with correlation function

$$R_{\tilde{A}_{ij\ell}}(t-s) = 8\pi^{3/2} \exp \left\{ -\frac{1}{64} \frac{(t-s)^2}{T^2} \right\}, \quad \ell = \perp, \parallel. \quad (17)$$

The differential equation model will allow for a readily implementable estimator for the problem.

In order to proceed, a particular problem decomposition may be made. Consider a $c(t)$ where $\tilde{A}_{ij\ell}(t) = c_{ij\ell}(t)$ such that

$$\begin{aligned} E \{c(t) c(s)\} &= \sum_{i=1}^p \alpha_i (\max(t, s)) \beta_i (\min(t, s)) \\ &= \underline{\alpha} (\max(t, s)) \underline{\beta} (\min(t, s)) \end{aligned}$$

for each ij and $\ell = 1, \dots, p$, where

$$\underline{\alpha} = [\alpha_1, \alpha_2, \dots, \alpha_p] \quad (19)$$

and

$$\underline{\beta} = \begin{bmatrix} \beta_1 \\ \beta_2 \\ \vdots \\ \beta_p \end{bmatrix} \quad (20)$$

Then $c(t)$ may be written (for each detector) as

$$c(t) = m(t) x(t)$$

where m and x will be defined later. This provides a mathematical model of $c(t)$ which satisfies the point temporal correlation function for $c(t)$. The definition of the proper m_p and x_p will now be given.

Let $A(t)$ be an arbitrary square $q_1 \times q_1$ matrix with finite-valued elements $a_{ij}(t)$. Define the state transition matrix, $\Phi(t, s)$ which is a $p \times p$ square matrix with elements $\Phi_{ij}(t, s)$ which satisfy the following differential equations coupled together

$$\frac{d \Phi_{ij}(t, s)}{dt} = \sum_{j=1}^p a_{ij}(t) \Phi_{ij}(t, s) \quad ; \quad i, j = 1, 2, \dots, p \quad (21)$$

with initial conditions

$$\Phi_{ij}(t_0, t_0) = \delta(i-j) \quad . \quad (22)$$

We may define $m(t)$ as the new vector

$$m(t) = [m_1(t), m_2(t), \dots, m_p(t)] \quad ,$$

where the i^{th} element is given as

$$m_i(t) = \sum_{j=1}^p \alpha_j \Phi_{ij}(t, t_0) \quad , \quad i = 1, 2, \dots, p \quad (23)$$

In order to define the column vector, $x(t)$, let us first define some auxiliary variables. Define $n(t)$ as the column vector

$$n(t) = \begin{bmatrix} n_1(t) \\ n_2(t) \\ \vdots \\ n_p(t) \end{bmatrix} \quad (24)$$

with the i^{th} element

$$n_i(t) = \sum_{j=1}^p \Phi_{ij}(t, t_0) \beta_j(t) \quad , \quad (25)$$

where β_j is the j^{th} element of the vector in Eq. (20).

Define $P(t)$ as the $p \times p$ matrix with ij^{th} element found as the solution to the following coupled set of differential equations

$$\begin{aligned} \dot{P}_{ij}(t) = & \sum_{k=1}^p a_{ik}(t) P_{kj}(t) + \sum_{k=1}^p P_{ik}(t) a_{jk}(t) + \left\{ n_i(t) - \sum_{k=1}^p P_{ik}(t) m_k(t) \right\} \\ & \times \left\{ n_j(t) - \sum_{k=1}^p P_{jk}(t) m_k(t) \right\}, \quad i, j = 1, 2, \dots, p \end{aligned} \quad (26)$$

with initial conditions

$$P_{ij}(t_0) = 0, \quad i, j = 1, 2, \dots, p.$$

Define $\gamma(t)$ to be the column vector

$$\gamma(t) = \begin{bmatrix} \gamma_1(t) \\ \gamma_2(t) \\ \vdots \\ \gamma_p(t) \end{bmatrix}, \quad (27)$$

such that

$$\gamma_i(t) = n_i(t) - \sum_{k=1}^p P_{ik}(t) m_k(t), \quad i = 1, 2, \dots, p. \quad (28)$$

The required column vector $x(t)$ is the solution to the coupled differential equations with i^{th} element

$$\dot{x}_i(t) = \sum_{k=1}^p a_{ik}(t) x_k(t) + \gamma_i(t) v(t), \quad (29)$$

where $v(t)$ is a white noise process with zero mean and covariance

$$E \{v(t) v(s)\} = \delta(t-s) \quad .$$

The initial condition of $x(t)$ is left unspecified. However, for the estimation problem, it is assumed that $x(t_0) = 0$, with the reliance on the interactions to force convergence.

We note here that a property of $\Phi(t, s)$ is that the solution to Eq. (29) may be written as follows for the i th element.

$$x_i(t) = \sum_{k=1}^p \Phi_{ik}(t, s) x_k(s) + \int_s^t \left(\sum_{k=1}^p \Phi_{ik}(t, \tau) \gamma_k(\tau) \right) v(\tau) d\tau \quad ,$$

$$i = 1, 2, \dots, p \quad . \quad (30)$$

From the statistics of $R_{\tilde{A}}$, we see that $c(t)$ is a Gaussian exponential which may be written as a simple power series,

$$E \{c(t) c(s)\} = 8\pi^{3/2} \sum_{\mu=0}^{\infty} \frac{\left\{ -\frac{1}{64} \frac{(t-s)^2}{T^2} \right\}^{\mu}}{\mu!}$$

$$\approx 8\pi^{3/2} \sum_{\mu=0}^1 \left\{ \left(-\frac{1}{64}\right) \frac{(t-s)^2}{T^2} \right\}^{\mu}$$

$$= 8\pi^{3/2} \left\{ 1 - \frac{1}{64} \frac{t^2}{T^2} + \frac{1}{32} \frac{ts}{T^2} - \frac{1}{64} \frac{s^2}{T^2} \right\} \quad . \quad (31)$$

This may be written as

$$E \{c(t) c(s)\} \approx \sum_{k=1}^4 \alpha_k(t) \beta_k(s) \quad (32a)$$

where

$$\alpha_1(t) = 8\pi^{3/2}$$

$$\alpha_2(t) = - \frac{8\pi^{3/2} t^2}{64 T^2}$$

$$\alpha_3(t) = \frac{8\pi^{3/2}}{32} \frac{t}{T}$$

$$\alpha_4(t) = - \frac{8\pi^{3/2}}{64}$$

$$\beta_1(s) = 1$$

$$\beta_2(s) = 0$$

$$\beta_3(s) = \frac{s}{T}$$

and

$$\beta_4(s) = \frac{s^2}{T^2} \quad (32b)$$

[Note that Eq. (32a) is unaffected if s and t are interchanged in Eq. (32b).]

For each of the two components of the amplitudes and each of the sixteen detectors, the models for the temporally-varying components may be written in terms of the previous development. Therefore, for each detector, the parallel component of amplitude will be given by four x 's denoted as $x_{1ij}^{\parallel}(t)$, $x_{2ij}^{\parallel}(t)$, $x_{3ij}^{\parallel}(t)$, and $x_{4ij}^{\parallel}(t)$, where this ij denotes the ij^{th} detector. The perpendicular components may be written as $x_{1ij}^{\perp}(t)$, $x_{2ij}^{\perp}(t)$, $x_{3ij}^{\perp}(t)$, and $x_{4ij}^{\perp}(t)$. The models for the x 's are found by first recognizing that the α_k 's and β_k 's for both the \parallel and \perp components for each detector are given in Eq. (32). These are used to form the m 's and n 's, as in Eq.'s (23) and (25). With the n 's and m 's, Eq. (26) is used to solve for the P 's. Eq. (28) is used to solve for the γ 's, and Eq. (29) may be used to simulate the x 's as well as for the estimator design. Again, we wish to state that there are 32

of these models, consisting of 4 components each. Once the x 's are formed, the measurement equation, as in Eq. (10), may be rewritten as

$$y_{ij}(t) = D_1^{ij}(\theta) \left\{ \left(\sum_{k=1}^4 m_k(t) x_{kij}^{\parallel}(t) \right)^2 + \left(\sum_{k=1}^4 m_k(t) x_{kij}^{\perp}(t) \right)^2 \right\} \\ + D_2^{ij}(\theta) \left(\sum_{k=1}^4 m_k(t) x_{kij}^{\parallel}(t) \right) + D_3^{ij}(\theta) + n_{ij}(t) , \\ i, j = 1 \dots 4 . \quad (33)$$

In order to find a discrete form for the models for the x 's, we may discretize the equation in Eq. (29). The reason for this is to develop a form that may be used in a digital computer.

The use of Eq. (30) and the known replacement of a Markov process noise term with a Markov sequence yields

$$x_k(n+1) = \sum_{\ell=1}^4 \Phi_{k\ell}(n+1, n) x_{\ell}(n) + \Gamma_k(n) w(n) , \quad (34)$$

where

$$\Gamma_k(n) = \int_{n\tau}^{(n+1)\tau} \sum_{\ell=1}^4 \Phi_{k\ell}(n+1, \tau) \gamma_{\ell}(\tau) d\tau , \quad (35)$$

and with $w(n)$ a white noise process, zero mean and variance,

$$\cos(w(n)) = \frac{1}{T} . \quad * \quad (36)$$

* See Bryson and Ho, Applied Optimal Control, Ginn Blaisdell, 1969.

One point to be noticed is that T is a function of rotation rate. Therefore, the Γ_k 's in Eq. (35) and the covariance in Eq. (36) are functions of the rotation rate. This is an explicit dependence.

The next section considers the adaptive estimator.

A.5. Adaptive Estimator

This section contains the development of the adaptive estimator structure for the problem. The structure is based upon a well-known expansion technique to linearize the nonlinear measurements. It will be assumed that the state equations are in the discrete time form [with, for example, $x(n)$ replacing $x(t)$]. We will use the notation $\hat{x}(n|n')$ to indicate the expectation of $x(n)$ based on the measurements up to time n' . We will use the notation $\hat{x}(n|n', \mathcal{P}_p)$ to imply the expectation of $x(n)$ based on the measurements up to n' and assuming that the parameter set \mathcal{P} has some specific values given by \mathcal{P}_p . We will write $Y(n) = \{y(n), y(n-1), y(n-2), \dots\}$.

With this notation, we have

$$\hat{x}_{\ell_{ij}}^{\perp}(n|n') = \int \hat{x}_{\ell_{ij}}^{\perp}(n|n', \mathcal{P}_p) p(\mathcal{P}_p | n') d\mathcal{P}_p, \quad (37)$$

and

$$\hat{x}_{\ell_{ij}}^{\parallel}(n|n') = \int \hat{x}_{\ell_{ij}}^{\parallel}(n|n', \mathcal{P}_p) p(\mathcal{P}_p | n') d\mathcal{P}_p, \quad (38)$$

where $\hat{x}_{\ell_{ij}}^{\parallel}$ denotes the ℓ^{th} component of the vector x for the parallel component on the ij^{th} detector, and similarly, for $\hat{x}_{\ell_{ij}}^{\perp}$. The term $p(\mathcal{P}_p | n')$ denotes the probability density function of \mathcal{P} conditioned on $Y(n')$.

The procedure to be followed is to find $\hat{x}(n|n', \mathcal{P}_p)$ for both the parallel and perpendicular components at each of the 16 detectors, and

then use these estimates in the calculation of the probabilities for the parameters. The form of the estimator conditioned on each parameter set is given as follows at each detector.

$$\begin{aligned}
 \hat{x}_{\ell, ij}^{\perp}(n+1 | n+1, \mathbb{P}_p) = & \hat{x}_{\ell, ij}^{\perp}(n+1 | n, \mathbb{P}_p) + K_{\ell, ij}^{\perp} \left\{ y_{ij}(n+1) \right. \\
 & - D_1^{ij}(\mathbb{P}_p) \left\{ \left(\sum_{k=1}^4 m_k(n+1) \hat{x}_{k, ij}^{\parallel}(n+1 | n, \mathbb{P}_p) \right)^2 \right. \\
 & \left. \left. + \left(\sum_{k=1}^4 m_k(n+1) \hat{x}_{k, ij}^{\perp}(n+1 | n, \mathbb{P}_p) \right)^2 \right\} \right. \\
 & - D_2^{ij}(\mathbb{P}_p) \left(\sum_{k=1}^4 m_k(n+1) \hat{x}_{k, ij}^{\parallel}(n+1 | n, \mathbb{P}_p) \right) \\
 & \left. - D_3^{ij}(\mathbb{P}_p) \right\} , \tag{39}
 \end{aligned}$$

and

$$\begin{aligned}
 \hat{x}_{\ell, ij}^{\parallel}(n+1 | n+1, \mathbb{P}_p) = & \hat{x}_{\ell, ij}^{\parallel}(n+1 | \mathbb{P}_p) + K_{\ell, ij}^{\parallel} \left\{ y_{ij}(n+1) \right. \\
 & - D_1^{ij}(\mathbb{P}_p) \left\{ \left(\sum_{k=1}^4 m_k(n+1) \hat{x}_{k, ij}^{\parallel}(n+1 | n, \mathbb{P}_p) \right)^2 \right. \\
 & \left. \left. + \left(\sum_{k=1}^4 m_k(n+1) \hat{x}_{k, ij}^{\perp}(n+1 | n, \mathbb{P}_p) \right)^2 \right\} \right. \\
 & - D_2^{ij}(\mathbb{P}_p) \left(\sum_{k=1}^4 m_k(n+1) \hat{x}_{k, ij}^{\parallel}(n+1 | n, \mathbb{P}_p) \right) \\
 & \left. - D_3^{ij}(\mathbb{P}_p) \right\} \tag{40}
 \end{aligned}$$

where

$$\hat{x}_{\ell, ij}^{\parallel}(n+1 | n, \mathbb{P}_p) = \sum_{k=1}^4 \Phi_{\ell k}(n+1, n) \hat{x}_{k, ij}(n | n, \mathbb{P}_p) , \tag{41}$$

and

$$\hat{x}_{\ell, ij}^{\perp}(n+1|n, \mathbb{P}_p) = \sum_{k=1}^4 \Phi_{\ell k}(n+1, n) \hat{x}_{k, ij}^{\perp}(n|n, \mathbb{P}_p) \quad ,$$

for $i, j, \ell = 1, 2, 3, 4$. (42)

For computations of the gain, it is necessary to first compute $V(n+1|n, \mathbb{P}_p)$, where $V(n+1|n, \mathbb{P}_p)$ is the approximation to the covariance of the mean square estimation error conditioned on \mathbb{P}_p at time $n+1$, given n measurements. Between measurements, the covariance elements may be computed as

$$V_{ij}^{k\ell, \parallel}(n+1|n, \mathbb{P}_p) = \sum_{\bar{k}=1}^4 \sum_{\bar{\ell}=1}^4 \Phi_{k\bar{k}}(n+1, n) \cdot V_{ij}^{\bar{k}\bar{\ell}, \parallel}(n|n, \mathbb{P}_p) \Phi_{\ell\bar{\ell}}(n+1, n) + \Gamma_k(n, \mathbb{P}_p) \Gamma_{\ell}(n, \mathbb{P}_p) \quad ,$$

(43)

where the superscript denotes the $k\ell^{\text{th}}$ element for the parallel component, and the subscript denotes the ij^{th} detector.

The equation for the perpendicular component is

$$V_{ij}^{k\ell, \perp}(n+1|n, \mathbb{P}_p) = \sum_{\bar{k}=1}^4 \sum_{\bar{\ell}=1}^4 \Phi_{k\bar{k}}(n+1, n) V_{ij}^{\bar{k}\bar{\ell}, \perp}(n|n, \mathbb{P}_p) \Phi_{\ell\bar{\ell}}(n+1, n) + \Gamma_k(n, \mathbb{P}_p) \Gamma_{\ell}(n| \mathbb{P}_p) \quad .$$

(44)

The cross covariance between the estimation error for the parallel and perpendicular components $V_{k\ell}^{\perp, \parallel}$ where the ij -detector dependence has been eliminated is given as

$$V_{k\ell}^{\perp, \parallel}(n+1|n, \mathbb{P}_p) = \Gamma_k(n, \mathbb{P}_p) \Gamma_{\ell}(n, \mathbb{P}_p) \quad .$$

(45)

The pertinent equations for the gain may be calculated as follows.

Denote

$$\frac{\partial h}{\partial x_{k,ij}^{\parallel}} = 2 D_{1,ij}(\mathbb{P}_p) \left(\sum_{k=1}^4 m_k(n+1) x_{k,ij}^{\parallel}(n+1) m_k(n+1) \right) + D_{2,ij}(\mathbb{P}_p) m_k(n+1), \quad (46)$$

and

$$\frac{\partial h}{\partial x_{k,ij}^{\perp}} = 2 D_{1,ij}(\mathbb{P}_p) \left(\sum_{k=1}^4 m_k(n+1) x_{k,ij}^{\perp}(n+1) \right) m_k(n+1). \quad (47)$$

Let

$$\begin{aligned} S_{ij}^p &= \sum_{n=1}^4 \frac{\partial h}{\partial x_{n,ij}^{\parallel}} \left(\sum_{\bar{n}=1}^4 V_{ij}^{n,\bar{n},\parallel}(n+1|n, \mathbb{P}_p) \frac{\partial h}{\partial x_{n,ij}^{\parallel}} + \sum_{\bar{n}=1}^4 V_{ij}^{n,\bar{n},\perp}(n+1|n, \mathbb{P}_p) \frac{\partial h}{\partial x_{n,ij}^{\perp}} \right) \\ &+ \sum_{n=1}^4 \frac{\partial h}{\partial x_{n,ij}^{\perp}} \left(\sum_{\bar{n}=1}^4 V_{ij}^{n,\bar{n},\parallel}(n+1|n, \mathbb{P}_p) \frac{\partial h}{\partial x_{n,ij}^{\parallel}} \right. \\ &\left. + \sum_{\bar{n}=1}^4 V_{ij}^{n,\bar{n},\perp}(n+1|n, \mathbb{P}_p) \frac{\partial h}{\partial x_{n,ij}^{\perp}} \right) + r_{ij}, \end{aligned} \quad (48)$$

where the partials are evaluated at $\hat{x}_{ij}^{\parallel}(n+1|n, \mathbb{P}_p)$, and $\hat{x}_{ij}^{\perp}(n+1|n, \mathbb{P}_p)$, respectively.

The Kalman gains are

$$\begin{aligned} K_{k,ij}^{\parallel} &= \left\{ \sum_{n=1}^4 V_{ij}^{k,n,\parallel}(n+1|n, \mathbb{P}_p) \frac{\partial h}{\partial x_{n,ij}^{\parallel}} \right\} \hat{x}_{ij}^{\parallel}(n+1|n, \mathbb{P}_p) + \sum_{n=1}^4 V_{ij}^{k,n,\parallel}(n+1|n, \mathbb{P}_p) \\ &\times \frac{\partial h}{\partial x_{n,ij}^{\perp}} \left\{ \hat{x}_{ij}^{\perp}(n+1|n, \mathbb{P}_p) \right\} S_{ij}^{\perp}, \end{aligned} \quad (49)$$

AD-A055 177

OPTICAL SCIENCES CO PLACENTIA CA
ADAPTIVE COMPENSATION TECHNIQUES.(U)

F/G 17/8

MAY 78 D L FRIED, E J SCHONHEINZ, R B ASHER

F30602-77-C-0099

UNCLASSIFIED

DR-105

RADC-TR-78-101

NL

5 OF 5
AD
A055 177



END
DATE
FILMED
7-78
DDC

and

$$K_{k,ij}^{\perp} = \left\{ \sum_{n=1}^4 V_{kn}^{\perp, \parallel} (n+1 | n, \mathcal{P}_p) \frac{\partial h}{\partial x_{ij}^{\parallel}} \right|_{\hat{x}^{\parallel} (n+1 | n, \mathcal{P}_p)} + \sum_{n=1}^4 V_{ij, kn}^{\perp, \perp} (n+1 | n, \mathcal{P}_p) \frac{\partial h}{\partial x_{ij}^{\perp}} \right|_{\hat{x}^{\perp} (n+1 | n, \mathcal{P}_p)} \} S_{ij}^{\perp -1} . \quad (50)$$

Then, at measurement

$$\begin{aligned} V_{ij}^{k\ell, \parallel} (n+1 | n+1, \mathcal{P}_p) &= \sum_{n=1}^4 \left\{ \delta(k-m) - K_{k,ij}^{\parallel} \frac{\partial h}{\partial x_{ij}^{\parallel}} \right|_{x^{\parallel} = \hat{x}^{\parallel}_{ij} (n+1 | n, \mathcal{P}_p)} \} \\ &\times V_{ij}^{m\ell, \parallel} (n+1 | n, \mathcal{P}_p) \\ &+ \sum_{n=1}^4 \left\{ -K_{k,ij}^{\perp} \frac{\partial h}{\partial x_{ij}^{\perp}} \right|_{x^{\perp} = \hat{x}^{\perp}_{ij} (n+1 | n, \mathcal{P}_p)} \} \\ &\times V_{ij}^{m\ell, \perp} (n+1 | n, \mathcal{P}_p) , \end{aligned} \quad (51)$$

and

$$\begin{aligned} V_{ij}^{k\ell, \perp} (n+1 | n+1, \mathcal{P}_p) &= \sum_{n=1}^4 \left\{ -K_{k,ij}^{\parallel} \frac{\partial h}{\partial x_{ij}^{\parallel}} \right|_{x^{\parallel} = \hat{x}^{\parallel}_{ij} (n+1 | \mathcal{P}_p)} \} \\ &\times V_{ij}^{m\ell, \parallel} (n+1 | n, \mathcal{P}_p) \\ &+ \sum_{n=1}^4 \left\{ \delta(k-m) - K_{k,ij}^{\perp} \frac{\partial h}{\partial x_{ij}^{\perp}} \right|_{x^{\perp} = \hat{x}^{\perp}_{ij} (n+1 | n, \mathcal{P}_p)} \} \\ &\times V_{ij}^{m\ell, \perp} (n+1 | n, \mathcal{P}_p) , \end{aligned} \quad (52)$$

The computations of the V 's yield an approximate measure of filter performance, as they are approximate mean square estimation error terms. The K 's are the extended Kalman filter gains conditioned on \mathbb{P}_p being the correct parameter vector. This algorithm, called the extended Kalman filter, yields an approximation to the optimal estimator conditioned on \mathbb{P}_p . The approximation made was that of linearizing about the current best \mathbb{P}_p -conditional estimate of the state.

In the above algorithm, the K 's weight the information. There will be 128 of these estimates, four for the parallel components and four for the perpendicular components on each detector. One subroutine may be written in order to take advantage of similar computations.

In order to compute the necessary probabilities for each \mathbb{P}_p , it is necessary to store the residuals in Eq. (39) and Eq. (40) for each detector. These residuals use the measurement minus the expected measurement terms in the above-mentioned equations. Also, it is necessary to store S_{ij} in Eq. (48) for each detector. The residuals will be denoted as v_{ij}^p contained in the measurements with the a priori dynamical information about the state. The weighting is a complex function of all the a priori knowledge of the system, including the goodness of the measurements as measured by the covariance of the measurement noise. If the measurement noise is low, the gains will be large. If the measurement noise is high, then the estimator will weight the a priori dynamical knowledge heavily. Then the probability of the p^{th} parameter is

$$\Pr (\mathbb{P}_p | Y(n+1)) = \frac{(\xi^p)^{-1/2} \exp \left(-\frac{1}{2} \psi_p \right) \Pr (\mathbb{P}_p | Y(n))}{\sum_{l=1}^q (\xi^l)^{-1/2} \exp \left(-\frac{1}{2} \psi_l \right) \Pr (\mathbb{P}_l | Y(n))} \quad (53)$$

where

$$\psi_p = \sum_{i=1}^4 \sum_{j=1}^4 (v_{ij}^p)^2 S_{ij}^p, \quad (54)$$

and

$$\xi_p = \prod_{i=1}^4 \prod_{j=1}^4 S_{ij}^p. \quad (55)$$

This recursive equation yields the required knowledge about the parameters. The S_{ij}^p 's yield the \mathbb{P}_p -dependent variance of the measurement residual system.

The initial conditions for $\hat{x}(0)$, $P(0)$, and $\Pr(\mathbb{P}_p)$ must be chosen for each channel and each possible parameter vector.

The initial probabilities are chosen based upon the a priori knowledge of the parameter grid structure. If all parameters are equally likely, then the initial probabilities may be chosen to be $\Pr(\mathbb{P}_p) = 1/q$ where it is assumed that there are q possible parameters. It may be noted that Eq. (53) is a recursive equation. That is, the last values of the probabilities, i.e., $\Pr\{\mathbb{P}_p | Y(n)\}$ are used to compute $\Pr\{\mathbb{P}_p | Y(n+1)\}$.

It is suggested that the algorithm be completely automated so that we may choose different and higher order expansions. Furthermore, it is suggested that the measurement partials be taken numerically.

With the above realizations algorithm assumed complete, the estimation algorithm proceeds as follows:

1. Initialize the initial guesses for the parameters. This is done by determining a grid for each possible parameter. Since there are seven parameters, this grid will be large. It is necessary to then choose the q 's possible parameter values for the starting grid discretization.

The initial probabilities may be initialized by letting the initial probabilities be $1/q$. This gives a uniform density for the initial probability density.

It is necessary to choose the initial estimates for the states. This includes each of the \mathbb{P}_p -conditional estimators. An adequate guess may be zero. It is necessary to determine initial values for the \mathbb{P}_p -conditional covariances, $V(0|0, \bar{\theta}_j)$. A good guess may be to take the maximum variance of uncertainty for each amplitude component and use this in the diagonal elements of the covariance matrix.

2. Once the initialization is accomplished, then the simulation is called to give the first set of detector measurements. This set should include any possible detector noise. If it does, then each noise term must come from an independent random number generator.

3. The detector measurements are processed through the \mathbb{P}_p -conditional estimator for each value of \mathbb{P}_p . This proceeds as previously given.

This includes both a propagation for the \mathbb{P}_p -conditional covariance between measurements, the calculation of the Kalman gain for the measurement system, the computation of the \mathbb{P}_p -conditional estimate of the state vector, and the updating of the covariance matrix at a measurement. Both the \mathbb{P}_p -conditional estimates, the \mathbb{P}_p -conditional covariances, the residuals as defined, and the term for the measurement covariances saved as output from this subroutine.

4. The probabilities of each \mathbb{P}_p are computed for each P . If the probability of one or several of the parameters goes to zero, then these parameters may be assumed not to be or even bound the true parameter set. Therefore, these parameters may be dropped from the grid structure.

It is advisable at this point to rediscritize the grid in order to more closely bound the true parameter vector. As time proceeds, the grid structure will become finer and finer until the parameter vector which is the true one is learned.

5. Once the \mathbb{P}_p -conditional estimates and the probabilities are obtained, then one can find the optimal estimate of the state. This is

$$\hat{\mathbf{x}}(n) = \sum \hat{\mathbf{x}}(n | n, \mathbb{P}_p) \Pr (\mathbb{P}_p | Y(n)) \quad .$$

It may be noted that the optimal estimate is a weighted sum of all the \mathbb{P}_p -conditional estimates where the weights are the respective probabilities representing the knowledge or uncertainty of each respective parameter.

6. The algorithm is repeated until the chosen final time. Since the amplitudes as well as the parameters are known, Monte Carlo may be used to develop a sample mean and sample variance of the estimation error if the many runs required in a Monte Carlo may be accomplished due to the increase in run time.

A.6. Conclusions

This report gives the formulation of the state space model realization for the baseline adaptive optics concept being considered in this contract, and gives the development of the adaptive estimator which will yield estimates of the states comprising the amplitude terms and the various system parameters necessary in the problem.

References for Addendum Section

1. A. Sage, Optimum System Control, Prentice-Hall, New York 1968
2. J. Thomas, Introduction to Statistical Communication Theory, John Wiley & Sons, 1969
3. J. B. Moore and B. D. O. Anderson, "Spectral Factorization of Time Varying Covariance Functions: The Singular Case," *Math. Sys. Thy.*, Vol. 4, No. 1, pp 10-23, 1970
4. L. Silverman, "Realization of Linear Dynamical Systems," *IEEE Trans. on Auto. Contr.*, Vol. AC-16, No. 6, pp. 554-567, December 1971
5. A. H. Jazwinski, Stochastic Processes and Filtering Theory, Academic Press, New York, 1970
6. T. P. McGarty, Stochastic Systems and State Estimations, John Wiley & Sons, New York 1974
7. T. Kailath and R. A. Geesey, "An Innovative Approach To Least Squares Estimation - Part IV: Recursive Estimation Given Lumped Covariance Functions," *IEEE Trans. on Auto. Contr.*, Vol. AC-16, No. 6, pp. 720-727, Dec. 1971
8. D. G. Lainiotis, "Optimal Adaptive Estimation: Structure and Parameter Adaptation," *IEEE Trans. on Auto. Contr.*, Vol. AC-16, No. 2, pp. 160-170, April 1971
9. R. M. Hawkes and J. B. Moore, "Adaptive Estimation Via Sequential Processing," *IEEE Trans. on Auto. Contr.*, Vol. 20, No. 1, pp. 137-138, February 1975
10. H. W. Sorenson, "Kalman Filtering Techniques," in Advances in Control Systems, C. T. Leondes, Editor, Academic Press, New York 1966
11. R. A. Singer and R. G. Sea, "Increasing the Computational Efficiency of Discrete Kalman Filters," *IEEE Trans. on Auto. Contr.*, Vol. AC-16, No. 3, pp. 254-257, June 1971

References, (continued)

12. J. Mendel, "Computational Requirements For a Discrete Kalman Filter," IEEE Trans. on Auto. Contr., Vol. AC-16, No. 6, pp. 748-758, December 1971.

MISSION
of
Rome Air Development Center

RADC plans and conducts research, exploratory and advanced development programs in command, control, and communications (C³) activities, and in the C³ areas of information sciences and intelligence. The principal technical mission areas are communications, electromagnetic guidance and control, surveillance of ground and aerospace objects, intelligence data collection and handling, information system technology, ionospheric propagation, solid state sciences, microwave physics and electronic reliability, maintainability and compatibility.

